



Control of Spillover Processes in Catalysis
-Porous and Patterned Electrodes

By

MAS RAHAYU JALIL

A Thesis Submitted for the Degree of Doctor Philosophy at
Newcastle University, United Kingdom

School of Chemical Engineering and Advanced Materials

April 2015

ABSTRACT

Electrochemical promotion of catalysis (EPOC) is a result of backspillover phenomena which involves the migration of backspillover (oxygen ionic) species through the tpb onto the catalyst surface under the influence of electrical potential application. The present work studies the occurrence and the role of the backspillover species and also the mechanisms of the related processes including factors controlling this phenomenon in a Pt/YSZ system which utilises a model catalyst or sputtered patterned electrodes. In comparison to the electrodes prepared by painting the commercially available Pt catalysts on YSZ, the geometric characteristics and the type and amount of impurities on the Pt surface should not vary significantly among the samples except the tpb length (of the 3rd batch samples). Therefore, the electrochemical processes at the tpb can be studied systematically and the electrochemical data should be reproducible which are not the case when electrodes prepared by using the commercially available catalysts are involved. The variability in the electrochemical behaviour (charge transfer reaction) of the Pt/YSZ system, as depicted by CV results under a nonreactive condition at 400 °C, of the Pt electrodes prepared by using the commercially available catalysts is demonstrated in the first part of the study. The three commercially available catalysts provided by ESL, Heraeus and Metalor are shown to contain different type and amount of impurities and to have different Pt surface morphology. The impurities were analysed by ICP-OES while the surface morphology was investigated by SEM. In the second part of the study, the focus was on the Pt/YSZ system utilising the patterned electrodes where the correlations between the oxygen charge transfer (oxygen activity) and the tpb length were investigated by CV, EIS and current overpotential experiments under a nonreactive condition at temperatures between 300 °C and 450 °C. The term oxygen activity in this thesis refers to the kinetics of the oxygen charge transfer reaction. A proportional relationship between the oxygen charge transfer and the tpb length was not observed and this is explained by the changes in Pt surface morphology throughout the experimental works and most important the formation of surface oxides at the tpb which blocks the charge transfer processes. However, the changes in the oxygen activity at the tpb can be observed from the correlation between the current density and the peak current from the CV results. Another interesting observation is the appearance of additional peak in CV after exposure to hydrogen which can be associated with either the decomposition of impurity oxides or

Pt oxides of different oxidation state at the binary interface. In the third part of the study, the catalytic and electrochemical behaviour of the system utilising the patterned electrodes was investigated during CO oxidation at temperatures between 300 °C and 450 °C. The Pt/YSZ system was found to exhibit (i) EPOC at 0.10 V, 0.20 V and 1.0 V, (ii) permanent EPOC and (iii) permanent poisoning effect. The backspillover species was found not only to enhance the catalytic rate but also to stop the open circuit rate oscillations and, at a high pO_2 , to restore the rate due to the permanent poisoning effect. Furthermore, five types of oxygen species are suggested to present at the tpb and on the Pt surface during the experimental works where the coverage of these species controls the amount of oxygen ionic species which can migrate through the tpb onto the Pt surface.

Nomenclature

List of acronyms

CV	Cyclic voltammetry
EDX	Energy dispersive x-ray spectroscopy
EPOC	Electrochemical promotion of catalysis
EIS	Electrochemical impedance spectroscopy
ICP-OES	Inductively coupled plasma-optical emission spectroscopy
MIEC	Mixed ionic-electronic conducting membranes
NEMCA	Non-faradaic electrochemical modification of catalytic activity
OCP	Open circuit potential
SEM	Scanning electron microscopy
SMSI	Strong metal-support interactions
STM	Scanning tunnelling microscopy
Tpb	Three phase boundary
TPD	Temperature programmed desorption
XPS	X-ray photoelectron spectroscopy
YSZ	Yttria stabilised zirconia

List of symbols

e	Electron charge (C)
ΔU_{WR}	Change in the catalyst potential (V)
U_{WR}^o	Open circuit potential (V)
$\Delta\Phi_W$	Change in the catalyst work function (eV)
η	Overpotential (V)
v	Scan rate (mVs^{-1})
I	Current (A)
I_o	Exchange current (Am^{-2})
r	Promoted catalytic rate ($\text{nmols}^{-1}\text{cm}^{-2}$)
r_o	Open circuit rate ($\text{nmols}^{-1}\text{cm}^{-2}$)
Δr	promotion-induced change in catalytic rate ($\text{nmols}^{-1}\text{cm}^{-2}$)
r_{ref}	Catalytic rate corresponding to a reproducible Pt free surface, i.e. with a negligible O^{2-} coverage on Pt ($\text{nmols}^{-1}\text{cm}^{-2}$)
r_{P-EPOC}	Open circuit rate after current interruption ($\text{nmols}^{-1}\text{cm}^{-2}$)
$r_{poisoning}$	Catalytic rate in the poisoned permanent EPOC steady state after negative current interruption ($\text{nmols}^{-1}\text{cm}^{-2}$)
t	time
τ	EPOC time constant(s)
τ_p	Promoter lifetime (s)
τ_r	gas-supplied reactants lifetime (s)
ρ	Rate enhancement ratio
γ	Permanent rate enhancement ratio
β	Rate poisoning index
ρ_n	Normalised rate enhancement ratio
Λ	Faradaic efficiency
N_{oPt}	Reactive oxygen uptake of the metal catalyst (mol)
N_{otpb}	Reduction of oxygen chemisorbed at tpb (mol)
F	Faraday's constant (Cmol^{-1})
N_{AV}	Avogadro's number (atom mol^{-1})
R	Gas constant ($\text{JK}^{-1}\text{mol}^{-1}$)
T	Temperature (K)

E	activation energy (KJmol ⁻¹)
ΔS	entropy (e.u.)
D _o	surface diffusion coefficient (cm ² s ⁻¹)
a _o	Oxygen activity
r _{Pt}	Atomic radius of Pt
A	Geometrical area of the Pt film (cm ²)
Å	Angstrom (10 ⁻⁸ cm)
d	Diameter of Pt crystallites(μm)
l	tpb length (cm)
l _{tpb}	tpb line length
R _{ct}	Area specific charge transfer resistance
ρ _{ct}	Intrinsic charge transfer resistivity
α	mean diffusion jump length
v	effective attempt frequency (s ⁻¹)
δ	the thickness of the spreading zone
τ _o	operational or electrochemical attack time constant
f	frequency (Hz)
ω	radial frequency
Φ	phase shift
Z	impedance

Acknowledgement

I would like to thank to the following persons who have helped me to complete this research course.

1. My supervisors, Prof. Ian S. Metcalfe and Dr. Evangelos Papaioannou, for their encouragement, guidance and supports throughout the research course.
2. Dr. Danai Poulidi for her guidance and help during the earlier stage of my studies.
3. Dr. Konstantin Vasilevskiy from the School of Electrical, Electronics and Computing Engineering (EECE) for providing patterned electrode samples.
4. Dr. Vasili Kasiutsich, from Manchester University for developing the quantum cascade laser CO₂ analyser.
5. Pauline and Dr. Isabel from the Advanced Chemical and Materials Analysis, Newcastle University for conducting SEM-EDX analyses.
6. Dr. David from the School of Chemistry, Newcastle University for carrying out ICP-OES analyses.
7. My colleagues, Sureena, Naimah, Maria Elena, Claire, Selgin, Henry, Arul, Rafael, Yousef and Prasna.
8. My family
9. Malaysians in Newcastle.
10. UTHM for the scholarship.

Table of Content

Abstract	i
Nomenclature	iii
Acknowledgement	vii
Chapter 1 Introduction	1
1.0 Research Background	1
1.1 Problem Statements	3
1.2 Hypotheses	4
1.3 Objectives of Study	5
1.4 Scopes of Study	6
1.5 Research Contributions	6
1.6 Limitations of Study	7
1.7 Structure of Thesis	8
Chapter 2 Literature review	9
2.0 Introduction	9
2.1 Electrochemical Promotion of Catalysis (EPOC)	9
2.1.1 Transient Behaviour	12
2.1.2 Advantages of EPOC	14
2.1.3 Model Reactions	14
2.1.4 EPOC by the Thermally Induced Oxygen Ionic Species	15
2.1.5 The Role of Backspillover Species	16
2.1.5.1 The Oscillatory Phenomenon during EPOC	17
2.1.5.2 Permanent EPOC	19
2.1.5.3 Permanent Poisoning Effect	21
2.1.6 The Role of Impurities on EPOC	22
2.1.7 Three Phase Boundary (tpb)	23
2.1.7.1 Tpb Length of a Porous Electrode	24
2.1.7.2 Tpb Length of a Patterned/Dense Electrode	25
2.1.8 Summary	26
2.2 Materials and Deposition Methods	26
2.2.1 Electrolyte	27
2.2.2 Catalyst / Electrode Materials	28

2.2.3	Electrode Deposition Method	28
2.2.4	Catalyst Surface Characteristics	29
2.2.4.1	Morphology	29
2.2.4.2	Impurities	30
2.3	Oxygen Charge Transfer in Pt/YSZ System	31
2.3.1	Anodic and Cathodic Reaction Paths	31
2.3.2	Electrochemical Investigations	32
2.3.2.1	Cyclic Voltammetry (CV) of the Pt/YSZ/O ₂ (g) System	32
2.3.2.2	Electrochemical Impedance Spectroscopy (EIS)	38
2.3.2.3	Current Overpotential	45
2.3.3	Limitations in Oxygen Charge Transfer	46
Chapter 3	Methodology	49
3.0	Introduction	49
3.1	Influence of Impurities on Oxygen Charge Transfer in a Pt/YSZ System	49
3.1.1	Sample Preparation	49
3.1.1.1	Electrolyte	50
3.1.1.2	Electrodes	50
3.1.2	Electrode Surface Characterisation	52
3.1.2.1	SEM-EDX	52
3.1.2.2	Analysis of Impurities	53
3.1.3	Reactor Design and Testing Rigs	54
3.1.4	Cyclic Voltammetry (CV) under Nonreactive Condition	56
3.2	Oxygen Charge Transfer in a Pt/YSZ System Utilising Patterned Electrodes	56
3.2.1	Sample Preparation	57
3.2.2	Electrode Surface Characterisation	59
3.2.3	Reactor Design and Testing Rigs	59
3.2.4	Electrochemical Characterisation under Nonreactive Condition	60
3.2.4.1	Geometry Dependence of the Charge Transfer Reactions by CV, EIS and Current Overpotential	60
3.2.4.2	Effect of 0.50 V Anodic Potential on Oxygen Charge Transfer Reactions	62

3.2.4.3	Repeatability Study	63
3.2.5	Verification of the Mechanisms of Patterned Electrode Activation and Deactivation Phenomena	63
3.2.6	Summary of the Electrochemical Characterisation Experiments	65
3.2.6.1	Electrochemical Characterisations	65
3.2.6.2	Repeatability	65
3.2.6.3	Verification of the Mechanisms of Electrode Activation and Deactivation Phenomena	67
3.3	Spillover Processes in a Pt/YSZ System Utilising patterned Electrodes	68
3.3.1	Electrode Surface Characterisation	68
3.3.2	Kinetic Experiments	68
3.3.2.1	Open Circuit Condition	68
3.3.2.2	Close Circuit Condition	70
3.3.3	Summary of the Experimental Works During the Investigations of the Origin of EPOC from the Utilisation of the Patterned Electrodes	70
3.3.3.1	Open Circuit Condition	71
3.3.3.2	Close Circuit Condition	72
3.4	Safety	72
3.4.1	Quantum Cascade CO ₂ Laser Analyser	72
3.4.2	Controls to Reduce Risks	73
3.4.2.1	Flammable Mixture	73
3.4.2.2	Leaks and Mass Flow Controller (MFCs)	73
3.4.2.3	Fume Cupboard Failure	73
3.4.2.4	Shut Down Procedure	74
Chapter 4	Influence of Impurities and Catalyst Surface Characteristics on the Oxygen Charge Transfer Reaction in a Pt/YSZ System	75
4.0	Introduction	75
4.1	Catalyst Surface Characterisations	75
4.1.1	SEM Images	75
4.1.2	ICP-OES Results	78
4.1.2.1	Effect of Sintering Time	79

4.2	Electrochemical Characterisations under a Nonreactive Condition	80
4.3	Further Discussions	83
4.4	Summary	83
Chapter 5	Oxygen Charge Transfer in a Pt/YSZ System Using Patterned Electrodes under a Non Reactive Condition	85
5.0	Introduction	85
5.1	Hypotheses	85
5.2	Geometry Dependence Studies	86
5.2.1	Electrochemical Impedance Spectroscopy (EIS)	87
5.2.1.1	Estimation of the Charge Transfer Resistance from the Diameter of the Semicircle	89
5.2.1.2	Arrhenius Plots of Conductance	90
5.2.2	Current Overpotential	92
5.2.2.1	Exchange Current Density	95
5.2.3	Cyclic Voltammetry (CV)	95
5.2.3.1	Effect of Scan Rate	97
5.2.3.2	Geometry Dependence	97
5.2.4	Summary	99
5.3	Repeatability Study	104
5.3.1	Correlation between Current Density and Cathodic Peak Height in CV	105
5.3.2	Electrode Deactivation and Activation Phenomena	108
5.3.2.1	Electrode Deactivation	109
5.3.2.2	Electrode Activation	112
5.3.3	Hydrogen Reduction	113
5.3.3.1	Surface Oxide Formation in the System Utilising Patterned and Porous Electrodes	115
5.3.3.2	200 μm 550 $^{\circ}\text{C}$ Kinetic Sample	121
5.3.3.3	Summary of Hydrogen Reduction Study	129
5.3.4	Summary	129

Chapter 6	Spillover Processes in a Pt/YSZ System Utilising Patterned Electrodes under a Reactive Condition	131
6.1	Introduction	131
6.2	Hypothesis	131
6.3	Spillover Phenomenon in the Pt/YSZ System Using the Patterned Electrodes	132
6.3.1	Open Circuit Condition	132
6.3.1.1	Surface Morphology by SEM Analyses	135
6.3.1.2	Repeatability Study	137
6.3.1.3	Summary	143
6.3.2	During Polarisation	143
6.3.2.1	Transient Responses of Different CO ₂ Analysers	147
6.3.2.2	Magnitude of EPOC effect	148
6.3.2.3	The Role of the Electrochemical Backspillover Species	152
6.3.3	After Current Interruption	157
6.3.4	Negative Polarisation	163
6.3.5	Correlations of Rates with the Open Circuit Potential	167
6.4	Summary	173
Chapter 7	Conclusions and Recommendations	175
7.0	Summary	175
7.1	Conclusions	177
7.2	Recommendations	178
	References	179
	Appendices	191

List of Figures

Figure 2.1: Schematic diagram of electrochemically induced spillover species onto a metal or Pt surface. The oxygen ions are transported through YSZ and discharged at the tpb and the discharged species migrate onto Pt electrode surface [9]	11
Figure 2.2: Schematic representation of a metal electrode deposited on a (a) O^{2-} conducting and (b) Na^+ conducting solid electrolyte which indicates the location of the metal-electrolyte double layer and of the effective double layer created at the metal-gas interface due to potential-controlled migration of backspillover species [34]	11
Figure 2.3: Catalytic rate versus time during an EPOC experiment [39]	12
Figure 2.4: Schematic diagram indicating the interfaces in a Pt/YSZ system	24
Figure 2.5: Conduction mechanism of a solid ion conductor	27
Figure 2.6: The potential sweep which results to cyclic voltammogram in	33
Figure 2.7: A typical cyclic voltammogram	34
Figure 2.8: CV of PLD films from the work of Mutoro et al. [8]: a) dense (dotted blue line) electrode where the tpb was successively enlarged (I–IV) by scratching; baselines drawn in as dashed red lines; b) dense electrode at the beginning of a measurement (dotted green line, “steady state1”) and after several experiments (continuous green line, “steady state2”)	36

Figure 2.9: Sinusoidal voltage input V at a single frequency f and current response I [89]	40
Figure 2.10: Complex impedance plot [89]	41
Figure 2.11: Typical current overpotential curve	46
Figure 2.12: Typical tafel plot	46
Figure 3.1:(a) Schematic of the electrodes arrangement and (b) the prepared Pellets/Electrolyte/Electrode	52
Figure 3.2: (a) Picture and (b) schematic of the electrochemical reactor	55
Figure 3.3: Schematic diagram of the experimental set up and rigs	55
Figure 3.4: Schematic diagram of the model catalyst or patterned electrodes	58
Figure 3.5: Schematic diagram of experimental set up of Pt/YSZ system using the patterned electrodes	59
Figure 4.1: SEM images of Pt films on YSZ of catalysts at 1000 and 10000 magnifications of the (a) fresh ESL 60 min, (b) fresh ESL 10 min (c) fresh Heraeus and (d) fresh Metalor	77
Figure 4.2: SEM images of Pt films on YSZ of catalysts at 1000 and 10000 magnifications of the ESL 60 min after electrochemical experiments	78
Figure 4.3: Voltammogram of ESL 10 min, ESL 60 min, Heraeus and Metalor at a scan rate of 30 mVs^{-1} , $400 \text{ }^\circ\text{C}$ and under the flow of 200 ml/min $20\% \text{ O}_2/\text{He}$	82

Figure 5.1: EIS spectra of the 4 μm , 40 μm and 400 μm at 400 $^{\circ}\text{C}$, under the flow of 100 mlmin^{-1} 20% O_2/He , the frequency was in the range between 0.1 Hz to 1000000 Hz	88
Figure 5.2: SEM images of the fresh patterned electrodes of (a) 40 μm , (b) 200 μm and (c) 400 μm at a nm scale (the images are provided by Dr. Danai Poulidi and Dr. Evangelos Papaioannou)	89
Figure 5.3: A semicircle with a centre (h,k) and a radius of h	90
Figure 5.4: The Arrhenius plots of low frequency conductance that are normalised to the electrode geometric (a) tpb length and (b) surface area of the 4 μm , 40 μm and 400 μm samples	91
Figure 5.5: Current overpotential curves of 4 μm , 40 μm , 200 μm , 400 μm samples at 350 $^{\circ}\text{C}$, 400 $^{\circ}\text{C}$ and 450 $^{\circ}\text{C}$ under a nonreactive condition (90 to 100 mlmin^{-1} 20 % O_2/He)	93
Figure 5.6: Current range of 4 μm , 40 μm and 400 μm samples at 350 $^{\circ}\text{C}$, 400 $^{\circ}\text{C}$ and 450 $^{\circ}\text{C}$ under a nonreactive condition 90 to 100 mlmin^{-1} 20 % O_2/He which are normalised to electrode geometric (a) width length scale and (b) surface area	94
Figure 5.7: Absolute values of exchange current densities (from the results of current overpotential experiments of 4 μm , 40 μm , 200 μm and 400 μm samples at 300 $^{\circ}\text{C}$, 350 $^{\circ}\text{C}$, 400 $^{\circ}\text{C}$ and 450 $^{\circ}\text{C}$ shown in Figure 5.5)	95
Figure 5.8: Cyclic voltammograms of the (a) 4 μm , (b) 40 μm and (c) 400 μm at 400 $^{\circ}\text{C}$ at different scan rate (10 mVs^{-1} , 20 mVs^{-1} , 30 mVs^{-1} , 50 mVs^{-1} and 100 mVs^{-1}) under a nonreactive condition 90 to 100 mlmin^{-1} 20 % O_2/He	96
Figure 5.9: Current range of 4 μm , 40 μm and 400 μm sample at scan rates of 20 mVs^{-1} , reactor temperature 400 $^{\circ}\text{C}$, 90 to 100 mlmin^{-1} 20% O_2/He	98

Figure 5.10: Cathodic peak heights from CV experiments of 4 μm , 40 μm and 400 μm samples at 400 $^{\circ}\text{C}$ and scan rates of 10 mVs^{-1} , 20 mVs^{-1} , 30 mVs^{-1} and 50 mVs^{-1}	98
Figure 5.11: SEM images of the 20 μm and 200 μm from the 1 st batch, (a) fresh and (b) after electrochemical experiments	101
Figure 5.12: SEM images of the 4 μm and 40 μm from the 3 rd batch , (a) fresh and (b) after electrochemical experiments	102
Figure 5.13: SEM images of the 200 μm and 400 μm from the 3 rd batch , (a) fresh and (b) after thermal treatment (c) electrochemical experiments	103
Figure 5.14: Current range during cyclic voltammetry of the 200 μm from the 3 rd batch, 350 $^{\circ}\text{C}$, 400 $^{\circ}\text{C}$ and 450 $^{\circ}\text{C}$, 20 mVs^{-1} , 100 mlmin^{-1} 20% O_2/He , -0.50 V to 0.10 V	106
Figure 5.15: Cathodic peak height from results of cyclic voltammetry at the reference experiment condition, 200 μm , 350 $^{\circ}\text{C}$, 100 mlmin^{-1} 20% O_2/He .	107
Figure 5.16: Correlation between the amount of oxygen atom and current range from the results of cyclic voltammetry experiments of 200 μm sample at the reference conditions, 20 mVs^{-1} (a) 350 $^{\circ}\text{C}$, 0.10 V, (b) 350 $^{\circ}\text{C}$, 0.20 V, (c) 400 $^{\circ}\text{C}$, 0.20 V and (d) 450 $^{\circ}\text{C}$, 0.20V	108
Figure 5.17: Impedance spectra of 400 μm at 400 $^{\circ}\text{C}$ under nonreactive condition, -0.45 V, before and after the exposure to 0.50 V	110
Figure 5.18: (a) Current range from the current overpotential curve and (b) voltammograms at 20 mVs^{-1} of the 400 μm , at 400 $^{\circ}\text{C}$, under nonreactive condition, 90 to 100 mlmin^{-1} , 20% O_2/He before and after exposure to a 0.50 V anodic potential	111

Figure 5.19: Linear sweep and CV results of the (a) 200 μm from the 3rd batch and (b) ESL 60 min, respectively, before and after exposure to hydrogen. The Linear sweep experiment of the 200 μm from the 3rd batch was conducted at 350 $^{\circ}\text{C}$, 100 mlmin^{-1} 20% O_2/He at scan rate of 20 mVs^{-1} . The CV experiment of the ESL 60 min sample was carried out at 400 $^{\circ}\text{C}$, 200 mlmin^{-1} 20% O_2/He and scan rate of 20 mVs^{-1} 116

Figure 5.20: Effect of holding time on the (a) amount of oxygen atoms and (b) current range, at 350 $^{\circ}\text{C}$, under nonreactive conditions. (i) 200 μm sample after H_2 reduction, this experiment was carried out after several linear sweep experiments at the same experimental condition, (ii) 200 μm sample after H_2 reduction, there was no other experiments carried out before this experiment after the H_2 reduction, (iii) 200 μm sample after experiment (ii) where the sample was not reduced prior to this experiment. 117

Figure 5.21: Voltammograms of 550 $^{\circ}\text{C}$ thermally treated 200 μm after kinetic sample at the reference condition before and after hydrogen reductions at 350 $^{\circ}\text{C}$, 4th cycle 122

Figure 5.22: Changes of the 1st and 2nd cathodic peak heights of the 200 μm 550 $^{\circ}\text{C}$ kinetic sample before and after 2 hours of exposure to hydrogen 123

Figure 5.23: Cyclic voltammograms of the 550 $^{\circ}\text{C}$ thermally treated 200 μm after kinetic sample at the reference condition after hydrogen reductions at 350 $^{\circ}\text{C}$, 50th cycle. 125

Figure 5.24: Voltammograms of the 200 μm 550 $^{\circ}\text{C}$ thermally treated of the 50th cycle, before and after exposure to hydrogen. The CV was carried out at 350 $^{\circ}\text{C}$ under the flow of 100 mlmin^{-1} 20% O_2/He , at a scan rate of 20 mVs^{-1} . 127

Figure 5.25: Voltammograms of the 200 μm 550 $^{\circ}\text{C}$ thermally treated of the 4th and the 50th cycle, before and after exposure to hydrogen. The CV was carried out 128

at 350 °C under the flow of 100 mlmin⁻¹ 20% O₂/He, at a scan rate of 20 mVs⁻¹.

Figure 6.1: SEM images of (a) 200 µm fresh untreated, before kinetic experiments, (b) 200 µm fresh treated at 550 °C, before kinetic experiments and (c) 200 µm fresh treated at 550 °C, after kinetic experiment. 136

Figure 6.2: Open circuit rates of 200 µm (1st sample) from the 3rd batch which are normalised to electrode geometric surface area at 340 °C during long term monitoring O₂ kinetic study at 3 kPa pO₂, 0.63 kPa pCO, total flow rate of 160 mlmin⁻¹ and the rates were measured by a quantum cascade CO₂ analyser. 139

Figure 6.3: Open circuit rates which were measured prior to 0.10 V and 0.20 V anodic polarisation during electrochemical experiments of the 200 µm (3rd sample in Table 6.2) from the 3rd batch at 3 kPa pO₂, 0.5 kPa pCO, 350 °C and total flow rate of 150 mlmin⁻¹. The rates were measured by Binos 100 CO₂ analyser and are normalised to electrode geometric surface area. 141

Figure 6.4: The effect of sintering temperature on open circuit rates of the 200 µm (1st sample after the long term monitoring study) and a fresh 400 µm from the 3rd batch. The rates were measured by a quantum cascade CO₂ analyser and are normalised to electrode geometric surface area. The experiments were carried out at 340 °C, 3 kPa pO₂, 0.63 kPa pCO, total flow rate of 160 mlmin⁻¹. Lower and upper limit correspond to the lowest and highest value during measurement, respectively. 142

Figure 6.5: The results of EPOC experiments of CO oxidation as a function of pO₂ under a fixed 0.5 kPa pCO at 350 °C, (a) 0.10 V and (b) 0.20 V, for the 200 µm from the 3rd batch 145

Figure 6.6: The results of EPOC experiments of CO oxidation as a function of pO₂ and pCO (under a fixed pCO=0.5kPa, pO₂=0.7kPa, respectively) at 340 °C, 1.0 V, for the 20 µm and 200 µm samples 146

Figure 6.7: Transient responses of EPOC experiments at 1.3 kPa pO ₂ , 0.5 kPa pCO, 350 °C, 150 mlmin ⁻¹ by using Xstream/Emerson and Binos 100 CO ₂ analyser	148
Figure 6.8: Transient responses during EPOC experiments of 200 μm from the 3 rd batch at 3 kPa pO ₂ , 0.5kPa pCO, and a total flow rate 150 mlmin ⁻¹ at (a) 350°C and 0.20 V, (b) 350 °C and -1.0 V, (c) 400 °C and 0.20 V	155
Figure 6.9: Transient responses during EPOC experiments of 200 μm from the 3 rd batch at 0.7 kPa pO ₂ , 0.5kPa pCO, 350 °C, and a total flow rate 150 mlmin ⁻¹ (a) and (c) 0.10 V, (b) -1.0 V, which demonstrate permanent EPOC effect	160
Figure 6.10: Permanent rate enhancement ratio from the transient responses at different oxygen feed composition of the (a) 20 μm, (b) 200 μm from the 1 st batch and (c) 200 μm from the 3 rd batch. The permanent rate enhancement ratio of the 20 μm (d) at different temperature and (e) and (f) correlation with the open circuit potential	161
Figure 6.11: Transient responses during EPOC experiments of 200 μm from the 3 rd batch at 350 °C, and 150 mlmin ⁻¹ which demonstrate permanent EPOC effect as a result of (i) oxygen storage [(a)4.6 kPa pO ₂ , 0.5kPa pCO, 0.10 V, (b) 4.6 kPa pO ₂ , 0.5kPa pCO, -1.0 V] and (ii) changes in Pt surface morphology [(c) 1 st experiment and (d) repeated experiment at 0.7 kPa pO ₂ , 0.5kPa pCO, 0.10 V]	162
Figure 6.12: Transient responses during EPOC experiments of 200 μm from the 3 rd batch at 0.7 kPa pO ₂ , 0.5kPa pCO, 350 °C, and a total flow rate 150 mlmin ⁻¹ (a) 0.10 V, (b) -1.0 V and (c) 0.10 V	164
Figure 6.13: Transient responses during EPOC experiments of the 200 μm from the 3 rd batch at 5 kPa pO ₂ , 0.5kPa pCO, 350 °C ,total flow rate 150 mlmin ⁻¹ and (a) 0.10 V, (b) -1.0 V and (c) 0.10 V	165

Figure 6.14: Open circuit rate and open circuit potential measured before the polarisation (a) 200 μm 1st batch, (b) 20 μm from the 1st batch, (c) 200 μm from the 3rd batch after electrochemical characterisation under nonreactive condition at 0.10 V, (d) 200 μm from the 3rd batch after electrochemical characterisation under nonreactive condition at 0.20 V 168

Figure 6.15: Electrochemical promoted rate and open circuit potential (a) 200 μm 1st batch, (b) 20 μm 1st batch, (c) 200 μm 3rd batch after electrochemical characterisation under nonreactive condition at 0.10 V, (d) 200 μm 3rd batch after electrochemical characterisation under nonreactive condition at 0.20 V 169

Figure 6.16: (a) Current and electrochemical promoted rate, (b) current and open circuit potential of the 20 μm and 200 μm from the 1st batch and the 200 μm from the 3rd batch 170

Figure 6.17: Transient responses of the 20 μm sample during EPOC studies at 340°C, 3kPa pO₂, 0.5kPa pCO, 1V, 150mlmin⁻¹ of the (a) first and (b) second experiments 171

List of Tables

Table 2.1: Findings of the Catalytic Rate Oscillations during EPOC by Other Researchers	18
Table 2.2: Summary of Permanent EPOC and Permanent Poisoning from EPOC Studies	23
Table 2.3: Results of Geometry Dependence Studies from Literatures	44
Table 3.1: Sintering program of the working, counter and reference electrodes	51
Table 4.1: Known impurities in YSZ and platinum found in the literature and present work	79
Table 4.2: Impurities in the three commercial platinum catalysts	79
Table 5.1. : Schematic representation of electrode processes and voltammograms of ESL and patterned electrodes before and after hydrogen reduction experiments, the reduction was carried out at 500 °C	120
Table 6.1: Catalytic rate of the fresh patterned electrodes which were measured by using a quantum cascade CO ₂ analyser	134
Table 6.2: Rate enhancement, faradaic efficiency and permanent rate enhancement ratio	148
Table 6.3: Results of EPOC experiments of CO oxidation	151
Table 6.4: Findings of the Catalytic Rate Oscillations during EPOC by Other Researchers	156

Table 6.5: Summary of Permanent EPOC and Permanent Poisoning from EPOC Studies	166
--	-----

Table 6.6: Type of oxygen species on Pt surface	174
---	-----

Chapter 1. Introduction

1.0 Research Background

The current work focuses on the electrochemical promotion of catalysis (EPOC) or non-faradaic electrochemical modification of catalytic activity (NEMCA) which has been studied and applied quite successfully for many catalytic systems (the term EPOC will be used in this thesis from now on). In EPOC, catalytic activity and selectivity of metal films in contact with electrolytes, both solid state and aqueous, can be varied in situ in a very pronounced and reversible manner via electrical potential application between the catalyst film and a counter electrode also in contact with the electrolyte. Vayenas and co-workers discovered this EPOC phenomenon in early 1980s and many types of reactions and systems have been studied today by many research groups. One of the practical utilisations of EPOC is in environmental catalysis, particularly in automotive pollution control. Recent investigations include implementation of EPOC on O^{2-} ionically conducting ceramics for automotive post-treatment (e.g., NO reduction, CO oxidation, hydrocarbons oxidation) and air cleaning (e.g., Volatile organic compounds oxidation) applications [1].

EPOC has been shown to be due to the catalytically promoting properties of ionic species which migrate onto the catalyst surface under the influence of the applied potential. These species accompanied by their compensating charge in the metal establish an overall neutral double layer on the gas exposed catalyst surface. The effective double layer affects the binding strength of chemisorbed reactants and reaction intermediates and thus affects the catalytic rate in a very pronounced and reversible manner [2]. After current interruption, the catalytic rate usually returns to the initial open circuit value, however, there are also cases where the rate remained at the highly active steady state [3,4] and at a value lower than the initial condition [5, 6].

The migration of the ionic species and the formation or the stabilisation of the effective double layer are influenced by catalyst surface microstructure and surface impurities. For a case of commercial catalysts, impurities may pre-exist on the catalyst surface and

catalyst surface characteristics may also be different as a result of the differences in catalyst manufacturing processes. The resulting catalyst films of different providers, therefore, may have different impurities [7, 8] and microstructure or morphology [8, 9] which can result to significant differences in the number of the available active sites (three phase boundary (tpb) interface) for the charge transfer reactions and hence exhibit different transient responses in EPOC. Furthermore, impurities cause changes in the catalyst work function and also can directly interact with the gas phase reactants and reaction intermediates and promoter or backspillover species [10]. Addition of an impurity (such as sodium) onto Pt catalyst has been shown to affect the catalyst catalytic and electrocatalytic activity, however, there was no evidence of the effect of such species on causing EPOC [10].

The effect of impurity and morphology on the catalyst catalytic and electrocatalytic behaviour interact and hence a special focus on either the contamination [8] or the morphology is necessary to obtain a clear evidence of the effect of each of these two factors on EPOC. A focus on the influence of impurities on EPOC can be obtained by adding a known amount of impurity onto a catalyst surface where the catalytic and electrocatalytic behaviour can be studied by analysing several samples with different amount of added impurities [10, 11]. However, for cases where the electrode is prepared by brushing or painting (manually), there should also a variation in the catalyst film thickness and amount among the electrodes (although using the same catalyst) where the morphology effect cannot simply be neglected. Besides that, impurities such as Si can also be introduced onto the catalyst surface during electrode preparation. A focus on the morphology, on the other hand, requires a clean sample or at least samples with a controlled amount and type of impurities. In other words, the samples should be similar in terms of the type and amount of impurities present on the Pt surface.

The variations or complexity in the electrode geometric (film thickness) and surface (morphology and impurities) characteristics of the porous electrodes prepared by using the commercially available catalysts led to difficulties in carrying out a systematic study on the geometric (such as tpb) dependence of the charge transfer reactions. These problems which also resulted to the experimental data which was not reproducible however can be solved through the application of model catalysts such as those prepared

by sputtering with known geometric tpb length [12-14]. Model catalysts prepared by sputtering have a controlled geometric characteristics and amount of impurities and are usually of a thin and dense electrode. However, there are limitations when this model catalyst was used where

- (i) significant changes in the morphology were observed as a result of anodic polarisation and heat treatment [15]
- (ii) surface oxidation at the catalyst active sites or tpb was unavoidable and was usually discussed in the literature as a cause of catalyst or electrode deactivation [15,16]

The electrode deactivation phenomenon is associated with a decrease in the oxygen activity at the tpb where the charge transfer reactions are hindered by the passive oxide layer at this interface [15]. For a case of a dense electrode, this decrease in the oxygen activity at the tpb causes an increase in the activity at other interfaces in the Pt/YSZ system such as at the Pt/YSZ (or binary) interface. In other words, oxygen activity at each of the interfaces in the system influence each other [8]. Since the deactivation phenomenon is particularly important in terms of the performance of the electrode, such as in EPOC where the processes occurring at the tpb is highly important, detail understanding of the processes occurring at each of these interfaces are therefore necessary.

1.1 Problem Statements

Variability in the electrochemical behaviour of a Pt/YSZ system are often reported in the literatures which could be due to the presence of different types of impurities in the raw materials used for the preparation of different samples [10]. To date, very little information is available on the possible influence of impurities on the charge transfer reactions and EPOC in a Pt/YSZ system. The presence of impurities on the catalyst surface requires a complex model to predict and explain the electrochemical behaviour of such a system [10]. As demonstrated by Ibrahim et al.[10], at high sodium (impurity) coverage, (i) sodium effect on the open circuit catalytic rate was more pronounced and (ii) the interaction between the sodium and oxygen (promoter) under the polarisation became significant. In order to simplify the model describing the electrochemical

behaviour of a Pt/YSZ system, (i) impurities should present (if there any) on the catalyst surface at the lowest possible amount so that the assumption of the negligible interaction with the promoter under the polarisation is valid or (ii) the type and amount of impurities present on the catalyst surface should not vary significantly among the samples so that the variables associated with impurities are minimised and a focus on the morphology or geometric characteristics can be obtained.

However, the commercially available catalysts should contain impurities and the manual preparation of the electrodes also can cause variation in the electrode geometric characteristics and hence the electrochemical data. This led to difficulties not only to explain the electrochemical behaviour but also to carry out a systematic study on the effect of certain geometric parameter such as the tpb length on the charge transfer reactions and hence EPOC. Therefore, (i) to systematically study the processes occurring at the tpb such as the backspillover processes which are associated with the origin of EPOC, the utilisation of a model catalyst with a focus on the tpb length is necessary. This can be obtained from the application of electrodes with controlled surface characteristics where the geometric parameters, such as the tpb length, film thickness and surface area, are well defined with a controlled amount of impurities (if there any) present on the catalyst surface.

1.2 Hypotheses

Based on the research background, the following hypotheses are developed.

- (i) Commercial catalysts contain impurities and the impurities influence (either by enhancing or hindering) the charge transfer reactions at tpb and hence has significant effect on EPOC.
- (ii) The complexity of the geometry characteristics of the patterned electrodes or model catalysts are reduced since the electrodes have a controlled geometry characteristics where the geometric tpb length is known and differs among samples of different width length scale. Therefore, geometry (tpb) dependence of the charge transfer reactions can be studied.
- (iii) Patterned electrodes (3rd batch samples) prepared by sputtering should have a controlled amount of impurities in comparison to those prepared manually by

using commercial catalysts. The patterned electrodes were prepared in three batches where the characteristics for each batch are described in Chapter 3 section 3.2. It is therefore assumed that variables associated with impurities (among different samples) are minimised. The question of whether the impurities are necessary for the occurrence of EPOC is not the focus of the present work involving the patterned electrodes.

- (iv) Tpb is susceptible to oxidation and the formation of surface oxide can hinder the charge transfer reactions at this interface [17,18]
- (v) Oxygen oxidation and reduction processes are occurring at various interfaces in the Pt/YSZ system using the patterned electrodes (such as tpb and binary interface (Pt/YSZ)) where the processes at an interface are dependent on the processes taking place at the other interfaces.

1.3 Objectives of Study

The objectives of the present work are to determine if the patterned electrodes can be utilised as a model catalyst where the focus was on the processes occurring at the tpb involving the backspillover phenomenon and on the factors controlling this process. The study included

- (i) the verification of the presence of impurities in commercial catalysts and the influence (which is assumed to interact with the effect of catalyst surface morphology) on the charge transfer reactions in a Pt/YSZ system.
- (ii) the utilisation of the patterned electrodes in electrochemical studies in which the focus was on the processes occurring at the tpb which is the most important interface associated with the backspillover phenomena.
- (iii) Investigations of the limitations (electrode deactivation and activation phenomena) and advantages of using electrodes with the patterned electrode design in the Pt/YSZ system. This is important in terms of determining the electrodes suitability as (i) the model catalyst and (ii) a catalyst in EPOC.

1.4 Scopes of Study

- (i) The study on the influence of impurities on the oxygen charge transfer reactions was carried out using three commercially available Pt catalysts. The experiments or analyses included surface (SEM and ICP) and electrochemical characterisations by cyclic voltammetry (CV) at low temperature and under atmospheric condition and a nonreactive condition in which the samples were exposed to the flow of 200 mlmin^{-1} 20% O_2/He at temperatures between $300 \text{ }^\circ\text{C}$ and $450 \text{ }^\circ\text{C}$.
- (ii) The study using the model catalyst or patterned electrodes included surface (SEM) and electrochemical characterisations by CV, electrochemical impedance spectroscopy (EIS), current overpotential under nonreactive condition and kinetic and electrochemical promotion (EPOC) experiments under reactive conditions at low temperature and under atmospheric condition. The electrodes were of different width length scale. Under the nonreactive condition, the electrodes were exposed to the flow of approximately 100 mlmin^{-1} 20% O_2/He while under the reactive condition, the electrodes were exposed to 5% CO/He , 20% O_2/He and He . The electrodes were also exposed to 5% H_2/He during chemical treatment study.

1.5 Research Contributions

The main contribution of the present work is the description of the electrochemical behaviour of the Pt/YSZ system utilising patterned electrodes in which (i) the role of backspillover species under polarisation, (ii) factors controlling the backspillover phenomena, and (iii) limitations (different than those described in **section 1.6**) during the utilisation of the patterned electrodes are discussed. The findings included

- (i) demonstration of the significant influence of impurities on the charge transfer reactions.
- (ii) repeatability study, which included chemical treatment, as an approach (i) to describe the tpb dependence of the catalytic rate and charge transfer reactions and (ii) to indicate the presence of impurity oxide or Pt oxide of different oxidation state at the binary interface.
- (iii) observations of EPOC at small anodic potential of 0.10 V and 0.20 V during CO oxidation at low temperature.

- (iv) the observation and the description of the mechanism of the permanent poisoning effect during CO oxidation.
- (v) the finding of a similarity in the role of the stored oxygen at the binary Pt/YSZ interface and Pt bulk with the backspillover species in controlling the surface oxygen activity, stabilising the effective double layer and enhancing the catalytic rate.
- (vi) a suggestion of five types of oxygen species which can present on the Pt surface during the experimental works where the coverage of these species on the Pt surface controls or influences the amount of oxygen ionic species which can migrate onto the Pt surface.
- (vii) surface oxides formation at tpb as the limiting factor of the charge transfer reactions and EPOC.
- (viii) durability of the patterned electrodes during the applications in the field (possible applications include (i) CO oxidation catalytic rate sensor (ii) EPOC)

1.6 Limitations of Study

Uncertainties of the results are associated with limitations in

- (i) the number of patterned electrode samples
- (ii) the design of the patterned electrodes where the electrodes are not completely dense and susceptible to oxidation
- (iii) the time to carry out the experiments
- (iv) the output of the Binos 100 CO₂ analyser where the transient results were digitised
- (v) carrying out chemical treatment at high temperature where the counter and reference electrodes are susceptible to damages
- (vi) data analyses where the utilisation of certain software may produce better demonstrations of the results
- (vii) in situ measurement where this type of investigation can further verify the findings of the current work

1.7 Structure of Thesis

Chapter 1 presents research backgrounds, problem statements, hypothesis, objectives, scopes of study, research contributions and limitations of study. Chapter 2 discusses the literature review while Chapter 3 describes the experimental procedures used in this study. Results are presented and discussed in Chapter 4, 5, and 6. Chapter 4 verifies the presence of impurities in the commercial catalysts and sintered Pt films and these impurities are shown to influence the charge transfer reaction where this effect interacts with the morphology of the Pt film. Chapter 5 presents the study on the tpb length dependence of the charge transfer reaction using the model catalyst where the discussions were on the effect of electrode morphology (microstructure and surface oxides). Chapter 6 present the role of backspillover species and mechanism of the backspillover processes in the Pt/YSZ system utilising the patterned electrodes. Chapter 7 presents the conclusions and recommendations for future works.

Chapter 2. Literature review

2.0 Introduction

Catalysis is the process in which the rate of a chemical reaction is either increased or decreased by means of a chemical substance known as a catalyst. A catalyst is not consumed by the reaction itself and may participate in multiple chemical transformations. The activity of catalysts can be increased by substances known as the promoters and the activity can be decreased by substances known as catalytic poisons. Homogeneous catalysts are those that are present in the same phase as the reactants while heterogeneous catalysts are those that are present in a different phase. In heterogeneous catalysis, promoters play an important role. Promoters can be added to the catalyst *ex situ*, during catalyst preparation or *in situ* via electrical potential or current application when the active phase is supported by an ionic or mixed-ionic-electronic conductor which can donate promoting species to the catalyst/gas interface via backspillover [19].

2.1 Electrochemical Promotion of Catalysis (EPOC)

The catalytic activity and selectivity of a porous catalyst film deposited on a solid electrolyte can be modified *in situ* in a very pronounced and reversible manner via electrical potential application between the catalyst film and a counter electrode also in contact with the electrolyte [20]. This phenomenon has been termed as electrochemical promotion of catalysis (EPOC) or non-faradaic electrochemical modification of catalytic activity (NEMCA) or *in situ* controlled promotion which has been studied and applied quite successfully for many catalytic systems. Catalytic oxidations of C_2H_4 , C_3H_6 and CO were among the catalytic systems being studied. Catalysts used in EPOC studies such as Platinum (Pt), Palladium (Pd) and Rhodium (Rh) were normally deposited on either a proton conductor, an ionic conductor or a mixed ionic-electronic conductor. The origin of EPOC has been studied by using analytical methods such as X-ray photoelectron spectroscopy (XPS) [21], work function measurements [22], scanning tunnelling microscopy (STM) [21], temperature programmed desorption (TPD) [23, 24] and scanning photoelectron microscopy [25], scanning electron microscopy (SEM) [7, 26-28], SEM/EDX [4,29,30] and cyclic voltammetry (CV) [7,31, 32].

The EPOC phenomenon is believed to be due to the electrochemically controlled migration of backspillover species from the solid electrolyte onto the gas exposed electrode surface through three phase boundary (tpb). Backspillover species can be $O^{\delta-}$ in the case of O^{2-} conductors such as Y_2O_3 -stabilized ZrO_2 (YSZ) and mixed ionic-electronic conductors such as TiO_2 or CeO_2 . For the case of Na^+ conductors such as β - and β'' - aluminas which are nonstoichiometric compounds corresponding to $Na_{1+x}Al_{11}O_{17+x/2}$ ($0.15 \leq x \leq 0.3$) and $Na_{1+x}M_xA_{11-x}O_{17}$, respectively, where M is a divalent metal such as Mg^{2+} , Ni^{2+} , Zn^{2+} , the backspillover is $Na^{\delta+}$ [33]. $O^{\delta-}$ can have a charge between O^- and O^{2-} [9], while for $Na^{\delta+}$ the charge is in the order of 0.8–0.5 [33].

The spillover effect can be described as the mobility of adsorbed species from one phase on which they easily adsorb (donor) to another phase where they do not directly adsorb (acceptor) [33]. Backspillover species such as $O^{\delta-}$ in the case of O^{2-} conductors act as normal promoters once they have migrated onto the metal surface. The species occupies the strongly bonded oxygen chemisorptions state while adsorbed oxygen from the gas phase populates the weakly bonded state. The reaction rate will be at a new steady state value when the backspillover species achieve a steady state coverage on the metal surface.

The electrical promotion operational principle is shown in Figure 2.1 [9]. Under the influence of the applied potential (between the catalyst and a catalytically inert counterelectrode, also deposited on the solid electrolyte), ionic species backspillover onto the catalyst surface accompanied by their compensating charge and establish an overall neutral effective double layer on the gas exposed catalyst surface. The effective double layer created at the metal-gas interface due to potential-controlled migration of backspillover species is shown in Figure 2.2 [34]. The presence of this effective double layer modifies the catalyst's work function and changes the binding strength of the chemisorbed reactants and reaction intermediates, thus affecting the catalytic rate [33, 34, 35].

The work function of a surface is the minimum energy which an electron must have to escape from the surface when the surface is electrically neutral [33]. Catalyst work function can be measured by using Kelvin probe [23, 34, 36-38] in which the correlation

between the applied potential and the change in the work function at the metal gas interface is described as [2, 34, 38]

$$e\Delta U_{WR} = \Delta\Phi_W \quad (1)$$

where ΔU_{WR} and $\Delta\Phi_W$ are the change in the catalyst potential and the work function, respectively.

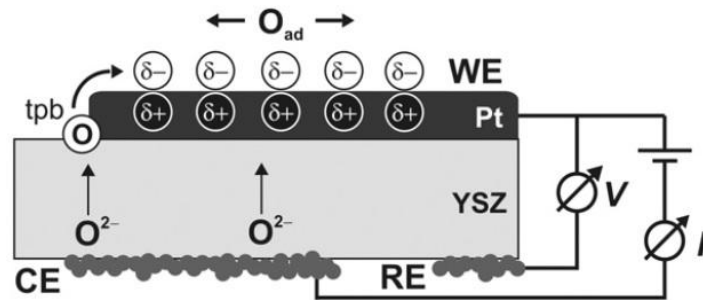


Figure 2.1: Schematic diagram of electrochemically induced spillover species onto a metal or Pt surface. The oxygen ions are transported through YSZ and discharged at the tpb and the discharged species migrate onto Pt electrode surface [9]

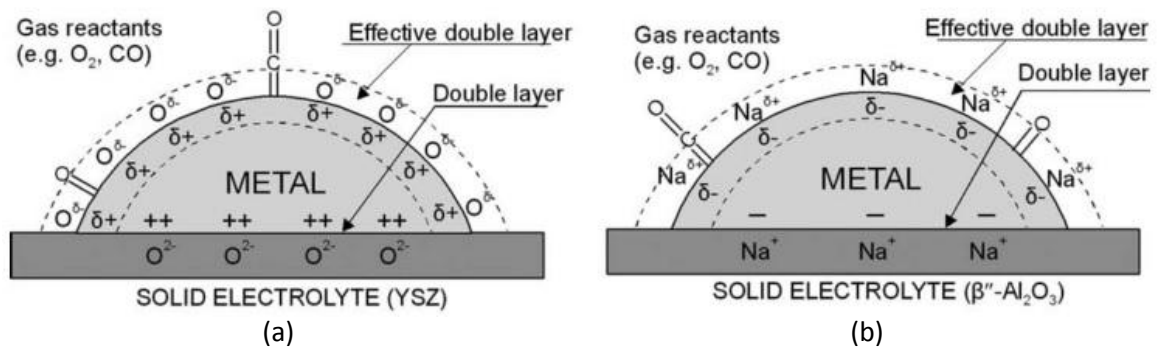


Figure 2.2: Schematic representation of a metal electrode deposited on a (a) O^{2-} conducting and (b) Na^+ conducting solid electrolyte which indicates the location of the metal-electrolyte double layer and of the effective double layer created at the metal-gas interface due to potential-controlled migration of backspillover species [34]

Upon varying the catalyst potential (or work function) of a given catalyst at constant temperature and gas composition, four types of the promoted catalytic rate dependence on the work function (or potential) can be observed which include [19]

- (i) an electrophobic reaction when the catalytic rate increases with catalyst work function and potential
- (ii) an electrophilic reaction when the catalytic rate decreases with catalyst work function and potential
- (iii) an inverted volcano type reaction when the rate passes through a minimum with the catalyst potential and work function
- (iv) a volcano type reaction when the rate passes through a maximum with the catalyst potential and work function.

For the electrophobic reaction, the positive potential increases the work function due to the O^{2-} or promoter supply onto the catalyst surface. The presence of this promoter weakens the chemisorptive bond of electron acceptor adsorbates and strengthens the chemisorptive bond of electron donor adsorbates [2]. The negative potential, however, should withdraw the promoter from the Pt electrode thus causing a decrease in the reaction rate [9].

2.1.1 Transient Behaviour

The typical catalytic rate versus time behaviour during an electrochemical promotion experiment is shown in Figure 2.3, where the catalytic rates, r_o ($I=0$) and r , are the rates under open and close circuit conditions, respectively.

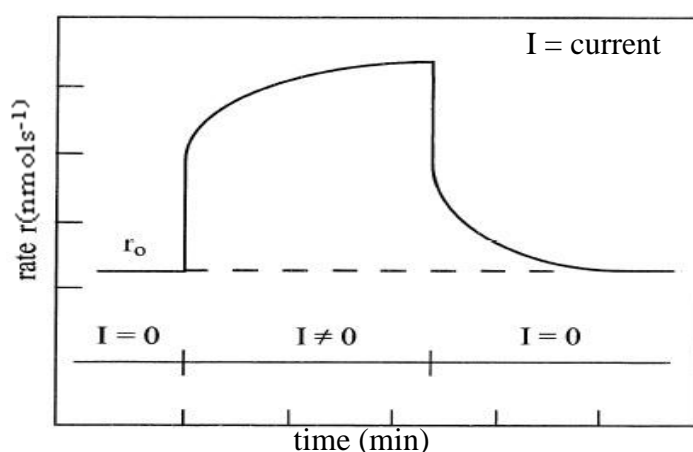


Figure 2.3: Catalytic rate versus time during an EPOC experiment [39]

The promoted rate, r , could be up to 200 times larger than the open circuit rate, r_o , after the application of an electric current, I , or a potential difference between working and the

reference electrode. The promotion-induced change in catalytic rate (mol O per s) can be expressed as

$$\Delta r = r - r_0 \quad (2)$$

The occurrence of the electrochemically controlled migration (backspillover) or promoting species from the solid electrolyte support to the metal gas interface is indicated by the long rate response time constants during constant current imposition [34]. This is equivalent to the time required to form a monolayer of $O^{\delta-}$ on the metal surface or for Δr to reach 63% of its steady state value when atomic oxygen is supplied at the tpb at a rate of $I/2F$ according to Faraday's law which is defined as the EPOC time constant, τ , [34]

$$\tau = 2FN_{oPt}/I \quad (3)$$

where N_{oPt} is the reactive oxygen uptake of the metal catalyst which is expressed in mol. The formation of these backspillover species at the tpb can be written as [34]



However, according to the sacrificial promoter mechanism, an O^{2-} arriving from the solid electrolyte support to the tpb can also desorb as O_2 or react with adsorbed CO to form CO_2 besides migrating (backspillover) at the metal/gas interface as a surface dipole [24]. Besides the EPOC time constant, another important parameter which is often used to describe the EPOC effect is the Faradaic efficiency, Λ , defined as [40]

$$\Lambda = \Delta r / (I/2F) \quad (5)$$

where Λ can also be approximated by [2]

$$|\Lambda| \approx 2 Fr_0/I_0 \quad (6)$$

where I_0 is the exchange current of the catalyst-solid electrolyte interface. If $|\Lambda| > 1$ then the reaction exhibits the EPOC effect. For oxidation reactions, Λ expresses the ratio of the

reaction rates of normally chemisorbed atomic oxygen on the promoted surface over that of backspillover oxide ions. It also describe the ratio of the average lifetimes τ_p and τ_r of the promoter and of the gas-supplied reactants, respectively, on the catalyst surface [34]

$$\Lambda = \tau_p/\tau_r \quad (7)$$

where this promoter lifetime τ_p can be directly obtained from the r versus time transient upon current interruption since the observed catalytic rate decrease is due to the consumption by the fuel of the promoting backspillover $O^{\delta-}$ species. Besides the faradaic efficiency, the rate enhancement ratio, ρ , defined as the ratio of the promoted, r , over open circuit catalytic rate, r_o , is also often used to determine the magnitude of the EPOC effect [40].

2.1.2 Advantages of EPOC

In EPOC, the promoting species that would normally have a short life-time on the catalyst surface can still be used as a promoter since its coverage on the catalyst surface can be fixed by setting an appropriate potential between the working and counter electrodes. This allows the direct examination of the effect of promoter coverage and of work function on the catalytic reaction kinetics [2]. It has been shown that the EPOC phenomenon is equivalent to the phenomenon of strong metal-support interactions (SMSI) [41] and the difference between EPOC and SMSI is that in the former case it is possible to control in situ the supply of the promoter on the catalyst surface.

2.1.3 Model Reaction (Carbon Monoxide Oxidation)

Electrochemical promotion has been studied for various catalytic reactions that included CH_4 , C_2H_4 , CO , SO_2 , C_3H_6 oxidations [3, 35, 42-52], NO reductions [20, 53-57] and CO_2 hydrogenations [58-60]. In the present work, CO oxidation over Pt catalyst was used as the model reaction during the EPOC study. Extensive studies on carbon monoxide (CO) oxidation over noble metal catalyst such as platinum (Pt) and palladium (Pd) have been carried out since these two metals are widely used as automobile catalytic exhaust

converters. The advantages of using CO oxidation over Pt catalyst as model reaction are as the followings [61]

- a. No side reactions in a CO oxidation reaction.
- b. The Pt-based catalyst was very stable towards the oxidation reaction.
- c. Information on CO oxidation is available due to its importance in the catalytic control of automobile emissions.

CO oxidation can be expressed as:



A pronounced EPOC effect with a rate enhancement ratio, ρ , of approximately 9 and a faradaic efficiency, Λ , of approximately 1500 when U_{WR} exceeded 0.4 V has been reported during study using CO oxidation as the model reaction [50]. Another study on CO oxidation over nano-dispersed Pt particles catalyst supported on YSZ under high vacuum conditions showed reaction rate enhancement by a factor of 500 at 300 °C [62]. The results of EPOC experiments on CO oxidation from literatures are indicated in Chapter 6 (Table 6.3).

2.1.4 EPOC by the Thermally Induced Oxygen Ionic Species

It has been established by Vayenas and co-workers that EPOC involves the migration of O^{2-} ionic species, from YSZ onto the Pt surface under the influence of polarisation. However, Vernoux et al. [63] has demonstrated that EPOC can be thermally induced without any electrical polarisation for a Pt/YSZ system involving nanoparticles of metallic catalysts supported on ionically conducting ceramics during propane deep oxidation. The occurrence of this thermally induced oxygen ionic species has also been described for a very thin and dense sputtered Pt layer (very low internal diffusion) [64]. This mechanism is similar to the effect of backspillover of O^{2-} induced by polarisation. The advantage of this effect is that it does not require electrical connections and complicated specific devices. In contrast to electrical polarisation, it may be difficult to

control in situ the thermal migration to achieve the optimal coverage of ionic promoters and the maximal catalytic rate [63].

As mentioned by Karoum et al. [65] in the literatures, the thermal migration ionic species from YSZ to the Pt surface, which contributed to the initial O^{2-} coverage on Pt without any polarisation, has often been neglected and assumed not to influence the catalytic rate measured at the open circuit condition. To observe a real impact of polarisation for a Pt/YSZ system where these thermally induced backspillover species present on the catalyst or Pt surface, a negative potential can be applied [64,65] where the negative polarisation causes the migration of O^{2-} ionic species from the Pt surface toward the electrolyte and this step assures the same Pt surface state before each anodic polarisation. Karoum et al. [65] also demonstrated the importance to define a normalised rate enhancement ratio from a reference value of the catalytic rate corresponding to a Pt surface state free of O^{2-} ions. The normalised rate enhancement ratio, ρ_n , is defined as

$$\rho_n = r/r_{ref} = r/r_{(-2V \text{ during 1 hour})} \quad (9)$$

where r_{ref} is not the open circuit catalytic rate which depends on the sample thermal history but the catalytic rate corresponding to a reproducible Pt free surface, i.e. with a negligible O^{2-} coverage on Pt.

2.1.5 *The Role of Backspillover Species in the Pt/YSZ System*

In EPOC, backspillover species (either induced by thermal effect or polarisation) acts as a promoter which can dramatically enhance the catalytic rate. The species however has been discussed in the literatures to also have other roles in the Pt/YSZ system such as

- (i) causing and or stopping oscillations in the catalytic rate,
- (ii) causing permanent EPOC effect and
- (iii) restoring the catalytic activity when the Pt surface is poisoned by oxides during a negative polarisation.

These roles and the mechanisms of the related processes are discussed below.

2.1.5.1 *The Oscillatory Phenomenon during EPOC*

Between 350 °C and 450 °C, PtO₂ and dissociatively chemisorbed oxygen can present on the catalyst surface where for long oxygen exposure time more of the oxygen of the PtO₂ (multilayer oxidation of Pt) present on the catalyst surface than that of the chemisorbed oxygen [66]. The oscillatory phenomenon such as during CO and ethylene oxidation at atmospheric pressure for a Pt/YSZ system is commonly associated in the literatures with the formation and decomposition of these surface oxides (PtO₂/PtO_x). The steady state and the oscillatory behaviour of CO oxidation on Pt depended on the catalyst pretreatment where the rate and emf oscillations of those produced on a peroxidised surface spike up and those produced on a prerduced surface spike down [66].

The application of the appropriate external voltages to the cell can cause either the appearance or disappearance of catalytic rate oscillations during CO [51, 66] and ethylene oxidation [10]. The findings of this oscillatory phenomenon during EPOC studies are listed in Table 2.1. This phenomenon was explained by the role of the electrochemical backspillover species which migrated from the electrolyte to the Pt surface in controlling or altering the oxygen activity on the catalyst surface during the potential application [51, 66]. Positive polarisation during CO oxidation which strengthened the Pt-CO interaction and weakened the Pt-O interaction enhanced the CO coverage on the catalyst surface which led to PtO_x decomposition and hence stopped the catalytic rate oscillations [51]. Oscillations which were induced during polarisation, on the other hand, can be explained by the decomposition of surface oxides via repulsive lateral interaction between the electrochemically controlled backspillover of O²⁻ on the catalyst surface and the oxygen of the surface oxide followed by surface reoxidation by gaseous O₂ [67].

Table 2.1: Findings of the Catalytic Rate Oscillations during EPOC by Other Researchers

Catalyst	Ratio to pO_2	Effect of Polarisation/ Promoter	Mechanism	References
Pt/YSZ, C_2H_4 oxidation Porous Pt film, Surface area: 0.88 cm^2 , Clean sample and 0.11% sodium coverage, T: $350 \text{ }^\circ\text{C}$	pC_2H_4/pO_2 : 0.5/8	Anodic and cathodic polarisations stopped catalytic rate oscillations	Not discussed	[10]
Rh/YSZ, C_2H_4 oxidation, Film thickness: $10 \text{ }\mu\text{m}$, Surface area: 2 cm^2 , T: $330 \text{ }^\circ\text{C}$	pC_2H_4/pO_2 : 0.58/1.8	Anodic polarisation caused oscillations of the catalytic rates	Interaction of the promoter with oxygen of the surface oxides and surface reoxidation by gaseous oxygen	[67]
Pt/YSZ, Sputtered Pt, CO oxidation Film thickness: 60 nm , T: $250 \text{ }^\circ\text{C}$	pCO/pO_2 : a.1.2/3 b.2/1	a. Anodic polarisation ($15 \text{ }\mu\text{A}$) stopped the rate oscillations. b. Cathodic polarisation ($-17 \text{ }\mu\text{A}$) caused a permanent oscillatory behaviour.	a. The enhanced CO coverage on Pt surface led to PtO_x decomposition b. CO depletion on Pt surface and surface PtO_x formation	[51]
Pt/YSZ, CO oxidation Porous, Film thickness: $5 \text{ }\mu\text{m}$, Surface area: 2 cm^2	pCO/pO_2 : 1/34	Negative polarisation stopped rate oscillations, positive polarisation led to rate oscillations (at high anodic currents)	Formation and decomposition of surface PtO_2 . Oscillatory mechanism is the same both under open circuit conditions and during oxygen pumping	[66]

2.1.5.2 Permanent EPOC

EPOC is in general a fully reversible process and the catalytic rate returns to the initial rate r_0 after the current interruption. However, there have been cases where the catalytic rate remained in a highly active steady state even after the current was interrupted and only returned to the initial catalytic rate after the application of a similar current of the opposite polarity [3, 68]. This phenomenon is termed permanent EPOC or persistent enhancement of the catalytic activity [3, 68-70]. Permanent EPOC can be studied or observed from the response of the catalytic rate after current interruption upon application of different anodic potential and polarisation at different time. The magnitude of the permanent EPOC can be quantified by a permanent rate enhancement ratio, γ , described in equation (8) [3,68].

$$\gamma = r_{P-EPOC}/r_0 \quad (10)$$

Where r_{P-EPOC} is the open circuit rate after current interruption and r_0 is the open circuit rate before polarisation. The permanent rate enhancement ratio from previous studies on EPOC is summarised in Table 2.2.

The catalytic rate transient response after current interruption was dependent on the (i) total anodic charge where γ increases via increase of the applied potential value [3], (ii) duration of polarisation [69, 71] and (iii) O_2 pressure [71]. In contrast to the catalytic rate after the current interruption, the steady state electrochemical promoted rate was independent on the duration of prolonged anodic polarisation under a reactive condition [71]. This suggests that the polarisation at a longer time (which causes an increase in the magnitude of the permanent EPOC) influenced a part of the system which was not exposed to the catalytic reaction [70, 71]. Permanent EPOC is therefore explained by the release of hidden or stored oxygen in non-gas exposed places (or in the subsurface region where it was not in contact with the reaction mixture) in the Pt/YSZ and Pt bulk upon anodic polarisation [3]. The application of a similar negative current, for example in a case of an electrophobic behaviour, serves as a fast and efficient way for the decomposition of the oxide species and the concomitant release of the stored charge species [3, 68].

The mechanism of the permanent EPOC is described as the following. Upon current interruption, the stored O species were migrated or released to the Pt/gas interface from the electrolyte support through tpb keeping the catalytic rate at the promoted state [3,71]. As discussed by Souentie et al. [3], the migration was caused by the O²⁻ electrochemical gradient between the Pt/gas and the Pt/YSZ interface. This subsequent migration of the backspillover species took place until electrochemical potential equilibrium was reached. The catalytic rate which was at the promoted state although under the open circuit condition is explained by the similarity of the role of this species with those induced during the polarisation where the presence of this previously stored (backspillover) species on Pt surface caused an increase in the Pt work function which resulted in the weakening of the Pt–O_{ads} strength and thus caused an increase in the catalytic rate. Besides oxygen storage at the binary interface and Pt bulk, the enhance coverage of the O²⁻ at Pt surface can also be caused by the local enrichment of the O²⁻ content of the YSZ.

The consumption of the hidden oxygen in the case of the C₂H₄ oxidation probe reaction after the current interruption can be expressed as:



The main reason for the quasi permanent effect was the large amount of stored oxygen and their slow diffusion towards the Pt/gas interface [68]. For cases where the PtO_x was near its instability area such as under a less oxidising condition, permanent EPOC was not observed. This instability could attribute to the immediate migration of the oxygen species to the Pt/gas interface after the current interruption and thus the permanent EPOC disappears and reversible EPOC was observed [3].

Besides the migration of the stored oxygen species, the irreversible morphology changes such as bubble formation and the role of dopants or additives such as Fe/FeO_x can also cause the permanent EPOC effect [4]. Morphology changes can alter the catalytic properties of the catalyst due to the appearance of atomic steps, differently oriented surfaces or the generation of structural defects. The iron oxide might either influence the microstructure or act as a reservoir for the promoting oxygen species where this oxide

might be more stable in comparison to the quickly consumed spillover oxygen after the current interruption.

2.1.5.3 Permanent Poisoning Effect

Besides the permanent EPOC effect, there are also cases where the catalytic rate remains at a value lower than the initial open circuit rate after the negative current interruption. This effect was defined as a permanent poisoning which is similar to the permanent EPOC effect. This effect is demonstrated in the work of Nakos et al. [5], who studied EPOC for methane oxidation reaction over Rh catalytic films interfaced with YSZ at temperatures from 350 °C to 550 °C in which after negative current interruption the catalytic rate was found to slowly increase but remained lower than the initial value. The rate poisoning index demonstrating this effect is

$$\beta = (r_o - r_{\text{poisoning}})/r_o \quad (12)$$

where $r_{\text{poisoning}}$ is the catalytic rate in the poisoned permanent EPOC steady state after negative current interruption and the values from previous EPOC studies are summarised in Table 2.3. Nakos et al. [5] associated this poisoning effect with the formation of a catalyst surface oxide by the strongly adsorbed species from the gas phase upon the negative polarisation. This effect has been described due to the slower thermal diffusion of O^{2-} backspillover to the catalyst surface and hence caused a lower O^{2-} coverage of the catalyst surface as a result to the difference in the chemical potential gradient between the electrolyte support and the catalyst surface in the presence of the surface oxides. A similar positive potential application however can restore the catalytic activity to the initial open circuit condition.

Besides the Rh catalyst, the poisoning of the Pt catalyst by Pt oxides which were formed on the catalyst surface during the sintering step performed in air explained the low reaction rates observed in the work of Poulidi et al. [72]. The catalytic activity however increased after hydrogen reduction at 800 °C which was explained either by the reduction of the oxides formed on the Pt catalyst surface or by the synergistic effect between the Pt and the surface of LSCF perovskite membrane that catalyses the reduction of the

perovskite surface. Reoxidation of either the Pt or the perovskite surface caused the subsequent deactivation.

2.1.6 The Role of Impurities on EPOC

Impurities (either by hindering or promoting properties) may significantly cause the observed rate modification in EPOC, via some interaction with the spillover species [10]. The work of Mutoro et al. [4] demonstrated the significant influence of iron (considered as impurity) on EPOC where the presence of iron on Pt (iron doped covering Pt film) appeared to cause the system to exhibit a permanent EPOC effect in comparison to the iron free covering Pt film [4]. This effect has been discussed in terms of the influence of iron on the catalyst microstructure or the role of iron as an oxygen reservoir.

In the work of Ibrahim et al. [10], however, a clear evidence that impurity (sodium) are necessary for the observation of EPOC in a Pt/YSZ system was not found although the presence of this species was found to significantly affect the Pt catalyst catalytic and electrocatalytic properties. The effect of sodium at low coverage became less pronounced at high oxygen partial pressure where no significant rate modification was observed. However, the two promoters (sodium and oxygen) were shown not to completely independent of each other especially at high sodium coverage (where the interaction with oxygen became more significant). This requires a complex model to fully predict and explain the behaviour of such a system.

Impurities may affect a catalytic reaction in a number of ways such as [10]

- (i) causing a change in the work function of the catalyst (long range effect) or by
- (ii) modifying the activity of catalyst sites in the vicinity of the impurity (sodium) species (short range effect) and
- (iii) creating different reaction intermediates and pathways through interactions with the gas phase reactants.

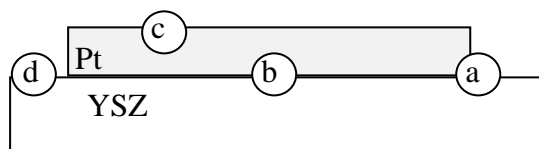
Table 2.2: Summary of Permanent EPOC and Permanent Poisoning from EPOC Studies

Catalyst	T (°C)	Ratio to pO ₂	γ	β	References
Sputtered Pt, Pt/YSZ, C ₃ H ₈ oxidation Film thickness: 150 nm, Surface area: 1.25 cm ²	350	pC ₃ H ₈ /pO ₂ : 0.2/4.5	1.2, 1.3		[3]
Sputtered Pt, Pt/YSZ, C ₂ H ₄ oxidation Film thickness: 1 μ m	375	pC ₂ H ₄ /pO ₂ : 0.2/8.2	1.7		[68]
Rh/YSZ, CH ₄ oxidation Film thickness: 10 μ m	430	pCH ₄ /pO ₂ : (a) 1.8/2 (b) 1.7/3.4		(a) 0.17 (b) 0.5	[5]
Sputtered Pd, Pd/YSZ, CH ₄ oxidation Film thickness: 380 nm, Surface area: 2cm ²	350	pCH ₄ /pO ₂ : (a) 2.6/1.9 (b) 1.4/2.8 (c) 1.3/4.5		(a) 0.10 (b) 0.12 (c) 0.16	[6]
Pt/YSZ, Iron doped Pt sample, C ₂ H ₄ oxidation	425	pC ₂ H ₄ /pO ₂ : 0.19/8.2	1.7 to 10		[4]

2.1.7 Three Phase Boundary (tpb)

Electrochemical reactions in the O₂(g)/Pt/YSZ system may occur at various interfaces or sites including Pt/YSZ, YSZ/O₂(g) and Pt/O₂(g) and the three phase boundary (tpb). As indicated in Figure 2.4, the three phase boundary is the region where all the interfaces meet (metal/gas/electrolyte). The site of an electrochemical reaction, however, depends on factors such as the temperature of operation, oxygen partial pressure and applied polarisation, electrode preparation method, electrode type, electrode microstructure, and the choice of electrode material [39]. For a O₂(g)/Pt/YSZ system where Pt is assumed

impermeable for oxygen, the electrochemical reaction which consists of electron exchange between gaseous O_2 and O^{2-} of the solid electrolyte can only take place at the tpb since the reaction involves reactants from the three phases. In the charge transfer reaction, oxygen dissociatively chemisorbed on Pt at the tpb ($O(tpb)$) and O^{2-} are supplied to or from the solid ion conductor. The number of tpb sites is strongly influenced by the electrode morphology and electrodes with a high number of tpb sites are expected to provide faster sensing responses and better resistance to ageing [73].



- a: Three phase boundary (tpb)
- b: Binary Interface (Pt/YSZ)
- c: Electrode surface (Pt/ O_2)
- d: Electrolyte surface (YSZ/ O_2)

Figure 2.4: Schematic diagram indicating the interfaces in a Pt/YSZ system

2.1.7.1 Tpb Length of a Porous Electrode

The length of the three phase boundary (tpb) of a porous electrode which is prepared by using commercially available catalysts can be estimated from the measured $N_{o,tpb}$ value which corresponds to the reduction of oxygen chemisorbed at the tpb. $N_{o,tpb}$ can be determined by integrating the cathodic peak of the cyclic voltammogram of the $O_2(g)/Pt/YSZ$ system. In calculating the tpb length, the effect of surface diffusion cannot be neglected and the surface diffusion coefficient of $O(a)$ on Pt(111) and Pt(100) has been expressed by Lewis and Gomer [74] as

$$D_o = \alpha^2 \nu \exp(\Delta S/R) \exp(-E/RT) \quad (13)$$

where α is the mean diffusion jump length, ν is the (effective) attempt frequency, ΔS is the entropy of activation, E is the activation energy, R is the gas constant and T is the temperature ($\alpha = 3\text{\AA}$, $\Delta S = 17 \text{ calmole}^{-1}\text{K}^{-1}$, $\nu = 10^{12} \text{ s}^{-1}$). For $T = 673 \text{ K}$, $D_o = 4 \times 10^{-11}$

cm^2s^{-1}). By using the surface diffusivity value, the thickness, δ , of the spreading zone can be estimated from

$$\delta = (D_o\tau_o)^{1/2}$$

where τ_o is the operational or electrochemical attack time constant. By using an average $\tau_o = 3\text{s}$, $\delta = 10^3 \text{\AA}$. By assuming a 1:1 of O:Pt stoichiometry and by using the atomic radius of Pt ($r_{\text{Pt}} = 1.4 \text{\AA}$), the average $N \approx \delta/2r_{\text{Pt}} \approx O(a)$ atoms diffuse and get reduced per tpb electrocatalytic site during the appearance of the cathodic peak could be estimated. The tpb length (l), then, could be estimated from

$$l = N_{\text{otpb}} \cdot N_{\text{AV}} (2r_{\text{Pt}})(2r_{\text{Pt}}/\delta) \quad (14)$$

where N_{AV} is Avogadro's number. The calculated tpb length, l , by using the above formula could be compared with the length calculated based on the information extracted from SEM images. From SEM images, the average diameter of Pt crystallites constituting the Pt catalyst films could be estimated. By assuming that the Pt film consists of Pt crystallites of uniform diameter d which were packed in a tetragonal arrangement and that those crystallites in contact with the flat YSZ electrolyte were half-spheres, each with a circular πd tpb contact with the electrolyte, tpb length, l , then can be estimated as [32]

$$l = \pi A/d \quad (15)$$

where A and d are the geometrical area of the Pt film and diameter of Pt crystallites, respectively. Besides the cyclic voltammogram and the SEM images, the number of tpb sites can also be quantified by using the impedance spectrum of the porous electrodes [73].

2.1.7.2 Tpb Length of a Patterned or Dense Electrode

In contrast to the porous electrodes prepared by using the commercial catalysts, the cathodic peaks in the cyclic voltammograms of dense electrodes may correspond to the charge transfer reactions at the binary interface and not at the tpb and therefore the

estimation of the tpb length by using equation (15) may not valid. The tpb length of dense electrodes is usually indicated by the geometric characteristics. However, in addition to the length of a particular geometric pattern, for example for patterned electrodes prepared by photomicroolithography, where smooth line edges were assumed, the length can also be attributed by [12]

- (i) the additional length due to the possible waviness (α) of the edge at a microscopic level and
- (ii) the tpb in the electrode film due to either inherent porosity of the substrate (electrolyte) and or due to the defects, such as pits, that may occur during sputtered film preparation or during heat treatments (l_{tpb0})

Therefore [12]

$$l_{tpb} = l_{tpbp}(1+\alpha) + l_{tpb0} \quad (16)$$

2.1.8 Summary

Based on the above review, the origin of EPOC is understood to be due to the migration of backspillover species from the solid electrolyte onto the catalyst metal surface under the influence of the applied potential. This effect or phenomenon caused a dramatic enhancement in the rate of reactions. In some cases the rate was not returned to the initial open circuit rate condition due to the permanent EPOC and permanent poisoning effects. This backspillover phenomenon also caused the appearance and disappearance of the catalytic rate oscillations. Many catalytic systems with various types of supports and catalysts have been studied by other researchers and not all commercial catalysts can exhibit EPOC. Besides that, the influence of impurities on EPOC has not yet been fully addressed in the literatures.

2.2 Materials and Deposition Methods

EPOC has extensively been studied for many catalytic systems of various types of support and catalysts or electrodes. The electrochemical behaviour or EPOC effect of the catalytic systems has been shown in the previous sections to depend on the type of materials (catalysts and support) and electrodes preparation methods. In this section, the

materials and electrode preparation methods which are commonly used in EPOC studies of the Pt/YSZ system are discussed.

2.2.1 Electrolyte

Catalysts used in EPOC are normally deposited on electrolyte materials that are either solid ionic conductors such as YSZ, proton conductors such as $\text{Ba}_3\text{Ca}_{1.18}\text{Nb}_{1.82}\text{O}_{9-\alpha}$, potassium conductor and mixed ionic-electronic conducting membranes (MIEC) such as LSCF ($\text{La}_{0.6}\text{Sr}_{0.4}\text{Co}_{0.2}\text{Fe}_{0.8}\text{O}_{3-\alpha}$). YSZ is the most common electrolyte used in EPOC studies involving catalytic oxidation reactions over noble metals such as Pt. The properties of the YSZ include

- a fluorite structure which has high oxygen deficiency and thus high ionic conductivity due to its ability to conduct O^{2-} .
- high chemical and thermal stability under a wide range of temperatures which is up to 1000°C [75].

For all the electrolyte materials, a driving force is required for oxygen ion to permeate through the membrane. This driving force can be either an electrical or a chemical potential gradient (i.e. gas component partial pressure). In addition, electrical neutrality criteria must be fulfilled. For example, oxygen is transported in the ionic form with a simultaneous flux of electrons in the opposite direction compensate the charge due to the oxygen flux [76]. The mechanism of conduction for a solid ion conductor is shown in Figure 2.5.

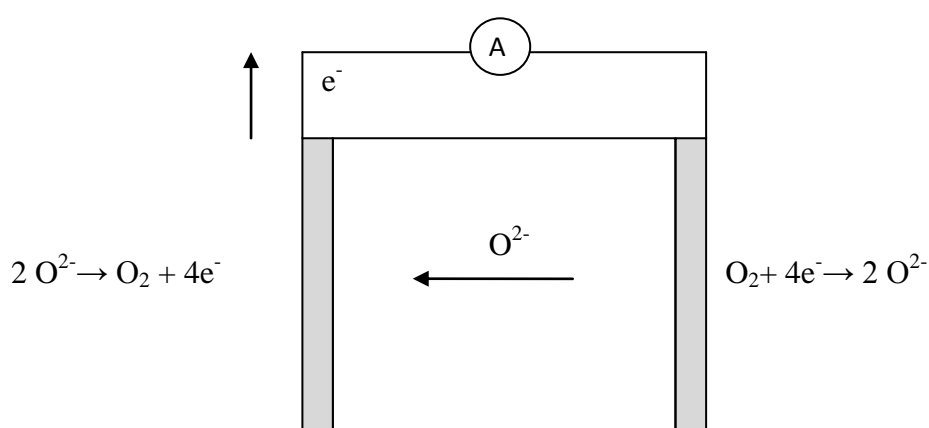


Figure 2.5: Conduction mechanism of a solid ion conductor

2.2.2 Catalyst / Electrode Materials

In EPOC studies, a working electrode also acts as the catalyst where the reaction of interest is occurring and it is commonly used in conjunction with an inert counter and a reference electrode. Gold (Au) is commonly used for the reference and counter electrodes. Choices of the working electrode depend on the reaction of interest. EPOC has been observed for a wide range of reactions in the presence of metal catalysts such as Pt, Pd, and Rh. For catalytic oxidation reaction, Pt is often used as the working electrode due to its characteristics as an important oxidation catalyst [32] with low oxygen solubility and diffusivity [77]. Based on the Pt characteristics, the present work uses Pt catalysts supported on YSZ as the working electrode under a nonreactive condition and during CO oxidation. In the case of Pt electrodes (in comparison with the LSM electrode), at temperature lower than 800 °C, the transport of oxygen through Pt is even smaller, therefore, the charge transfer reaction in the case of Pt/YSZ system can be concluded to occur almost exclusively at tpb. Besides that, platinum is a better electrocatalyst for oxygen reduction on YSZ than LSM based on the intrinsic charge transfer resistivity values at 800 °C [32].

2.2.3 Electrode Deposition Method

Porous metal films prepared by painting the commercially available Pt pastes or resins with a brush followed by calcinations [8, 24, 45, 48, 78, 79] has extensively used in EPOC studies of a Pt/YSZ system. The commercially available Pt catalysts included Engelhard Clal 6926 [48, 80], Engelhard A1121 [24,78,79] and Engelhard M60313 [48]. The catalytic systems using these catalysts have been shown to exhibit EPOC. However, Pt paste from Demetron did not show any work function change and a difference between the Engelhard and Demetron paste was organic solvent [81]. This indicates that not all commercial (Pt) catalysts can cause work function change and hence exhibit EPOC.

Besides that, Pt electrodes can also be prepared by screen printing [8,70] and sputtering [51, 58, 62 ,64, 82, 83]. Sputtering Pt from a Pt target onto YSZ samples is an alternative way of preparing Pt catalysts (of less contaminants and porosity) in which the method was developed to construct a model catalyst [9]. The sputtered Pt electrochemical catalyst

was shown to have better characteristics for the electrochemical promotion of catalysis than Pt paste due to their greater dispersion value and higher polarisability [64]. Besides sputtering, model catalysts can also be prepared by [9]

- (i) optical lithography, which was a technique from semiconductor technology, to prepare microstructured Pt/YSZ electrodes. However, Pt layers produced using this technique were not dense and still exhibited pores, and
- (ii) pulsed laser deposition at elevated sample temperature or annealing to prepare a dense (111) oriented Pt films. Pt layers prepared by pulse laser deposition were dense, contained no pores and structurally well defined.

However, the morphology of dense electrodes is susceptible to changes after polarisation which was not the case of porous electrodes prepared by using the commercially available catalysts [26]. This is because dense electrodes have less tpb in comparison to the porous electrodes in which bubbles and or cracked bubbles can be formed during anodic polarisation due to gas tightness.

2.2.4 Catalyst Surface Characteristics

As discussed in the previous sections, catalyst films are often prepared by using different materials (commercially available catalysts) and methods. Therefore, the resulting films may have different microstructure or morphology [8, 39] and impurities [8, 9]. These variations could result in significant differences in the tpb length which could affect the catalytic and electrocatalytic behaviour of these electrodes and this explains the variation in the electrochemical data (reproducibility issue) which often reported for O₂(g)/Pt/YSZ system. In the liquid state, reproducible electrode studies relied on the use of pure components with a minimum impurity levels [8].

2.2.4.1 Morphology

The morphology of an electrode depends on the material and the preparation method and may significantly affect the electrode behaviour. Mutoro et al. [26] demonstrated differences in the electrode microstructures and the features in the cyclic voltammogram (CV) as a result of different materials and preparation methods. The theoretical background of CV is described in detail in *section 2.3.2.1*. The differences observed in

the cyclic voltammograms are the shape, position and number of cathodic peaks. Besides that, electrode morphology also depends on the sintering temperature [39] and sintering time [84]. Increasing the sintering time leads to densification and grain growth which causes reduction in porosity and the tpb length [84].

2.2.4.2 Impurities

Impurities affect the characteristics of oxygen charge transfer in the Pt/YSZ system and this is demonstrated by the features in the CV [8, 10] where impurities may give rise to different peaks [8]. For example, in the work of Mutoro et al. [8], CV of two identically prepared porous electrodes from two different pastes having the same structure (XRD) and a comparable microstructure (SEM), but a different composition in terms of contamination (ToF-SIMS) are different in terms of the current density, peaks position, shoulder or hysteresis including the appearance of small peaks which was usually hidden under the main peak.

Depending on the nature of the impurities they may hinder (by blocking catalyst active sites or the tpb) or enhance (if catalytically active) the catalytic or electrocatalytic activity. Electrochemical behaviour could be affected by impurities due to changes in the binding of spillover species to the catalyst surface which can be caused by the surface segregation of impurities [85]. Impurities found in platinum (Pt) and YSZ and methods used for their determination are indicated in Chapter 4 (Table 4.1).

In Pt and YSZ samples, silicon (Si) has been known as the main contaminant. Even high purity electrolyte and electrode materials are often Si-contaminated as observed in work of Mutoro et al. [8]. Si was found in

- a. YSZ and high purity Pt samples
- b. Pt|YSZ system after temperature treatment
- c. Pt|YSZ system during electrochemical polarisation

Si can be introduced in the Pt/YSZ system during electrode preparation works. YSZ surface is often polished with SiC papers prior to the electrode or catalyst deposition on the YSZ pellet (by painting with a brush). However, the amount of Si introduced during

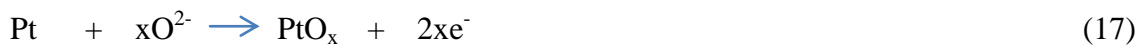
this preparation work can be minimised by cleaning the pellets with isopropyl alcohol in ultrasonic cleaners [28, 86, 87].

2.3 Oxygen Charge Transfer in Pt/YSZ System

In this section, oxygen reduction and oxidation processes in a Pt/YSZ system which can take place at Pt/gas, Pt/YSZ and YSZ/gas and three phase boundary (tpb) interfaces are discussed.

2.3.1 Anodic and Cathodic Reaction Paths

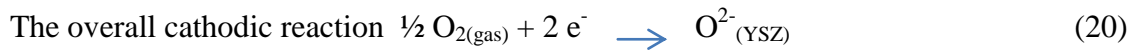
The overall charge transfer reactions in a Pt/YSZ system can be described by the two electrochemical reactions which are not independent and may strongly influence each other [7]. The electrochemical reactions are



The two anodic reaction paths which share the same reactants O^{2-} (the charge carrier in YSZ) and contribute to the sum of the currents are described as the followings [7]



In the first path, O^{2-} originating from the electrolyte releases two electrons to Pt at the Pt/YSZ interface to form PtO compound which remains at the electrode and accumulates [7,12]. In the second path, O^{2-} which reaches the tpb region forms a chemisorbed oxygen atom by releasing two electrons to the electrode, and desorb to the gas phase as molecular O_2 . Besides that, this process can also occur at Pt/gas interface which is related to the phenomenon of oxygen backspillover from the tpb [7]. Besides that, oxygen can also be incorporated on the free YSZ surface, where electron conduction in YSZ from Pt to the oxygen reduction sites on the free YSZ surface is required [12].



can be splitted as the followings [15]

i. adsorption of oxygen on Pt surface



ii. dissociation of molecular oxygen on Pt surface



iii. surface diffusion of adsorbed atomic oxygen to the tpb



iv. incorporation of oxygen at tpb into YSZ including charge transfer



2.3.2 Electrochemical Investigations

Details of the oxygen charge transfer processes in a Pt/YSZ system can be obtained from the results of electrochemical investigations that include cyclic voltammetry (CV), electrochemical impedance spectroscopy (EIS) and current overpotential. These techniques are described below.

2.3.2.1 Cyclic Voltammetry (CV) of the Pt/YSZ/O₂(g) System

Cyclic voltammetry (CV) is a technique is commonly used for the investigation of the oxygen charge transfer in the Pt/YSZ/O₂(g) system. Cyclic voltammetry can provide information such as the coverage of adsorbed species and tpb length [32]. Cyclic voltammetry studies of the Pt/YSZ/O₂(g) system involve the oxidation or reduction of oxygen species by placing the gaseous oxygen in contact with the Pt electrode surface and force the electron transfers by applying a positive or negative potential on the Pt surface. Oxygen species might gain or transfer electrons from or to the Pt surface once the surface became negative or positive and thus cause a measurable current through the circuit.

In this technique, the potential is applied between the reference and the working electrodes and the potential ramped with a scan rate (V/s) linearly versus time. The current is measured between the working electrode and the counter electrode. During CV when a set potential is reached, the electrode's potential ramp is reversed. The forward

scan produces a current peak for any species that can be reduced (or oxidized depending on the initial scan direction) through the range of the potential scanned and the reverse scan produces a peak for the species that can be oxidised. As the potential reaches the reduction potential of the reactive species, the current will temporarily increase, and then decrease again as the concentration of these species is depleted close to the electrode surface. If the redox couple is reversible then when the applied potential is reversed, it will reach the potential that would reoxidise the product formed in the first reduction reaction, and produced a current of reverse polarity from the forward scan. This oxidation peak would usually have a similar shape to the reduction peak. The potential sweep which results to cyclic voltammogram is indicated in Figure 2.6 while the typical cyclic voltammogram is shown in Figure 2.7.

The most interesting features in the voltammograms which indicative of the charge transfer reactions (or the oxidation and reduction of oxygen) in the Pt/YSZ system are the anodic (at V_{pa} and I_{pa}) and cathodic peak (at V_{pc} and I_{pc}) currents as indicated in Figure 2.7. In solid state CV the occurrence of current peaks have been reported for a wide range of temperature, oxygen partial pressures [32] and for electrodes which were prepared by various methods [4, 40]. The peaks are commonly associated to the processes which occurs at either Pt/YSZ interface [8, 16, 88] or tpb [8, 15, 16, 32]. Other processes such as the formation of Pt oxides at the Pt/gas interface, surface oxidation of YSZ, morphology changes due to surface migration of electrode material and bubble formation are not causing peaks in the voltammograms [8].

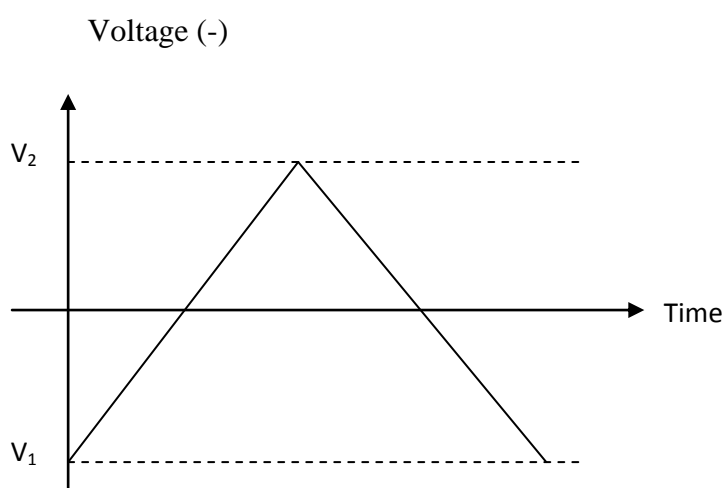


Figure 2.6: The potential sweep which results to cyclic voltammogram in Figure 2.7

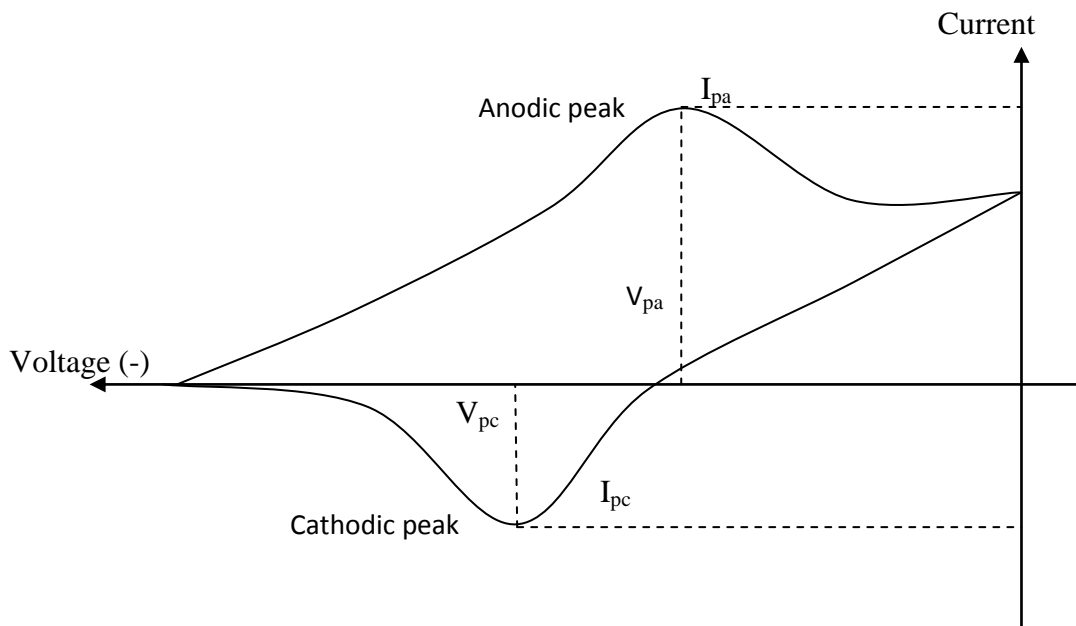


Figure 2.7: A typical cyclic voltammogram

The cathodic and the anodic peak currents are strongly dependent on the temperature [32] and the scan rate, v , [7, 32]. The effect of increasing temperature on the features in the CV is a gradual positive shift of the peak potential and an increase in peak size to a maximum which then decreases abruptly and vanishes at a higher temperature. The effect of scan rate, v , on the other hand, includes:

- a. the shifting of the peak potentials towards more negative values, the growth of the peak current [4, 7, 32] and pronounced anodic wave, which related to the reverse of the charge transfer process, with increasing scan rate, v [7],
- b. one broad and less well defined cathodic peak at higher sweep rates while no cathodic peak appears at very small rates [8],
- c. vertical shift or vertical hysteresis (ΔI) which is proportional to v [8]. ΔI is voltammogram thickness at zero potential which corresponds to the amount of current used to charge the Pt/YSZ interface, and
- d. linear increase of the peak height (I_p) with v [32]. However, when the electronic transfer at the catalyst surface is fast and the current is limited by the diffusion of oxygen species to the electrode surface, the I_p will be proportional to the square root of v ,

where the most useful information can be extracted with v between 5 and 200 mVs^{-1} [32]. In a typical CV of dense film electrodes, three regions are commonly observed which are [16]:

1. pseudocapacitive current region due to the very small tpb length,
2. a range where the cathodic peak appears. The charge reflected by this peak depends on the amount of oxygen pumped prior from the CE to the interface Pt/YSZ, which also influence its peak position, and
3. the strong current increase in the anodic peak range reflects the beginning of an anodic peak.

The interface corresponds to the cathodic peaks of electrodes of different surface characteristics or surface morphology is not necessary the same [8]. Cyclic voltammograms of a Pt/YSZ system using a dense electrode provide details on the processes which take place at the Pt/YSZ or the binary interface [8, 16] while the voltammograms of a porous electrode give information on the processes occurring at the tpb [8, 16, 32]. These can be explained by the oxygen activity at both tpb and Pt/YSZ interface during the anodic polarisation. The oxygen activity at tpb of a porous electrode should be higher than that of a dense electrode because in the system utilising the porous electrode oxygen has to diffuse only a small distance to reach the tpb [16]. The findings of the geometry dependence of the charge transfer reaction from literatures are indicated in Table 2.3.

In order to verify the interface associated with the peaks, a correlation between the peak height and current density measured during the CV can be studied as demonstrated in the work of Mutoro et al. (2009), which is described in Figure 2.8 [8]. Mutoro et al. [8] demonstrates (Figure 2.8) the influence of increasing the tpb length by successively scratching the Pt film after every experiment (from I to IV) where the current density increased and the peak area decreased, mainly in the cathodic region (the cathodic peak potential was not shifted). The increase of the tpb length which is not associated with an enlargement of the cathodic peak area demonstrates that the process corresponding to this peak does not take place at the tpb.

Therefore, a proportional relationship between the peak height and the current density should be observed when the processes are occurring at the tpb. An inversely proportional relationship, on the other hand, indicates processes which take place at the binary interface. This is explained by the fraction of oxygen ions transported through YSZ which is consumed by different possible microscopic processes due to the influence of the electrode morphology [8]. For a case of a dense electrode, where the oxygen activity at the Pt/YSZ interface can be assumed to be at a larger extent than the activity at the tpb, a large cathodic peak should be observed. Besides that, the changes in the number of available sites for the charge transfer reactions such as the tpb (due to the changes in the morphology) of a dense electrode during the experimental works or electrode applications, can be identified from the changes in the cathodic peak height or area. For example, an increase in the tpb length can cause a decrease in the cathodic peak height or area. This is explained by an increasing amount of oxygen ion consumption, which is transported through YSZ, at tpb and thus cause less oxide formation at the Pt/YSZ interface [8]. The processes causing peaks in the voltammograms are further discussed below.

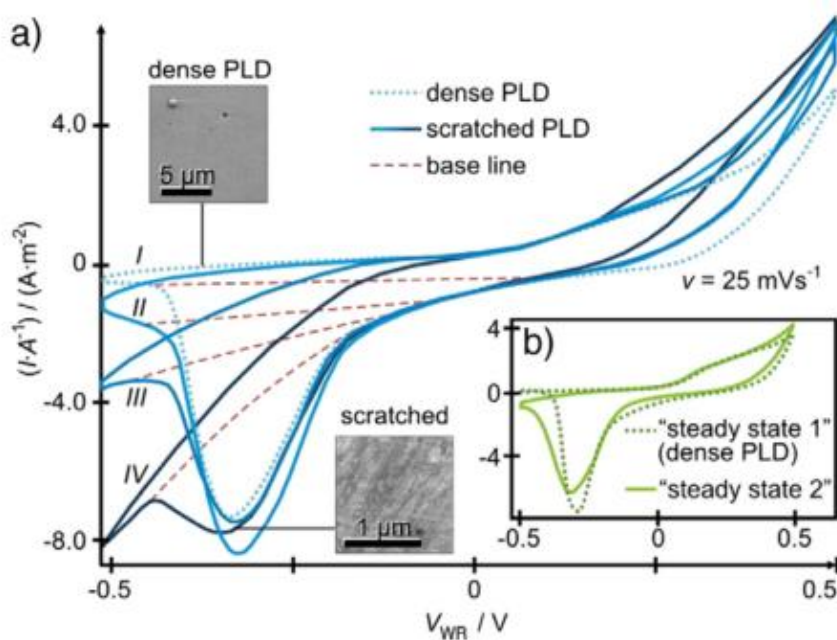


Figure 2.8: CV of PLD films from the work of Mutoro et al. [8]: a) dense (dotted blue line) electrode where the tpb was successively enlarged (I–IV) by scratching; baselines drawn in as dashed red lines; b) dense electrode at the beginning of a measurement

(dotted green line, “steady state1”) and after several experiments (continuous green line, “steady state2”)

i. Pt/YSZ Interface

Peaks in the voltammograms can be assigned to Pt oxides formation and decomposition at the Pt/YSZ interface [7, 16, 88] when the peak area is proportional to the contact area at Pt/YSZ [8]. However, Mutoro et al. [8] did not support the existence of a Pt oxide at the Pt/YSZ interface, because Pt oxide was not observed experimentally by using XRD and XPS/XPEEM. In addition to Pt oxides, impurity oxides can also contribute to the peak associated with processes occurring at this binary interface [8,16] where a big cathodic peak is the convolution of the decomposition of Pt and impurity oxides [8]. However, the evidence of the contribution of impurities to this peak has not yet been shown in literatures. Furthermore, to assign a peak to a certain impurity is also difficult since more than one impurity can present at the interface such as impurities that were detected on a nm thick region of the YSZ surface by using SIMS [8]. Pöpke et al. [88], however, believed that impurities present at Pt/YSZ interface are not causing the cathodic peaks. Instead, two different oxygen species can be formed at this interface upon polarisation which includes oxygen in an adsorbed state at low coverages and oxygen in Pt oxide at high coverages and the formation of the oxides at this binary interface extending to the tpb should cause electrode degradation [88]. Therefore, there is an uncertainty whether the cathodic peaks in a cyclic voltammogram are caused by Pt or impurity oxides decomposition at Pt/YSZ interface and this depends on the type and preparation of the electrodes [8].

ii. Growth of Pt Oxide Layer from Pt/YSZ toward Pt Bulk

Another process which can be assigned to a peak in the voltammograms is the growth of Pt oxide layer from the binary Pt/YSZ interface toward the Pt bulk [7, 69, 71] where this process is slow and follows a $t^{1/2}$ kinetic [7]. This process is consecutive to the process associated with the formation of oxides at the binary interface and in this process, oxygen should be stored in the Pt electrode itself, however, the possibility that oxygen is stored in the YSZ at the vicinity of the anodically polarised Pt electrode cannot be excluded [7].

iii. Spillover Oxygen

Backspillover oxygen, either O^{2-} or $O^{\delta-}$, can be assigned to cathodic peaks in the voltammograms [7, 32, 71] when the corresponding peak area is proportional to the tpb length [8]. However, spillover oxygen or species do not necessarily cause a peak or additional peak in the voltammograms because for any sample having tpb, spillover oxygen can be generated [8] and in contrast to Jaccoud et al. [7], Vayenas et al. [32] and Xia et al. [72], Mutoro et al. [8] assigned this peak to the presence of contaminations rather than to spillover oxygen.

The reduction of oxygen chemisorbed at the tpb and associated with the occurrence of spillover oxygen species is expressed in equation (20d) [32]. The reverse of the charge transfer reaction, on the other hand, causes the appearance of an anodic peak according to equation (20). The anodic peak area, however, could be a factor of 10 smaller than the corresponding area of the cathodic peak due to the fact that reaction described by equation (20) is competing with direct oxygen chemisorption from the gas phase to the tpb according to reaction [32]



where O(a) is oxygen dissociatively chemisorbed on the gas exposed catalyst surface. Direct O(tpb) formation from $O_2(g)$ is also possible.

2.3.2.2 Electrochemical Impedance Spectroscopy (EIS)

Besides features in the CV, the responses from the electrochemical impedance spectroscopy (EIS) measurements can also provide details of the oxygen charge transfer. Impedance demonstrates the ability of a circuit to resist the flow of electrical current, represented by the “real impedance” term and also reflects the ability of a circuit to store electrical energy, reflected in the “imaginary impedance” term. Impedance can be defined as a complex resistance encountered when current flows through a circuit composed of various resistors, capacitors, and inductors. This definition is applied to both direct current (DC) and alternating current (AC). In experimental situations the electrochemical

impedance is normally measured using excitation AC voltage signal, V , with small amplitude, V_A , (expressed in volts) applied at frequency, f , (expressed in Hz or s^{-1}). The voltage signal $V(t)$, expressed as a function of time t , has the form [89]

$$V(t) = V_A \sin(2\pi ft) = V_A \sin(\omega t) \quad (22)$$

where ω is the radial frequency of the applied voltage signal (expressed in radians/second) . The radial frequency is related to the applied AC frequency f as described [89] by

$$\omega = 2\pi f \quad (23)$$

Electrochemical impedance is normally measured using a small excitation signal so that the cell's response is pseudo-linear. In the linear system, the current response to a sinusoidal voltage input will be a sinusoid at the same frequency but shifted in phase as indicated in Figure 2.9. In a linear system, the response current signal $I(t)$ is shifted in phase (ϕ) and has a different amplitude, I_A [89]

$$I(t) = I_A \sin(\omega t + \phi) \quad (24)$$

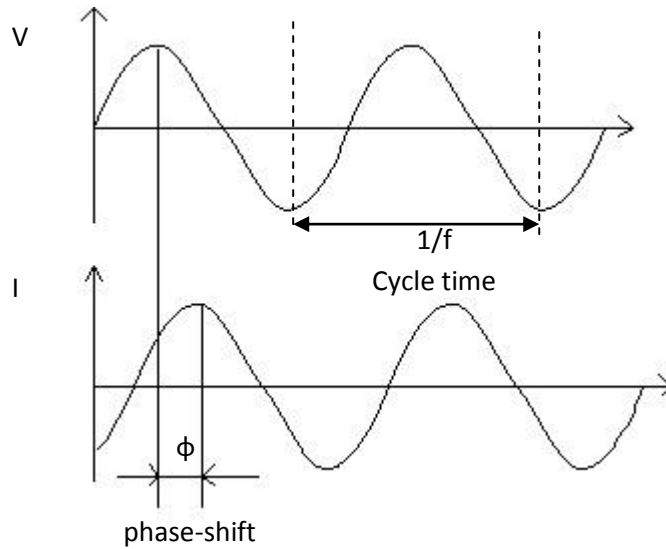


Figure 2.9: Sinusoidal voltage input V at a single frequency f and current response I [89]

The impedance of the system as can be calculated by an expression analogous to Ohm's Law [89]

$$Z^* = V(t)/I(t) = V_A \sin(\omega t) / I_A \sin(\omega t + \phi) = Z_A \sin(\omega t) / \sin(\omega t + \phi) \quad (25)$$

The impedance is therefore expressed in terms of a magnitude, Z_A , and a phase shift, Φ . with Eulers relationship [89],

$$\exp(j\phi) = \cos \phi + j \sin \phi \quad (26)$$

The impedance can be expressed as a complex function. The potential and the current response can be described as [89],

$$V(t) = V_A e^{j\omega t} \quad (27)$$

$$I(t) = I_A e^{j\omega t - j\phi} \quad (28)$$

The impedance is then represented as a complex number that can be expressed in complex mathematics as a combination of real or in phase (Z_{REAL}) and imaginary or out of phase (Z_{IM}) parts as indicated in Figure 2.10 [89]

$$Z^* = V/I = Z_A e^{j\phi} = Z_A (\cos \phi + j \sin \phi) = Z_{\text{REAL}} + j Z_{\text{IM}} \quad (29)$$

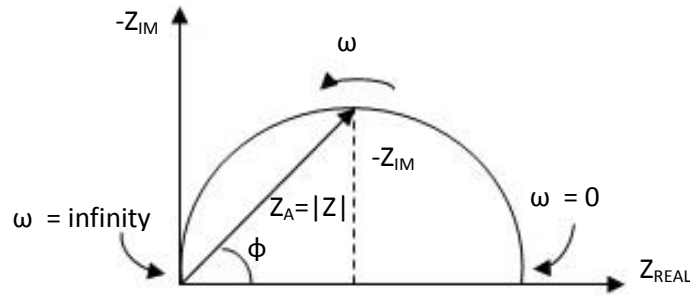


Figure 2.10: Complex impedance plot [89]

And the phase angle ϕ at a chosen radial frequency ω is a ratio of the imaginary and real impedance components [89]

$$\tan \phi = Z_{\text{IM}}/Z_{\text{REAL}} \text{ or } \phi = \arctan (Z_{\text{IM}}/Z_{\text{REAL}}) \quad (30)$$

a. Graphical Representation

Impedance plots (Nyquist plot) generally consist of two arcs, one due to the bulk of the sample and the other due to electrodes where an additional arc which is due to grain boundaries can also present in the plot [90]. The analysis of the impedance plot can provide the details of the oxygen charge transfer in a Pt/YSZ system. The high frequency intercept of the arc on the real axis (the first semicircle of the higher frequency range) of the impedance spectra indicates the ohmic resistance when it is similar among samples (or electrodes) of different tpb length [12, 90, 91]. The low frequency intercept corresponds to the total resistance (or charge transfer resistance) of the half cell between the working and the reference electrodes which is related to the rate determining step of the electrochemical oxygen exchange reaction [12, 91]. The charge transfer resistance depends on the tpb length, oxygen partial pressure and temperature [12]. The charge

transfer resistance is inversely proportional to temperature [12, 90]. In addition to the semicircles, a high frequency shoulder can also be observed in the plot and for a single crystalline YSZ electrolyte where grain boundaries can be excluded as a cause of the impedance feature, this shoulder can be assigned to electrode related processes [14]. Opitz and Fleig [14] interpreted the shoulder in the impedance spectra observed in their work as a contribution of a capacitively locked path which depends on the availability of a finite oxygen source between Pt and YSZ such as oxygen in closed pores along the binary interface (internal tpb) and if this oxygen reservoir can be filled and emptied by the oxide ion flux in YSZ a serial connection of a capacitor and a resistor can be used to describe such a situation.

The information in the Nyquist plot, however, is not complete since there is no detailed indication of the frequency at which the impedance is measured for every point. For a detailed presentation of the experimental data, the plot must be labelled with the corresponding frequency values. The determination of low impedance values from the Nyquist plot, which typically observed at very high frequencies, is difficult [89].

b. Analysis of the geometry dependence of the oxygen charge transfer

The geometry dependence of the oxygen charge transfer can be determined from the Arrhenius plots of the conductance or the inverse of the charge transfer resistance that are normalised either to the (i) tpb length or (ii) catalyst surface area versus the reciprocal of temperature, T^{-1} [13, 14]. The true geometry dependence is reflected in the plots where all the regression lines fall together [14]. Besides that, the plot of the conductance versus the tpb length can indicate a tpb related process in which a linear relation for each temperature with the regression lines intersecting the origin should be observed in this plot [12, 14]. Besides the geometry dependence, the activation energies and the type of connection of the involved resistive processes; parallel connections result in a concave shape and serial connections lead to a convex shape, can also be determined from the Arrhenius diagram [13].

c. *Area specific charge transfer resistance*

The area specific charge transfer resistance, R_{ct} , is given by [12]

$$R_{ct} = \rho_{ct}/l_{tpb} \quad (31)$$

where l_{tpb} is the tpb line length and ρ_{ct} is the intrinsic charge transfer resistivity. ρ_{ct} is microstructure independent and is a fundamental parameter that can be used to compare two electrode materials. The adsorption process, dissociation of molecular species into atomic species, migration of molecular or atomic species to the tpb region, the occurrence of electron transfer reaction and the transfer of ions across the tpb region may be included in the R_{ct} . As demonstrated by equation (31), if the electrochemical reaction occurs at tpb, the charge transfer resistance is inversely proportional to the tpb line length.

Table 2.3: Results of Geometry Dependence Studies from Literatures

Catalysts	T (°C)	R^{-1} ($\text{ohm}^{-1}\text{cm}^{-2}$)	Geometry dependence/ Mechanism	References
<p>Pt/YSZ, Patterned electrode, photomicrolitography and sputtering</p> <p>Pt lines on a circular YSZ disks: 20 to 200 μm width</p> <p>Tpb length: 50 to 500 cm^{-1}</p> <p>Surface area: 0.785 cm^2</p> <p>Film thickness: 1 μm, 10^{-3} to 1 atm O_2</p>	650 to 800	10^{-2} to 10^{-1}	Tpb	[12]
<p>Pt/YSZ, Sputtered,</p> <p>Circular Pt</p> <p>Film thickness: 500 nm</p>	700 to 900	10^{-4} to 10^{-1}	Tpb	[14]
<p>Pt/YSZ, Dewetted Pt by Pulsed laser deposition,</p> <p>Circular Pt</p> <p>Film thickness: 70 to 100 nm</p> <p>Tpb length: 300 to 600 mcm^{-2}</p> <p>Surface area: 16 mm^2</p>	400	10^{-3} to 10^{-2}	Tpb	[15]
<p>Pt/YSZ, Sputtered,</p> <p>Film thickness: 350 nm</p>	300 to 700	10^{-6} to 10^{-2}	<p>300 to 400°C: Area</p> <p>550 to 700 °C: Tpb</p>	[92]

2.3.2.3 Current Overpotential

The details of the charge transfer reactions can also be obtained from the results of the current overpotential experiments. A typical current overpotential curve is shown in Figure 2.11. The most significant information which can be extracted from the current overpotential results is the exchange current (I_0). I_0 can be obtained by plotting the current (I) vs the overpotential (η) in a Tafel plot as indicated in Figure 2.12. The overpotential (η) is given by [9]

$$\eta = V_{WR}(I) - V_{WR}(I=0) \quad (32)$$

which is defined as the difference between the potential at chemical equilibrium and the potential when an electric current is flowing.

I_0 expresses the electrocatalytic activity of the interface (tpb) for the charge transfer reaction under consideration [32] or a measure of how fast ions are discharged at the interface metal/solid ionic described in the Butler-Volmer equation [9].

$$I/I_0 = \exp(\alpha_a F\eta/RT) - \exp(\alpha_c F\eta/RT) \quad (33)$$

where α_a and α_c denote the symmetry of the activation barrier with respect to initial or final state in the corresponding potential diagram (usually around 0.5). A low I_0 means that the interface has to be strongly polarised in order to generate a certain electric current as compared to a high I_0 which means low polarisability [9]. The exchange current (density) should also be proportional to the tpb length since it is exactly at this interface that the electrocatalytic charge transfer reaction is taking place [32]. A direct experimental proof for the proportionality between the electrocatalytic activity in solid electrolyte cells and reactive oxygen uptake at the tpb was demonstrated by Vayenas et al. [32] who compared the N_{otpb} values of different catalyst film with the corresponding I_0 values at a fixed temperature and pO_2 .

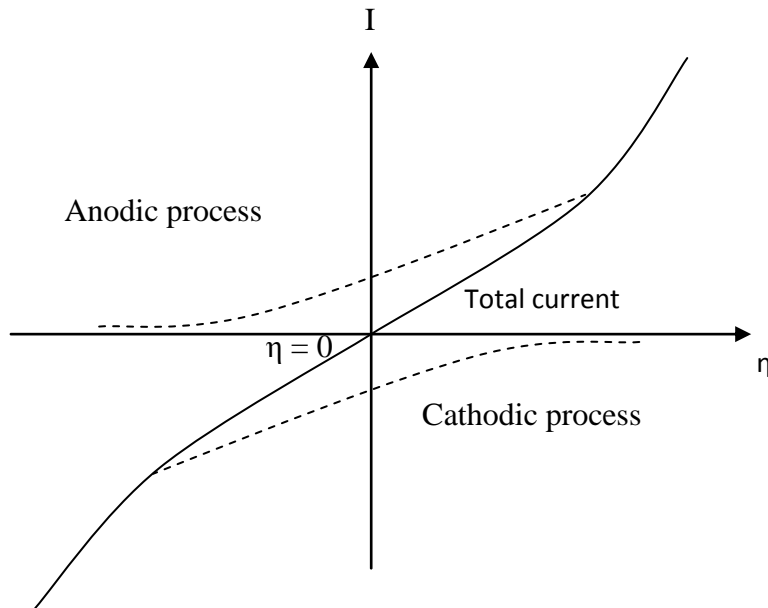


Figure 2.11: Typical current overpotential curve

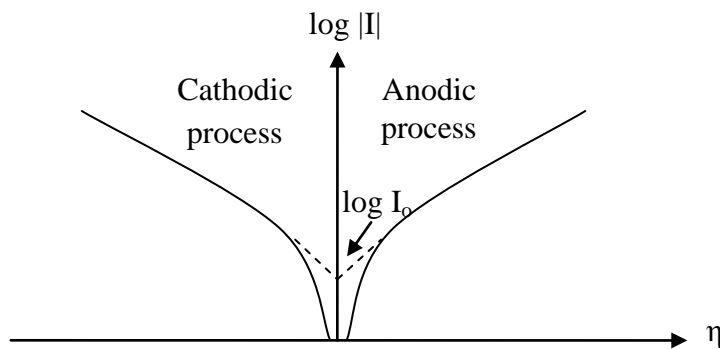


Figure 2.12: Typical tafel plot

2.3.3 Limitations in Oxygen Charge Transfer

The formation of Pt oxide at tpb, which is reducing or inhibiting, can limit the oxygen exchange reaction at this interface. This is usually associated with the electrode deactivation (Pt oxide formation) and also activation phenomena (Pt oxide decomposition) in a Pt/YSZ system [15,16]. Pöpke et al. [15] proposed the formation of ultra-thin and very thin Pt oxide layers on the Pt/gas interface extending to tpb which hinder the oxygen exchange reactions. Pt oxide layer can be formed on Pt surface at

atmospheric pressure [93]. The presence of Pt oxide and its amount are strongly depended on the experimental conditions, such as temperature, oxygen partial pressure, and oxygen flux towards the electrode during anodic polarisation [16].

The most stable Pt oxide species on YSZ has been shown to be PtO [94] and Pt oxide decomposes at $T > 370$ K [95]. Between 650 K and 700 K, PtO is nearly completely reduced although traces of PtO (possibly stabilised at the Pt nanoparticles/support interface) could be observed up to 1000 K. A two steps thermal decomposition process $\text{PtO}_2 \rightarrow \text{PtO} \rightarrow \text{Pt-metal}$ was observed and the highest stability PtO species was found for Pt/ZrO₂ system upon annealing in O₂ [94]. However, changes in electrode morphology such as cracking of the barrier layers and or a roughening of the Pt surface close to the tpb can hinder the formation of this covering Pt oxide film [15].

The investigation of the deactivation and activation phenomenon requires details on the processes occurring at the tpb. However, there are limited experimental possibilities to investigate the tpb (*in situ*) and therefore Pöpke et al. [88] suggested to first study the binary Pt/YSZ interface by carrying out electrochemical investigation techniques such as cyclic voltammetry (CV) and then focus on the tpb by taking the gas phase into consideration. The presence of oxides on the gas exposed surface can be verified by exposing the catalyst to hydrogen in which an increase in the number of Pt active sites can be observed after the reduction step [72].

Chapter 3. Methodology

3.0 Introduction

The methodology is structured based on the objectives of the present work which focused on (i) the influence of impurities on oxygen charge transfer in the Pt/YSZ system using porous electrodes and (ii) oxygen charge transfer and backspillover processes in the Pt/YSZ system utilising a model catalyst (patterned electrodes). The methodology describes experiment rigs, materials and procedures of sample preparation, surface characterisations, and electrochemical experiments.

3.1 Influence of Impurities on Oxygen Charge Transfer in a Pt/YSZ System

This section demonstrates the methodology of the investigation of the oxygen charge transfer in a Pt/YSZ system utilising porous electrodes which were prepared by using Pt catalysts from three providers which include ESL(5542), Heraeus (RP 10003-12) and Metalor (M603B).

3.1.1 *Sample preparation*

In this work, the electrochemical cell was of a single pellet type and consisted of a three electrode system which includes working, reference and counter electrodes. The working electrode was platinum (Pt) catalyst while the counter and the reference electrodes were gold. The solid electrolyte was YSZ in a pellet form. A number of samples were prepared for each Pt catalyst. The prepared samples were used for the investigation on (i) electrode surface characteristics (such as porosity and grain size) by scanning electron microscope (SEM), (ii) distribution of different elements via energy-dispersive x-ray spectroscopy (EDX), (iii) impurity content of the Pt film by inductively coupled plasma in conjunction with atomic emission spectroscopy (ICP-OES) and (iv) electrochemical characterisation via cyclic voltammetry (CV) experiments. Samples preparation and the geometric characteristics are described below.

3.1.1.1 Electrolyte

The YSZ pellets were prepared by uniaxially pressing of approximately 2.2 g of YSZ powder 8 mol% yttria (Lot E1626, 1 kg, $7.1 \text{ m}^2 \text{ g}^{-1}$ $0.6 \mu\text{m}$, PI-KEM LTD) at 3 tons by using a 20 mm diameter die. The final disc was approximately 2 mm thick and after a sintering program the final diameter and thickness were approximately 15 mm and 1.5 mm, respectively. The YSZ pellets were sintered by using the following program:

- a. Ramp to 1200 °C at a rate of $1 \text{ }^\circ\text{Cmin}^{-1}$
- b. Ramp to 1500 °C at a rate of $2 \text{ }^\circ\text{Cmin}^{-1}$
- c. Dwell at 1500 °C for 4 hours
- d. Ramp to room temperature at $1 \text{ }^\circ\text{Cmin}^{-1}$

The sintered YSZ pellets were polished with SiC paper and washed with isopropyl alcohol in an ultrasonic cleaner for 3 minutes, then rinsed with deionised water and dried and weighed.

3.1.1.2 Electrodes

The working electrodes were prepared by depositing Pt film on the polished and cleaned YSZ pellets on one side (half) of the pellet by using a brush. The deposited Pt films were then sintered by using the program, as indicated in Table 3.1, which was recommended by the providers. Similar to the working electrode, the reference and counter electrodes were also deposited on YSZ pellets by painting Metalor (A1118) gold resin by using a brush. The counter electrode was painted in a symmetrical face to face arrangement to the working electrode on the opposite sides of the YSZ pellet. The reference electrode was painted at a distance of approximately 2 mm to the counter electrode at the same side of the YSZ pellet. The sintering program of the counter and reference electrode films are also demonstrated in Table 3.1. The schematic of the electrode arrangement and the prepared pellet deposited with ESL Pt catalyst, respectively, are indicated in Figure 3.1.

Table 3.1: Sintering program of the working, counter and reference electrodes

Electrodes	Providers	Sintering Program
Working (Pt)	ESL (5542)	<ol style="list-style-type: none"> 1. Ramp to 980 °C at 20 °Cmin⁻¹ 2. Dwell at 980 °C for either 10 min (this was recommended by the provider) or 60 min (this was to study the effect of sintering time on the electrode surface characteristics) 3. Ramp to room temperature at 20 °Cmin⁻¹
	Heraeus (RP 10003-12)	<ol style="list-style-type: none"> 1. Ramp to 90 °C at 0.5°Cmin⁻¹ 2. Dwell at 90 °C for 15 min 3. Ramp 850 °C at 20 °Cmin⁻¹ 4. Dwell at 850 °C for 7 min 5. Ramp to room temperature at 20 °Cmin⁻¹
	Metalor (M603B)	<ol style="list-style-type: none"> 1. Ramp to 400 °C at 10 °Cmin⁻¹ 2. Dwell at 400 °C for 2 hours 3. Ramp to 850 °C at 10 °Cmin⁻¹ 4. Dwell at 850 °C for 2 hours 5. Ramp to room temperature at 10 °Cmin⁻¹
Counter & Reference (Au)	Metalor (A1118)	<ol style="list-style-type: none"> 1. Ramp to 400 °C at 10 °Cmin⁻¹ 2. Dwell at 400 °C for 2 hours 3. Ramp to 800 °C at 10 °Cmin⁻¹ 4. Dwell at 800 °C for 2 hours 5. Ramp to room temperature at 10 °Cmin⁻¹

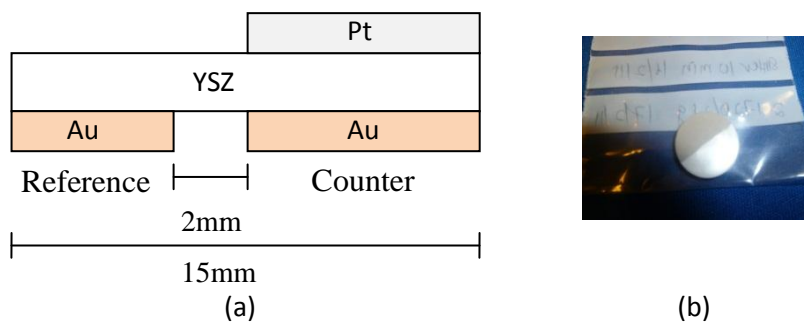


Figure 3.1: (a) Schematic of the electrodes arrangement and (b) the prepared Pellets/Electrolyte/Electrode

3.1.2 Electrode Surface Characterisation

This section demonstrates surface characterisation of the prepared samples which includes SEM-EDX and ICP analyses.

3.1.2.1 SEM-EDX

The morphology and microstructure of a catalyst film can be analysed by using scanning electron microscopy (SEM) which is commonly used in conjunction with energy dispersive x-ray spectroscopy (EDX) [4, 29, 30]. One of the most important information which could be extracted from the SEM images is the catalyst particle size. For a specimen to be analysed by SEM, the specimen must be electrically conductive. SEM magnification can range from 10 to 500 000 times or 6 orders of magnitude. EDX, on the other hand, is commonly used to determine the elemental distribution on the catalyst film [4, 30]. EDX analysis is based on the principle that each element has a unique atomic structure.

In the current work, the sintered Pt films were analysed by using the SEM (FEI XL30 ESEM-FEG)/EDX (Rontec and Quantac Software) with a specialist of the scanning electron microscopy of the Chemicals & Materials Analysis Service (ACMA) unit at the Newcastle University. The analyses were carried out on the fresh and used samples. The used samples were those which have been exposed to CV experiments. The analysis was to determine catalyst surface morphology before and after the experiments at different

magnifications (such as 350, 1000 and 10000 magnifications) and to investigate the presence of surface impurities. EDX measures the presence of the elements to a depth of several micrometers into the sample surface and therefore was used in the present work only for simple identification of significant elements [10].

3.1.2.2 *Analysis of Impurities*

Pt catalysts from the commercial are expected to contain impurities where the amount and type of impurities are varied among different providers. The presence of impurities, such as metal cations, on the catalyst surface is also expected to affect the catalyst catalytic and electrocatalytic properties. Since the presence of the impurities at a depth below EDX detection limit cannot be observed from the surface investigation, another determination method is necessary. Metal impurities [96] including Pt [97] in a Pt sample can be analysed by using inductively coupled plasma (ICP). ICP has been extensively used for trace metal determination in various type of analyses such as in environmental [98, 99], foods [100] and drugs [101] studies. ICP was often used in conjunction with other analytical instruments such as Mass Spectroscopy (MS) and Atomic Emission Spectroscopy (AES/OES). Inductively coupled plasma mass spectrometry (ICP-MS) is highly sensitive for the determination of metals and several non-metals at a concentration of below one part per trillion (ppt). In the work of Zhang et al. [96], ICP-AES method has been used to study 13 impurity elements in a highly pure platinum sample. This method was proven to be accurate, and can be applied to the analysis of 99.9-99.995% pure platinum.

In the current work, platinum resins and pastes and the sintered Pt films of the samples from the three providers were analysed for metal impurities by using ICP in conjunction with atomic emission spectroscopy (ICP-OES). Prior to the ICP-OES analysis, the following samples were digested by using an aqua regia solution.

- i. Pt resin/pastes of the three catalysts
- ii. Sintered Pt film on YSZ (Pt/YSZ pellet) of the three catalysts
- iii. YSZ pellet
- iv. Blank

The aqua regia solution was prepared by mixing concentrated nitric acid (ultra pure grade) and concentrated hydrochloric acid (ultra pure grade) in a volume ratio of 1:3, respectively. Approximately 25 mg Pt samples of each provider and the pellets were placed in 50 ml beakers. The aqua regia solution was then added to each beaker and the solutions were heated on a hot plate until all residues were completely dissolved. Whatman filter papers no 1 were used to filter the solution once the solutions have reached room temperature. The final solution was then diluted in 100 ml volumetric flasks. 10% nitric acid which was diluted in deionised (DI) water solution was used to clean glassware used in the sample preparation process. The prepared samples were then sent to the Advanced Chemicals & Materials Analysis Service (ACMA) Unit at Newcastle University for impurity determination by using ICP-OES. To consider any trace metals that could have present in the deionised (DI) water and acids or may have been introduced during preparation works from glassware, etc., blank samples were also prepared and analysed using the ICP-OES.

3.1.3 Reactor Design and Testing Rigs

Figure 3.2 shows the schematic diagram and picture of electrochemical reactor while Figure 3.3 shows the schematic diagram of the experimental set up and rigs. The reactor consists of a quartz tube of approximately 30 ml volume closed with stainless steel (Swagelok vacuum fitting) fittings. It is a single chamber reactor where all electrodes were exposed to the same gas atmosphere. Gold wires were used to provide electrical connection to the electrodes and keep the sample pellet suspended in the reactor. A four-bore alumina tube (from Alfa Aesar) was used in order to isolate the three gold wires and the (K-type) thermocouple (used to measure the temperature inside the reactor) in order to avoid short-circuiting. The thermocouple was placed in proximity of the surface of the working electrode. As indicated in Figure 3.2, the reactor was placed in a furnace which was equipped with a heat control system. A mass flow control system (Hasting Instruments, Model 400) was used to adjust and control feed or gases flow rate while the reactor operated under atmospheric pressure.

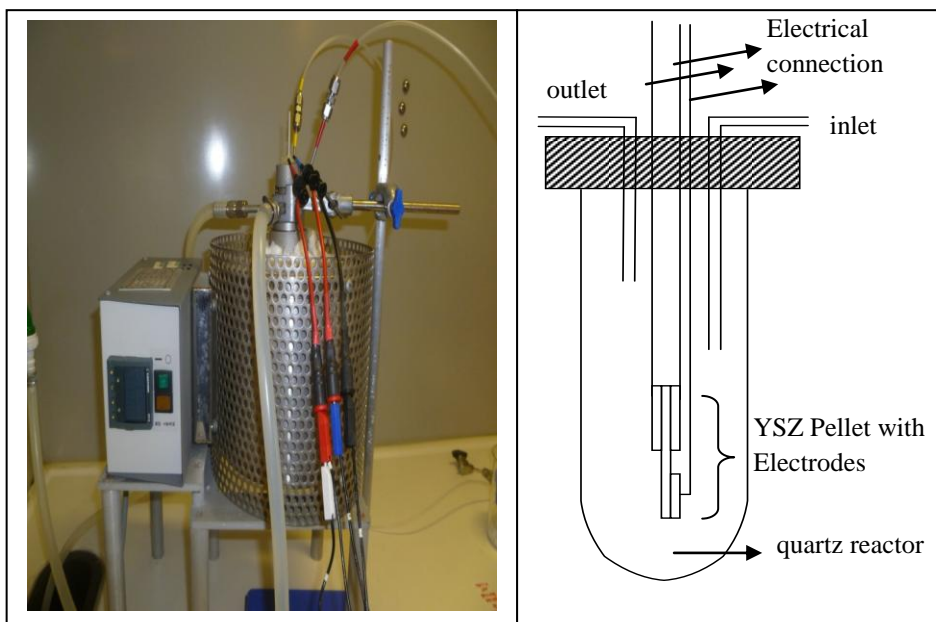


Figure 3.2: (a) Picture and (b) schematic of the electrochemical reactor

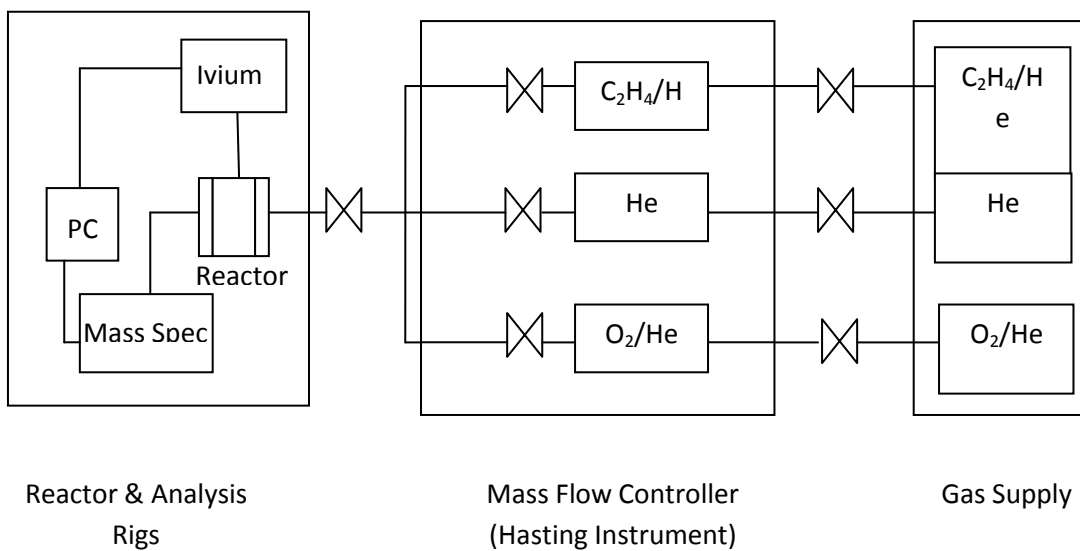


Figure 3.3: Schematic diagram of the experimental set up and rigs

3.1.4 Cyclic Voltammetry (CV) under Nonreactive Condition

The charge transfer reactions in the Pt/YSZ system using the commercial catalysts were studied by cyclic voltammetry (CV). In this work, an IVIUM Compactstat (potentiostat/galvanostat) unit was employed during the CV experiments which were carried out on samples that included ESL 10 min, ESL 60 min, Heraeus, and Metalor under a nonreactive condition at 400 °C. ESL 10 min and ESL 60 min are ESL samples which were sintered at 10 min and 60 min, respectively. Prior to the CV, the reactor temperature was increased from room temperature to the temperature of interest at 10 °Cmin⁻¹ and the reactor was flushed with helium. A flow of 200 mlmin⁻¹ 20% O₂/He was then exposed to the sample and once the reactor temperature was stable, the open circuit potential (OCP) was monitored. Cyclic voltammetry was carried out once the OCP was stable.

During CV, the voltage was scanned from -1.0 V to 0.50 V where the scan rates, v , were 1, 5, 20, 30, 50 and 100 mVs⁻¹ and for each v the experiment was carried out for three cycles. For the ESL and Heraeus samples where cathodic peaks were not observed during the CV, the samples were exposed to 5% H₂/He at 800 °C. This step was to remove surface oxides which may block the tpb. After the exposure to hydrogen, CV was repeated at the same experimental condition. The features in CV of each of the samples were compared and discussed in terms of the electrode surface morphology and impurity content.

3.2 Oxygen Charge Transfer in a Pt/YSZ System Utilising Patterned Electrodes

As demonstrated later in Chapter 4, there is a necessity of utilising a model catalyst in order to exclude the influence of impurities and to carry out a systematic investigation of geometry (tpb) dependence of the oxygen charge transfer which cannot be obtained from the study using the porous electrodes. This section, therefore, describes the methodology of the investigation of the oxygen charge transfer in a Pt/YSZ system using a model catalyst in which the focus was on the tpb.

The model catalyst is a patterned electrode which has been fabricated for several width length scales. The geometric characteristics are indicated in **Appendix A**. The samples were prepared in three batches. For the 1st batch sample, both the geometric surface area and tpb length are different among the samples of different width length scale. The distance between the Pt lines however are similar, which is 20 μm . In contrast to the 1st batch, the 2nd and the 3rd batch electrodes have a more controlled geometric characteristic where the geometric surface area is similar while the tpb length differs among the samples of different width length scale. In this case, the distance between the Pt lines of each sample is similar to the electrode width length scale. Besides that, the 2nd batch samples have been thermally treated at 550 °C and 600 °C by the Electrical Engineering School, Newcastle University. The 2nd batch samples were thermally treated in N₂ for 5 minutes at atmospheric pressure.

3.2.1 *Sample Preparation*

The Pt/YSZ system using the patterned electrodes is similar to the cell utilising the porous electrodes. The electrochemical cell is also a single pellet type and consists of three electrode system. The working electrode was platinum (Pt) catalyst, the counter and the reference electrodes were gold (Au) and the solid electrolyte was YSZ. The patterned electrodes were prepared with solid electrolyte pellets composed of single crystalline YSZ by a lift off procedure. The YSZ (substrate) has a thickness of 0.5 mm. The cleaning of the substrate was carried out by using the following process steps:

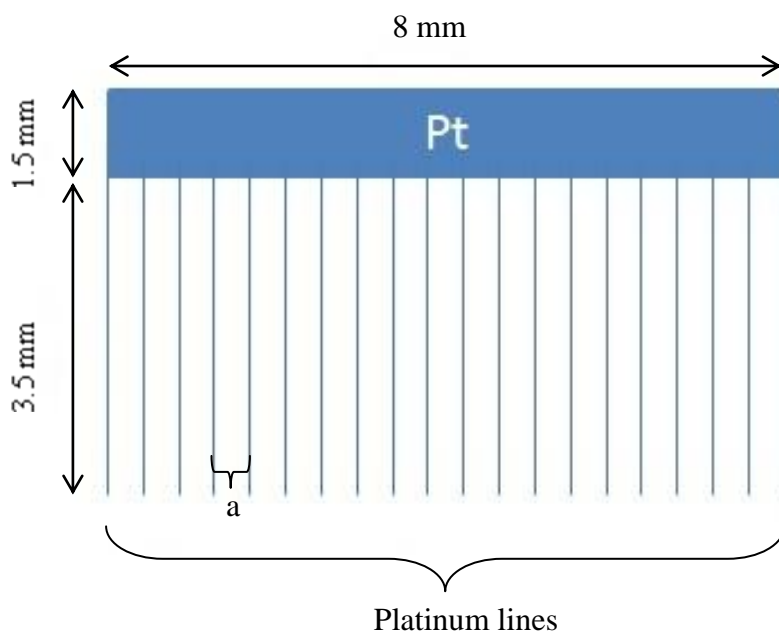
1. Degreasing with organic solvent
2. Soaking in ultrasonic bath of H₂SO₄/H₂O₂ for 5min at 80 °C
3. RCA procedure
4. Drying in N₂ gas flow

The sputtered Pt films, as indicated in Figure 3.4, were then obtained via deposition of Pt film on one side of the YSZ pellets by DC magnetron sputtering at 9 mtorr in Argon at room temperature. The resulted Pt film thickness was 80 nm. A photoresist AZ-5214E was used for the patterning. The Au film (counter and reference electrodes) were obtained by electron beam deposition at the base pressure of $5 \cdot 10^{-6}$ torr also at room temperature.

A photoresist AZ-5214E was used for patterning which result an Au film with thickness of 80 nm. After the deposition, during the lift off procedure, the samples were immersed in N,N-dimethylformamide in an ultrasonic bath at 80 °C followed by rinsing in DI water and dried in N₂ gas flow.

The lift off process steps:

1. Preparation of the substrate
2. Deposition of the sacrificial stencil layer
3. Patterning the sacrificial layer (ex. etching), creating an inverse pattern
4. Deposition of the target material
5. Washing out the sacrificial layer together with the target material on its surface
6. Final pattern



Batch	Pt finger/line width length Scale (μm)	a: Distance between Pt finger/line (μm)
1 st	2	20
	20	20
	200	20
2 nd & 3 rd	4	4
	40	40
	200	200
	400	400

Figure 3.4: Schematic diagram of the model catalyst or patterned electrodes

3.2.2 Electrode Surface Characterisation

In the current work, the surface of the patterned Pt films were also analysed by using the SEM/EDX with a specialist of the scanning electron microscopy of the Chemicals & Materials Analysis Service (ACMA) unit at the Newcastle University. Similar to the porous electrodes, the analyses were carried out on the fresh and used samples in which the used samples were those which have been exposed to either kinetic and or electrochemical experiments. The analyses were also conducted at different magnifications such as 350, 1000 and 10000.

3.2.3 Reactor Design and Testing Rigs

The schematic diagram of the experimental set up and electrochemical reactor utilising the patterned electrodes are indicated in Figure 3.5. The experimental set up is very similar to the system using the porous electrodes except that the patterned electrode sample was held in the reactor by a sample holder in order to avoid sample damage and short-circuiting. Also, gases flow rate was adjusted and controlled by using a mass flow control system (Hasting Instruments, Model 400).

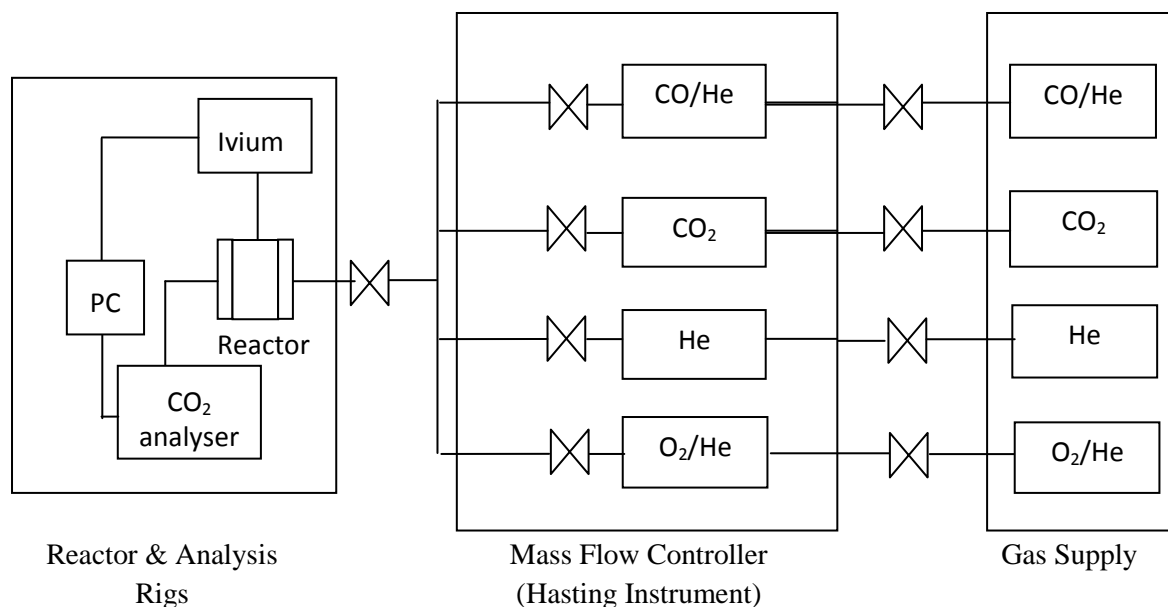


Figure 3.5: Schematic diagram of experimental set up of Pt/YSZ system using the patterned electrodes

3.2.4 *Electrochemical Characterisation under Nonreactive Condition*

This section demonstrates the electrochemical characterisations of the Pt/YSZ system using the patterned electrodes. In contrast to the porous electrodes, the study was more comprehensive in which electrochemical impedance spectroscopy (EIS) and current overpotential experiments were also carried out in addition to CV. Similar to the porous electrodes, an IVIUM Compactstat (potentiostat/galvanostat) unit has been used during the experiments. These experiments were carried out under a nonreactive condition under the flow of 20 % O₂/He at temperatures between 300 °C and 450 °C.

Prior to the experiments, the reactor was flushed with helium and the reactor temperature was increased from room temperature to the temperature of interest at 10 °Cmin⁻¹. The reactor was then exposed to the flow of 90 to 100 mlmin⁻¹ 20% O₂/He and once the reactor temperature was stable, the open circuit potential (OCP) was monitored. After the OCP was stable, the experiments which focused on

- (i) the geometry dependence of the oxygen charge transfer
- (ii) the repeatability study where the changes of the catalyst electrochemical properties (deactivation and activation phenomena) were monitored throughout the experimental works and
- (iv) the verification of the factors causing the electrode deactivation and activation phenomena

were carried out. The experiments are summarised in Table 3.2.

3.2.4.1 *Geometry Dependence of the Charge Transfer Reactions by CV, EIS and Current Overpotential*

As demonstrated in Table 3.2, CV, EIS and current overpotential experiments were carried out by using 4 µm, 40 µm and 400 µm where the results were compared to obtain a correlation between the geometric characteristics (tpb) and the oxygen charge transfer or activity in the Pt/YSZ system.

a. *Cyclic Voltammetry*

During CV, depending on the reactor temperature, the voltage was scanned within -1.0 V to 0.50 V. The scan rates, v , were 10, 20, 30, 50 and 100 mVs^{-1} and the experiments were carried out for four cycles for each scan rate. The experiments were repeated for at least two times. However, it will be shown later in Chapter 5 that the features of the voltammograms (such as the current range) were changing when the experiments were repeated. The analyses of the data (including data from the repeated experiments) were carried out by studying the changes in the features of the voltammograms throughout the experimental works. The current range was measured by adding the highest anodic and cathodic current during the CV. The amount of oxygen associated with the oxide decomposition during cathodic scan was measured by integrating the cathodic current (reduction) peak. The geometric characteristics were correlated with the current range, reduction peak height and area.

b. *Electrochemical Impedance Spectroscopy (EIS)*

Electrochemical Impedance spectroscopy (EIS) measurement system integrates an AC measurement unit (frequency-response analyser), a potentiostat/galvanostat, and an electrochemical cell in contact with the investigated sample [89]. In the present work, the EIS measurements were carried out in a frequency range between 0.1 Hz and 1000 kHz with a resolution of 5 points per decade [14] at a potential between -0.50 V to 0.50 V. The frequency range has been chosen to ensure minimal change in the system during measurement. This is because a very low frequency limit can result in a very long time for the collection of a complete scan and for systems that are changing with time (e.g. due to corrosion, growth of a film etc.) this implies that the system has changed during the course of the data collection [89]. The EIS is also measured using a small excitation signal so that the cell's response is pseudo-linear.

The EIS measurements at the same experimental conditions were repeated for at least two times. The impedance spectra which resulted from the experiments were analysed in terms of the diameter of the impedance semicircles (which corresponds to the charge

transfer resistance) in a certain frequency range. The charge transfer resistance has been estimated by using the equation of a circle (described in chapter 5, section 5.2.1). The reciprocal of the charge transfer resistance is the conductance which was then divided by the electrode geometric characteristics in order to produce Arrhenius plots for the analyses of the geometry dependence of the oxygen charge transfer.

c. Current Overpotential

During the current overpotential study, the applied voltage was held constant for 300 s and the corresponding current was recorded for every 0.2 s. The applied voltage during the experiments of the 4 μm , 40 μm and 400 μm from the 3rd batch was between -0.50 V to 0.50 V. During the study of the 200 μm from the 3rd batch, the voltage was in the range between -1.0 V and 0.10 V. After the study within this range was completed the range has been increased to 0.20 V. The step size varied from, with smaller step widths close to equilibrium for the case of the 200 μm . In order to exclude the effect of charging current of the interfacial electrode capacitor [101], only the last 50 points, which almost exclusively reflect the faradaic current of the respective voltage, were averaged and taken into account for further analysis. In order to obtain the overpotential, η , the contribution of the ohmic overpotential caused by YSZ was subtracted by using resistance values determined from impedance measurements [15]. The experiments were repeated for at least two times.

3.2.4.2 Effect of 0.50 V Anodic Potential on Oxygen Charge Transfer Reactions

An exposure to a large anodic potential can cause electrode morphological changes such as bubbles and cracked bubble formation which can increase the tpb length of a sample and hence affect sample's electrochemical properties. In order to observe this effect, the oxygen charge transfer in the Pt/YSZ system was also investigated at an anodic potential which is smaller than 0.50 V by using the 400 μm . The small anodic potential is 0.10 V and the procedure is described in Table 3.2. The 400 μm was only exposed to the 0.50 V anodic potential during linear sweep at 400 °C. During the linear sweep, the anodic

potential of 0.50 V was held at 9 different times and the voltage was scanned from -0.50 V to 0.50 V at a scan rate of 20 mVs⁻¹.

3.2.4.3 Repeatability Study

As described later in Chapter 5, the geometry dependence of the oxygen charge transfer reaction cannot be observed from the results of the electrochemical characterisation of the electrodes of different width length scale. The next step was therefore to focus on and analyse the changes in the data of one sample and try to correlate it with parameters that can be associated with the number of the available sites for the charge transfer reactions.

In this case, a detail analysis on the changes in the electrochemical results of a 200 µm from the 3rd batch throughout the experimental works was conducted. This was obtained by carrying out a reference experiment, which was CV with scan rates of 10 mVs⁻¹, 20 mVs⁻¹ and 30 mVs⁻¹, after each electrochemical experiment (CV, EIS, current overpotential and kinetic/EPOC) at each temperature (350 °C, 400 °C and 450 °C) and before carrying out the experiments on a different day. The detail procedure is indicated in Table 3.2. Besides the 200 µm, similar analyses were also carried out on the 400 µm to study the reproducibility of the electrochemical data when the model catalysts were utilised. However, the study was less comprehensive than that of the 200 µm.

3.2.5 Verification of the Mechanisms of Patterned Electrode Activation and Deactivation Phenomena

From the results of the repeatability study which is discussed later in Chapter 5, patterned electrode deactivation and activation phenomena are associated with the formation and decomposition of surface oxide at the tpb. In order to verify the mechanism of the processes occurring at the tpb or at the gas exposed interface, the 200 µm (which is the same sample which has been used during the repeatability study) and the 200 µm 550 °C kinetic samples were exposed to the flow of 5% H₂/He. The 200 µm 550 °C thermally treated sample has been used in CO oxidation experiments (described in **section 3.3.2.1**) prior to this study. Since the focus was on the processes occurring at the tpb, a

comparison with the results of similar experiments of those of a high tpb density electrode is necessary. These results are therefore compared with the responses during CV before and after the exposure to hydrogen of the porous electrode prepared by using the ESL catalyst.

The exposure to hydrogen (reduction) should remove oxides at the gas exposed interface and hence increase the available tpb (sites) for the oxygen charge transfer reaction. This should affect the oxygen activity at the other (non-gas exposed) interfaces in the system. These changes can be observed from the differences in the features in CV or linear sweep before and after the exposure to hydrogen. For the case of the 200 μm , linear sweep experiments at 350 $^{\circ}\text{C}$ under the nonreactive condition (flow of 100 mlmin^{-1} 20 % O_2/He) were carried out before and after the exposure to 100 mlmin^{-1} 5% H_2/He at 500 $^{\circ}\text{C}$. During the linear sweep, the 200 μm was exposed to a 0.50 V anodic potential in which the 0.50 V was held at 9 different times and the voltage was scanned from -1.0 V to 0.50 V with a scan rate of 20 mVs^{-1} . Before exposing the sample to the 5% H_2/He , the reactor was flushed with helium to completely remove oxygen in the reactor. During the exposure to hydrogen, OCP was monitored and once the OCP was stable at a very small value or close to 0 V the gas flow was switched to helium to completely remove the remaining hydrogen in the reactor. Then, the sample was exposed to flow of 100 mlmin^{-1} 20 % O_2/He and the linear sweep was repeated.

During the hydrogen reduction study of the 200 μm , the counter and the reference electrodes were damaged (the surface was not conductive) when the sample was exposed to the 100 mlmin^{-1} 5% H_2/He at 500 $^{\circ}\text{C}$. The experimental condition during the hydrogen reduction of the 200 μm 550 $^{\circ}\text{C}$ kinetic sample was therefore adjusted to prevent similar damages from occurring on both electrodes. This sample was then exposed to 70 mlmin^{-1} 5% H_2/He at a lower temperature which was 350 $^{\circ}\text{C}$. CV experiments were carried out before and after the exposure to hydrogen. Most of the CV experiments were carried out for 50 cycles where the voltage was scanned from -0.50 V to 0.20 V with a scan rate of 20 mVs^{-1} . The effect of exposing the sample to hydrogen at different time on the features in the voltammograms was also investigated where the duration of exposure varied from 2 hours to 7.5 hours.

3.2.6 Summary of the electrochemical characterisation experiments

The experiments were carried out under a 90 to 100 mlmin⁻¹ 20 % O₂/He flow except during kinetic and EPOC studies.

3.2.6.1 Electrochemical Characterisations

Hypothesis:

Oxygen charge transfer or activity in a Pt/YSZ system, particularly at tpb, can be systematically investigated through the utilisation of the model catalyst or patterned electrodes of different width length scale.

Objective:

To study geometry (tpb length) dependence of the charge transfer reactions.

Samples and Experimental Conditions:

Samples: 4 μm, 40 μm, 400 μm

Experiments: CV, EIS and current overpotential

Temperature: 300 °C to 450 °C

Potential Range: -0.50 V to 0.50 V

Procedure:

For each sample, the electrochemical experiments were carried out first at a lower temperature.

3.2.6.2 Repeatability

Hypothesis:

The analyses of the changes in the electrochemical data of one sample throughout the experimental works should provide details of oxygen charge transfer or activity in the Pt/YSZ system using the patterned electrodes.

Objectives:

- a. To develop a correlation between the changes in the electrochemical data and the changes in number of the charge transfer reaction sites (tpb).
- b. To associate the results with the electrode deactivation and activation phenomena.

Samples and Experimental Conditions:

(i) Sample: 200 μm

Experiments: CV, EIS and current overpotential

Temperature: 350 °C, 400 °C and 450 °C

Potential range: -1.0 V to 0.10 V and 0.20 V.

Procedure:

1. Electrochemical experiments under the nonreactive condition at 0.10 V at 350 °C.
2. CV was carried out after each electrochemical experiment at this temperature where this CV serves as a reference experiment. The voltage was scanned from -0.50 V to 0.10 V at scan rates of 10 mVs^{-1} , 20 mVs^{-1} and 30 mVs^{-1} .
3. The experiments were continued at the same temperature with EPOC at various pO_2 pressure at constant pCO (0.5 kPa) at a total flow rate of 150 ml (STP) min^{-1} .
4. Reference (CV) experiment at the same temperature.
5. The temperature was increased to 400 °C. Experiments 1 to 4 were carried out at this temperature.
6. Reference (CV) experiment at 350 °C.
7. The temperature was increased to 450 °C. Experiments 1 to 4 were carried out at this temperature.
8. Reference (CV) experiment at 350 °C.
9. Experiments 1 to 8 were carried out by increasing the anodic potential to 0.20 V.

(ii) Sample: 400 μm

Experiments: CV, EIS and current overpotential, linear sweep, reverse potential

Temperature: 300 °C to 450 °C

Potential Range: -0.50 V to 0.10 V (small), -0.50 V to 0.50 V (large), this is the same work described in objective a under the electrochemical characterisation study.

Procedure:

1. Electrochemical experiments at 0.10 V at 300 °C, 350 °C, 400 °C and 450 °C.
2. Linear sweep at 400 °C where the sample was exposed to the 0.50 V.
3. CV was then carried out at the same temperature at 5 different scan rates from -0.50 V to 0.50 V followed by a reverse potential at a scan rate of 20 mVs⁻¹ from 0.40 V to 0.10 V.
4. Study at 0.10 V was repeated by carrying out CV at 400 °C where the voltage was scanned between -0.50 V and 0.10 V and the scan rate was 20 mVs⁻¹.
5. The studies were then continued with reverse potential, EIS, CV and current overpotential by exposing the sample to the 0.50 V at 350 °C, 400 °C and 450 °C. Study at 0.10 V was repeated after these experiments.

3.2.6.3 Verification of the Mechanisms of Electrode Activation and Deactivation Phenomena

Hypothesis:

The formation and decomposition of surface oxides at tpb caused the observed electrode deactivation and activation phenomena.

Objective:

To verify the presence of surface oxides at the tpb.

Samples and Experimental Conditions:

Sample: (a) 200 μm (the same sample which was used in the repeatability study), (b) 200 μm 550 °C kinetic sample and (c) ESL sample (the same work described in **section 3.1.4**)

Procedure: Chemical treatment was carried out on these samples to investigate the processes occurring at the gas exposed interface

- (i) The 200 μm was exposed to 5% H₂/He at 500 °C. Linear sweep experiment was carried out before and after the chemical treatment.
- (ii) The 200 μm 550 °C kinetic sample was exposed to 5% H₂/He at 350 °C at different time. CV were carried out before and after the treatment.
- (iii) The ESL sample was exposed to 5% H₂/He at 800 °C. CV were carried out before and after the treatment.

3.3 Spillover Processes in a Pt/YSZ System Utilising Patterned Electrodes

The origin of EPOC has been investigated by using the Pt/YSZ system utilising the model catalyst under the open and close circuit conditions. The summary of the experimental works are listed in Table 3.3.

3.3.1 Electrode Surface Characterisation

The electrode surface morphology were analysed before and after the exposure to the experimental conditions.

3.3.2 Kinetic Experiments

The experimental set up, electrochemical reactor and testing rigs during the kinetic experiments were those used during the study using the patterned electrode under the nonreactive condition. The electrochemical reactor operates differentially where a small volume of approximately 30 ml reactor has been used and a low conversion (below 5%) was expected. This was to avoid complications due to reverse reaction and therefore the reaction rates can be measured accurately. The gases used were provided by BOC Limited. Feed or gases flow rate were adjusted and controlled by a mass flow control system (Hasting Instruments, Model 400) while the reactor was operated under atmospheric pressure. The reaction rates were expressed in terms of moles of CO₂ produced from the outlet of the reactor per unit area per unit time. The geometric surface area was used for the rate calculations. An IVIUM Compactstat unit was employed during the experiments under polarisation and the effect of polarisation on the catalytic rate or the magnitude of EPOC was quantified by the rate enhancement ratio, ρ , and faradaic efficiency, Λ . The catalytic reaction exhibits EPOC when $|\Lambda| > 1$.

3.3.2.1 Open Circuit Condition

As demonstrated in Table 3.3, the kinetic of CO oxidation under the open circuit condition was investigated by using the patterned electrodes from the 1st, 2nd and 3rd batch. Prior to the experiments, the samples were exposed to the flow of helium and the

reactor temperature was increased from room temperature to the temperature of interest at $10\text{ }^{\circ}\text{Cmin}^{-1}$. The reactor was then exposed to the reactant gases at 150 mlmin^{-1} and once the reactor temperature was stable, the open circuit rate was monitored. The kinetic experiments under the open circuit condition included

- (i) $2\text{ }\mu\text{m}$, $20\text{ }\mu\text{m}$ and $200\text{ }\mu\text{m}$ from the 1st batch at $340\text{ }^{\circ}\text{C}$ with a total flow rate of $150\text{ ml (STP)min}^{-1}$ by varying either $p\text{O}_2$ or $p\text{CO}$ at constant $p\text{CO}$ (0.5kPa) or $p\text{O}_2$ (0.7kPa), respectively. A custom built quantum cascade laser CO_2 analyser was used to measure the outlet CO_2 concentration during the experiments. The response time was 1.5 s and the rate was calculated by using stable outlet CO_2 concentration. The calibration of the quantum cascade laser CO_2 analyser was carried out accordingly by using a 100 ppm CO_2 which was supplied by the BOC limited. The uncertainty associated with the quantum cascade laser CO_2 analyser was $\leq 5\%$.
- (ii) a $4\text{ }\mu\text{m}$ and a $200\text{ }\mu\text{m}$ from the 3rd batch during CO oxidation at different $p\text{O}_2$ and constant $p\text{CO}$ at $300\text{ }^{\circ}\text{C}$ where the rate measurement was carried out by using the quantum cascade CO_2 analyser.
- (iii) a $200\text{ }\mu\text{m}$ from the 3rd batch (a different sample than that which has been used in the electrochemical characterisation experiments under the nonreactive condition) where the rate was measured continuously during a long term monitoring catalytic rate study. The rate was also measured by using the quantum cascade CO_2 analyser.
- (iv) (a) the $200\text{ }\mu\text{m}$ which has been exposed to the reactive condition during the long term monitoring study in *experiment (iii)* and (b) a $400\text{ }\mu\text{m}$ from the 3rd batch (a different sample than that which has been polarised during the electrochemical characterisation studies under the nonreactive condition). The catalytic rate was measured also by the quantum cascade laser CO_2 analyser to study the influence of sintering temperature on the catalyst catalytic property.
- (v) A $550\text{ }^{\circ}\text{C}$ thermally treated $200\text{ }\mu\text{m}$ from the 2nd batch where the rates were measured by using the quantum cascade CO_2 analyser.

- (vi) repeatability of the catalytic rate by analysing the open circuit value during a transient study using a 200 μm from the 3rd batch (the procedure is demonstrated in *section 3.3.2.2*). This is the same sample which has been used during the electrochemical experiments under the nonreactive condition and the rate measurements were carried out by using a Binos 100 CO₂ analyser. The error associated with the Binos 100 CO₂ analyser was $\leq 5\%$.

3.3.2.2 Closed Circuit Condition

Prior to polarisations, the open circuit catalytic rates were measured. Once the open circuit catalytic rate was stable, the OCP and current were measured for 5 minutes and then the samples were polarised either at positive or negative potential as demonstrated in Table 3.3. The initial coverage of ionic species on the catalyst surface [65] was assumed to be negligible before the polarisation and should not significantly influence the rate measured under the open circuit condition. The study includes

- (i) 20 μm and 200 μm from the 1st batch. The 20 μm was polarised at 1.0 V while the 200 μm was polarised at ± 1.0 V and ± 2.0 V. The catalytic rate was also monitored after the anodic or cathodic current interruption. Catalytic rate measurements were carried out by using the quantum cascade CO₂ analyser.
- (ii) 200 μm from the 3rd batch as a function of pO₂ under a fixed 0.5 kPa pCO at 350 °C with a total flow rate of 150 mlmin⁻¹. This is the 200 μm sample which has been used or polarised during the electrochemical characterisation studies under the nonreactive condition. In most experiments, the CO₂ concentration from the reactor outlet was measured by using a Binos 100 CO₂ analyser. Since the output of the Binos 100 CO₂ analyser was digitised, the transient result at 1.3 kPa pO₂, 0.5 kPa pCO and 350 °C is compared with the output of the Xstream/Emerson analyser.

3.3.3 Summary of the Experimental Works During the Investigation of the Origin of EPOC from the Utilisation of the Patterned Electrodes

The samples were kept in air at room temperature during no experimental works except for the 200 μm from the 3rd batch which has been used in a long term monitoring study.

3.3.3.1 Open Circuit Condition

Hypothesis:

The open circuit catalytic rate of the Pt/YSZ system utilising the patterned electrode is tpb dependent

Objectives:

- a. To compare the catalytic rate of samples of different width length scale
- b. To analyse electrode surface morphology before and after kinetic experiments
- c. To analyse the changes in the catalytic rate of one sample (repeatability study)

Samples and Experimental Conditions:

Objective a:

1. 2 μm , 20 μm , 200 μm from the 1st batch

CO oxidation by varying (i) $p\text{O}_2$ at constant $p\text{CO}$ and (ii) $p\text{CO}$ at constant $p\text{O}_2$, 340 °C 150 mlmin^{-1} .

2. 200 μm after a long term monitoring study and 400 μm from the 3rd batch

The samples were sintered at different temperature in the range between 340 °C to 550 °C, CO oxidation at 340 °C, 3 kPa $p\text{O}_2$, 0.63 kPa $p\text{CO}$.

3. 4 μm and 200 μm from the 3rd batch

CO oxidation by varying $p\text{O}_2$ at constant $p\text{CO}$, 300 °C.

Objective b:

SEM analyses on the electrode surface before and after the kinetic experiments

Objective c:

1. 200 μm from the 3rd batch, fresh sample

Long term monitoring CO oxidation study at 340 °C, 160 mlmin^{-1} , 3 kPa $p\text{O}_2$ and 0.63 kPa $p\text{CO}$. This sample was kept in helium or reactant gases at 340 °C when there was no experimental works.

2. 200 μm from the 2nd batch, was thermally treated at 550 °C, fresh sample

CO oxidation at 150 mlmin^{-1} , 3 kPa $p\text{O}_2$, 0.5 kPa $p\text{CO}$.

3. 200 μm from the 3rd batch, the same sample which has been used during electrochemical experiments under the nonreactive condition.

Open circuit rate measurements during transient (repeated) experiments of CO oxidation at 350 °C, 150 mlmin⁻¹, 3kPa pO₂ 0.5 kPa pCO.

4. 200 µm after a long term monitoring study and 400 µm from the 3rd batch

The same works described in **objective a** item 2.

3.3.3.2 Close CircuitCondition

Hypothesis:

The Pt/YSZ system using the patterned electrodes exhibits EPOC which is associated with the occurrence of electrochemical backspillover species

Objectives:

- a. To determine the occurrence of backspillover species in the Pt/YSZ system using the patterned electrodes
- b. To investigate the roles of the backspillover species in the system during positive and negative polarisations and after the current interruption.

Samples and Experimental Conditions:

1. 20 µm, 200 µm from the 1st batch

CO oxidation by varying (i) pO₂ at constant pCO and (ii) pCO at constant pO₂, 340 °C, 150 mlmin⁻¹, 1.0 V.

2. 200 µm from the 3rd batch

CO oxidation by varying pO₂ at constant pCO, 350 °C to 450 °C, 150 mlmin⁻¹, 0.10 V,

3.4 Safety

This section discusses safety concerning quantum cascade CO₂ laser analyser and controls taken to reduce risks during the experimental works.

3.4.1 Quantum Cascade CO₂ Laser Analyser

The Quantum Cascade CO₂ Laser Analyser contains a Class 3R laser where training of this equipment has been given in the laboratory and also by the University Safety Office

(Laser Safety training). However, the experiments were carried out with the sensor lid shut and secured in place. For this case, the sensor was considered as a Class 1 laser where the protective control measures for normal use was not required. Furthermore, the laser current driver could only be switched on by using a key which was always kept separately from the current driver when the sensor was switched off.

3.4.2 Controls to Reduce Risks

3.4.2.1 Flammable Mixture

During the hydrogen reduction study, before exposing the patterned electrodes to the 5% H₂/He, the remaining oxygen in the reactor (from previous experiments) was completely removed by flushing the reactor with helium. This was to prevent the creation of flammable mixture. For a similar reason, after the exposure to hydrogen, the remaining hydrogen in the reactor was also completely removed by switching the gas flow to helium before exposing the sample to 20 % O₂/He.

3.4.2.2 Leaks and Mass Flow Controller (MFCs)

Leaks and Mass Flow Controller (MFCs) failure could occur. These can be indicated by the total flow at the outlet which was used to manually monitor reactor stability. The CO₂ laser analyser and Binos 100 CO₂ analyser provided online analysis of the outlet gas and therefore, any fluctuation in the reaction mixture that could lead to the creation of a flammable mixture (due to MFC failure) could be detected quickly. For this case, the experiment must be shut down.

3.4.2.3 Fume Cupboard Failure

There was a possibility to encounter fume cupboard failure during experimental works and therefore, a flammable mixture could be created in the fume cupboard. However, the failures could be detected on the same day and the mixture of the gases could have been released before the gases reach the flammability level, since a normal working hour is not longer than 10 hours per day. Exposures to hydrocarbon and CO are monitored by sensors that are available at the laboratory

3.4.2.4 Shut down procedure

After completing the experiments, the furnace was switched off. Then, gas valves under the work bench were switched off, followed by valves in the fume cupboard and then valves in the cylinder cabinet.

Chapter 4. Influence of Impurities and Catalyst Surface Characteristics on the Oxygen Charge Transfer Reaction in a Pt/YSZ System

4.0 Introduction

This chapter discusses the influence of catalyst microstructure and impurities on the oxygen charge transfer reaction in a Pt/YSZ system. Pt/YSZ systems utilising platinum (Pt) paste and resins from three different providers that were ESL (5542), Heraeus (RP 10003-12) and Metalor (M603B) were studied and compared. To determine the effect of sintering time on the microstructure and impurity content, two ESL samples that are ESL 10 min and ESL 60 min were sintered at different time. The microstructure was investigated by SEM while the impurities were determined by ICP-OES. To compare the electrocatalytic behaviour, cyclic voltammetry (CV) experiments at 400 °C under a nonreactive condition were carried out.

4.1 Catalyst Surface Characterisations

4.1.1 SEM Images

SEM images of the Pt films of the three catalysts on the prepared YSZ pellets are shown in Figure 4.1. Based on these images, the average diameter of crystallites constituting the Pt catalyst films used in this work on YSZ ranged from 0.5 to 2 μm . The SEM images suggest that ESL and Heraeus may have a more porous structure in comparison to the microstructure of the Metalor sample (denser microstructure). However, this observation is inconclusive since in the present work, the SEM images can only provide qualitative view about pore size. In all cases, the obtained EDX spectra did not show any peaks for elements other than Pt. This observation indicates that if there are any impurities present on the catalyst films they were below the EDX detection limit.

Besides that, the results evidence different microstructures for different sintering times revealed by SEM images. Figures 4.1(a) and 4.1(c) correspond to the ESL films for different sintering times. Based on these figures, it is suggested that sintering the Pt catalyst film for 60 minutes may result to a less porous microstructure than sintering the

film for only 10 minutes. This finding is in agreement with the findings of Badwal and Ciacchi [84] where densification and grain growth due to increasing sintering time led to reductions in Pt film porosity and the extent of the three phase boundary (tpb).

Changes in the microstructure of Pt film after electrochemical experiments were also investigated based on the SEM image shown in Figure 4.2. The image indicates the microstructure of Pt film after the electrochemical experiments was similar to the microstructure of the fresh sample shown in Figure 4.1 (a). This result was in agreement with the findings of Mutoro et al. [26] where the structure of a porous catalyst film was not visibly affected by polarisation during electrochemical experiments which suggests that oxygen could freely emerge from tpb without having to form cavities or bubbles as the case of dense or pulsed laser deposition electrodes. This observation is important to serve as a comparison with the microstructures of a model catalyst or patterned electrodes which are discussed in **Chapter 5**. The SEM images, at this stage, showed that Pt catalyst film of different providers and sintering program (or time) would result in different surface morphology.

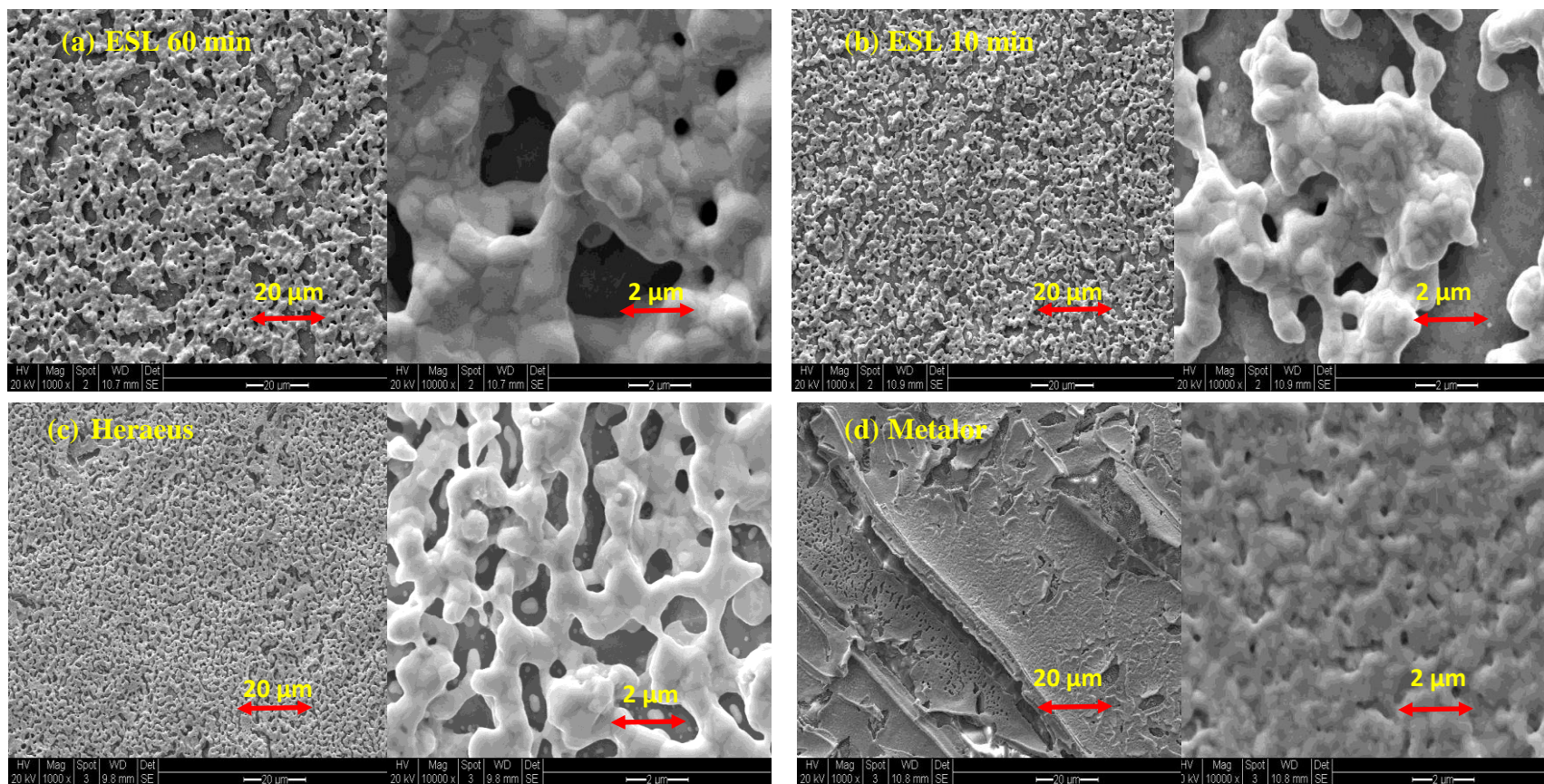


Figure 4.1: SEM images of Pt films on YSZ of catalysts at 1000 and 10000 magnifications of the (a) fresh ESL 60 min, (b) fresh ESL 10 min (c) fresh Heraeus and (d) fresh Metalor

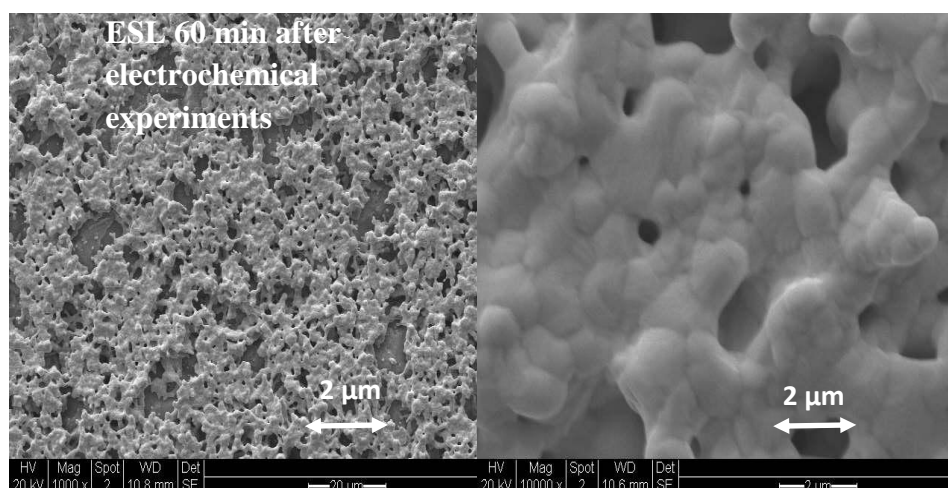


Figure 4.2: SEM images of Pt films on YSZ of catalysts at 1000 and 10000 magnifications of the ESL 60 min after electrochemical experiments

4.1.2 ICP-OES Results

Next, the ICP-OES results of the three Pt catalysts and the sintered films, as shown in Table 4.1 and Table 4.2, are discussed. The quantitative analysis was at this point inconclusive as the level of trace elements found in the deionised (DI) water was of the same order of magnitude as the impurities in the catalysts and therefore significant error is associated with the calculation of the absolute values of the impurities concentration. As can be seen in Table 4.2 a range of impurities was found in the three catalysts in concentrations that ranged from 0.001 % to 1.234 % wt. However, different impurities were found in the sintered films in concentration that ranged from 0.002 % to 1.595 % wt. This is anticipated as a lot of the impurities may migrate from the bulk to the surface of the catalyst film and volatilise during the sintering process. Moreover, during the electrode preparation impurities could have also been introduced from the YSZ substrate.

In terms of their (impurities) effect on catalytic and electrocatalytic performance, the most important impurities are those found on the catalyst films after sintering. The sintered ESL catalyst films contained mainly Bi and Si. The sintered Heraeus film contained Bi of approximately 0.336 % wt., Pb, Ca and Si. The Metalor catalyst film showed only 0.04 % wt. Bi as the main impurity which is lower than that of the ESL

samples. The different type and amounts of impurities in each catalyst and the sintered films are expected to cause differences in the catalyst catalytic and electrocatalytic behaviour as some of these elements may have promoting properties while others may cause active-site or tpb blocking.

4.1.2.1 Effect of Sintering Time

Winkel et al. [102] had shown that as the temperature treatment time increases heavy metal concentration decreases. In the current work, this is demonstrated by the ICP results in which the longer the sintering time of the Pt film, either among the same or different providers, the lesser impurity remains on the Pt surface. For the case of the ESL samples, this is indicated by the lower concentration of Bi which was found in the ESL 60 min film (0.185 % wt.) than that of the ESL 10 min film (1.595 % wt.). Besides that, the Metalor film, which has the longest sintering time among the catalysts (2 hours), appears to have a lower level of impurities while the Heraeus and ESL 10 min films have more impurities remaining on the Pt surface.

Table 4.1: Known impurities in YSZ and platinum found in the literature and present work

Sample	Analytical methods	Impurities	Reference
YSZ (111) single crystal without Pt electrode	Tof-SIMS	Na, K, Ca, Cr, Al, C, Si, Mg, Fe	[8]
Commercial Pt paste without sintering aid	GDMS glow discharge mass spectrometry	Fe, Pd, Rh, Al, Cr, Si	[8]
10 mg samples of pure platinum metal	Ion Exchange Chromatography and Ge (Li spectrometry)	Au, Cu, Ir, K, La, Mn, Pd and Zn	[104]
Highly pure Pt	ICP-AES	Mg, Mn, Cu, Ag, Fe, Zn, Au, Ir, Ni, Pb, Rh, Al, Pd	[96]
Pt resins/pastes	ICP-OES	Bi, Ca, Au, Zn, Fe, Ni, Cr, Si	Present work
Sintered Pt films	ICP-OES	Bi, Si, Ca, Pb	Present work

Table 4.2: Impurities in the three commercial platinum catalysts

Providers	Impurities in catalysts		Impurities in sintered catalyst films	
	Impurities Content	wt.%	Impurities Content	wt.%
ESL	Bi	1.234	60 min sample: Bi	0.1855
	Ca	0.1743		
	Au	0.0188		
	Cr	0.0228	10 min sample: Bi	1.595
	Zn	0.0209	Si	0.6333
	Fe	0.0108		
	Ni	0.0070		
Heraeus	Zn	0.0117	Bi	0.3356
	Si	0.0590	Pb	0.2219
	Fe	0.0184	Si	0.9825
	Ni	0.0059		
	Cr	0.0030		
	Au	0.0006		
Metalor	Fe	0.0364	Bi	0.0400
	Si	0.0260		
	Cr	0.0082		
	Ni	0.0044		
	Zn	0.0033		
	Au	0.0006		

4.2 Electrochemical Characterisations under a Nonreactive Condition

This section presents the features in the CV of the Pt/YSZ system using the three catalysts and correlates the features with the impurities and the morphology of the sintered catalyst films. The voltammograms obtained at 400 °C for the four samples, which includes Heraeus, Metalor, ESL 60 min and ESL 10 min, are shown in Figure 4.3. The scan rate during the CV was 30 mVs⁻¹ and the voltage was scanned from -1.0 V to 0.50 V under the flow of 200 mlmin⁻¹ 20% O₂/He. As depicted in the voltammograms of the ESL, Heraeus and Metalor catalysts, electrode surface morphology and impurities influence the oxidation and reduction of oxygen species in the Pt/YSZ system. These are manifested in the form of differences in the current range and the shape, size and position of the cathodic peaks in the voltammograms.

The current range of the four catalysts varies by almost two orders of magnitude with Heraeus exhibiting the lowest while ESL 10 min the highest which are $22 \mu\text{Acm}^{-2}$ and $800 \mu\text{Acm}^{-2}$, respectively. The current range of ESL 60 min is smaller than that of the ESL 10 min (ESL 10 min is assumed to be more porous than ESL 60 min based on the SEM images in Figure 4.1). The current range of ESL 60 min however is larger than that of the Metalor (Metalor should have least porosity based on Figure 4.1). These findings support the assumption on the porosity of the catalyst films discussed above in **section 4.1.1** since we expect that the sample of highest porosity shows the highest current (which is observed for the ESL 10 min). The smallest range which is observed for the Heraeus sample (which should be the case of the metalor) may indicate the interaction of the effects of morphology and impurities on the charge transfer reaction as discussed further below.

As indicated in Figure 4.3, a cathodic peak is observed in all cases and since the films are of a high tpb density (porous electrodes) the peaks are assigned to the reduction of oxygen chemisorbed at the tpb [32] as described in equation 20(d). The cathodic peaks which corresponds to oxide decomposition in the Metalor and Heraeus voltammogram are within -0.10 V to -0.30 V. The peaks in the ESL 60 min is broader which is within -0.10 V to -0.60 V. The peak of ESL 10 min, however, is observed at a more negative potential (which is within -0.20 V and -0.45 V which indicates more stable oxide formation at the tpb) in comparison to the other samples. Similar to the ESL 60 min, the ESL 10 min sample which has the highest Bi content also shows broad cathodic peaks during the CV. A study conducted by Arul Raj and Vasu [105] indicated that the cathodic peak broadens for an electrochemical system that contains Bi (i.e. the charge transfer process becomes slower). Anodic peak which corresponds to the reverse of the charge transfer reaction [32], however, is barely detectable in the voltammograms of the three catalysts which indicates that $\text{O}_{(\text{tpb})}$ was formed primarily from $\text{O}_{2(\text{g})}$ and not from O^{2-} .

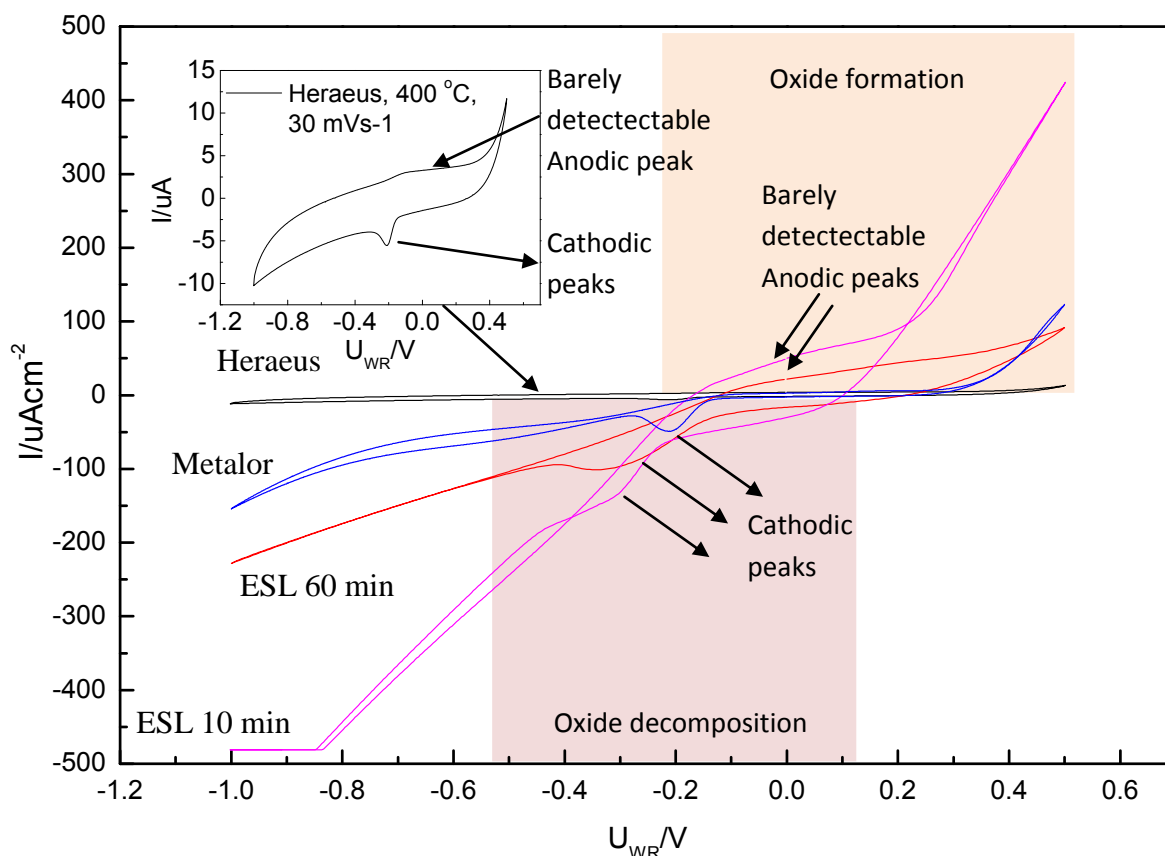


Figure 4.3: Voltammogram of ESL 10 min, ESL 60 min, Heraeus and Metalor at a scan rate of 30 mVs^{-1} , $400 \text{ }^\circ\text{C}$ and under the flow of $200 \text{ ml/min } 20\% \text{ O}_2/\text{He}$

These findings show that both microstructure and the amount and type of impurities of the catalyst film affect the charge transfer reactions. As was discussed earlier, both ESL and Heraeus catalysts should have a more porous structure than that of the Metalor and therefore the former should have higher tpb length than the later. This has been indicated by the cathodic behaviour of the voltammograms of the different samples where the sample of highest porosity and hence highest tpb length (ESL 10 min) shows highest current during the CV. However, we must recall that as discussed earlier the four catalyst films have different impurity content. The Heraeus sample has a higher Si content in comparison to the other three samples in addition to a moderate amount of Bi and Pb. The high Si content may be the reason why such low current are observed for this sample as Si can cause blocking of the tpb and slow down the charge transfer reaction [8]. Finally, the Metalor which has the highest purity of the four studied films studied here, shows very distinct cathodic peaks.

4.3 Further Discussions

The experiments conducted here had allowed us to gain an insight into the effect of catalyst microstructure and impurities on the charge transfer reactions. It would be very difficult however to predict the performance of the four catalyst films under catalytic and electrocatalytic conditions mostly due to the differences in the type and or amount of impurities found in each one. Both morphology and impurities effect may interact. The more porous microstructure should provide more active sites (tpb) for the charge transfer reactions to occur. However, the impurities may affect the catalytic behaviours of the samples in different ways either by promoting or poisoning (e.g. by blocking the catalyst active sites) the catalyst and therefore it would be very hard to predict what the overall effect would be. As an example, a study conducted on a Bi-promoted Pt(111) surface indicated that the rate of CO oxidation could be increased by the addition of Bi as it helps reduce the adsorbate energies on the catalyst surface due to the lower d-band centre energy for the Pt-Bi surface [106]. In contrast, Si is in general known to block catalyst active sites or poisoning the catalyst [8]. Moreover under the electrochemical promotion of catalysis (EPOC) condition the effect of impurities may change again. The impurities which may have a spectator role under open circuit may become activated under the polarisation and vice versa. Therefore, the EPOC behaviour of these systems should be further investigated in order to fully assess the role of these impurities.

4.4 Summary

The present work has shown that the three catalysts (i) contain different types and amount of impurities and (ii) the surface characteristics of the sintered films are different (impurities and morphology) where these factors influence the charge transfer processes in the Pt/YSZ system depicted by the features in the CV. Furthermore, the effect of both of impurities and morphology may interact which suggests that any of these factors cannot be disregarded and therefore a complex model is required to describe the charge transfer processes when porous electrodes prepared by using these catalysts are involved. Besides that, the geometric characteristics of the porous electrodes, such as film thickness, should vary among sample of the same and different providers since the electrodes were manually prepared by brushing the catalyst on the YSZ surface. Therefore, in order to reduce the complexity of geometry characteristics and for the

samples to have a similar amount and type of impurities, the utilisation of a model catalyst such as those prepared by sputtering is necessary. This is discussed in detail in Chapter 5 and 6.

Chapter 5. Oxygen Charge Transfer in a Pt/YSZ System Using Patterned Electrodes under a Non Reactive Condition

5.0 Introduction

Chapter 4 concludes that the utilisation of a model catalyst is necessary in order to reduce the complexity of geometry characteristics and to have samples of similar type and amount of impurities. This chapter demonstrates the utilisation of the model catalyst during the study of oxygen charge transfer in a Pt/YSZ system. The model catalysts are patterned electrodes of different width length scale in which the geometric characteristics have been described in Chapter 3 and **Appendix A**. The study included electrochemical experiments under a nonreactive condition at low temperature which consists of cyclic voltammetry (CV), electrochemical impedance spectroscopy (EIS) and current overpotential. The findings show that there are limitations in the application of the patterned electrodes as the model catalyst and hence treatments which can be carried out to minimise the limitations are therefore recommended. Besides that, an approach of investigating the behaviour of the system when the patterned electrodes are used under the limiting conditions is suggested.

5.1 Hypotheses

As discussed in Chapter 4, porous electrodes prepared by using catalysts of different providers have different impurity content and catalyst surface characteristics. Besides that, the geometric characteristics can also vary as a result of electrode preparation method. These differences lead to variations in electrochemical data and hence cause complexity in explaining the electrochemical behaviour of the Pt/YSZ system and to conduct a systematic investigation of the effect of a certain geometric parameter (such as the tpb length) on the charge transfer reactions and EPOC.

The patterned electrodes, on the other hand, were prepared by sputtering in which similar type and amount of impurities should present on the Pt surface for all samples in comparison to the porous electrodes. Also, the patterned electrodes were fabricated in such a way that samples of different geometric tpb length can be obtained. As described

in Chapter 3, this is well presented by the 3rd batch electrodes which have a more controlled geometric characteristic where all the samples are similar in the geometric surface area and Pt film thickness while differ in the tpb length. Since the geometric tpb length of the patterned electrodes is known for a given electrode surface area, it is expected that the electrochemical behaviour of the system in which the focus was on the charge transfer processes occurring at the tpb can be well demonstrated.

In this work, the charge transfer reaction at the tpb should be able to be described from the analyses of the electrochemical data of the patterned electrode of different (known) tpb length although the charge transfer is known can also occur at the other interfaces in the system. Besides that, processes which can take place at the tpb, such as surface oxide formation and decomposition, and changes in the electrode morphology, which can alter the tpb length of a sample, are in the same order of magnitude among the samples of different width length scale. In other words, it is assumed that (i) surface oxides formation per tpb length and (ii) the increase and or decrease of the tpb length per electrode surface area throughout the experimental works do not significantly vary among samples of different width length scale. Therefore these processes should not affect the correlation which is tried to be developed between the electrochemical data and the tpb length. It is assumed that tpb length is the only variable which has significant influences on the electrochemical behaviour when the results of patterned electrodes of different width length scale were compared.

5.2 Geometry Dependence Studies

This section presents the electrochemical results of the patterned electrodes of different width length scale which are compared to observe the geometry (tpb) dependence of the charge transfer reactions. The results consist of those obtained during the electrochemical impedance spectroscopy (EIS), current overpotential and cyclic voltammetry (CV) experiments which were carried out by using 4 μm , 40 μm , 400 μm and 200 μm samples from the 3rd batch under the nonreactive condition (where the electrodes were exposed to approximately 100 mlmin⁻¹20% O₂/He at temperatures between 300 °C and 450 °C).

5.2.1 Electrochemical Impedance Spectroscopy (EIS)

Figure 5.1 shows the impedance spectra of the 4 μm , 40 μm and 400 μm at 400 °C while Figure 3 in **Appendix C** indicates the impedance spectra of the 40 μm and 400 μm at different temperature. The impedance spectra of the samples consisted of two semicircles, at low and high frequency range, respectively. In this work, grain boundaries can be excluded in the impedance spectra as YSZ is a single crystalline [14]. Similar to the findings of Reddy et al. [90], the resistance values decrease with temperature for all samples. For all the samples of different width length scale, the radius of the first semicircles at a higher frequency range at each temperature and at most of the potential used during the EIS measurements are similar where the values decrease with temperature. Therefore, the charge transfer resistance represented by the first semicircle is taken as the bulk ionic resistance in the sample.

In contrast to the radius of the first semicircle, significant differences were observed in the radius of the second semicircle (at the lower frequency range) in the 4 μm , 40 μm , and 400 μm EIS spectra at each temperature and at most of potential used. The charge transfer resistance values at the lower frequency range are due to the electrodes which are related to the rate determining step of the electrochemical oxygen exchange reaction. Smallest length scale should exhibit lowest resistances due to the higher tpb length while the largest length scale should exhibit highest resistances. However, this is not observed in most of the EIS spectra in the current work and this is discussed in section 5.2.4.

Besides that, the resistance from the impedance spectroscopy experiments is three order magnitudes lower than the values in the previous works utilising dense electrodes [13,14,102]. The lower resistance measured in the current work indicates that the patterned electrodes are not as dense as those used by the other researchers. This is also supported by the SEM images of the patterned electrodes at a nm scale indicated in Figure 5.2. The images are provided by Dr. Danai Poulidi and Dr. Evangelos Papaioannou in which the analysis was conducted at the University of Giessen.

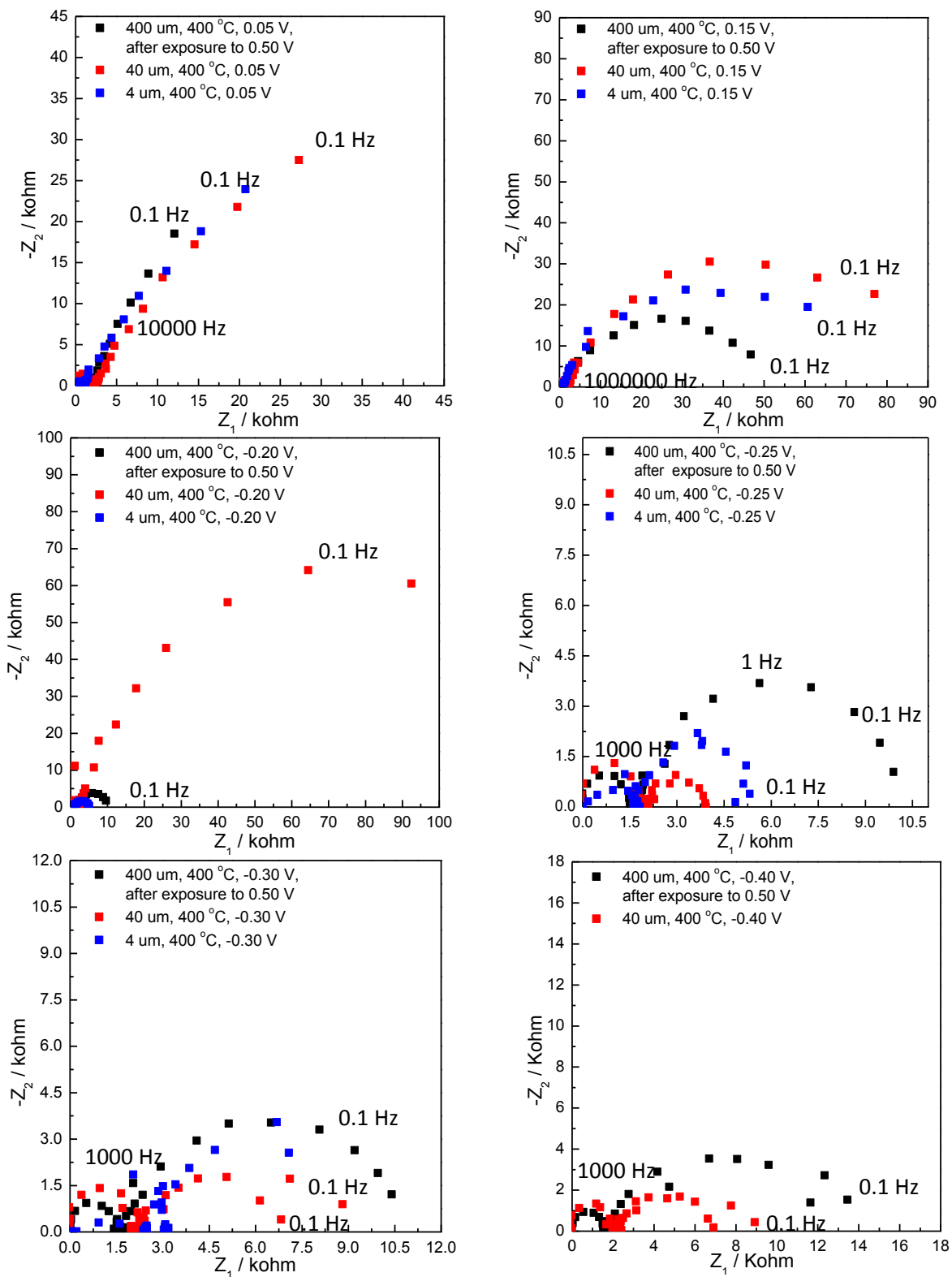
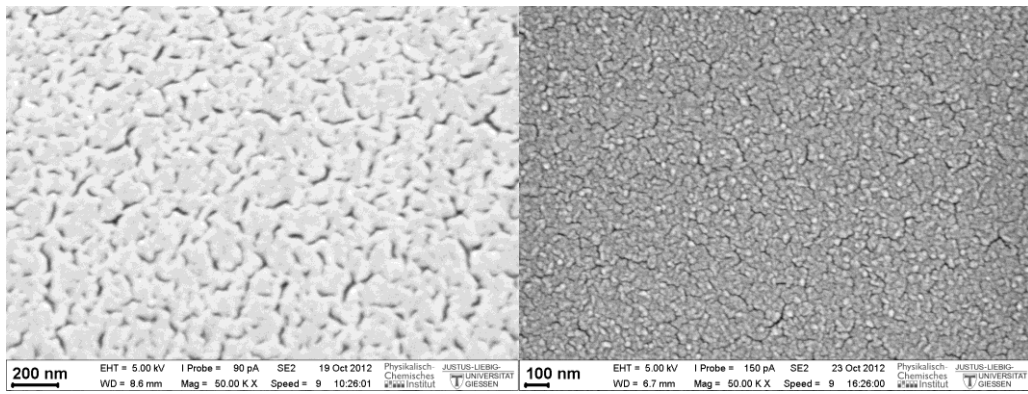
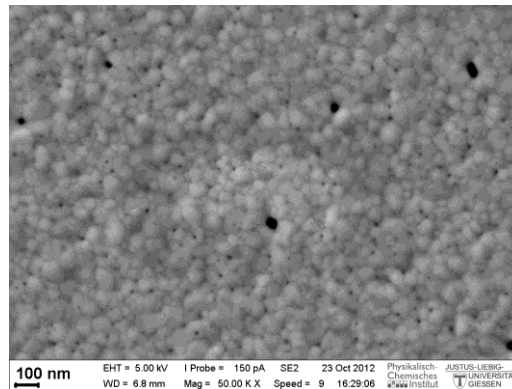


Figure 5.1: EIS spectra of the 4 μm , 40 μm and 400 μm at 400 $^\circ\text{C}$, under the flow of 100 mlmin^{-1} 20% O_2/He , the frequency was in the range between 0.1 Hz to 1000000 Hz



(a) 40 μm

(b) 200 μm



(c) 400 μm

Figure 5.2: SEM images of the fresh patterned electrodes of (a) 40 μm, (b) 200 μm and (c) 400 μm at a nm scale (the images are provided by Dr. Danai Poulidi and Dr. Evangelos Papaioannou)

5.2.1.1 Estimation of the Charge Transfer Resistance from the Diameter of the Semicircle

The charge transfer resistance or the diameter of the second semicircle from the impedance spectra were approximated by using equation (34) which is the equation of a circle.

$$(x-h)^2 + (y-k)^2 = \text{radius}^2 \quad (34)$$

x and y are the values of Z_1 and $-Z_2$ for each frequency from the impedance spectra (as indicated in Figure 5.3), respectively. The equation is simplified by inserting (h,0) as (h,k) and h as radius.

$$(x-h)^2 + (y)^2 = h^2 \quad (34a)$$

$$x^2 - 2hx + h^2 + y^2 = h^2 \quad (34b)$$

$$x^2 + y^2 = 2hx \quad (34c)$$

$$h = x^2 + y^2 / (2x) \quad (34d)$$

$$\text{Charge transfer resistance} = 2h \quad (34e)$$

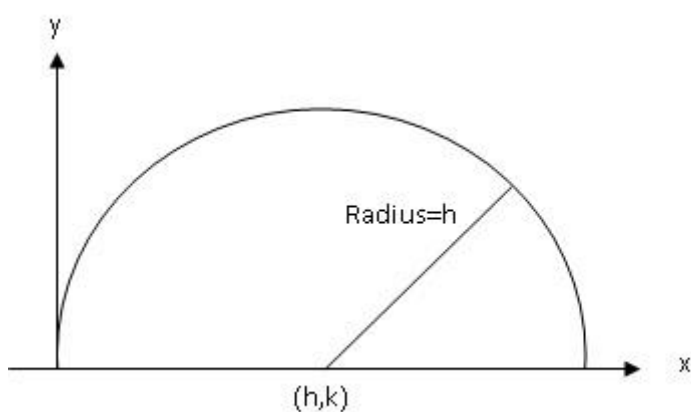
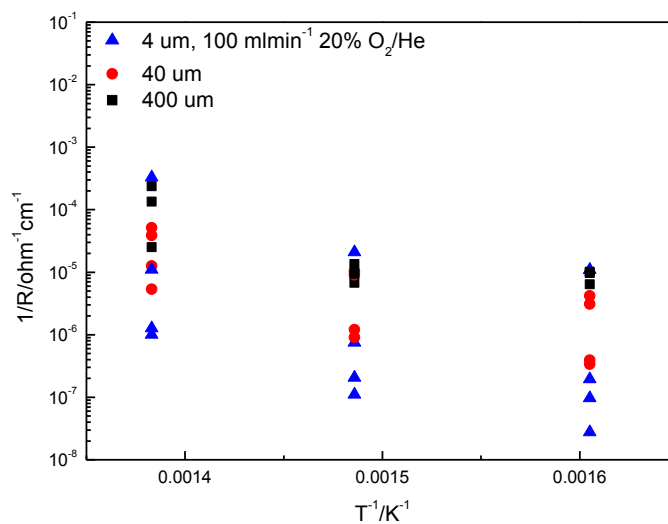


Figure 5.3: A semicircle with a centre (h,k) and a radius of h

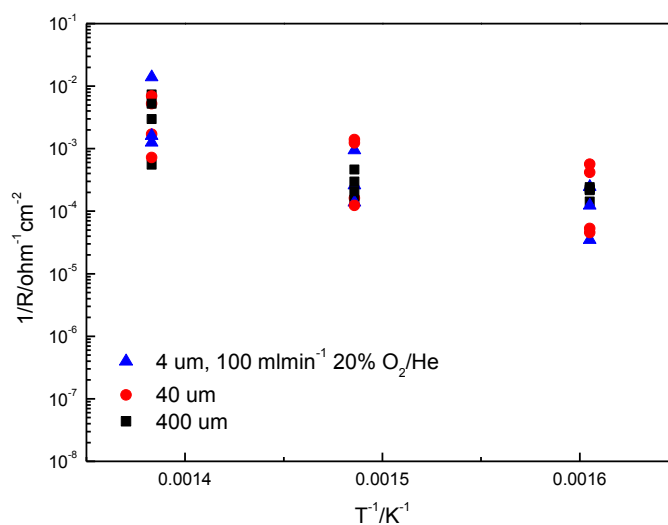
5.2.1.2 Arrhenius Plots of Conductance

The conductance (or the inverse of the charge transfer resistance) from the impedance spectra of 4 μm , 40 μm and 400 μm at each applied potential, at 350 $^{\circ}\text{C}$, 400 $^{\circ}\text{C}$ and 450 $^{\circ}\text{C}$ are shown in **Table 2 in Appendix C**. The experiments were carried out under the flow of 20% O_2/He . The charge transfer resistances were approximated by using equation (34e). The inverse of the charge transfer resistance or the conductance was normalised either to the geometric tpb length or to the geometric surface area. Then, the normalised conductance was plotted versus the reciprocal of temperature, T^{-1} . This plot, which is indicated in Figure 5.4, is the Arrhenius plot of conductance. The plot is analysed to investigate the geometry dependence of the charge transfer reaction in the Pt/YSZ system utilising the patterned electrodes. According to Opitz and Fleig [14], the geometry dependence of the charge transfer reaction is observed when all the regression lines in the

Arrhenius plots fall together. From the Arrhenius plots, regression lines of the area related conductance fall together at low and high frequency range which should not be the case of the tpb related conductance. The tpb dependence of the conductance and hence the charge transfer reactions is therefore not observed from the Arrhenius plots.



(a)



(b)

Figure 5.4: The Arrhenius plots of low frequency conductance that are normalised to the electrode geometric (a) tpb length and (b) surface area of the 4 μm , 40 μm and 400 μm samples

5.2.2 *Current Overpotential*

Figure 5.5 shows the plots of current overpotential of the 4 μm , 40 μm , 200 μm and 400 μm samples at 350 $^{\circ}\text{C}$, 400 $^{\circ}\text{C}$, and 450 $^{\circ}\text{C}$. The current overpotential plots of the 4 μm , 40 μm , 200 μm and 400 μm samples indicate a butler-volmer exponential current voltage relationship at low cathodic potential while a diffusion limitation behaviour is shown at high cathodic potential. The measured current range which are normalised to sample width length scale and electrode surface area are shown in Figure 5.6. The observed current range is in accordance to Pöpke et al. [15] and two order magnitudes higher than the values reported by Opitz et al. [102]. As indicated in Figure 5.6 (a), current range, which is normalised to the width length scale, decreases as width length scale increases (or tpb length decreases). No definite conclusion however can be derived from the correlation between the current range, which is normalised to the catalyst surface area, and the tpb length as described by Figure 5.5 (b).

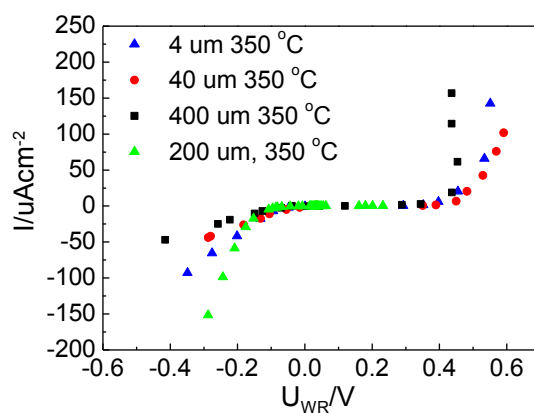
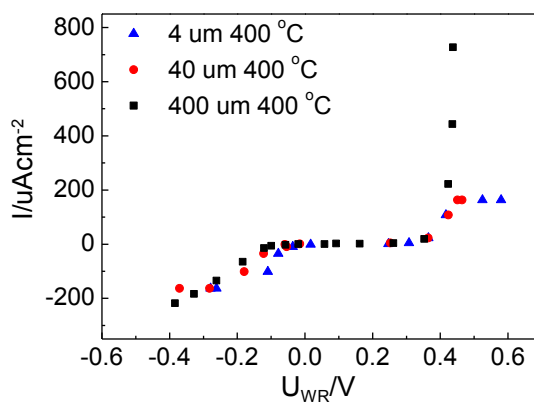
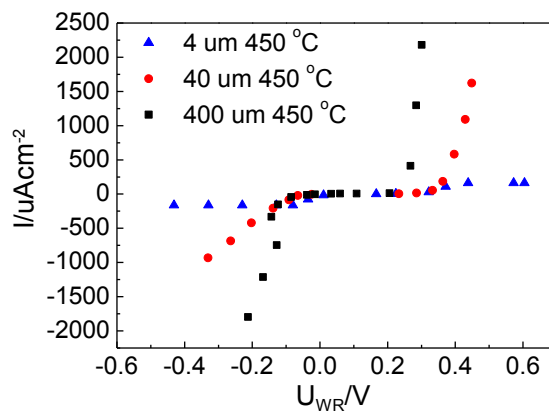
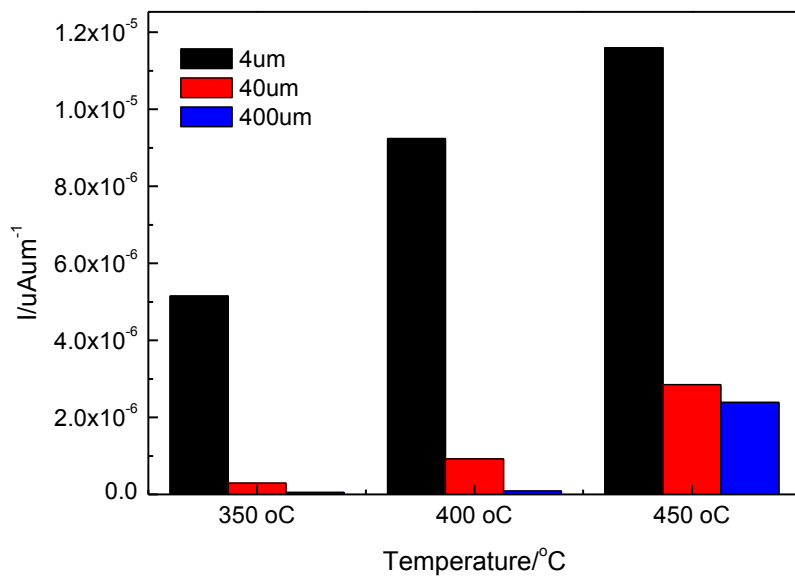
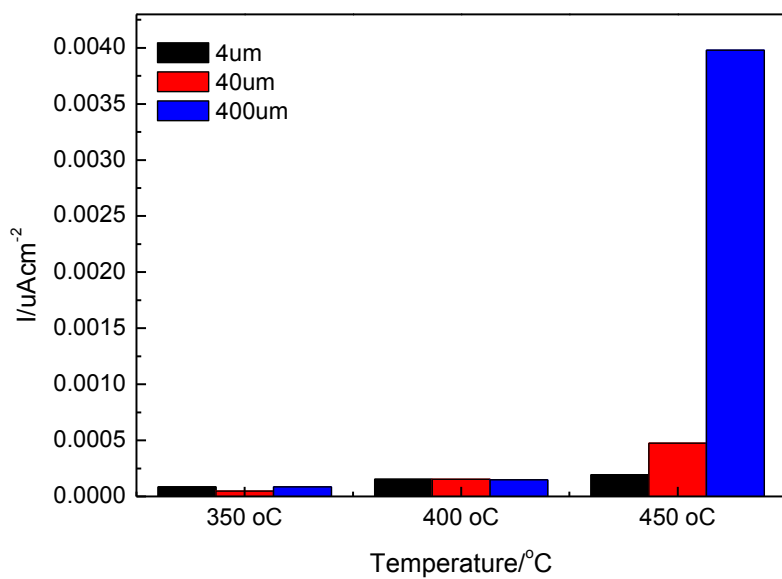


Figure 5.5: Current overpotential curves of 4 μm , 40 μm , 200 μm , 400 μm samples at 350 $^{\circ}\text{C}$, 400 $^{\circ}\text{C}$ and 450 $^{\circ}\text{C}$ under a nonreactive condition (90 to 100 mlmin^{-1} 20 % O_2/He)



(a)



(b)

Figure 5.6: Current range of 4 μm , 40 μm and 400 μm samples at 350 $^{\circ}C$, 400 $^{\circ}C$ and 450 $^{\circ}C$ under a nonreactive condition 90 to 100 $mlmin^{-1}$ 20 % O_2/He which are normalised to electrode geometric (a) width length scale and (b) surface area

5.2.2.1 Exchange Current Density

Exchange current density, I_0 , provides a measure of how fast ions are discharged at the metal/solid ionic interface [9] and can be extracted from the tafel plots [32]. Figure 5.7 shows I_0 extracted from the tafel plots of the 4 μm , 40 μm , 200 μm and 400 μm (from the results shown in Figure 5.5). The exchange current density should be proportional to the tpb length since it is exactly at this interface that the electrocatalytic charge transfer reaction is taking place [32]. However, as indicated in Figure 5.7, this is not observed except at 300 $^{\circ}\text{C}$.

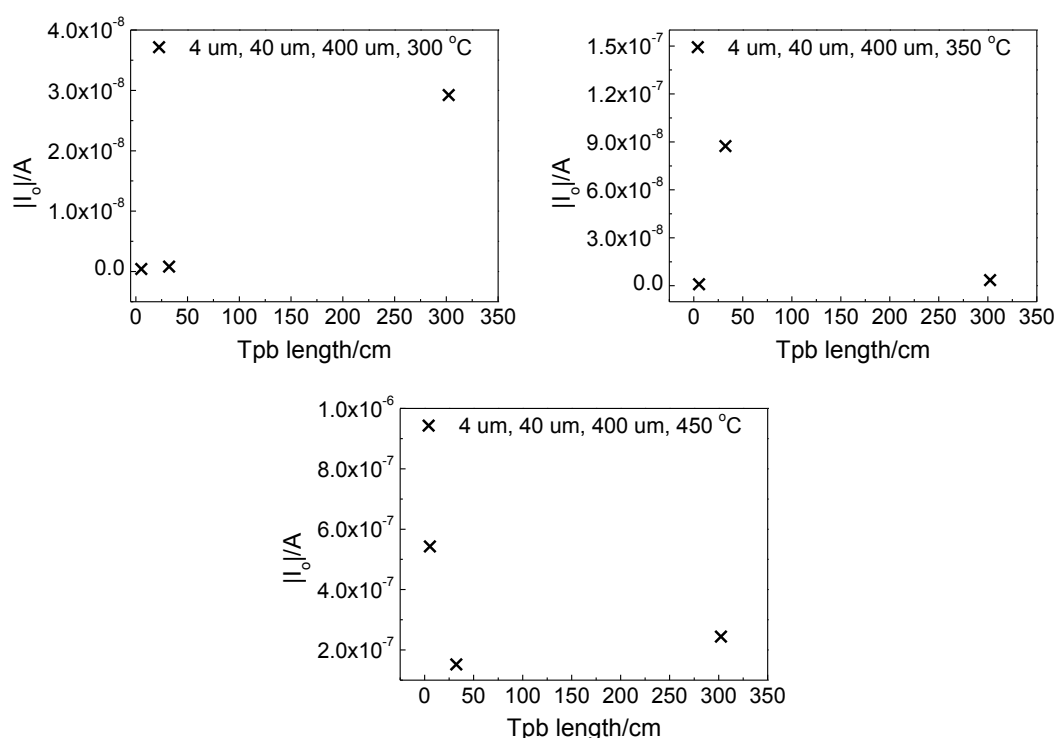


Figure 5.7: Absolute values of exchange current densities (from the results of current overpotential experiments of 4 μm , 40 μm , 200 μm and 400 μm samples at 300 $^{\circ}\text{C}$, 350 $^{\circ}\text{C}$, 400 $^{\circ}\text{C}$ and 450 $^{\circ}\text{C}$ shown in Figure 5.5)

5.2.3 Cyclic Voltammetry (CV)

Cyclic voltammograms of the 4 μm , 40 μm and 400 μm at 400 $^{\circ}\text{C}$ at different scan rate (10 mVs^{-1} , 20 mVs^{-1} , 30 mVs^{-1} , 50 mVs^{-1} and 100 mVs^{-1}), which had been exposed to a 0.50 V anodic potential, under a nonreactive condition are indicated in Figure 5.8.

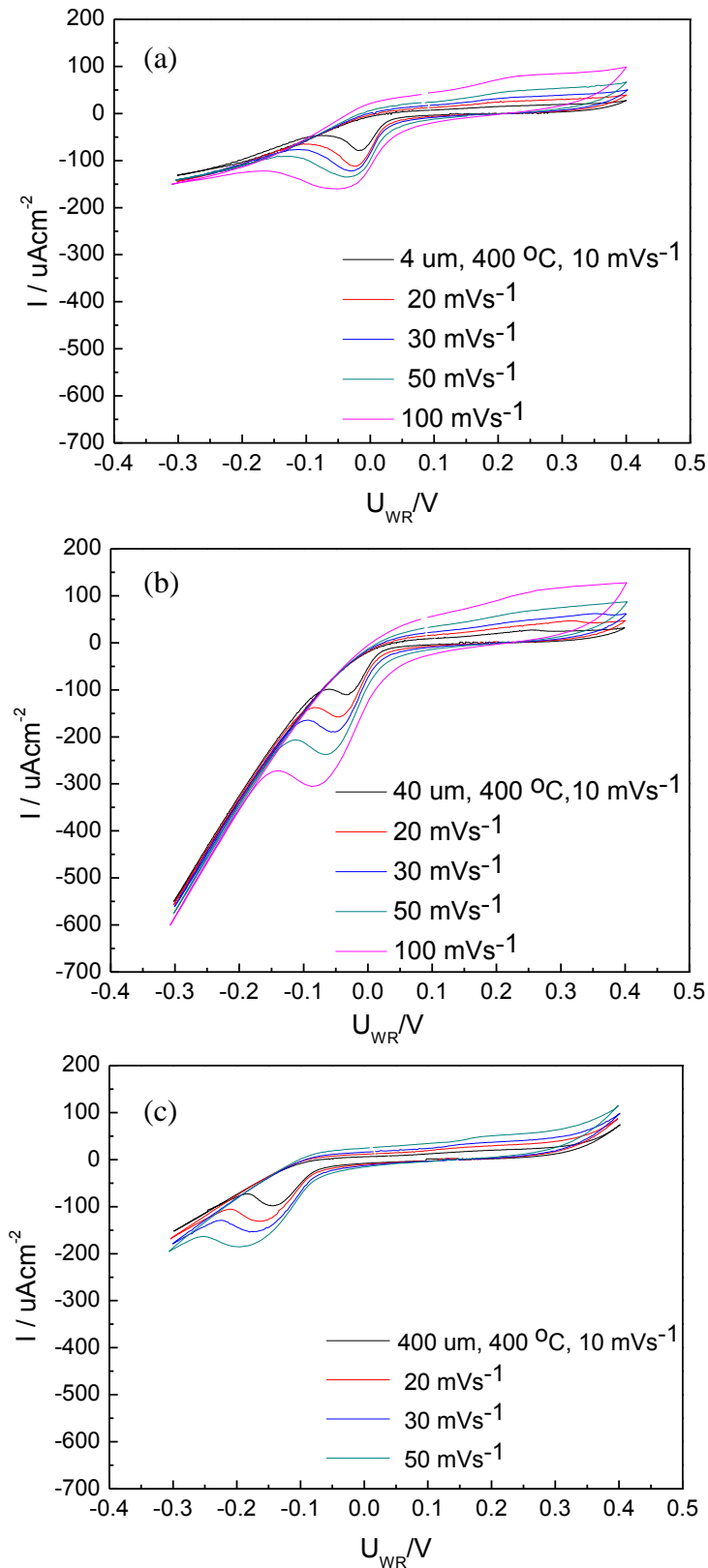


Figure 5.8: Cyclic voltammograms of the (a) 4 μm , (b) 40 μm and (c) 400 μm at 400 $^{\circ}\text{C}$ at different scan rate (10 mVs^{-1} , 20 mVs^{-1} , 30 mVs^{-1} , 50 mVs^{-1} and 100 mVs^{-1}) under a nonreactive condition 90 to 100 mlmin^{-1} 20 % O_2/He

5.2.3.1 Effect of Scan Rate

As shown in Figure 5.8, cathodic peaks are observed for all samples at all scan rates. As the scan rate increased, features of the voltammograms changed where the cathodic peaks current grow and the peak potentials shifted toward more negative values. The cathodic peaks were observed between the potential of 0.05 V and -0.30 V for the 4 μm , between 0.20 V and -0.20 V for the 40 μm samples and between -0.05 V and -0.30 V for the 400 μm sample. The peaks are commonly assigned in the literatures to the decomposition of Pt and or impurity oxides either at tpb or Pt/YSZ interface which will be discussed below in detail.

5.2.3.2 Geometry Dependence

Next, the voltammograms of the 4 μm , 40 μm and 400 μm which are shown in Figure 5.8 are compared to study the geometrical or tpb dependence of the charge transfer reaction in the Pt/YSZ system. Figure 5.9 indicates current range of the 4 μm , 40 μm and 400 μm which was calculated from the highest anodic and cathodic current during the CV. The 40 μm exhibits the highest current range while the 4 μm shows the lowest current range. The current range of the 400 μm sample was smaller than that of the 40 μm sample and almost similar to the range of the 4 μm sample. As shown in Table Appendix A, the geometric tpb length of the 4 μm , 40 μm and 400 μm samples are 302.3 cm, 32.3 cm and 5.3 cm, respectively. Based on the geometric tpb length, the 4 μm sample should exhibit the highest current range while the 400 μm should show the lowest current range and these were not observed in the current work. These should not be the case for a Pt/YSZ system which exhibits a tpb dependence of the charge transfer reaction.

Then, the correlation between peak height and the tpb length was studied. In most cases during the CV, the correlation between the peak height and the tpb length is not linear at 400 °C. For example, the nonlinear relationship (from the result of one experiment) is indicated in Figure 5.10. This finding is consistent with those observed during EIS and current overpotential where the tpb dependence of the charge transfer reactions is not well described by the geometry dependence studies. Moreover, since the linear relationship between the cathodic peak heights from the CV and the tpb length cannot be observed, the spillover species which can migrate through tpb and strongly adsorb at Pt/gas

interface is unlikely to cause the peaks in the voltammograms [8]. The peaks therefore are assigned to the decomposition of Pt and or impurity oxides at the Pt/YSZ interface and this is verified in **section 5.3**.

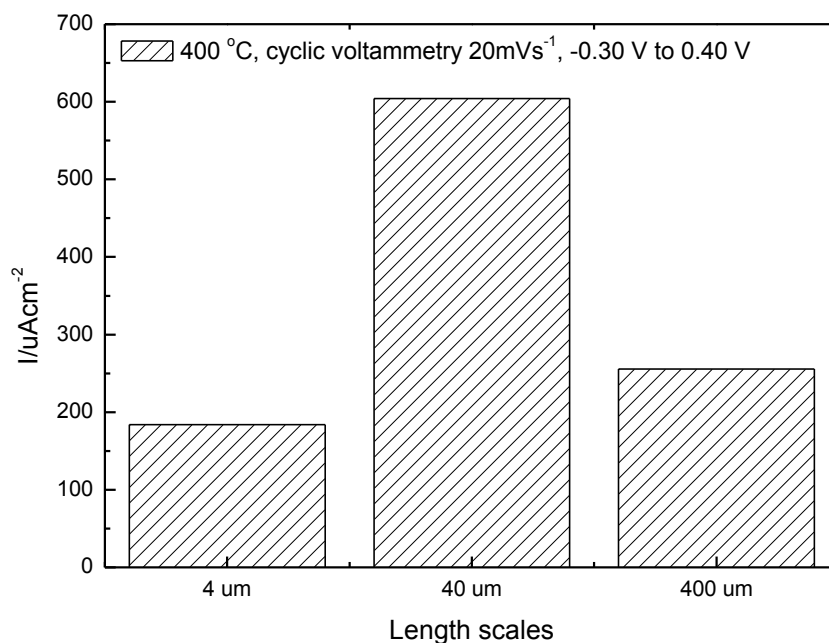


Figure 5.9: Current range of 4 μm , 40 μm and 400 μm sample at scan rates of 20 mVs⁻¹, reactor temperature 400°C, 90 to 100 mlmin⁻¹ 20% O₂/He

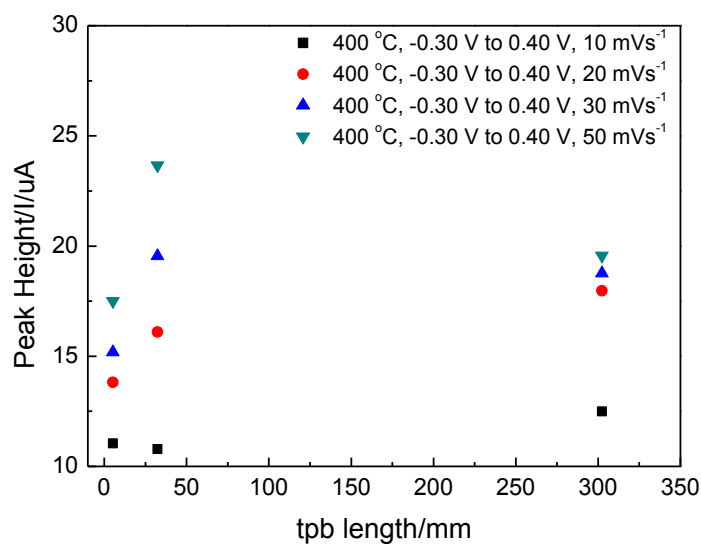


Figure 5.10: Cathodic peak heights from CV experiments of 4 μm , 40 μm and 400 μm samples at 400 °C and scan rates of 10 mVs⁻¹, 20 mVs⁻¹, 30 mVs⁻¹ and 50 mVs⁻¹

5.2.4 Summary

Investigation of the oxygen charge transfer dependence on the tpb length is important since electrochemical reactions involving reactants/electrode/electrolyte take place at tpb and this should be able to be described by the utilisation of the model catalysts or the patterned electrodes which are well characterised geometrically. However, the tpb dependence of the charge transfer reactions was not observed by comparing the electrochemical results of the patterned electrodes of different width length scale under the nonreactive condition. This observation can be explained by limitations due to

- (i) the structure of the patterned electrodes which is not completely dense although denser than that of the porous electrodes prepared by using the commercially available catalysts. Since the Pt surface area is similar among the electrodes of different width length scale, there should be additional tpb due to the porosity within the Pt lines and Pt block where 50 % of the total surface area (except for the 2 μm) is contributed by the Pt block. Therefore, the geometric tpb length (along the Pt lines) shown in Chapter 3 may only provide a lower limit of the actual length in which the actual tpb length may not differ significantly among the patterned electrodes.
- (ii) The tpb interface which may have been significantly blocked or hindered by passive oxide layer and therefore more charge transfer reactions took place at interfaces other than the tpb such as at the Pt/YSZ (this assumption is further verified in **section 5.3**). The tpb at the edge or along the Pt lines should be susceptible to oxidation. Based on this assumption, more oxides should be formed at the tpb of the electrode which has more Pt lines or of the smallest width length scale. This factor explains the lower current range of the 4 μm electrode, which is of the smallest width length scale, than that of the 400 μm electrode, which is of the largest length scale, at 400 $^{\circ}\text{C}$ and 450 $^{\circ}\text{C}$.
- (iii) the delamination of the Pt film which contributed to the decrease in the sample tpb length. The tpb length can decrease as a result of the formation of larger pores from small pores or cavities at the binary interface as a result of the effect of temperature. During the electrode fabrication, defects may be formed between Pt and YSZ interface such as small cavities or closed pores that can store oxygen and thus lead to the internal tpb and the oxygen in the pores can electrochemically exchange [14]. Increasing the reactor temperature before carrying out any

- (iv) electrochemical experiments may cause delamination of Pt film and or the formation of larger pores from the small cavities. The formation of larger pores from the small pores for the same Pt/YSZ surface area caused a decrease in the internal and external tpb available for the electrochemical exchange reaction. This effect is similar to the blocking of oxides at the tpb although the mechanism is different.
- (v) the changes in the electrode morphology caused by the formation of bubbles and or cracked bubbles which has significantly changed the tpb length and therefore the differences in the tpb length as described by the geometric length are no longer valid. This change in the electrode morphology is indicated by the SEM images of the Pt surface at μm scale after the sample has been exposed to the electrochemical experiments as shown in Figure 5.11 to 5.13. However, the order of magnitude of the changes in the electrode morphology should not be significantly different among the samples since the samples were exposed to almost similar experimental conditions. This is described in **Table 3 in Appendix C** by the average bubble diameter per Pt electrode surface area of the 4 μm and 40 μm which is in the same order of magnitude.

(a) Fresh

(b) After electrochemical experiments

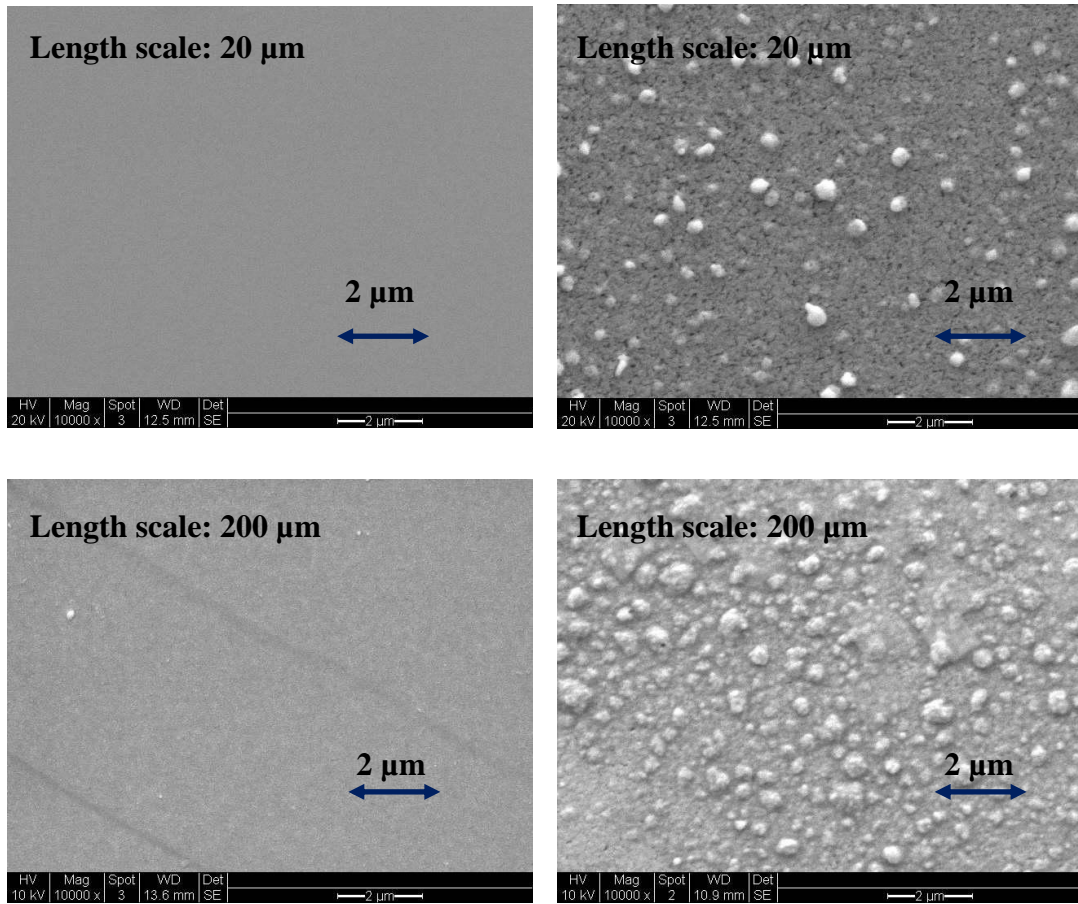
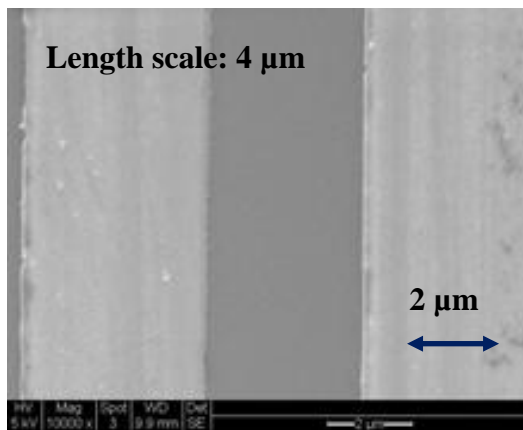


Figure 5.11: SEM images of the 20 μm and 200 μm from the 1st batch, (a) fresh and (b) after electrochemical experiments

(a) Fresh



(b) After electrochemical experiments

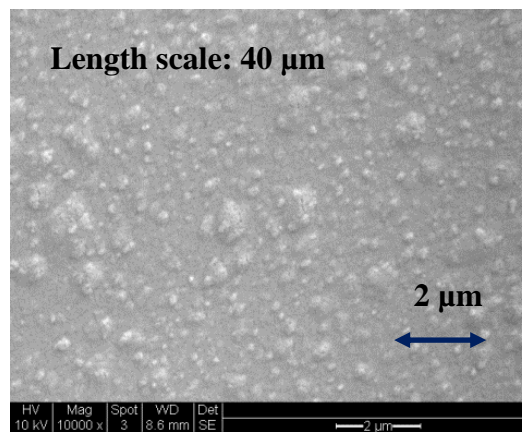
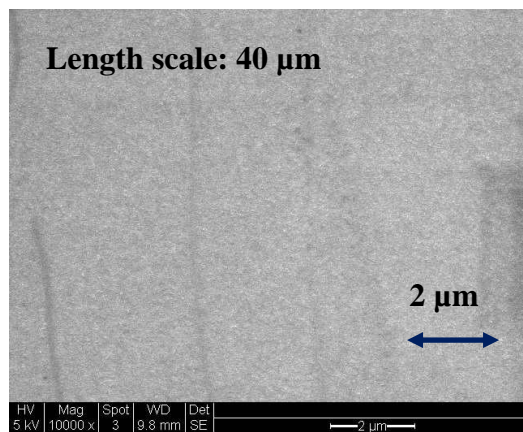
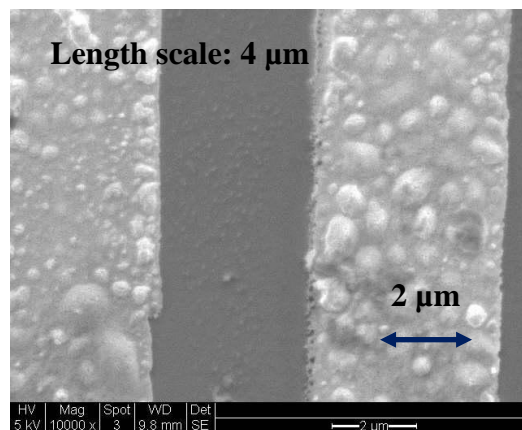
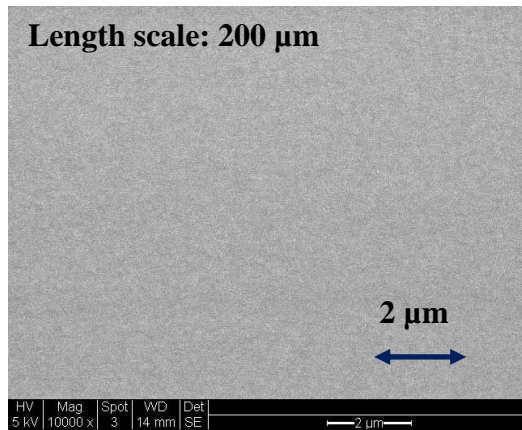
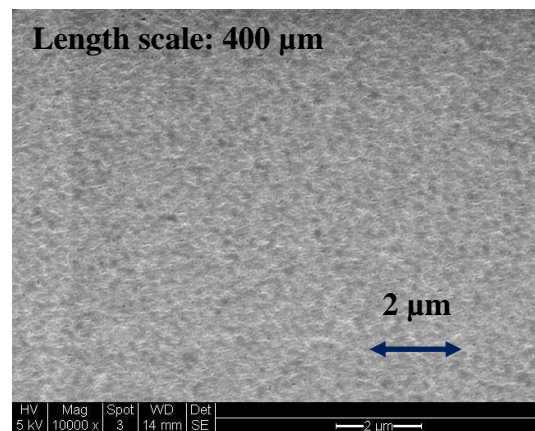
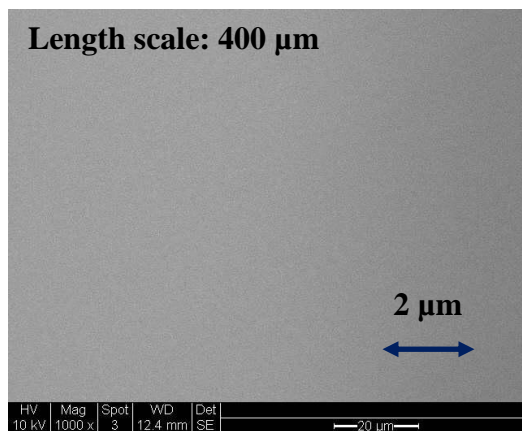
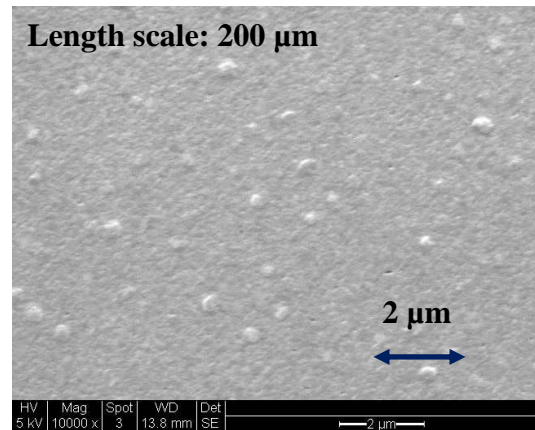


Figure 5.12: SEM images of the 4 μm and 40 μm from the 3rd batch , (a) fresh and (b) after electrochemical experiments

(a) Fresh



(b) After thermal treatment



(c) After electrochemical experiments

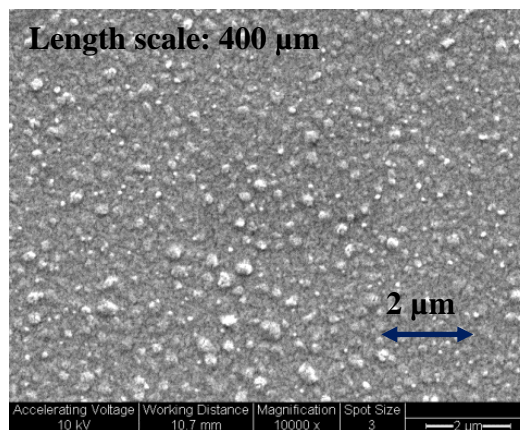


Figure 5.13: SEM images of the 200 μm and 400 μm from the 3rd batch , (a) fresh and (b) after thermal treatment (c) electrochemical experiments

5.3 Repeatability Study

The geometry dependence of the oxygen charge transfer in the Pt/YSZ system utilising the patterned electrodes cannot be demonstrated by the electrochemical results under the nonreactive condition discussed in the previous section. The complexity in developing a correlation between the electrochemical data and the tpb length has been suggested to be associated with the limitations due to the (i) patterned electrode design (which is not a completely dense surface structure) and or (ii) processes or changes occurring on the electrode surface. In order for the patterned electrodes to be utilised in the field and as a model catalyst (in a broader context), it is necessary to identify the factors which contribute to the changes in the electrode surface throughout its application or exposure to the experimental conditions. This can be obtained by monitoring the changes in the electrochemical data by focusing on the results of one sample and this analysis is termed in the present work as a repeatability study.

As demonstrated by Mutoro et al. [8], changes in electrode surface morphology for a case of a dense sample which resulted to the increase in the tpb length causes an increase in the total amount of oxygen exorporated during anodic polarisation at the tpb. This reduces the fraction of oxygen ions transported through YSZ to the Pt/YSZ interface where less oxide is then formed at this binary interface. In other words, changes in the tpb length cause changes in the oxygen activity in the system. Most important, the activity at the tpb can provide an insight into the activity at the binary interface and vice versa.

As also described by Mutoro et al. [8], the changes in the current density (mainly in the cathodic region) are associated (proportional) with the changes in the tpb length. This suggests that the analyses which focus on the changes in the current density during CV should allow us to have an insight on the changes in the tpb length and hence the changes of the oxygen activity at the tpb. Also, it has been suggested during the geometry dependence study (**section 5.2**) that cathodic peaks in the CV of the patterned electrodes provide information on the oxidation and reduction processes at the Pt/YSZ interface. Therefore, the analyses on the changes in the features in CV should provide details of the changes in oxygen activity at the tpb and the Pt/YSZ interface and thus the geometry dependence of the oxygen charge transfer which cannot be obtained from the electrochemical results of patterned electrodes of different width length scale.

The next step is therefore to correlate the processes taking place at the binary interface with those occurring at the tpb by focusing on the changes of the features in the CV of the 200 μm from the 3rd batch. The CV is a reference experiment which was carried out after exposing the 200 μm to each of the electrochemical experiments which included CV, EIS, current overpotential and kinetic and or EPOC. The features in the reference CV which were analysed were the current density and cathodic peak area. The changes in these features are then associated with the changes in number of the available sites for the charge transfer reactions which is in this case is the tpb. The reference experiments were carried out under a nonreactive condition

- (i) after each electrochemical experiment at each temperature (350 °C, 400 °C and 450 °C),
- (ii) at the reference condition at 350 °C after all the electrochemical experiments at each temperature were completed and
- (iii) before carrying out electrochemical experiments after the sample was left overnight in the reactor in air at room temperature.

In addition to the results of the 200 μm , the changes in the electrochemical data of the 400 μm are also included and discussed in this section. This is to determine if the changes of the electrochemical data to the experimental conditions are similar among the electrodes of different width length scale in which this analysis provides details on the reproducibility of the data when the patterned electrodes are utilised.

5.3.1 Correlation between Current Density and Cathodic Peak Height in CV

Figure 5.14 and 5.14 indicate the current density from the CV of the 200 μm at the reference condition after each of the electrochemical experiments at 350 °C, 400 °C and 450 °C. As demonstrated in the figures, a decrease and an increase in the current density are observed throughout the experimental works. This behaviour is associated with the electrode deactivation and activation phenomena. Before carry out further discussions on these phenomena and the mechanisms of the related processes, first, the current density is correlated with the cathodic peak area. This is to determine if there is a correlation between the changes in the tpb length and the changes in the oxygen activity at the binary interface.

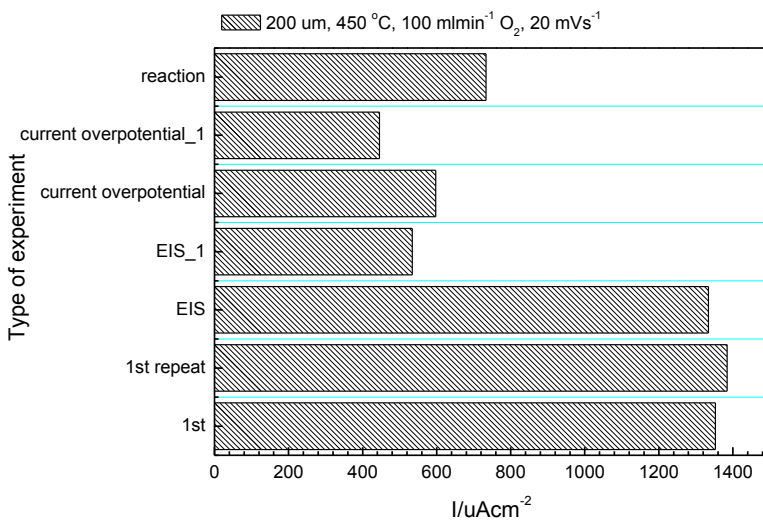
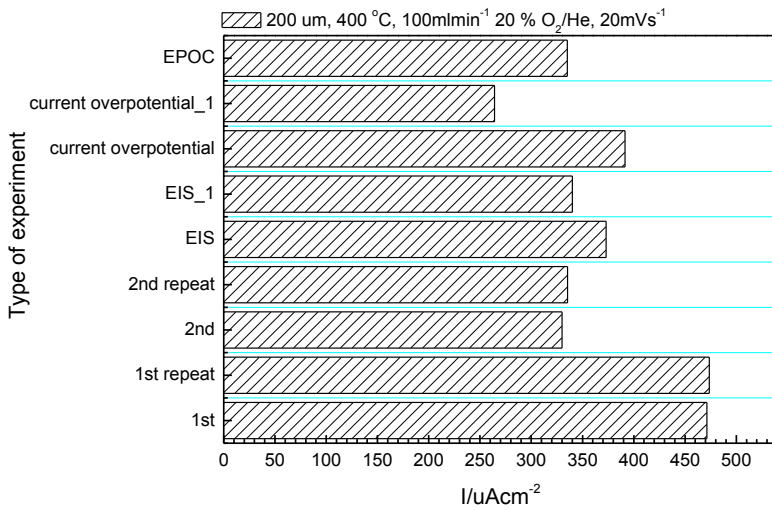
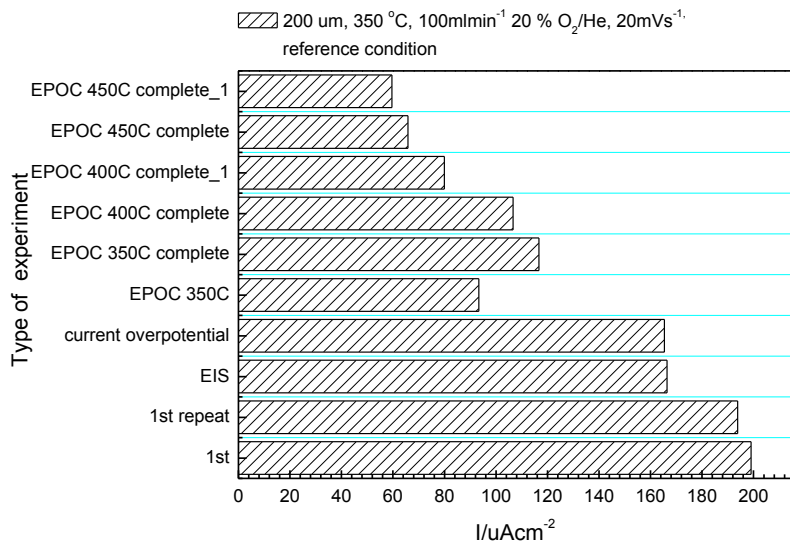


Figure 5.14: Current range during cyclic voltammetry of the 200 μm from the 3rd batch, 350 °C, 400 °C and 450 °C, 20 mVs⁻¹, 100 mlmin⁻¹ 20% O₂/He, -0.50 V to 0.10 V

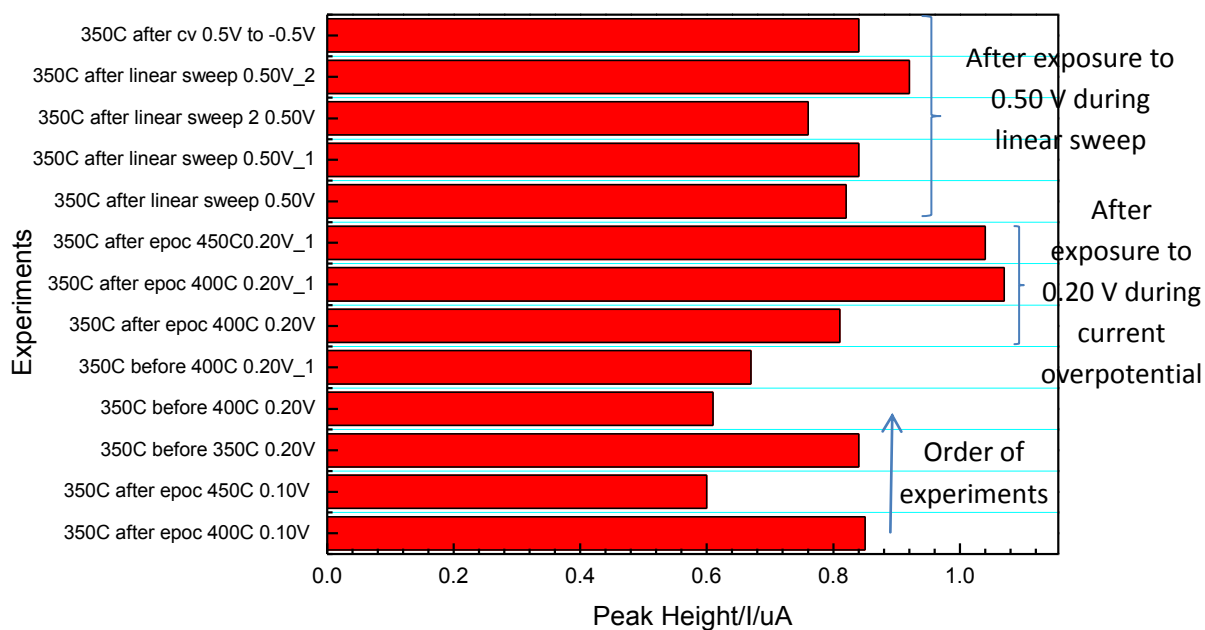


Figure 5.15: Cathodic peak height from results of cyclic voltammetry at the reference experiment condition, 200 μm , 350 $^{\circ}\text{C}$, 100 mlmin^{-1} 20% O_2/He .

The cathodic peaks from the voltammograms of the reference experiments were integrated to determine the amount of oxygen atom. The integrated values were then correlated with the current density also from the reference voltammograms and this is indicated in Figure 5.16. From the figure, the amount of oxygen atom is found to be inversely proportional to the current density at 350 $^{\circ}\text{C}$, 400 $^{\circ}\text{C}$ and 450 $^{\circ}\text{C}$. This relationship supports the cathodic peak assignment to the decomposition of Pt and or impurity oxides at Pt/YSZ or the binary interface. This is because if the peak corresponds to the decomposition of Pt and or impurity oxides at the tpb we should observe a proportional relationship between the current density and the amount of oxygen atom or current peak. Most important, this observation suggests the dependence of the oxygen activity at both interfaces in which oxygen activity at tpb can be described by a decrease or an increase in the oxygen activity at the Pt/YSZ interface.

Besides that, this finding suggests minimal delamination (if any) of the Pt film. This is because a decrease in the current density in the current work and thus the tpb length did not reduce the formation of Pt and or impurity oxides at the binary interface which should

not be the case when significant delamination is involved. Delamination should cause a significant reduction in the tpb and Pt/YSZ interface which are available for the charge transfer reactions. Therefore, there should be less formation of oxides at both of these interfaces which should be indicated by a decrease in the cathodic peak area in the CV [15] throughout the experimental works. However, this is not observed during the CV experiments on the 200 μm .

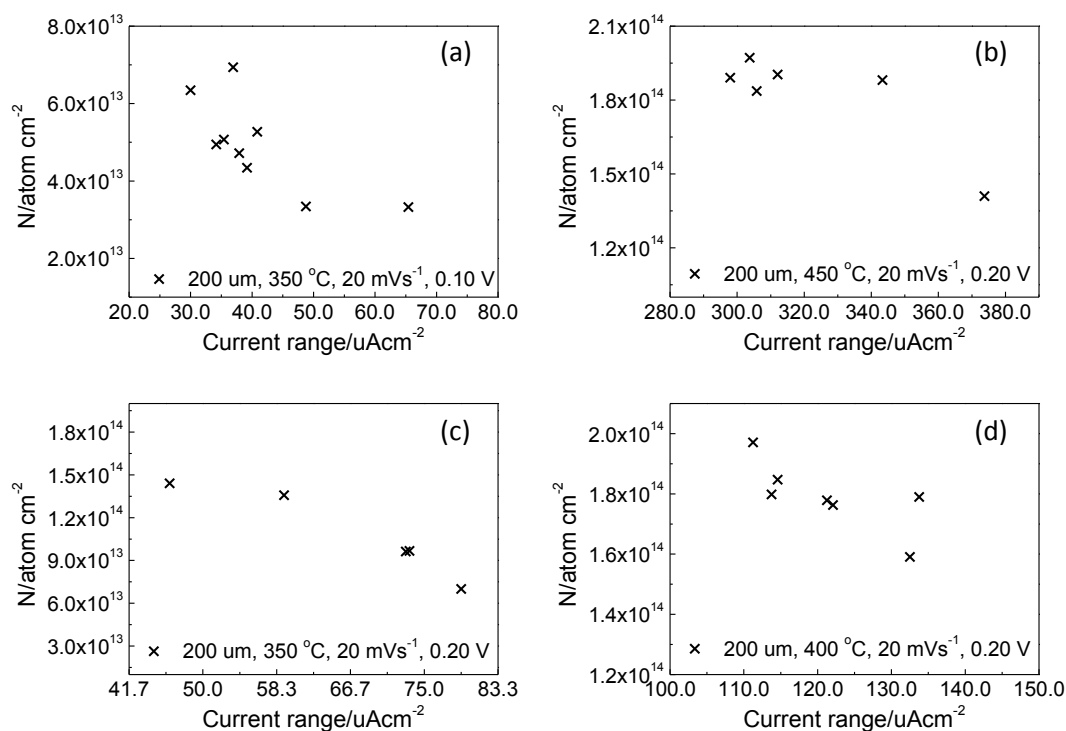


Figure 5.16: Correlation between the amount of oxygen atom and current range from the results of cyclic voltammetry experiments of 200 μm sample at the reference conditions, 20 mVs^{-1} (a) 350 $^{\circ}\text{C}$, 0.10 V, (b) 350 $^{\circ}\text{C}$, 0.20 V, (c) 400 $^{\circ}\text{C}$, 0.20 V and (d) 450 $^{\circ}\text{C}$, 0.20V

5.3.2 Electrode Deactivation and Activation Phenomena

The deactivation and activation of the patterned electrodes can be studied by analysing the changes in the electrochemical data such as current density and charge transfer resistance [15,16]. These phenomena are associated with (i) oxide formation at tpb and (ii) bubble and or cracked bubble formations. Oxidation of Pt can take place without electrochemical driving force in air under ambient oxygen pressure at elevated temperature which is within the thermodynamic stability range of Pt and or impurity

oxide, while the formation of bubbles and or cracked bubbles, as indicated in Table 5.1, are usually caused by the exposure to a large anodic potential [15] and also the effect of reaction and due to temperature gradient. Bubbles and or cracked bubbles formation can contribute to the electrode activation by providing more tpb interface and by hindering the formation of Pt oxide film [15].

5.3.2.1 Electrode Deactivation

As indicated in Figure 5.14, the current density of the 200 μm from the 3rd batch at 400 °C and 450 °C, decreases when the reference (CV) experiments were repeated after the 200 μm was left in the reactor overnight (in air at room temperature) during no experimental works. This result suggests that the deactivation of the 200 μm could be caused either by the processes occurring on the electrode surface during no experimental works or when the reactor temperature was increased to the temperature of interest before carrying out any experiments.

As mentioned above, the formation of a passive oxide layer at tpb is one of the possible explanations of the decrease in the oxygen activity (or oxygen charge transfer) at this interface [15]. This is further demonstrated by the peak, corresponds to the decomposition of Pt and or impurity oxide at the Pt/YSZ interface, which is only observed in the voltammograms when there is a significant decrease in the current density. This has been discussed in **section 5.3.1**. Another possible explanation of the deactivation phenomenon is Pt film delamination which can occur when the reactor temperature was increased to the temperature of interest before carrying out the electrochemical experiments. However, as described in **section 5.3.1**, this effect should be minimal.

This deactivation phenomenon was also observed during the electrochemical characterisations under the nonreactive condition of the fresh 4 μm , 40 μm , and 400 μm samples from the 3rd batch. In comparison to the 4 μm and 40 μm , more electrochemical experiments were carried out on the 400 μm which included studies at a small (0.10 V) and a large anodic (0.50 V) potentials. Therefore, the patterned electrodes deactivation and activation phenomena are further discussed by the results of the 400 μm . The responses of the electrochemical impedance spectroscopy (EIS) measurements at 400 °C and -0.45 V as shown in Figure 5.17 are similar to those of the CV and current

overpotential of this sample, as indicated in Figure 5.18. Therefore, this phenomenon can be demonstrated by discussing the results of the EIS measurement of the 400 μm .

The deactivation of the 400 μm after the exposure to the 0.50 V anodic potential is indicated by a significant increase in the charge transfer resistance. This observation is similar with the changes of the charge transfer resistance of a high tpb density sample demonstrated by Pöpke et al. [16]. The sample in the work of Pöpke et al. [16] was prepolarised by anodic potentials prior to the impedance measurement (which was carried out close to the open circuit potential) and the deactivation has been described due to the oxidation of Pt at the tpb during the anodic polarisation which led to a kinetic hindrance for the oxygen exchange.

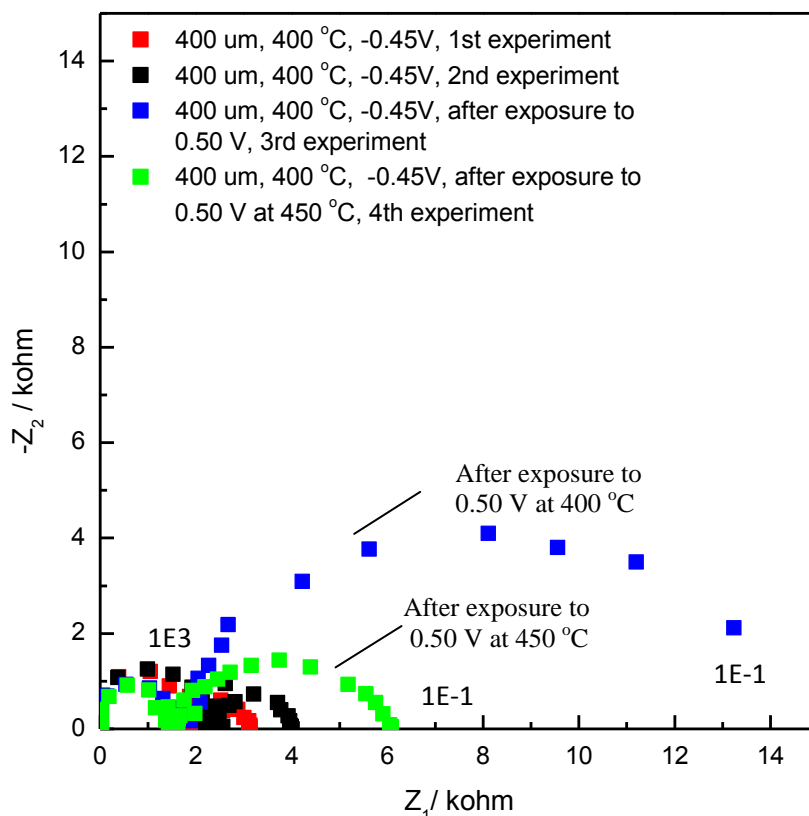


Figure 5.17: Impedance spectra of 400 μm at 400 $^{\circ}\text{C}$ under nonreactive condition, -0.45 V, before and after the exposure to 0.50 V

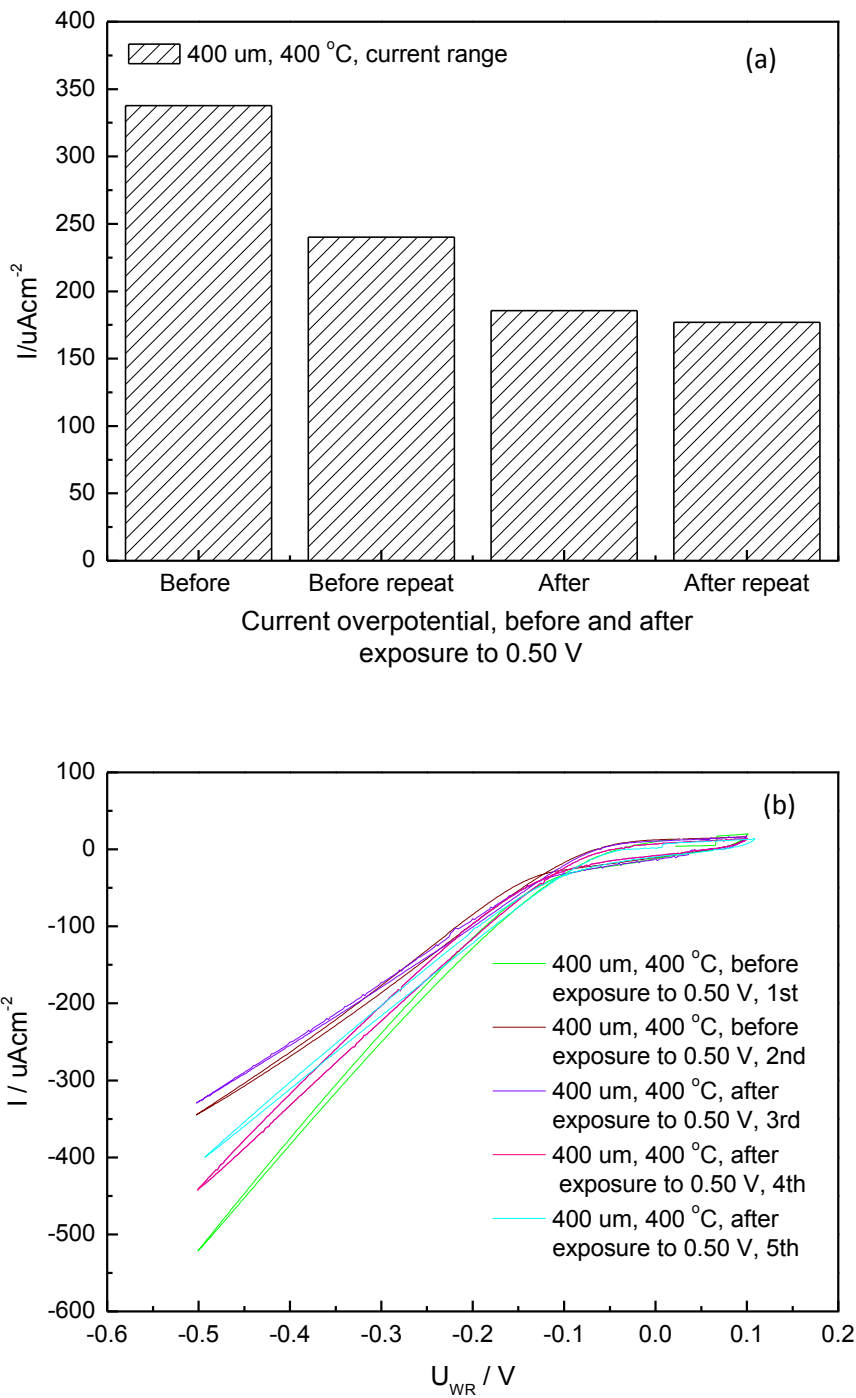


Figure 5.18: (a) Current range from the current overpotential curve and (b) voltammograms at 20 mVs^{-1} of the $400\text{ }\mu m$, at $400\text{ }^{\circ}C$, under nonreactive condition, $90\text{ to }100\text{ mlmin}^{-1}$, $20\%\text{ O}_2/\text{He}$ before and after exposure to a 0.50 V anodic potential

In the current work, the 400 μm was exposed to the 0.50 V anodic potential during a linear sweep experiment at 400 $^{\circ}\text{C}$. The EIS measurement was carried out after a CV experiment (which was carried out after the linear sweep). The exposure to the 0.50 V anodic potential at 400 $^{\circ}\text{C}$ during the electrochemical experiments should lead to electrode activation caused by the morphology activation effect due to the formation of bubbles and or cracked bubbles [15] as indicated by the SEM images in Table 5.1. This activation effect which is not observed after the exposure to the 0.50 V at 400 $^{\circ}\text{C}$, therefore, could be caused by the formation of oxide layer at tpb [16] within the experimental works where this oxide cannot be completely decomposed during the negative (-0.45 V) polarisation. Besides that, there is a possibility that the 400 μm surface structure may also have not changed significantly during the exposure to 0.50 V at 400 $^{\circ}\text{C}$ because a defective structure should cause a smaller blocking [16] and this is not observed current work.

5.3.2.2 *Electrode Activation*

Figure 5.14 and 5.15 also demonstrate the activation of the 200 μm , although not as significant as the deactivation phenomenon. This is indicated by an increase in the current density of the 200 μm when the reference experiment was carried out right after the electrochemical experiments that included EIS, current overpotential, kinetic and EPOC. This electrode activation can be explained by

- (i) the decomposition of surface oxides at tpb (a) by the -1.0 V negative polarisation during current overpotential and EPOC experiments and or (b) by CO during the kinetic and EPOC experiments and or (c) during anodic polarisation/oxygen pumping under the nonreactive condition.
- (ii) an increase in the tpb length due to the morphology activation effect [15] such as the formation of bubbles and or cracked bubbles caused by the effect of temperature and or prolonged 0.10 V polarisations during EPOC experiments.

For the case of the 400 μm , the morphology activation effect due to the exposure to anodic potential as described by Pöpke et al. [15] can only be observed in the EIS spectra at -0.45 V after further exposure to the 0.50 V at 450 $^{\circ}\text{C}$ during electrochemical experiments that included EIS, CV and current overpotential. This is indicated by the increase in the conductance which is close to (although lower than) the values of the first

and second EIS experiments which were carried out before the exposure to the 0.50 V.

The significant increase in the conductance could be due either to

- (i) the significant increase in the tpb length caused by the formation of bubbles and or cracked bubbles at 450 °C which can hinder the formation of Pt oxide film [15] or
- (ii) the decomposition of oxides at tpb during negative polarisation [16] at 450 °C
- (iii) the removal of surface oxides at tpb by oxygen during the experiments (during anodic polarisation/oxygen pumping) which were carried out under the flow of 20% O₂/He.

This electrode activation of the 400 µm by anodic polarisation after electrochemical experiments at 450 °C is also demonstrated by the reverse potential voltammograms of the 400 µm at 400 °C after the exposure to the 0.50 V at 450 °C as indicated in **Appendix C**. As can be seen in the voltammogram, there is an increase in the current density and thus tpb length accompanied by a decrease in the cathodic peak area or oxide formation at the binary interface (smaller cathodic peak) during the repeated reverse potential experiments.

The morphology activation effect suggests insignificant delamination of the Pt film of the 400 µm which could be due to the effect of temperature and polarisations. If the significant decrease in the current density and increase in the charge transfer resistance after the 0.50 V polarisation were due to the delamination of the Pt film, the current density and resistance cannot return to the values which are close to the results during the first measurement before the exposure to the 0.50 V. However, this is not the case in the current work.

5.3.3 Hydrogen Reduction

In the previous sections, it has been shown that the oxygen activity at the tpb which cannot be demonstrated by comparing the results of the patterned electrodes of different width length scale can be described by analysing the changes in the oxygen activity from the results of one sample or one length scale. This can only be observed at a condition when the tpb is assumed to be significantly blocked by surface oxides (in which a decrease in the oxygen activity at the tpb causes an increase in the activity at Pt/YSZ interface and vice versa). The formation and decomposition of surface oxides at the tpb

has also been associated with the patterned electrode deactivation and activation phenomena. Therefore, it is important in the current work to verify the presence of the oxides at the tpb and the influence on the behaviour of the Pt/YSZ system since this is considered as a limitation in the application of the patterned electrodes in the field or as a model catalyst.

Oxides at the gas exposed interfaces such as tpb and Pt/gas can be removed by exposing the sample to hydrogen. The removal of oxides at tpb should increase the number of the available sites for the charge transfer reactions and hence increase the oxygen activity at this interface which should be indicated by an increase in the current density (during CV) or conductance (during EIS). Since the processes occurring at the tpb and the binary interface are dependent on one another, this should be accompanied by a decrease in the oxygen activity at the Pt/YSZ.

Hydrogen reduction studies therefore were carried out on the 200 μm from the 3rd batch and the 200 μm 550 °C kinetic sample from the 2nd batch. In this study, changes in the current density and cathodic peak height of either a linear sweep or CV were analysed before and after the exposure to the hydrogen. The results of the experiments which were carried out prior to the reduction serve as a reference condition. In order to further verify the features in the voltammogram corresponded to the processes taking place at the tpb and the Pt/gas interface, the results are also compared with those of a similar study which was carried out by using a porous electrode (of a high tpb density) which was prepared by using the ESL catalyst. From this study the following hypotheses have been further verified and are discussed in detail below.

- (i) cathodic peaks observed in the voltammograms are due to the decomposition of Pt and or impurity oxides at the Pt/YSZ interface,
- (ii) the formation and decomposition of surface oxides at tpb contributed to the deactivation and activation of the electrode observed throughout the electrochemical experiments and
- (iii) Pt film delamination is not the major cause of the electrode deactivation.

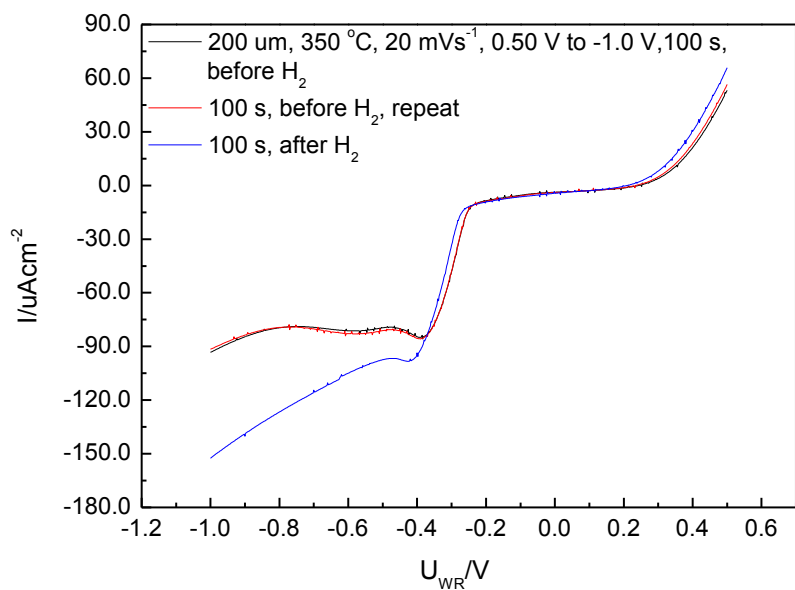
5.3.3.1 Surface Oxide Formation in the System Utilising Patterned and Porous Electrodes

The verification of the surface oxide formation at the tpb of the 200 μm from the 3rd batch (which is the same sample which has been used in the irreversibility study discussed in the previous sections) was conducted by (i) analysing the changes in the features in the linear sweep voltammograms during the hydrogen reduction study and (ii) by comparing the findings with the changes in the cyclic voltammogram of a porous electrode (also during hydrogen reduction study) which was prepared by using the ESL catalyst. Figure 5.19 (a) demonstrates the linear sweep voltammogram of the 200 μm sample at 350 °C before and after the hydrogen reduction. The sample was exposed to hydrogen at 500 °C. The effect of holding time on the (a) amount of oxygen atoms and (b) current range at 350 °C during the linear sweep are demonstrated in Figure 5.20. CV result of the ESL electrode which was carried out at 400 °C under a nonreactive condition before and after exposing this sample to hydrogen is shown in Figure 5.19(b). Table 5.1 demonstrates the electrode processes of the two systems (patterned and porous electrodes) which was modelled based on the linear sweep and CV results.

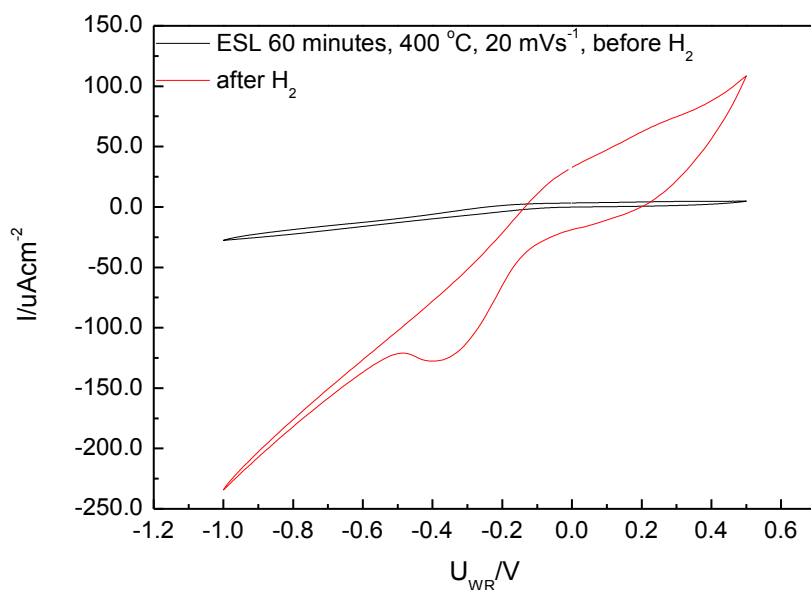
(a) 200 μm from the 3rd batch

In the system utilising the patterned electrode, during the linear sweep prior to the exposure to hydrogen as indicated in Figure 5.19 (a), two peaks were observed in the voltammograms and the assignment of these two peaks to the types of the involved species depends on the results of similar experiment after the hydrogen reduction. The second peak was observed after 40 s of holding time at the 0.50 V anodic potential.

As indicated in Figure 5.19(a) and Figure 5.20, an increase in the current density and reduction in cathodic peak areas were observed after the hydrogen reduction experiment. This result suggests that after the reduction there is an increase in the oxygen activity at the tpb and a decrease in the oxide formation. If the oxides are those formed at the tpb, an increase in the oxygen activity at this interface should lead to an increase in the peak height and area which is not observed in the current work. The peaks are therefore assigned to the processes occurring at the non-gas exposed interface such as at Pt/YSZ and Pt bulk.

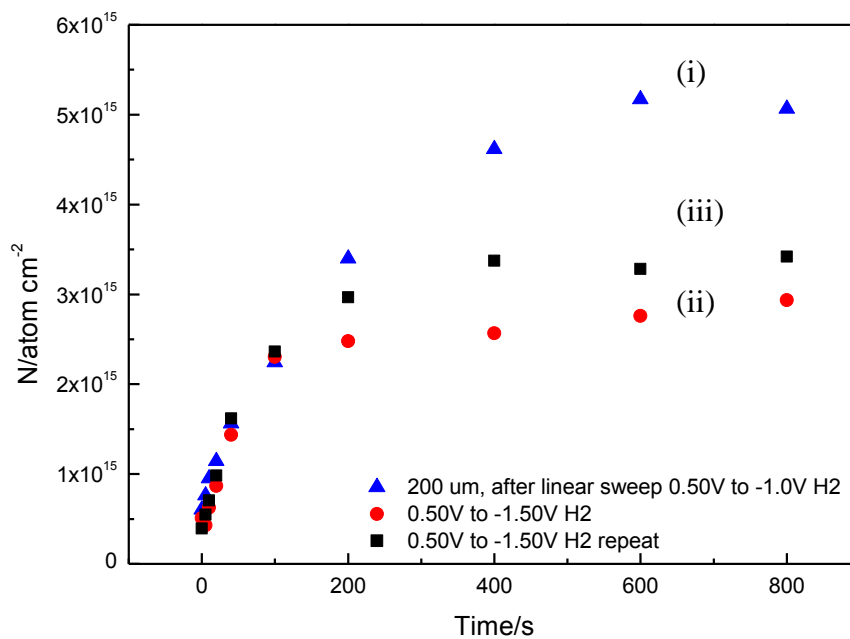


(a)

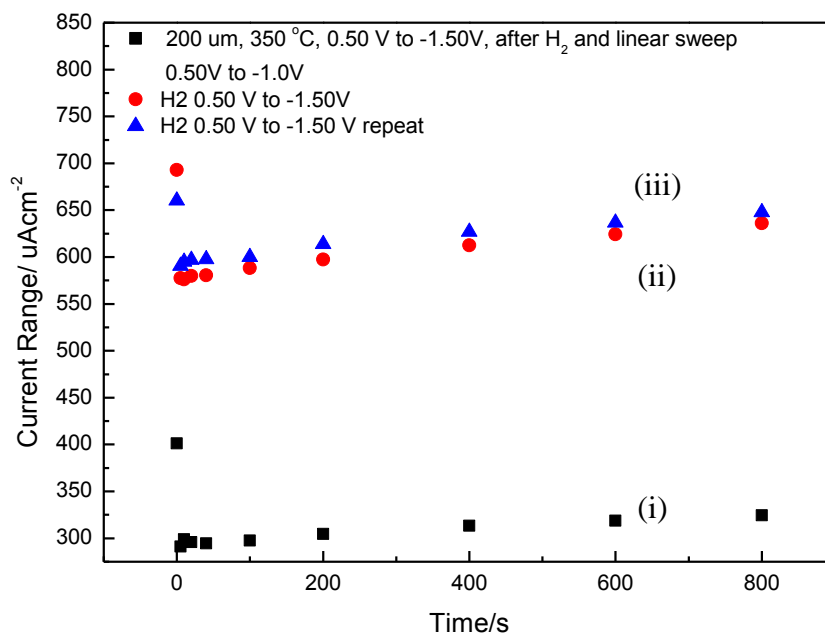


(b)

Figure 5.19: Linear sweep and CV results of the (a) 200 μm from the 3rd batch and (b) ESL 60 min, respectively, before and after exposure to hydrogen. The Linear sweep experiment of the 200 μm from the 3rd batch was conducted at 350 $^{\circ}\text{C}$, 100 mlmin^{-1} 20% O_2/He at scan rate of 20 mVs^{-1} . The CV experiment of the ESL 60 min sample was carried out at 400 $^{\circ}\text{C}$, 200 mlmin^{-1} 20% O_2/He and scan rate of 20 mVs^{-1}



(a)



(b)

Figure 5.20: Effect of holding time on the (a) amount of oxygen atoms and (b) current range, at 350 °C, under nonreactive conditions. (i) 200 μm sample after H₂ reduction, this experiment was carried out after several linear sweep experiments at the same experimental condition, (ii) 200 μm sample after H₂ reduction, there was no other experiments carried out before this experiment after the H₂ reduction, (iii) 200 μm sample after experiment (ii) where the sample was not reduced prior to this experiment.

The first peak in the linear sweep voltammogram in Figure 5.17(a) can be assigned to the oxide decomposition at the binary interface which is similar to the finding discussed in the previous sections and of Jaccoud et al. [7]. The second peak, however, cannot be assigned to spillover species adsorbed on the Pt surface at Pt/gas interface as suggested by Jaccoud et al. [7]. This peak is assigned to the growth of Pt and or impurity oxide layer from the binary Pt/YSZ interface toward the bulk of Pt electrode [7,69,71]. This oxygen storage may explain permanent EPOC observed during the experiments of the 1st and 3rd batch samples [69, 71] presented in Chapter 6.

Besides that, the hydrogen reduction study on this sample has shown that the delamination effect is very minimal. Hydrogen reduction experiment involved the removal of oxides at Pt/gas and tpb interface. Exposing this sample to hydrogen at 500 °C has significantly caused an increase in the current density and thus indicates an increase in the charge transfer reaction sites at tpb due to the removal of oxides at the interface. Building up of Pt and or impurity oxides layer at the tpb, therefore, is more significant in causing the observed reduction in the current density.

(b) ESL 60 min Catalyst

Before exposing the ESL sample to hydrogen, CV experiments were carried out at 400 °C under a nonreactive condition and the voltammogram, as shown in Figure 5.19(b). During the CV a small current density was observed and there was no occurrence of cathodic peaks where these should not be the case of a porous electrode. This result suggests that most of the tpb may have been blocked by oxides which hinder the charge transfer reactions from occurring at this interface. Since cathodic peak is also not observed, oxides may have also not significantly formed at Pt/YSZ interface [8]. Table 5.1 (i) demonstrates these effects.

After exposing the sample to hydrogen, a significant increase in the current density from 32.5 μAcm^{-2} to 342.9 μAcm^{-2} , and a well defined cathodic peak with a peak area of 38.6 μAs are observed. The significant increase in the current density and peak area is caused by the removal of oxides at tpb as demonstrated in Table 5.1(ii). This is because an increase in the number of the available tpb for the charge transfer reactions causes an increase in oxides formed (during anodic polarisation) at this interface. The peaks which


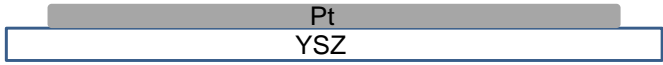

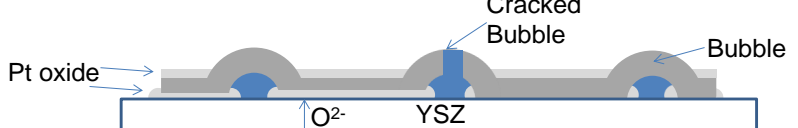
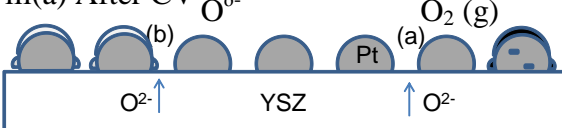
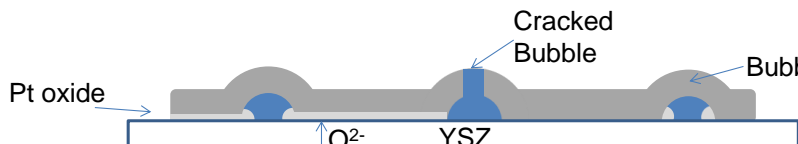
are only observed after the removal of oxides at the interfaces therefore can be assigned to spillover species which can strongly adsorb on Pt surface [7,32,71].

(c) *Description of the Developed Model (demonstrated in Table 5.2)*

Porous electrode which was prepared by using the ESL catalyst, which has a higher tpb length is more stable morphologically [16] than that of the patterned electrodes, as indicated by SEM images in Figure 4.1. Therefore, as demonstrated in Table 5.1, there are no changes in the morphology of the porous electrode throughout the experimental works. Surface oxides are formed at the tpb and Pt/gas interfaces of the fresh sample. Exposure to the hydrogen removed oxides at the tpb and the Pt/gas interfaces. Surface reoxidation takes place at the tpb and the Pt/gas interfaces after the CV experiments.

Patterned electrodes, on the other hand, is denser than that of the porous electrode and hence as described in Table 5.1, there are changes in the morphology in the form of bubbles and cracked bubbles. After the kinetic and electrochemical experiments, oxides are formed at the tpb, Pt/gas and Pt/YSZ interfaces. During the hydrogen reduction experiment, only oxides at the tpb and Pt/gas are removed.

Table 5.1 : Schematic representation of electrode processes of (a) ESL 60 min and (b) patterned electrodes which are modelled based on CV and linear sweep results, respectively, before and after exposure to hydrogen

ESL Porous Electrode	Patterned Electrodes, 200 μm
<p>i(a) Fresh, before CV</p> 	<p>i(b) Fresh, before kinetic and electrochemical experiments</p> 
<p>ii(a) After exposure to hydrogen</p> 	<p>ii(b) After kinetic and electrochemical experiments</p> 
<p>iii(a) After CV</p> 	<p>iii(b) After exposure to hydrogen</p> 

5.3.3.2 200 μm 550 $^{\circ}\text{C}$ Kinetic Sample

The occurrence of surface oxide formation at the gas exposed interface of the 200 μm 550 $^{\circ}\text{C}$ kinetic sample was investigated by analysing the features in CV before and after the hydrogen reduction at 350 $^{\circ}\text{C}$. The results are shown in Figure 5.21. In contrast to the 200 μm , this sample was exposed to hydrogen at a lower temperature which is 350 $^{\circ}\text{C}$. As mentioned in Chapter 3, this is to prevent damages of the counter and the reference electrodes which have been encountered during the hydrogen reduction study of the 200 μm . However, the hydrogen reduction which was carried out at this low temperature could not significantly remove surface oxides at the tpb. This can be observed from the large differences between the current density measured (i) after the first and second reduction and also between (ii) the second and the fifth reductions (Figure 5.21).

To further demonstrate the increase in the oxygen activity at the binary interface during anodic polarisation, at a condition where the tpb is significantly blocked by surface oxides, CV of this sample was carried out at a larger number of cycles. During the CV, current in the cathodic region in the voltammograms of this sample decreases from cycle to cycle and converges to a new steady state [16]. Besides that, two cathodic peaks which are observed in the voltammograms are more pronounced at a larger number of cycles. In contrast to Pöpke et al. [16], this relaxation process in the current work is associated with the blocking effect of surface oxides at tpb because the patterned electrodes are not completely dense where there should be a large number of the available tpb for the charge transfer reactions.

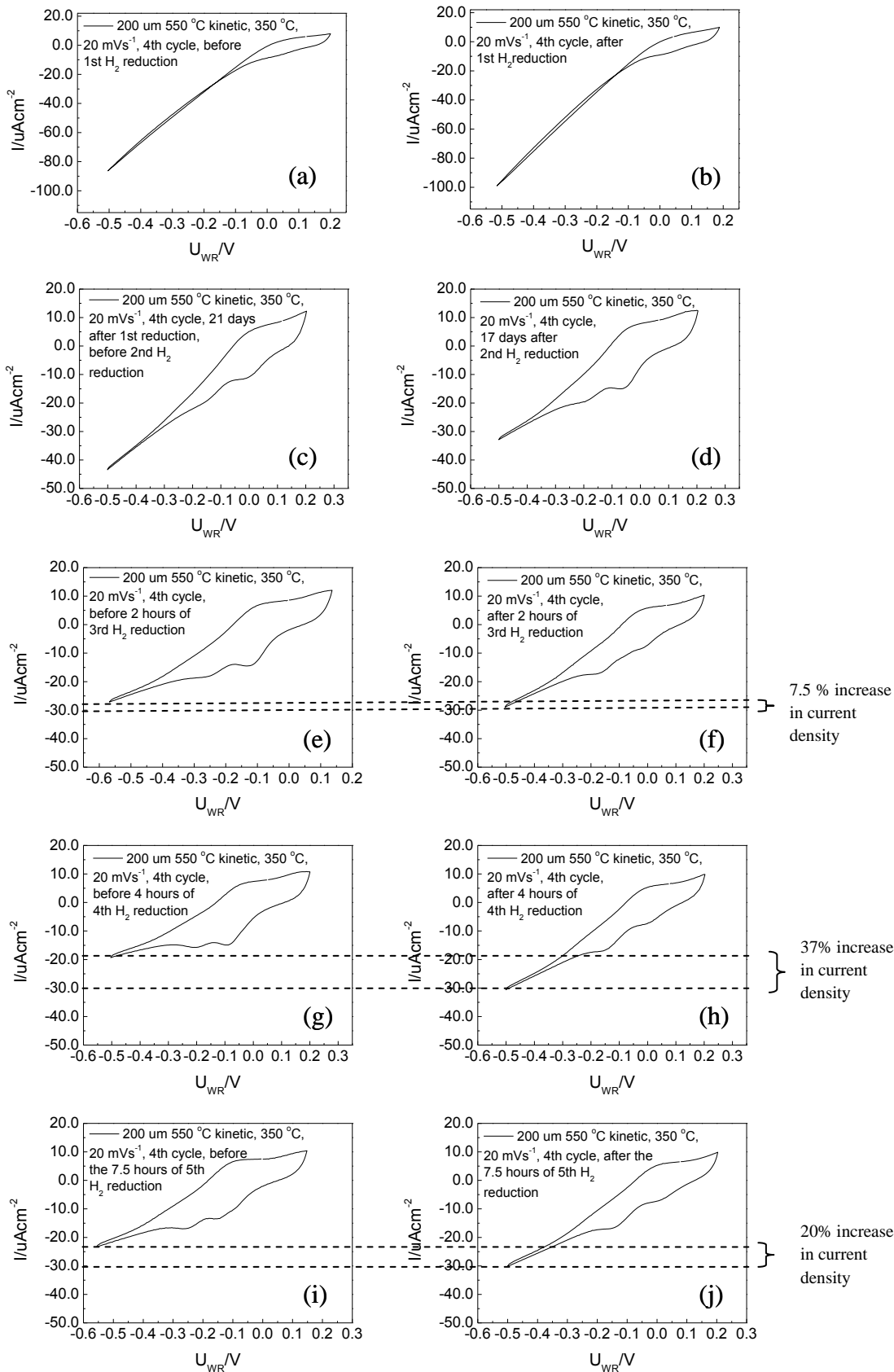


Figure 5.21: Voltammograms of 550 °C thermally treated 200 μm after kinetic sample at the reference condition before and after hydrogen reductions at 350 °C, 4th cycle

(i) *Interface Associated with the Two Peaks*

In order to support the above argument on the interface associated with the oxygen activity depicted by the two peaks, the changes in the peak height before and after the exposure to hydrogen, as shown in Figure 5.22, during the CV are discussed. After the exposure to hydrogen, oxygen activity at the tpb should increase which should decrease the oxide formation at the binary interface. This mechanism is verified by the changes in both peaks heights where the height decreases after the reduction and this is significantly observed for the first peak. Furthermore, by increasing the number of cycle during the CV (where the current density decreases), the height of the first peak increases significantly. The height of the second peak was also increases however the increase was less pronounced than that of the first peak. Moreover, the height of the second peak also does not change significantly after the exposure to hydrogen although the reduction was carried out for a long time. As mentioned above, the first peak is assigned to the decomposition of oxides at Pt/YSZ while the second peak can be assigned to the growth of Pt and or impurity oxide layer from the binary interface toward the bulk of the Pt electrode.

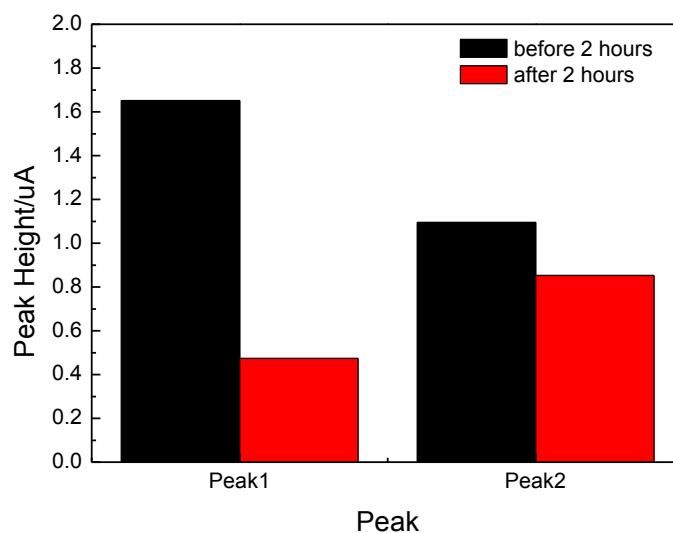


Figure 5.22: Changes of the 1st and 2nd cathodic peak heights of the 200 μm 550 $^{\circ}\text{C}$ kinetic sample before and after 2 hours of exposure to hydrogen

(ii) *Surface Oxide Formation*

Next, the changes in the responses of the CV are analysed to investigate when the surface oxides are significantly formed, either during the experiments under the nonreactive condition or when the sample was left in the reactor in air at room temperature. Figure 5.21 indicates there is a significant decrease in the current density and pronounced cathodic peaks during CV which was repeated after 21 days leaving the sample in air at room temperature. The first cathodic peak in voltammogram (c) which is more defined and larger than that of voltammogram (a) and (b) suggests pronounced oxide formation at the binary interface during experiment (c). Based on this result, the significant surface oxide formation is found to occur during or within the 21 days of no experimental works.

The formation of new oxide layer during no experimental works is also described by the responses in experiment (d) which was carried out after experiment (c). Before experiment (d) the sample was again exposed to hydrogen at 350 °C, however, the CV experiment which should be carried out right after the reduction was not conducted due to problems associated with the experimental equipment. The next experiment was only carried out 17 days after the hydrogen reduction and a further decrease in the current density is observed as indicated in voltammogram (d). The result suggests that after experiment (c), some of the surface oxides at the tpb may have been removed during the exposure to hydrogen. However, during 17 days of no experimental works new oxide layer may have been formed. Furthermore, the first cathodic peak in voltammogram (d) indicates the formation of thermodynamically more stable oxides at the Pt/YSZ interface in which the peak shifted to a more negative potential and is larger than that in the voltammogram (c).

(iii) *Effect of Exposing the Sample to Hydrogen at Different Time*

The effect of hydrogen exposure time on the features in the CV of the 200 μm 550 $^{\circ}\text{C}$ kinetic sample is demonstrated in Figure 5.23. Exposing the sample to hydrogen at a longer time should remove more oxides at the tpb and Pt/gas interface. This is indicated in Figure 5.21 where an exposure of 4 hours to hydrogen caused a more significant increase in the current density, which is 37%, than the increase after the exposure of 2 hours, which is 7.5%. Exposing the sample to hydrogen for 7.5 hours caused 20% increase in the current density. An interesting observation is that the repeatability of experimental data after the reduction was observed after the 2 hours, 4 hours and 7.5 hours exposure to hydrogen, as indicated in Figure 5.21 and 5.23 where the voltammograms overlap at similar current density. Therefore, the exposure to hydrogen at low temperature (350 $^{\circ}\text{C}$) even for a very long time (more than 2 hours) does not cause significant changes in the current density and hence the removal of surface oxides at tpb.

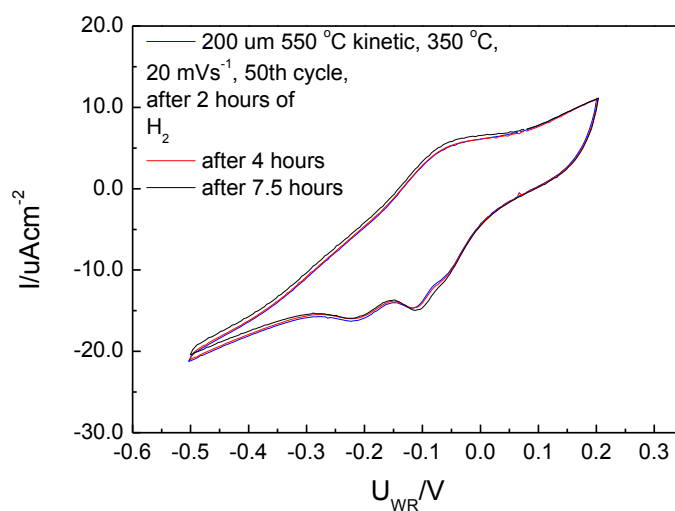


Figure 5.23: Cyclic voltammograms of the 550 $^{\circ}\text{C}$ thermally treated 200 μm after kinetic sample at the reference condition after hydrogen reductions at 350 $^{\circ}\text{C}$, 50th cycle

Another interesting finding is that an additional cathodic peak, which is indicated in Figure 5.23 and 5.24, is observed after the reduction at a larger number of cycles or when a steady state is almost reached during the CV. This peak is within the potential range of the first peak which has been previously assigned to the decomposition of Pt and or impurity oxides at Pt/YSZ and is more defined at a scan rate which is higher than 20 mVs^{-1} . Furthermore, this peak can only be observed when the CV was carried out not long after the reduction (or before deactivation of the electrode after the reduction due to the formation of new oxides at tpb). As indicated in Figure 5.23 and 5.24, the peak is difficult to be identified during CV which was carried out approximately a day after the reduction. Therefore, this peak can be caused by the decomposition of either impurity oxides [8] or Pt oxide of different oxidation state which overlap with a larger peak of the previously assigned to the decomposition of Pt and or impurity oxides. The observation of this peak can be explained by a decrease in the amount of oxygen being consumed in the processes taking place at Pt/YSZ interface due to an increase in the amount of oxygen involves in the reactions occurring at the tpb after the hydrogen reduction. When less oxide is formed at the binary interface, the decomposition of either impurity oxides or Pt oxides of different oxidation state may have become more significant and hence can be observed in the voltammograms.

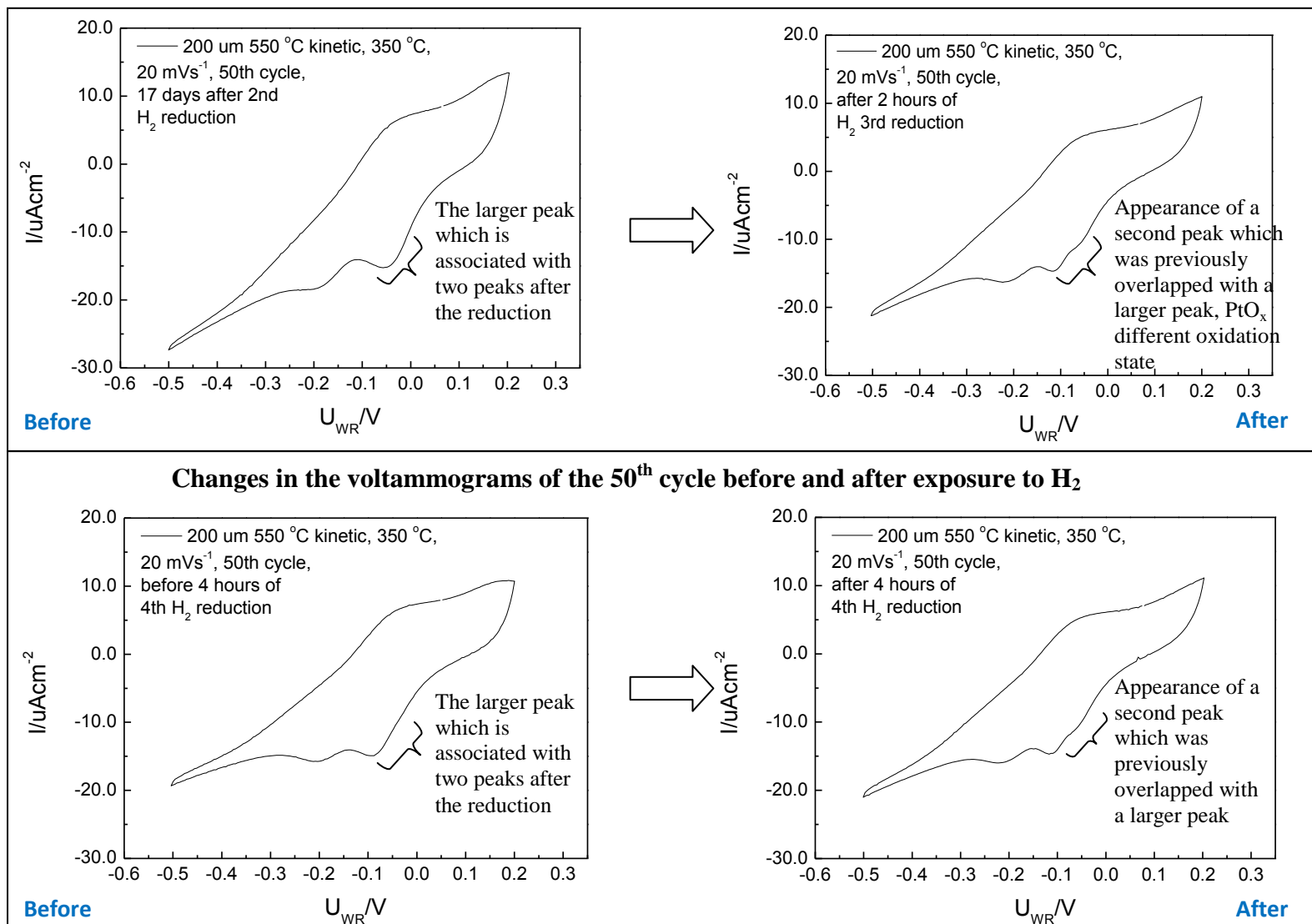


Figure 5.24: Voltammograms of the 200 μm 550 $^{\circ}\text{C}$ thermally treated of the 50th cycle, before and after exposure to hydrogen. The CV was carried out at 350 $^{\circ}\text{C}$ under the flow of 100 mlmin^{-1} 20% O₂/He, at a scan rate of 20 mVs^{-1} .

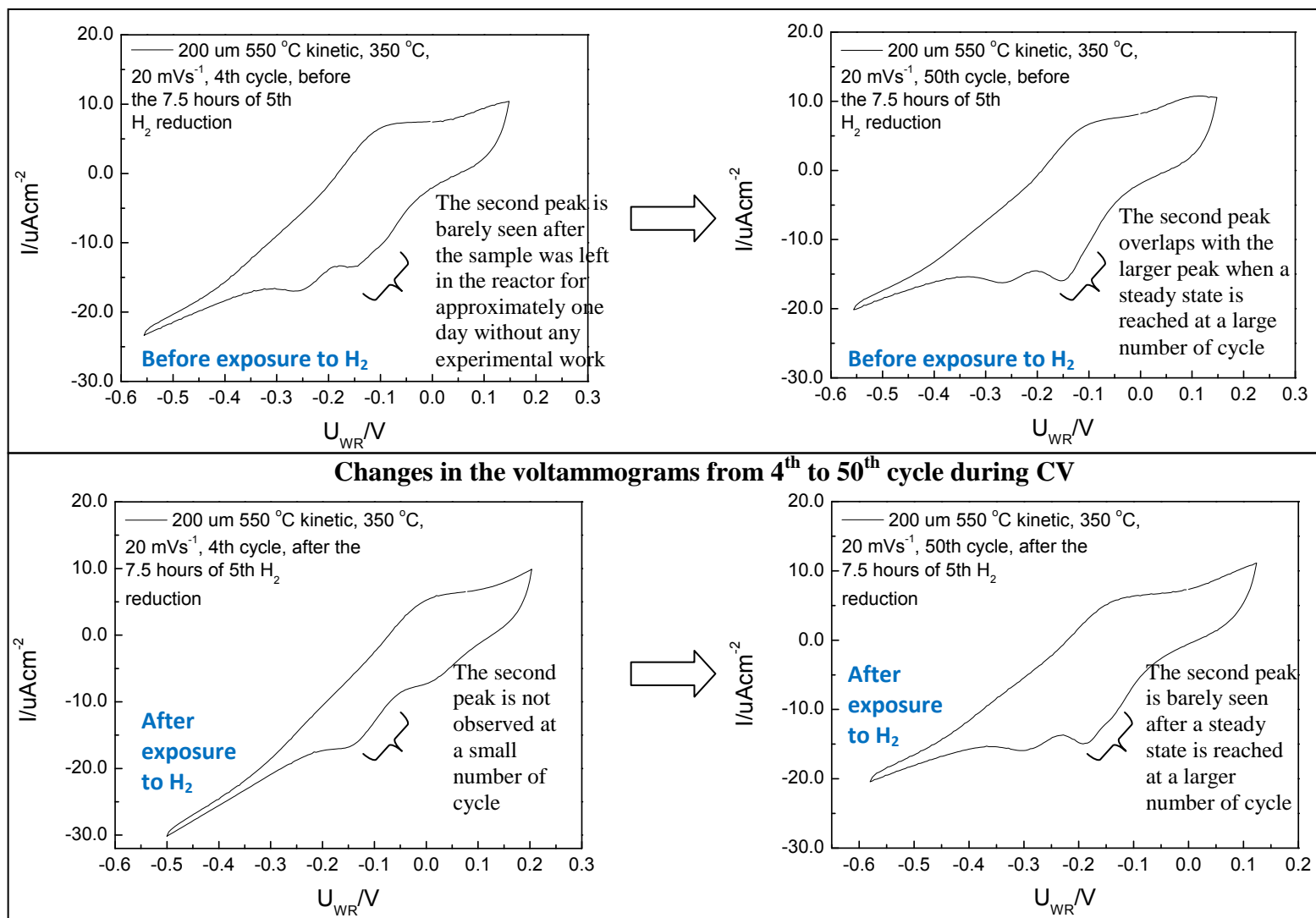


Figure 5.25: Voltammograms of the 200 μm 550 $^{\circ}C$ thermally treated of the 4th and the 50th cycle, before and after exposure to hydrogen. The CV was carried out at 350 $^{\circ}C$ under the flow of 100 $mlmin^{-1}$ 20% O_2/He , at a scan rate of 20 mVs^{-1} .

5.3.3.3 Summary of Hydrogen Reduction Study

The results of hydrogen reduction study of the ESL and the patterned electrodes are compared and discussed. Based on the features in the cyclic and linear sweep voltammograms in Table 5.2, a similarity is observed in terms of the changes of (increase in) the current density after the exposure to hydrogen. These changes can be explained by the changes occurring at the tpb or gas exposed interface after the reduction. By exposing both systems to hydrogen, oxides at the tpb and the Pt/gas interface can be removed which can result to an increase in the number of the available tpb interface for the charge transfer reaction (or the oxygen activity at this interface). Therefore, the similarity in the increase in the current density, despite of the differences in the surface characteristics of both electrodes as indicated by the SEM images in Figure 4.1 and Figure 5.11 to 5.13, indicates the increase in the tpb length which therefore further verifies the presence or formation of surface oxides at tpb in the Pt/YSZ system using the patterned electrodes. This finding demonstrates that the electrode can be activated by exposing it to hydrogen. This is clearly demonstrated by the 200 μm where the current density returns to the value which is close to the value at a condition when there is less blocking of oxides at the tpb.

The changes of the peak height in the cathodic region of the two systems, however, are different which is due to the differences in the interface associated with the oxide formation. After the reduction, there is an increase in the oxygen activity at the tpb while there should be a decrease in oxide formation at the Pt/YSZ interface and Pt bulk. This correlation can only be observed from the results of the patterned electrodes which is denser than the ESL catalyst. The spillover processes, however, are not indicated in the voltammograms of the patterned electrodes in which, as discussed by Mutoro et al. [8] spillover species are not necessary causing additional peaks in the voltammogram. In contrast, the spillover processes are depicted by the peaks in the CV of the ESL catalyst and this is in agreement with the findings of [7,69,107].

5.3.4 Summary

In summary, the repeatability study suggests oxygen charge transfer in the Pt/YSZ system using the patterned electrodes occurs not only at tpb but also at the binary interface where there is also oxygen storage at Pt bulk. Electrode deactivation and activation phenomena

have been described as a result of Pt and or impurity oxide formation and decomposition at tpb and this has been verified by the results of hydrogen reduction experiments. It appears that the study provided details on

- (i) the geometry dependence of the charge transfer reactions when a conclusion cannot be derived by comparing the electrochemical data of patterned electrodes of different width length scales.
- (ii) the limiting factor which has significant effects on the performance of the patterned electrodes. This is important in term of the durability of the electrodes during the application in the field and the suitability of the patterned electrodes as a model catalyst and
- (iii) The type of treatments such as exposing the sample to hydrogen to prevent or minimise electrode deactivation.

Chapter 6. Spillover Processes in a Pt/YSZ System Utilising Patterned Electrodes under a Reactive Condition

6.1 Introduction

In this chapter, the results of kinetic experiments under open and close circuit conditions are presented and discussed. The objective was to determine if the Pt/YSZ system utilising the patterned electrodes can exhibit NEMCA or EPOC in which this behaviour indicates the occurrence of the spillover processes in the system either thermally or electrochemically. The application of the patterned electrodes is assumed can demonstrate EPOC mechanism due to the role of the backspillover species including factors controlling this process.

6.2 Hypotheses

As described in Chapter 3, patterned electrodes which were prepared by sputtering are similar in terms of the geometric surface area and film thickness while different in terms of the geometric tpb length where the length decreases with increasing width length scale. Besides that, small amount of impurities (which should be less than those present on the catalyst films of the commercially available materials) is assumed to present on the patterned electrodes surface, in which the interaction of the impurities with the promoter (backspillover species), induced by thermal effect and or polarisation, under the reactive condition can be neglected [10]. Therefore, a simple model can be used to describe the behaviour of the system toward EPOC in which the focuses of the present work are on the backspillover species, $O^{\delta-}$, and the three phase boundary (tpb).

Similar to the backspillover mechanism suggested by Vayenas and his co-workers, in this model, $O^{\delta-}$ is assumed to migrate onto the Pt surface through tpb under the influence of positive polarisation (and or due to thermal effect) and only interact with the reactive components and intermediates and this should cause a dramatic increase in the catalytic rate. During the negative polarisation, $O^{\delta-}$ is removed from the Pt surface and the opposite observation is expected. The migration of this species onto the Pt surface and the formation of the effective double layer are strongly dependent on

- (i) the electrode morphology and hence the tpb length (EPOC effect should be more pronounced for sample of a higher tpb length)
- (ii) the composition of the reactive mixture such as oxygen partial pressure
- (iii) the temperature and
- (iv) the magnitude of the applied potential.

6.3 Backspillover Phenomenon in the Pt/YSZ System Using the Patterned Electrodes

In this section, the evidence of the backspillover phenomenon in the Pt/YSZ system utilising the patterned electrodes was obtained by studying the behaviour of the system under open and close circuit conditions. This is described by the origin of EPOC and permanent EPOC in which the origin of EPOC is associated with the electrochemical [32] and the thermal [63] migration of the O^{2-} ions while the origin of the permanent EPOC is linked to the occurrence of oxygen storage [3, 68, 71] and changes in catalyst morphology [4]. The study includes

1. *kinetic studies* to observe if the open circuit catalytic rate is tpb dependent in which if this is true then the behaviour can be associated with the occurrence of the thermally induced backspillover species (EPOC without electrical connections)
2. *transient studies* to demonstrate the occurrence of the electrochemical backspillover species

From the results of the kinetic and transient studies, the following mechanisms are found to describe the behaviour of the Pt/YSZ system using the patterned electrodes under the (i) open circuit condition, (ii) during the positive and negative polarisations and (iii) after the current interruption.

6.3.1 Open Circuit Condition

Under a reactive condition at a temperature between 300 °C and 450 °C without the electrical connection, backspillover processes can occur in the Pt/YSZ system using the patterned electrodes. This involves the migration of the thermally induced O^{2-} from the YSZ to the Pt surface through the tpb. Similar to the electrochemical backspillover species, the migration of the thermally induced backspillover O^{2-} creates a double layer

which can interact electrostatically with covalently chemisorbed reactants and intermediates and alter their binding strength and thus causes changes in the catalytic rate. Since the migration of the thermally induced O^{2-} is also through tpb, a tpb dependence of the catalytic rate should be observed.

To verify this phenomenon, the results of CO oxidation under the open circuit condition by using fresh samples from the 1st and the 3rd batch which are listed in Table 6.1 are discussed in terms of the geometry dependence. The tpb length dependence of the catalytic rate should be indicated by a proportional relationship between the tpb length and the rate. As demonstrated in Table 6.1, the catalytic rate dependence on the tpb length was not observed from the results of the 1st batch samples. This can be explained by the geometric surface area and the tpb length which vary among the samples of different width length scale where the effect of both geometric characteristics may interact. In contrast to the 1st batch samples, the tpb length of the 3rd batch samples is different while the surface area is similar among the samples of different width length scale and therefore it was expected that a correlation between the tpb length and the catalytic rate can be observed. However, similar to the 1st batch samples, the tpb length dependence of the catalytic rate could not be observed.

Table 6.1: Catalytic rate of the fresh patterned electrodes which were measured by using a quantum cascade CO₂ analyser

Samples/Length scales	Experimental conditions	Rate (nmols ⁻¹ cm ⁻²)
1 st Batch: 2 μm, 20 μm, 200 μm	Temperature = 340 °C pO ₂ = 3 kPa pCO = 0.5 kPa	2 μm: 456 20 μm: 15 200 μm: 119
3 rd Batch: 200 μm, 400 μm	Temperature = 340 °C pO ₂ = 3 kPa pCO = 0.6 kPa	200 μm: 127 400 μm: 147 Rate of 200 μm > rate of 400 μm, during experiments after the sample has been sintered at a temperature higher than 340 °C
3 rd Batch: 4 μm, 200 μm	Temperature = 300 °C pO ₂ = 3 kPa pCO = 0.5 kPa	4 μm: 6 200 μm: 11

6.3.1.1 Surface Morphology by SEM Analyses

Since the rate dependence on the tpb length cannot be found, the assumption of the formation of the effective double layer by the thermally induced O^{2-} which influences the catalytic activity may not be valid or if it is valid then the Pt surface may have been fully covered by the double layer (the Pt electrode is a thin film). To further verify this finding, the SEM images of the patterned electrodes before and after the exposure to the thermal treatment and kinetic experiments as shown in Figure 6.1 are then analysed. From the images, the electrode morphology after the sample has been exposed to the thermal treatment and kinetic experiments is found to be different from the surface of the fresh sample where bubble formation is observed. This morphology change is similar to those caused by polarisation discussed in the literatures which is known to increase the tpb length. The changes which occurred on the sample which has not been polarised can therefore be explained by the mechanism described by Mutoro et al. [4] on the effect of electrochemical migration of the backspillover species on the partly porous sample except that in this case the bubbles are formed due to the thermal migration of O^{2-} . This oxygen needed to escape to the gas phase and since the Pt film is denser than that of the porous electrodes, there was a built up of oxygen pressure underneath the catalyst film which caused the bubble formation. Besides that, the bubbles could also be formed as a result of Pt film delamination due to the effect of temperature. This effect however is not significant as demonstrated in Chapter 5. The question of whether the Pt surface is fully covered by the double layer is further explained by the results of the transient study in **section 6.3.2.3**.

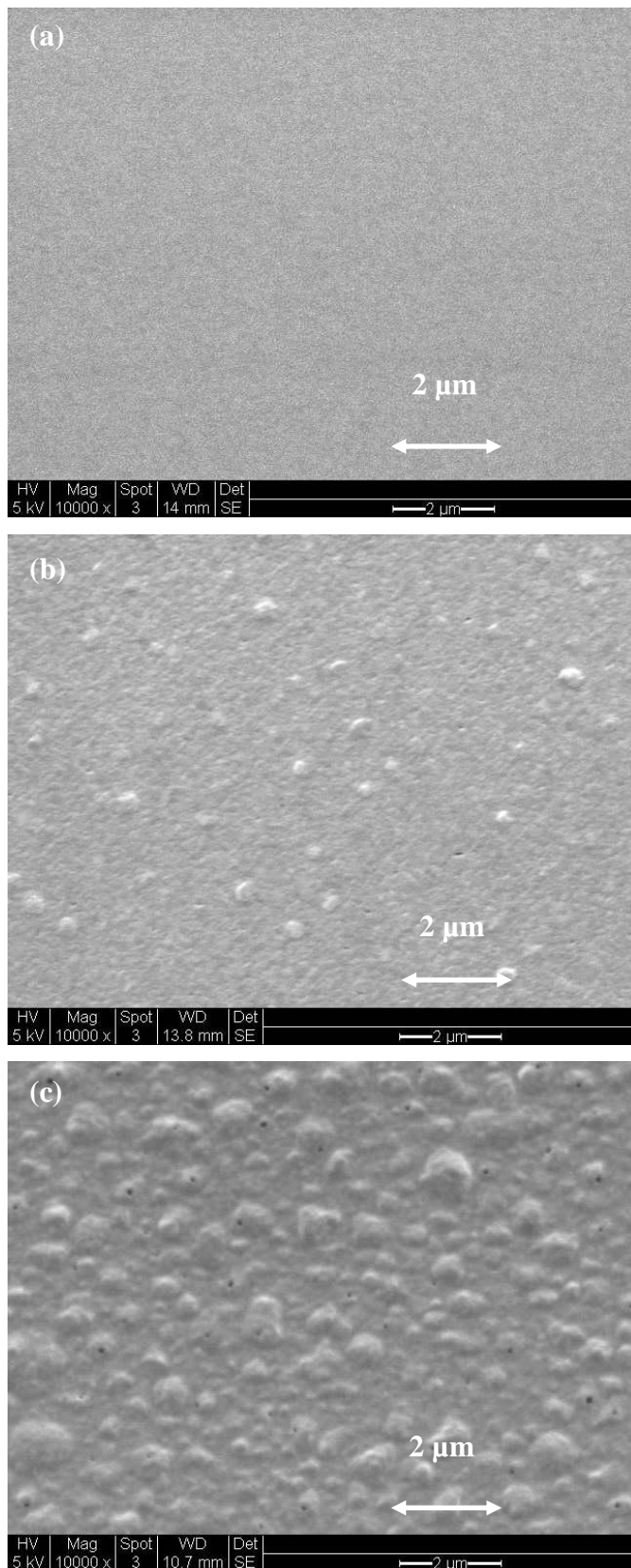


Figure 6.1: SEM images of (a) 200 μm fresh untreated, before kinetic experiments, (b) 200 μm fresh treated at 550 °C, before kinetic experiments and (c) 200 μm fresh treated at 550 °C, after kinetic experiments

6.3.1.2 Repeatability Study

As discussed in the previous section, the tpb dependence of the catalytic rate was not observed. However, the formation of bubbles in Figure 6.1 suggests the migration of the thermally induced O^{2-} onto the Pt surface and the mechanism is similar to those of the electrochemical O^{2-} . To further verify this mechanism, the analysis was then continued by focusing on the results of the patterned electrode of one length scale. It appears that the rate dependence on the tpb length can be observed by analysing the changes in the catalytic rates of one sample throughout the experimental works. This type of analysis, which is termed in the present work as the repeatability study, can serve as another approach of demonstrating the catalytic rate dependence on tpb for a Pt/YSZ system where a correlation associated with the geometric characteristics cannot be developed although the electrodes were fabricated in such a way that the electrodes geometrical and compositional complexity are reduced. The changes in rates in this case are associated with the changes in electrode surface morphology or characteristics which occurred during the (i) kinetic experiments under the reactive condition and (ii) electrochemical characterisation experiments under the nonreactive condition (which were carried out prior to the exposure to the reactive condition). The changes included a decrease and an increase in the tpb interface (number of active sites) available for the charge transfer reactions.

The decrease in the tpb length described in this thesis is the reduction of the number of active sites at tpb or some of the tpb sites have become inactive and this has been described in Chapter 5 due to the presence of passive oxide layer at this interface. The presence of surface oxides can hinder charge transfer reactions at this interface [15]. The increase in the the number of active sites, on the other hand, is caused by the formation of bubbles and or cracked bubbles and also the removal of the surface oxides. Factors that can cause the removal of the surface oxides are described in details in Chapter 5. The results of kinetic experiments which can demonstrate this dependence are discussed below.

As discussed below, the history of the samples (either fresh or has been thermally treated or used in other experiments) varies among the samples. These experiments were carried out in this manner to understand the kinetics of the samples which have been exposed to

different experiment conditions. This is particularly important in terms of the future applications of the patterned electrodes where the patterned electrodes may require treatments prior to its utilisation and or during its applications so that the electrodes can perform at its optimum condition. As mentioned previously, during this repeatability study, the results appear to demonstrate the tpb dependence of the catalytic rate.

i. 1st sample: 200 μm , 3rd batch, fresh sample during a long term monitoring study

In this experiment, a 200 μm from the 3rd batch, which has not been thermally treated or used in other experiments, has been used in a long term monitoring O₂ kinetic study where the catalytic rate was measured at one experimental condition (340 °C, 160 mlmin⁻¹, 3 kPa pO₂ and 0.63 kPa pCO) and the sample was left in either helium or reactant gases at 340 °C during no experimental works. The purpose of carrying out this experiment was to observe changes in the catalytic rate over time and to associate the changes with the reactor environment and most probably changes that may occur on the catalyst or electrode surface.

As indicated in Figure 6.2, the rate did not decrease throughout the experimental works, however, increased although slightly and stabilised at a higher value. The increase in the rate can be associated with a slight increase in the tpb length caused by the changes in Pt surface morphology (such as the formation of bubbles) due to the effect of temperature (gradient) and or the built up oxygen (thermally induced ionic species) pressure underneath the Pt film. The effect of temperature treatment in changing Pt surface morphology and hence exhibiting a higher catalytic rate was observed for another sample of a similar width length scale which has been thermally treated at 550 °C and discussed below.

Since the reaction can occur either at tpb and or Pt/gas interfaces, the results of this long term monitoring study indicate minimal changes on the electrode surface, and these changes did not decrease the catalytic rate. Keeping the temperature at 340 °C under a less oxidising condition or under an active state by exposing the sample to either helium or reactant gases, respectively, overnight or when there was no experimental works may

prevent significant changes on the electrode surface characteristics (microstructure and the building up of surface oxide layer).

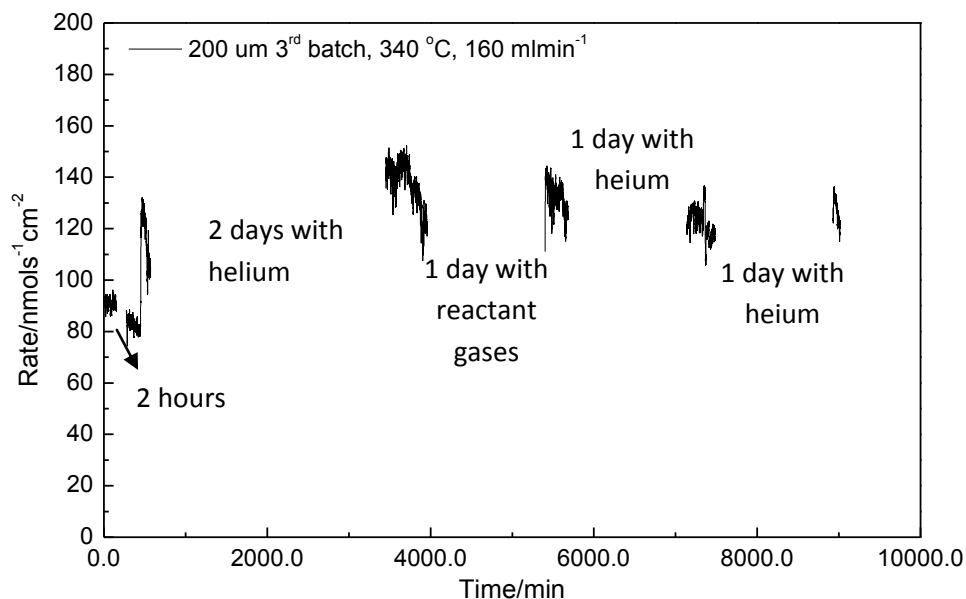


Figure 6.2: Open circuit rates of 200 μm (1st sample) from the 3rd batch which are normalised to electrode geometric surface area at 340 $^{\circ}\text{C}$ during long term monitoring O_2 kinetic study at 3 kPa p_{O_2} , 0.63 kPa p_{CO} , total flow rate of 160 mlmin^{-1} and the rates were measured by a quantum cascade CO_2 analyser.

ii. 2nd sample: 200 μm , 2nd batch, 550 $^{\circ}\text{C}$ thermally treated, fresh

The 2nd sample is a 200 μm from the 2nd batch where it has been thermally treated at 550 $^{\circ}\text{C}$ by the Electrical Engineering School, Newcastle University. This sample has not been used in other experiments before the kinetic O_2 study. SEM images of the sample before and after the kinetic experiments are shown in Figure 6.1. As indicated by the SEM image, the electrode surface of the 2nd sample is different than the surface of the untreated 1st sample. Bubbles were formed (during the thermal treatment and throughout the experimental works) due to the thermal migration of oxygen ionic species in which these species need to escape to the gas phase and since the Pt film of the patterned electrode is denser than that of the porous electrodes, there was a built up oxygen pressure underneath the catalyst film. The formation of small bubbles on this 2nd sample could have resulted to an increase in the tpb length and thus caused a higher catalytic rate than that of the 1st sample which was 247 $\text{nmols}^{-1}\text{cm}^{-2}$ and 127 $\text{nmols}^{-1}\text{cm}^{-2}$, respectively. The higher

catalytic rate of the 2nd samples than that of the 1st sample suggests the open circuit rate dependence on the catalyst surface morphology and hence the tpb length.

iii. 3rd sample: 200 μm , 3rd batch, the sample has been exposed to electrochemical experiments

The 3rd sample is also a 200 μm from the 3rd batch which has been exposed to a 0.10 V and 0.20 V anodic potential during electrochemical characterisation and EPOC experiments. The rate measurement was carried out by using a Binos 100 CO₂ analyser and the experiments were carried out at 350 °C and 0.5 kPa pCO by varying O₂ pressure. The details of the experiment 1 to 5 are demonstrated in Chapter 3. In contrast to the 1st sample, this sample was left in air at room temperature when there was no experimental works. As indicated in Figure 6.3, significant changes in the catalytic rate over time or stabilisation of the rate throughout the experimental works at a lower value are observed. This is in contrast to the findings during the long term monitoring study (1st sample) discussed above.

As verified by the results of irreversibility studies under a nonreactive condition and hydrogen reduction experiments which were carried out on this sample which is presented in the Chapter 5, passive oxide layer formation at tpb hindered charge transfer reactions at this interface. This effect may have resulted to the observed reduction of the catalytic rate over time. This decrease of the rate which was not observed during the long term monitoring study of the 1st sample supports the conclusion of the study under the nonreactive condition where the decrease in the catalytic performance is due the processes occurring at the tpb and Pt/gas interfaces when the sample was left in air at room temperature or when the temperature was increased to the temperature of interest or to be more precise caused by surface oxidation and oxide formation cannot be avoided and keeping the sample in helium during no experimental works can minimise the formation at tpb and on Pt surface. Since similarity is observed between the changes of the open circuit rate and current density over time, the open circuit rate of this sample is hence tpb dependence.

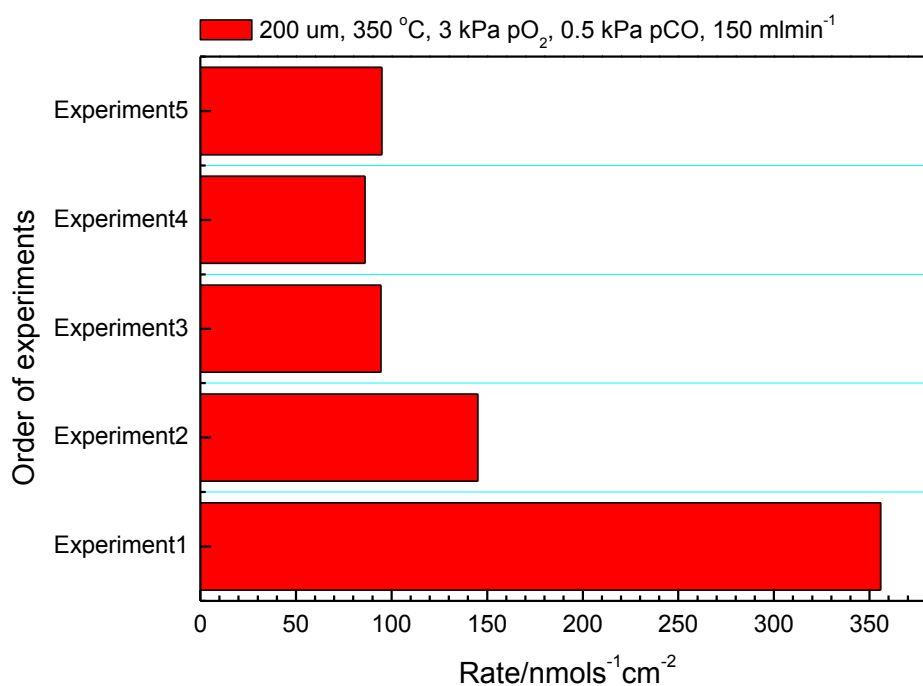


Figure 6.3: Open circuit rates which were measured prior to 0.10 V and 0.20 V anodic polarisation during electrochemical experiments of the 200 μm (3rd sample) from the 3rd batch at 3 kPa pO_2 , 0.5 kPa pCO , 350 $^\circ\text{C}$ and total flow rate of 150 mlmin^{-1} . The rates were measured by Binos 100 CO_2 analyser and are normalised to electrode geometric surface area.

iv. The 200 μm , the 1st sample which has been used during the long term monitoring study and a fresh 400 μm (4th sample)

The rate dependence on tpb and blocking effect of oxides at gas exposed interface are further demonstrated by the results of kinetic experiments which were carried out on the 1st sample (which has been exposed to the reactive condition during the the long term monitoring study) and the 4th sample which is a fresh 400 μm from also from the 3rd batch. In this study both samples were sintered at 340 $^\circ\text{C}$, 400 $^\circ\text{C}$, 500 $^\circ\text{C}$, 550 $^\circ\text{C}$ and 600 $^\circ\text{C}$ for two hours in air. After sintering at each temperature, rate measurement was carried out at 340 $^\circ\text{C}$, 3kPa pO_2 and 0.63 kPa pCO . The experiments were not carried out on the same day. In contrast to the long term monitoring study, these samples were left in air at room temperature when there was no experimental works.

The effect of sintering temperature on open circuit rates are indicated in Figure 6.4. By comparing the catalytic rates of both samples, tpb dependence is observed after the sample has been sintered at temperature higher than 340 °C. This can be associated with the occurrence (and the effect) of the thermally induced backspillover species. At higher temperature, the migration of this ionic species from the YSZ onto the Pt surface became more significant due to the higher ionic conductivity of the YSZ.

Besides that, by analysing the changes in the catalytic rate for each sample, the rate decreases as the sintering temperature increases. Passive oxide layer, which may have formed when the samples were left in the reactor in air either at room temperature or when the temperature was increased to the temperature of interest or during the sintering process, could have possibly blocked the tpb interface and caused a decrease in the catalytic rate. The hindering effect of the surface oxides at tpb has been discussed above and verified in Chapter 5. The results also suggest both effects of temperature and formation of surface oxides at tpb interact.

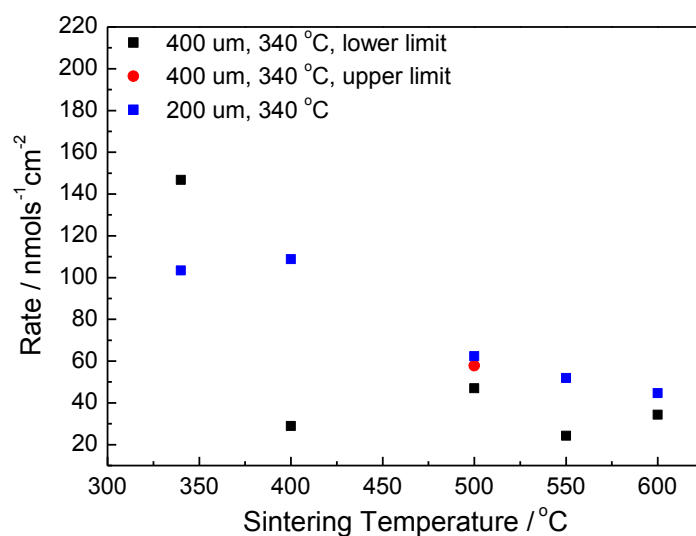


Figure 6.4: The effect of sintering temperature on open circuit rates of the 200 μm (1st sample after the long term monitoring study) and a fresh 400 μm from the 3rd batch. The rates were measured by a quantum cascade CO₂ analyser and are normalised to electrode geometric surface area. The experiments were carried out at 340 °C, 3 kPa pO₂, 0.63 kPa pCO, total flow rate of 160 mlmin⁻¹. Lower and upper limit correspond to the lowest and highest value during measurement, respectively.

6.3.1.3 Summary

The catalytic rate dependence on the tpb length was only observed from the results of the repeatability study. The tpb dependence of the catalytic rate which was not observed when the results of different width length scales are compared can be explained by the same factors causing the complexity in developing the oxygen charge transfer dependence on the tpb length as described in Chapter 5 (**section 5.2.4**).

6.3.2 During Polarisation

The catalytic rate under the open circuit condition which has been suggested in the previous section is dependent on the tpb length where this is associated with the occurrence of the thermally induced backspillover O^{2-} . Under the influence of polarisation, both the thermal and the electrochemical backspillover species can coexist where the additional O^{2-} coverage from the electrochemical backspillover processes should increase the density of the effective double layer and hence cause an increase in the catalytic rate. In this section, the occurrence and the role of the electrochemical backspillover species during polarisation are demonstrated based on the results of EPOC experiments.

The experiments were carried out on the 20 μm and 200 μm from the 1st batch and 200 μm from the 3rd batch. During the experiments, the 1st batch samples were polarised at 1.0 V while the 3rd batch sample was polarised at smaller anodic potential of 0.10 V and 0.20 V and a cathodic potential of -1.0 V. The purpose of polarising the 3rd batch sample at the smaller anodic potential was to determine if the amount of O^{2-} migrated onto the Pt surface under the influence of the small potential is sufficient to form an effective double layer which can change the Pt work function and hence cause catalytic rate enhancement (lower limit). The CO_2 concentration from the reactor outlet of the 1st and the 3rd batch samples were measured by using a quantum cascade CO_2 analyser and a Binos 100 CO_2 analyser, respectively.

The results of CO oxidation transient experiments of the 200 μm from the 3rd batch as a function of $p\text{O}_2$ under a fixed 0.5 kPa $p\text{CO}$ at 350 °C are demonstrated in Figure 6.5 while

the results of transient experiments of the 1st batch samples which were carried out as a function of pO₂ and pCO under a fixed 0.5 kPa pCO and 0.7 kPa pO₂, respectively, at 340 °C are indicated in Figure 6.6. The results show that the Pt/YSZ system using patterned electrodes from both batches exhibited reversible and permanent EPOC which suggests the occurrence of the backspillover phenomenon in which the behaviour in most cases is electrophobic. The correlation between the oxygen pressure and open circuit potential (OCP), as demonstrated in Figure 6.5 and 6.6, is in accordance to the following equations [107].

$$a_o = p_{O_2}^{1/2} \exp\left(\frac{2FU_{WR}^o}{RT}\right) \quad (35)$$

$$\frac{1}{2} \ln p_{O_2} = \ln a_o - \frac{2FU_{WR}^o}{RT} \quad (36)$$

$$p_{O_2} \propto -U_{WR}^o \quad (37)$$

where a_o is the oxygen's thermodynamic activity and U_{WR}^o is the OCP in which $U_{WR}^o < 0$. Besides that, a proportional relationship is also observed between the promoted catalytic rate and (i) oxygen pressure and (ii) faradaic efficiency as demonstrated by equation (38) and equation (39), respectively.

$$r \propto p_{O_2} \quad (38)$$

$$r \propto \Lambda \quad (39)$$

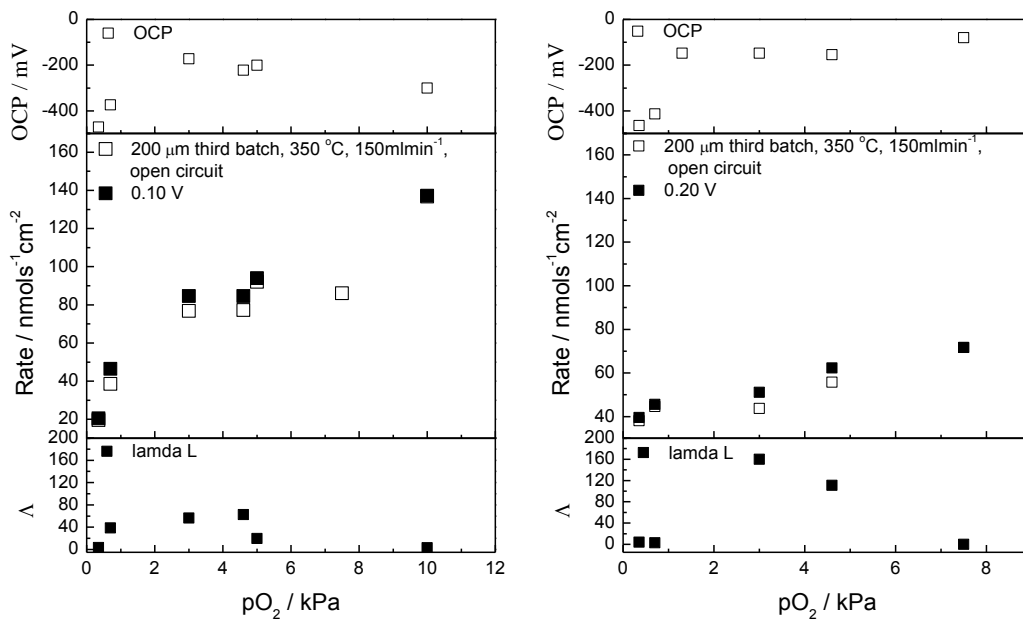


Figure 6.5: The results of EPOC experiments of CO oxidation as a function of pO_2 under a fixed 0.5 kPa pCO at 350 $^{\circ}C$, (a) 0.10 V and (b) 0.20 V, for the 200 μm from the 3rd batch

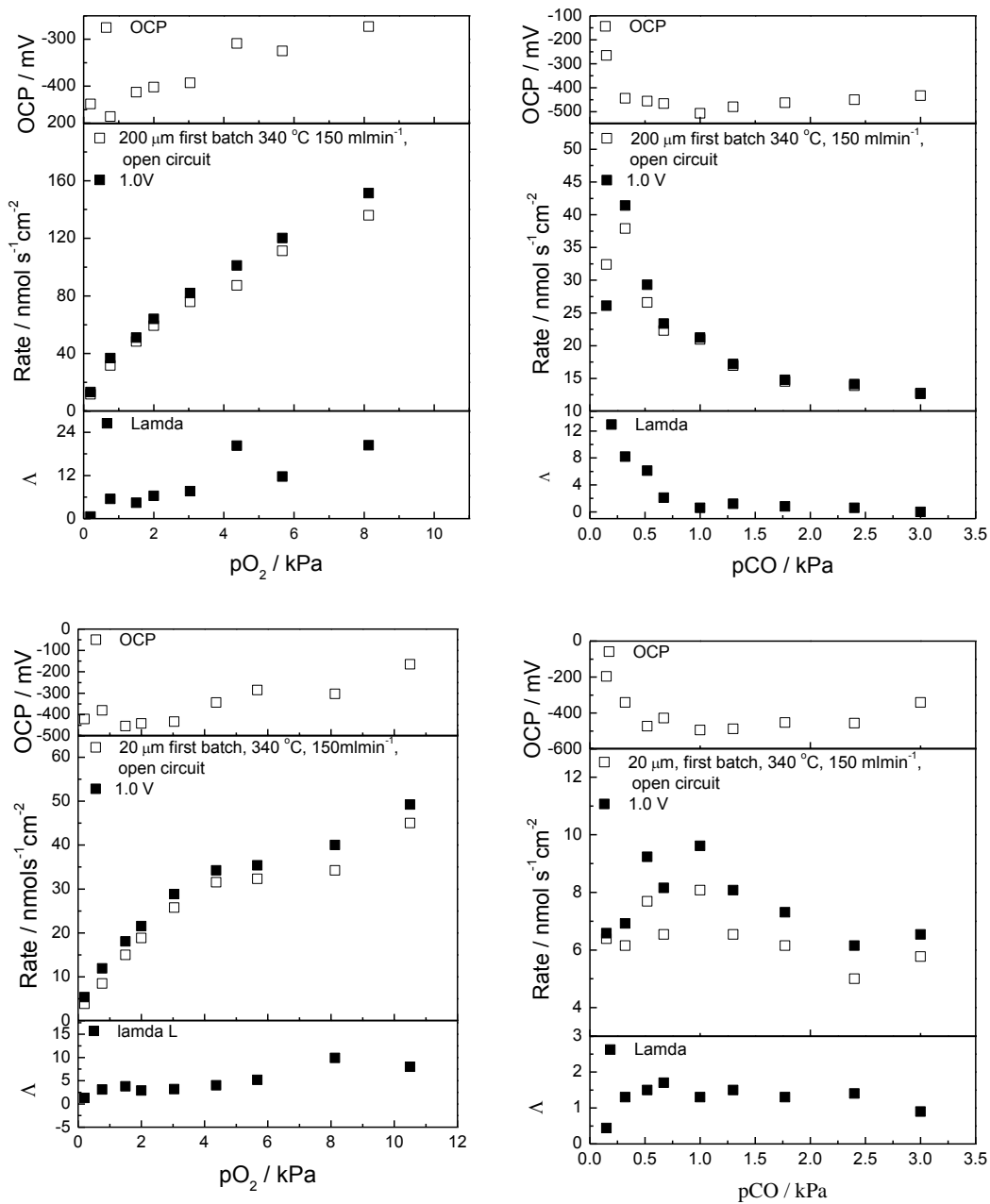


Figure 6.6: The results of EPOC experiments of CO oxidation as a function of pO₂ and pCO (under a fixed pCO=0.5kPa, pO₂=0.7kPa, respectively) at 340 °C, 1.0 V, for the 20 μm and 200 μm samples

6.3.2.1 Transient Responses of Different CO₂ Analysers

Figure 6.7 shows the transient responses of the 200 μm from the 3rd batch, which were measured by the Binos 100 CO₂ analyser and Xstream/Emerson analyser. As indicated in the figure the transient responses of the Binos 100 CO₂ analyser were digitised. In order to determine the reliability of the output of the Binos 100 CO₂ analyser, CO₂ concentration from the reactor outlet during an EPOC experiment of the 200 μm from the 3rd batch at 1.3 kPa pO₂, 0.5 kPa pCO and 350 °C was measured in conjunction with an Xstream/Emerson analyser. This is because the transient responses of the Xstream/Emerson analyser are not digitised where a gradual change (either increase or decrease) in the rate can be observed. The output of the quantum cascade CO₂ laser analyser was also not digitised however there was a technical problem with this analyser and therefore a comparison can only be made with the Xstream/Emerson analyser.

As can be seen in Figure 6.7, the output of the Xstream/Emerson analyser was also higher than that of the Binos 100 CO₂ analyser. Despite of the differences, the responses to the anodic polarisation and the changes in the catalytic rates after the current interruption are similar. From this observation, the output of the Binos 100 CO₂ analyser, although digitised, is considered as reliable to the extent of demonstrating the responses of the catalytic rates (either decrease or increase and the order of the magnitude of the changes) to the experiment conditions such as reactants concentration, temperature and polarisation.

The study which is demonstrated in Figure 6.7 indicates an electrophilic behaviour where the catalytic rate decreases with the anodic polarisation which is not discussed in other sections in this thesis. This was only observed at this oxygen pressure for this 200 μm sample. Since CO is an electron donor and oxygen is an electron acceptor, the small positive polarisation at this oxygen pressure could be possibly strengthened the Pt-CO interaction and weakened the Pt-O interaction which led to an enhanced CO coverage on the Pt surface and to PtO_x decomposition and hence caused the electrophilic behaviour [52]. However, during the early EPOC study or experiments of this 200 μm sample, a permanent EPOC with an electrophobic behaviour was also observed with a rate enhancement ratio of 1.15 and a faradaic efficiency of 42. This change in the behaviour from electrophobic to electrophilic at the same experimental conditions is suggested in

the current work to be associated with the changes occurring on the catalyst surface throughout the experimental works.

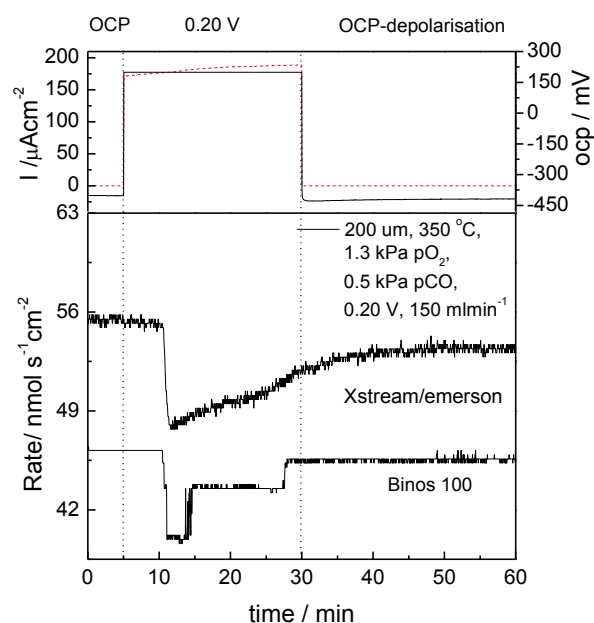


Figure 6.7: Transient responses of EPOC experiments at 1.3 kPa pO_2 , 0.5 kPa pCO , 350 °C, 150 $mlmin^{-1}$ by using Xstream/Emerson and Binos 100 CO_2 analyser

6.3.2.2 Magnitude of EPOC effect

The magnitude of the EPOC effect is discussed based on the values of the rate enhancement ratio, ρ , and faradaic efficiency, Λ . The magnitude of the permanent EPOC and permanent poisoning EPOC effect, on the other hand, are described by the permanent rate enhancement ratio, γ , and rate poisoning index, β , respectively. The values are indicated in Table 6.2 and compared with those reported in the literatures as indicated in Table 6.3. The mechanisms of the permanent EPOC and permanent poisoning EPOC effect are described later in detail in **section 6.3.3**. In the current work, the Λ and ρ values are within those using porous and sputtered Pt electrodes reported in the literatures. The Λ values reported in the present work are considerably smaller than those reported for porous electrodes due to the much shorter tpb length of the patterned electrode catalyst film in comparison to those of a porous or a high tpb density electrode [4].

Table 6.2: Rate enhancement, faradaic efficiency and permanent rate enhancement ratio

Batch	Samples (μm)	ρ	Λ	γ
1 st	20	1.1-1.4	1.3-9.9	1.1-1.2
	200	1.1-1.2	0.54-20	1.0-1.1
3 rd	200 1) 0.10 V 2) 0.20 V	1) 1.0-1.3 2) 1.0-1.2	1) 3.2-63 2) 2.7-160	1) 1.0-1.2 2) 1.2

As indicated in Table 6.2, although the 200 μm from the 3rd batch was polarised at a much smaller anodic potential, this sample exhibits a larger range of Λ , which is between 3 and 160, than that of the 20 μm and 200 μm from the 1st batch, which is between 0.5 and 20. An interesting observation is that the ρ values are very similar for samples from both batches regardless of the large differences in the applied anodic potential. The insignificant influence of the magnitude of anodic polarisation on the promoted catalytic rate during the EPOC experiments is discussed by studying the following equations [108].

$$\ln\left(\frac{r}{r_o}\right) = \alpha e \frac{\Delta U_{WR}}{K_b T} \quad (40)$$

$$\ln\left(\frac{r}{r_o}\right)_{0.10\text{ V}, 0.20\text{ V}, 350\text{ }^\circ\text{C}} \approx \ln\left(\frac{r}{r_o}\right)_{1.0\text{ V}, 340\text{ }^\circ\text{C}} \quad (40\text{ a})$$

$$\alpha \Delta U_{WR, 0.10\text{ V}, 0.20\text{ V}} \approx \alpha \Delta U_{WR, 1.0\text{ V}} \approx 1.2 \quad (40\text{ b})$$

and for an electrophobic reaction, $0 < \alpha < 1$. Assuming α is similar in both cases,

$$\Delta U_{WR, 0.10\text{ V}, 0.20\text{ V}} \approx \Delta U_{WR, 1.0\text{ V}} \quad (40\text{ c})$$

which cannot be true. The similarity of the ρ value therefore can be explained by the large differences in the electrode polarisability among the samples of different geometric characteristics (1st and 3rd batch). This is supported by the current value measured during the polarisation which is similar in the order of magnitude for all of the samples. This means that the patterned electrode from the 1st batch (low I_o) has to be strongly polarised (1.0 V) in order to generate a similar electric current with the 3rd batch (high I_o) sample which was only polarised at 0.10 V and 0.20 V [9]. This finding suggests that EPOC

effect for the Pt/YSZ system using the patterned electrodes is limited by the electrode design and processes occurring at the tpb (possibly along Pt lines) as suggested in Chapter 5.

The Pt/YSZ system utilising the patterned electrode, therefore, can be electrochemically promoted at a small anodic potential (0.10 V and 0.20 V), although exhibits small magnitude of rate enhancement ratio. This electrochemical promotion at a small anodic potential and the observed permanent EPOC phenomenon suggest that electrical energy requirement (polarising the catalyst for only a short time) can be reduced [83] through the utilisation of the patterned electrodes. Besides that, the electrode is suitable to be used as a model catalyst where the backspillover phenomenon was able to be demonstrated.

Table 6.3: Results of EPOC experiments of CO oxidation

Pt/YSZ System	T (°C), I(μA)	Ratio pCO to pO ₂	ρ/Δr	Λ	Reference
Porous Pt Film thickness: 5 μm, Surface area: 2 cm ²	(1) T: 412 °C, a. I: 400 μA, b. -400 μA	0.047/1	a. Δr: 1.68 E-7 gmole CO ₂ s ⁻¹ b. Δr: -0.51E-7 gmole CO ₂ s ⁻¹	a. Λ: 81 b. Λ: 24.6	[66]
Porous Pt Film thickness: 1.1 μm Surface area: 1 cm ²	(1) T: 225 °C, a. I: 1 μA, b. I: -1 μA (2) T: 400 °C, I: 100 μA	(1) 2.5/8 (2) 2.5E-6/1	(1) a. ρ: 1.3 b. ρ: 0.8 (2) ρ: 1.3	(1) a. Λ: 11.4 b. Λ: 9.6 (2) Λ: 0.4	[109]
Sputtered Pt Film thickness: 60 nm	T: 250 °C, a. I: 15 μA b. I: -17 μA	a. 1.2/3 b. 1.2/6	a. ρ: 0.19 b. ρ: 4	a. Λ: -450 b. Λ: 530	[51]
Magnetron sputtered Pt Film thickness: 1 μm Surface area: 0.35 cm ²	T: 300 °C, I: 4 μA	3.4/1	ρ: 1.3	Λ: 2.7	[71]
Magnetron sputtered Pt Film thickness: 80 nm Surface area: 0.145 cm ² to 0.372 cm ²	(1) T: 340 °C, 1.0 V, I: 28 to 200 μA (2) T: 350 °C, 0.10 V and 0.20 V, I: 4.7 to 53 μA	0.40/1 to 21/1	ρ: 1.0 to 1.4	Λ: 1.3 to 160	Present work

6.3.2.3 The Role of the Electrochemical Backspillover Species

The Pt/YSZ system utilising the patterned electrodes have been shown to exhibit EPOC which is known as a result of the backspillover phenomenon. To have a detail understanding on the role of the electrochemical backspillover species in the system during the polarisation, the transient responses of the 200 μm from the 3rd batch during constant applied positive (0.10 V, 0.20 V) and negative potentials (-1.0 V) were analysed and discussed below. The EPOC experiments were carried out at various $p\text{O}_2$ at constant $p\text{CO}$ (0.5 kPa), 350 °C and 400 °C with a total flow rate of 150 mlmin^{-1} at

- (a) no prior polarisation at the OCP where only the thermally induced O^{2-} can migrate onto the Pt surface
- (b) 0.10 V and 0.20 V anodic potential where both the thermal and electrochemical O^{2-} can migrate and present on the Pt surface
- (c) -1.0 V cathodic polarisation where O^{2-} cannot migrate to the Pt surface or O^{2-} are removed from the Pt surface

The occurrence and the role of the species are discussed in this section in terms of the oxygen pressure and temperature.

(i) Oxygen Pressure

1. low $p\text{O}_2$:

At 0.35 $\text{kPa}p\text{O}_2$ EPOC was not observed. This is because most of the O^{2-} which migrated from the YSZ to the tpb during the anodic polarisation desorb as O_2 .

2. high $p\text{O}_2$:

Condition 1 – There are no fluctuations in the open rate

In this case, surface oxides may present at insignificant coverage on the Pt surface where the interaction with the thermally induced O^{2-} species is also insignificant. Therefore, the formation and decomposition of these oxides which is commonly associated with the catalytic rate oscillation cannot be observed from the transient results. During polarisation, the migrated electrochemical O^{2-} spreads along the

Pt/gas interface and forms an effective double layer and hence causes the enhancement of the catalytic rate (EPOC).

Condition 2—There are fluctuations in the open circuit rate

As described in Figures 6.8, fluctuations of the open circuit rate were observed during the experiments of the 200 μm from the 3rd batch which were stopped during the positive and negative polarisation. This phenomenon can be associated with the occurrence of the thermally induced O^{2-} , electrochemically induced O^{2-} and the formation and decomposition of surface oxides. In this case, the thermally induced O^{2-} accompanied by the image charge in metal form surface dipole can form an overall neutral dipole layer or an effective double layer on the Pt surface. This double layer alters the binding strength of the covalently chemisorbed reactants such as surface oxides and hence causes oxides decomposition (adsorbed oxygen from the gas phase occupies the weakly bonded oxygen chemisorption state). Since the amount of the thermally induced O^{2-} which migrates onto the Pt surface is considerably very small in comparison to those produced during positive polarisation, the double layer is not dense and is susceptible to desorption which can cause surface re-oxidation by gaseous oxygen.

During the positive polarisation, the electrochemical induced O^{2-} also accompanied by the image charge migrated onto the Pt surface. Since the electrochemically and the thermally induced O^{2-} are similar, the addition of O^{2-} during the anodic polarisation on the Pt surface, which has already occupied by the thermally induced O^{2-} , stabilised the double layer. The stabilisation of this double layer as a result to the increase in the promoter or O^{2-} coverage on the Pt surface caused the catalytic rate to stabilise and remain at the higher limit of the oscillation during the anodic polarisation. This phenomenon can be further demonstrated by the repulsive lateral interaction of the backspillover O^{2-} with oxygen of the surface oxides which weakens the Pt– O_{ads} strength and hence led to surface oxides decomposition. Since there was a constant supply of O^{2-} during the positive polarisation, surface oxidation did not reoccur. This phenomenon was not only observed during the positive polarisation but also after the positive current interruption and during the negative polarisation as described in Figure 6.8 (b). This phenomenon which is observed after the anodic current interruption

demonstrates the role of the stored oxygen species in also stabilising the effective double layer and hence the catalytic rate (similar role with the electrochemical backspillover species). This phenomenon is verified by the transient results during the negative polarisation where after the negative current interruption the rate returned to the open circuit rate of the experiment in Figure 6.8 (a). The occurrence and the role of this stored oxygen species in the system is further described in **section 6.3.3**.

During the negative polarisation, on the other hand, the enhanced CO coverage on the Pt surface led to surface oxides decomposition and hence the oscillations were stopped. After the negative current interruption, the oscillations reappeared however the rate spiked down to a value during the -1.0 V polarisation. The 0.20 V polarisation at this oscillating rate increased and stabilised the rate to the value observed during positive polarisation of the experiment in Figure 6.8 (a). The oscillation and spiking down of the catalytic rate after the negative current interruption where the rate can only be restored to the initial condition or stabilised during the positive polarisation is explained by the formation of the strongly adsorbed surface oxides during the negative polarisation. This is further demonstrated in **section 6.3.4**. The fluctuations of the catalytic rate during EPOC studies by other researchers and current work and the mechanism describing the phenomenon are indicated in Table 6.4.

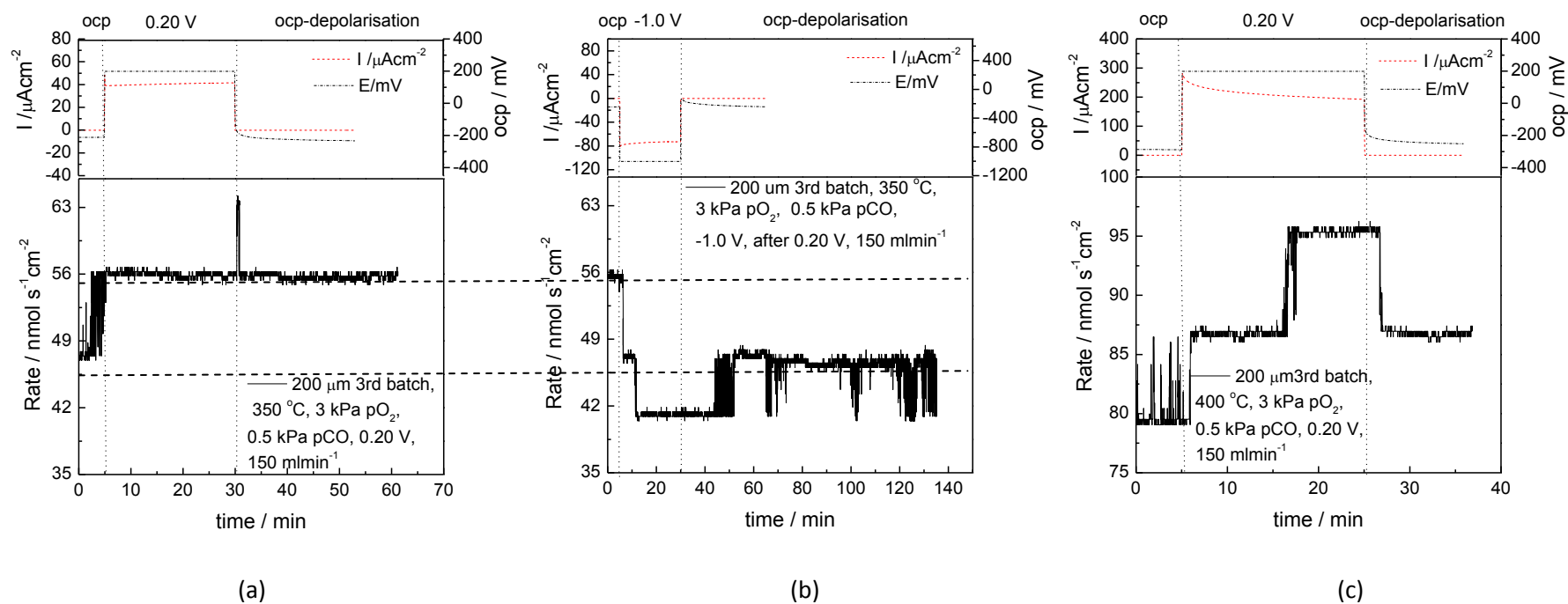


Figure 6.8: Transient responses during EPOC experiments of 200 μm from the 3rd batch at 3 kPa pO_2 , 0.5kPa pCO , and a total flow rate 150 mlmin^{-1} at (a) 350 $^{\circ}\text{C}$ and 0.20 V, (b) 350 $^{\circ}\text{C}$ and -1.0 V, (c) 400 $^{\circ}\text{C}$ and 0.20 V

Table 6.4: Findings of the Catalytic Rate Oscillations during EPOC by Other Researchers

Catalyst/Model Reaction/Temperature	Ratio to pO ₂	Effect of Polarisation/ Promoter	Mechanism	References
Pt/YSZ Porous Pt film, Surface area: 0.88 cm ² , Clean sample and 0.11% sodium coverage, C ₂ H ₄ oxidation, T:350 °C	pC ₂ H ₄ /pO ₂ : 0.5/8	Anodic and cathodic polarisations stopped catalytic rate oscillations	Not discussed	[10]
Rh/YSZ Film thickness:10 μm, Surface area: 2 cm ² , C ₂ H ₄ oxidation, T: 330 °C	pC ₂ H ₄ /pO ₂ : 0.58/1.8	Anodic polarisation caused oscillations of the catalytic rates	Interaction of the promoter with oxygen of the surface oxides and surface reoxidation by gaseous oxygen	[67]
Sputtered Pt Film thickness: 60 nm, CO oxidation T: 250 °C	pCO/pO ₂ : a.1.2/3 b.2/1	a. Anodic polarisation (15 μA) stopped the rate oscillations. b. Cathodic polarisation (-17 μA) caused a permanent oscillatory behaviour.	a. The enhanced CO coverage on Pt surface led to PtO _x decomposition b. CO depletion on Pt surface and surface PtO _x formation	[51]
Porous Pt/YSZ Film thickness: 5 μm, Surface area: 2 cm ² , CO oxidation	pCO/pO ₂ : 1/34	Negative polarisation stopped rate oscillations, positive polarisation led to rate oscillations (at high anodic currents)	Formation and decomposition of surface PtO ₂ . Oscillatory mechanism is the same both under open circuit conditions and during oxygen pumping	[66]
Sputtered Pt Pt/YSZ Film Thickness: 80 nm Surface area: CO oxidation, T: 340 °C and 350 °C	pCO/pO ₂ : 0.5/0.7 0.5/3 0.5/4.6	Anodic and cathodic polarisations stopped rate oscillations	Anodic: Repulsive lateral interaction of the promoter with oxygen of the surface oxides led to PtO _x decomposition Cathodic: Enhanced CO coverage on the Pt surface led to PtO _x decomposition	Present work

(ii) *Temperature*

At 350 °C and high pO_2 , as demonstrated in Figure 6.8, the effective double layer only causes the catalytic rate to remain at the highest limit of the open circuit rate oscillations and does not cause further rate enhancement. At 400 °C during the study at 0.20 V, on the other hand, a further increase in the catalytic rate which is higher than the highest limit of the rate oscillations under the open circuit condition was observed. This increase in the catalytic rate during the polarisation which is not observed at 350 °C can be explained by the correlation between the time constant, τ , and the measured current, I , during the polarisation at both temperatures described by equation (3) in Chapter 2.

The measured current, I , during the study at 400 °C is higher than the value measured at 350 °C. This is because at 400 °C, YSZ conductivity is higher than that at 350 °C and more charge transfer therefore occurs at the tpb during the polarisation. From equation (3), less $O^{\delta-}$ species should present (at a lower coverage) on the catalyst surface when the sample is polarised at 350 °C than that during the polarisation at 400 °C (for approximately similar polarisation time) and therefore at 350 °C the $O^{\delta-}$ species only stabilises the formed effective double layer (by the thermally induced $O^{\delta-}$ species) and hence the catalytic rate. The increase in the $O^{\delta-}$ species coverage during polarisation at 400 °C causes the formation of a denser effective double layer which resulted to a further increase of the catalytic rate.

Besides that, at 400 °C and 450 °C, the application of a small anodic potential of 0.10 V did not cause changes in the catalytic rate. This could be possibly due to a high oxygen activity at the tpb (under the open circuit condition) which is indicated by the high OCP measured at these temperatures. This observation can be associated with the higher YSZ ionic conductivity at a higher temperature and hence the occurrence of the thermally induced backspillover species.

6.3.3 *After Current Interruption*

As described in Figure 6.9, after current interruption, the promoted catalytic rate either returned to the initial condition or remained at the highly (promoted rate) steady state

condition. For the later, it is termed permanent EPOC and is explained by the release of stored oxygen at Pt/YSZ and Pt bulk upon anodic polarisation. Upon current interruption, the stored O^{2-} migrates to the Pt/gas interface from the YSZ through the tpb, spreads along the Pt/gas interface, occupies the strongly bonded oxygen chemisorption state (which was previously occupied by the electrochemical O^{2-}) and hence maintaining the effective double layer stability and keeping the catalytic rate at the promoted state. This stability of the effective double layer due to the role of the stored O^{2-} species also prevents the reoccurrence of the fluctuations of the catalytic rate (discussed in the previous section) after the current interruption. Besides that, the oxygen storage which is associated with the permanent EPOC phenomenon also explains the observations during the EPOC experiments when further positive polarisations did not cause changes in the catalytic rate. In this case, positive or anodic polarisation only affected the part of the system (binary interface) which is not exposed to the gas phase.

As demonstrated by Souentie et al. [3] and Souentie et al. [68], the migration of the stored O^{2-} backspillover species from the YSZ to the Pt/gas interface through the tpb was caused by the O^{2-} electrochemical gradient between the Pt/gas and the binary (Pt/YSZ) interface. This subsequent migration of the O^{2-} backspillover species took place until electrochemical potential equilibrium was reached. In addition to the interfacial and bulk PtO_x formation, local enrichment of the O^{2-} content of the YSZ could also contribute to the enhance coverage of the O^{2-} at Pt surface which causes the highly active open circuit steady state.

To verify and hence further demonstrate the mechanism of the permanent EPOC phenomenon due to the migration of the stored oxygen at the part of the system which is not exposed to the gas phase, correlations of the permanent rate enhancement ratio, γ , with temperature, oxygen concentration in the feed, and OCP, as indicated in Figure 6.10, are studied. As can be seen in Figure 6.10, an increase in the oxygen concentration in the feed (which also causes an increase in the OCP as described in **section 6.3.2**) at 340 °C and 350 °C causes a less pronounced permanent EPOC effect for the 20 μm and 200 μm from the 1st and the 3rd batch, respectively. This relationship could be not observed for the 200 μm from the 1st batch since γ between each reading of this sample is very similar (much smaller differences) in comparison to the other two samples.

An inversely proportional relationship between the permanent rate enhancement ratio and the OCP is described in Figure 6.10(f) and equation (41). Besides the OCP, the permanent rate enhancement ratio of the 20 μm is also found to be inversely proportional to the oxygen concentration in the feed and temperature demonstrated in equation (42) and equation (43), respectively. Decreasing the temperature and oxygen concentration in the feed causes a lower oxygen activity at tpb which is indicated by a decrease in the OCP. The lower the oxygen activity at tpb and Pt surface resulted in a larger local electrochemical potential gradient between the Pt/YSZ and Pt/gas interface and therefore caused the more pronounced effect of this permanent EPOC. However, a definitive conclusion cannot be made on the inversely proportional relationships described in Figure 6.10 (a-f). This is because the data for each length scale were obtained from the experiments which were carried out by using one sample.

$$\gamma \propto \frac{1}{V_{WR}^o} \quad (41)$$

$$\gamma \propto \frac{1}{pO_2} \quad (42)$$

$$\gamma \propto \frac{1}{T} \quad (43)$$

The application of a negative current restores the catalytic activity to the initial condition where it leads to the decomposition of the oxide species and the concomitant release of the stored charge species as described in Figure 6.9 and 6.11 (a and b). In addition to the stored oxygen at the non-gas exposed interface in the Pt/YSZ system, changes in the electrode surface morphology such as the formation of bubbles and or cracked bubbles which increase the tpb length also cause the observed permanent EPOC phenomena. However, for the case involving the microstructure changes the application of a negative current cannot restore the catalytic activity to the initial condition. This is demonstrated in Figure 6.11 (c and d). Table 6.6 summarises the permanent EPOC effect reported in the literatures and in the present work.

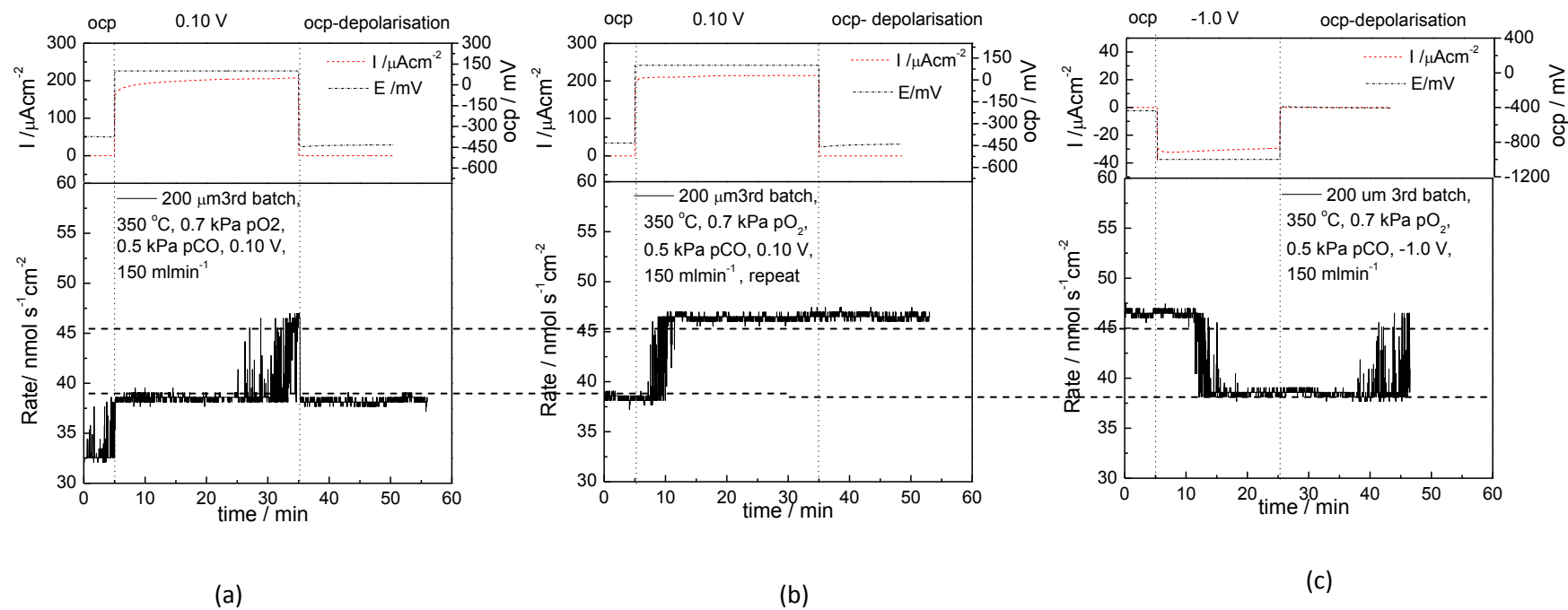


Figure 6.9: Transient responses during EPOC experiments of 200 μm from the 3rd batch at 0.7 kPa pO_2 , 0.5 kPa pCO , 350 °C, and a total flow rate 150 mlmin^{-1} (a) and (c) 0.10 V, (b) -1.0 V, which demonstrate permanent EPOC effect

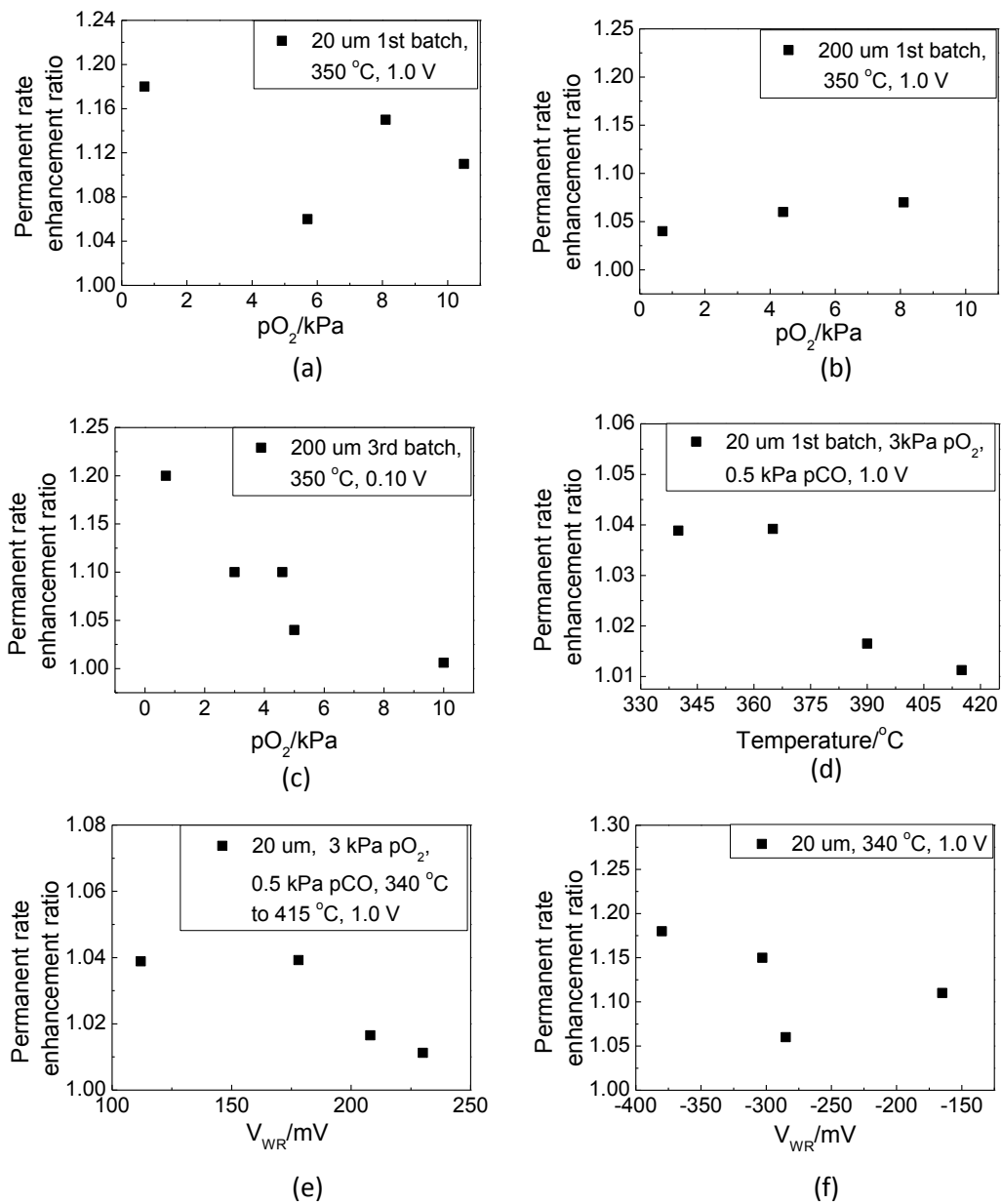


Figure 6.10: Permanent rate enhancement ratio from the transient responses at different oxygen feed composition of the (a) 20 μm , (b) 200 μm from the 1st batch and (c) 200 μm from the 3rd batch. The permanent rate enhancement ratio of the 20 μm (d) at different temperature and (e) and (f) correlation with the open circuit potential

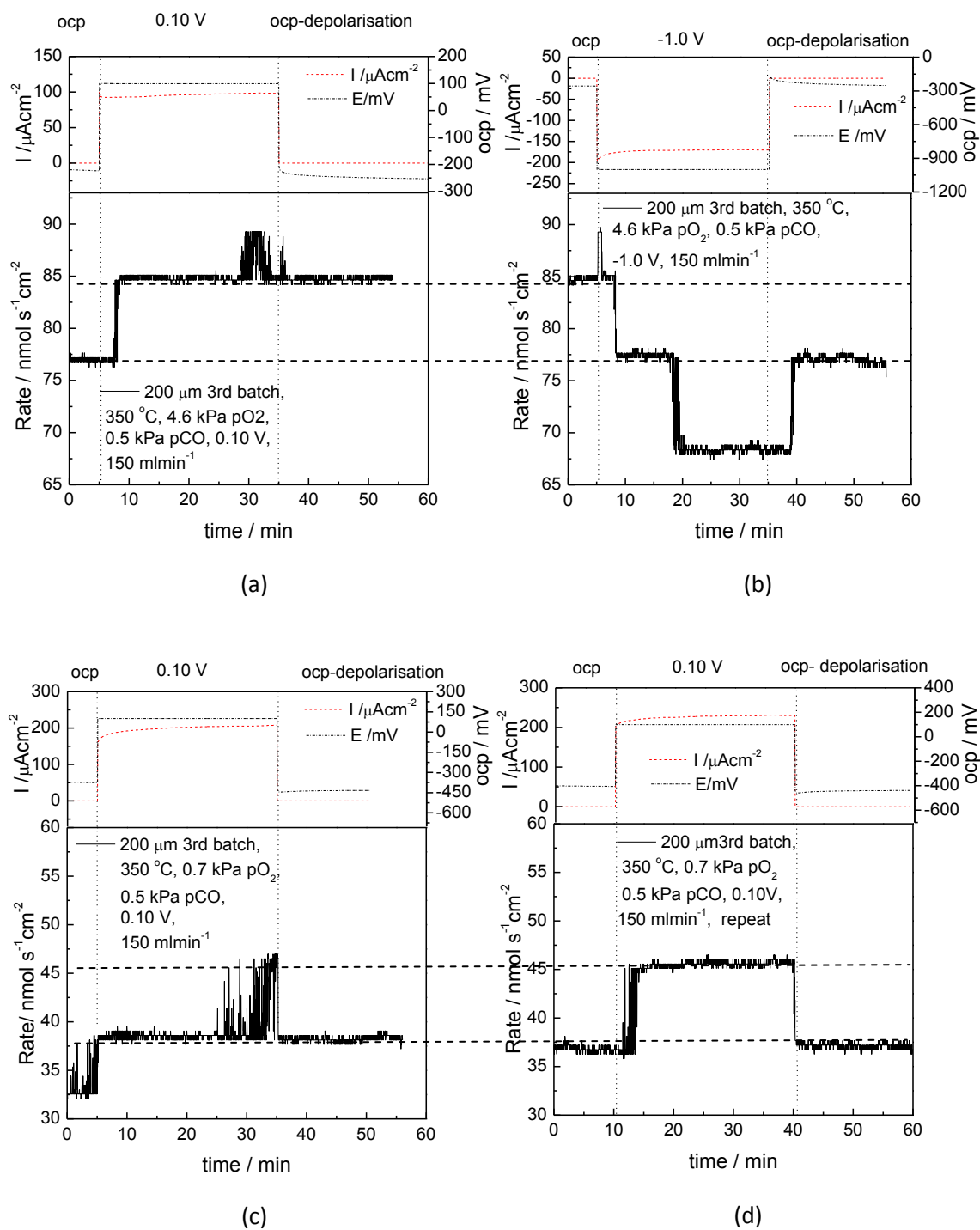


Figure 6.11: Transient responses during EPOC experiments of 200 μm from the 3rd batch at 350 $^{\circ}\text{C}$, and 150 mlmin^{-1} which demonstrate permanent EPOC effect as a result of (i) oxygen storage [(a) 4.6 kPa pO_2 , 0.5kPa pCO , 0.10 V, (b) 4.6 kPa pO_2 , 0.5kPa pCO , -1.0 V] and (ii) changes in Pt surface morphology [(c) 1st experiment and (d) repeated experiment at 0.7 kPa pO_2 , 0.5kPa pCO , 0.10 V]

6.3.4 Negative Polarisation

Upon the negative polarisation, O^{2-} are removed from the Pt surface and hence caused a decrease in the catalytic rate and after the negative current interruption, the rate returned to the initial open circuit condition. However, there are cases where the rate remained at a value lower than the initial condition after the current interruption which is demonstrated in Figure 6.8(b), Figure 6.12(b) and Figure 6.13(b). This behaviour is termed as the permanent poisoning effect. This is explained by surface oxides which can easily be formed at the tpb and on the Pt surface by the strongly adsorbed species from the gas phase during the negative polarisation. At high pO_2 such as at 5 kPa and 10 kPa the catalytic activity can be restored by the anodic potential application as demonstrated in Figure 6.13(c). However, at 0.7 kPa pO_2 as indicated in Figure 6.12(c), the strongly adsorbed oxides could not be decomposed during the anodic polarisation. The permanent poisoning effect is first time reported for a study involving CO oxidation. The permanent poisoning effect observed by other researchers is indicated in Table 6.5.

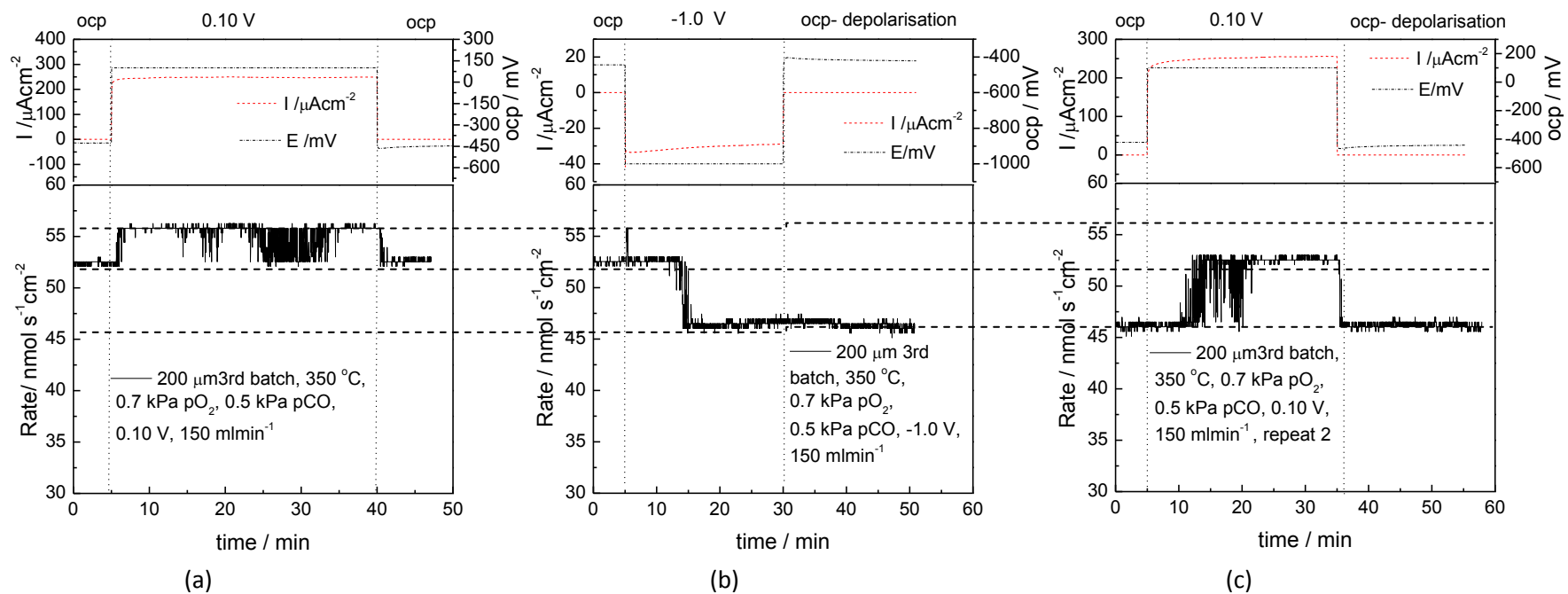


Figure 6.12: Transient responses during EPOC experiments of $200 \mu\text{m}$ from the 3rd batch at 0.7 kPa pO_2 , 0.5 kPa pCO , $350 \text{ }^\circ\text{C}$, and a total flow rate 150 mlmin^{-1} (a) 0.10 V , (b) -1.0 V and (c) 0.10 V

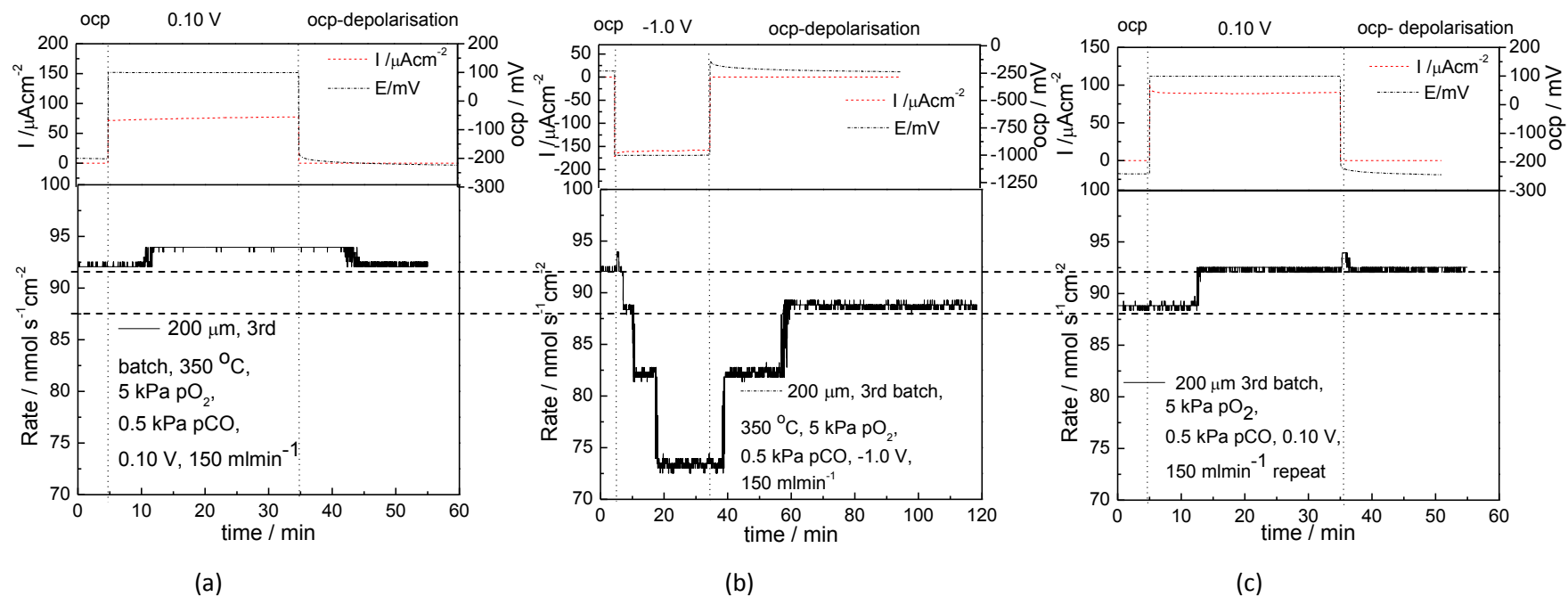


Figure 6.13: Transient responses during EPOC experiments of the 200 μm from the 3rd batch at 5 kPa pO_2 , 0.5 kPa pCO , 350 $^{\circ}\text{C}$, total flow rate 150 mlmin^{-1} and (a) 0.10 V, (b) -1.0 V and (c) 0.10 V

Table 6.5: Summary of Permanent EPOC and Permanent Poisoning from EPOC Studies

Catalyst	T (°C)	Ratio to pO ₂	γ	β	References
Sputtered Pt , Pt/YSZ, C ₃ H ₈ oxidation Film thickness:150 nm, Surface area: 1.25 cm ²	350	pC ₃ H ₈ /pO ₂ : 0.2/4.5	1.2, 1.3		[3]
Sputtered Pt, Pt/YSZ, C ₂ H ₄ oxidation Film thickness: 1 μ m	375	pC ₂ H ₄ /pO ₂ : 0.2/8.2	1.7		[68]
Sputtered Pd, Pd/YSZ, CH ₄ oxidation Film thickness: 380 nm, Surface area: 2cm ²	350	pCH ₄ /pO ₂ : (a) 2.6/1.9 (b) 1.4/2.8 (c) 1.3/4.5		(a) 0.10 (b) 0.12 (c) 0.16	[6]
Rh/YSZ, CH ₄ oxidation Film thickness: 10 μ m	430	pCH ₄ /pO ₂ : (a) 1.8/2.0 (b) 1.7/3.4		(a) 0.17 (b) 0.50	[5]
Pt/YSZ, Iron doped Pt sample, C ₂ H ₄ oxidation	425	pC ₂ H ₄ /pO ₂ : 0.19/8.2	1.7 to 10		[4]
Magnetron sputtered Pt, Pt/YSZ, CO oxidation Film thickness: 80 nm Surface area: 0.145 cm ² to 0.372 cm ²	340, 350	pCO/pO ₂ : 0.50/0.70 0.50/5.0 0.50/10	1.0 to 1.2	0.12, 0.03	Present work

6.3.5 Correlations of Rates with the Open Circuit Potential (OCP)

The backspillover phenomena and the mechanisms of the related processes occurring at the tpb involving O^{2-} in the Pt/YSZ system utilising the patterned electrodes have been discussed in the previous sections. In this section, the phenomena and mechanisms are further discussed by studying the catalytic rates and current relationship with the OCP as described in Figure 6.14 to 6.16. This is because OCP measures the oxygen activity at tpb [9] and OCP dependence of the rates and current should indicate tpb dependence of both data. However, this analysis is not conclusive since the data described in Figure 6.14 to 6.16 were only obtained from the experiments of only one sample for each length scale.

The first correlation is between the catalytic rate (open and close circuit) and the OCP and this is indicated in Figure 6.14 and 6.15. From the correlation, a proportional relationship is found between both the catalytic rates and the OCP and this is described by equation (44) and equation (45). The proportional relationship of the electrochemical promotion rate with the OCP can be explained by the electrochemical reactions involving reactants from the gas/electrode/electrolyte phase which can only take place at the tpb. The similar relationship with the OCP of both the open circuit and the electrochemical promoted catalytic rate suggests a tpb dependence of the open circuit rate. This finding not only support the discussions on the rate dependence on the tpb length in the previous sections but also the results of the electrochemical characterisations under a nonreactive condition which demonstrated a tpb dependence of the charge transfer reaction (in Chapter 5). Besides that, the proportional relationship of the catalytic rate with the OCP suggests the potential of utilising the patterned electrodes as a CO oxidation rate sensor [51].

$$r_o \propto V_{WR}^o \quad (44)$$

$$r \propto V_{WR}^o \quad (45)$$

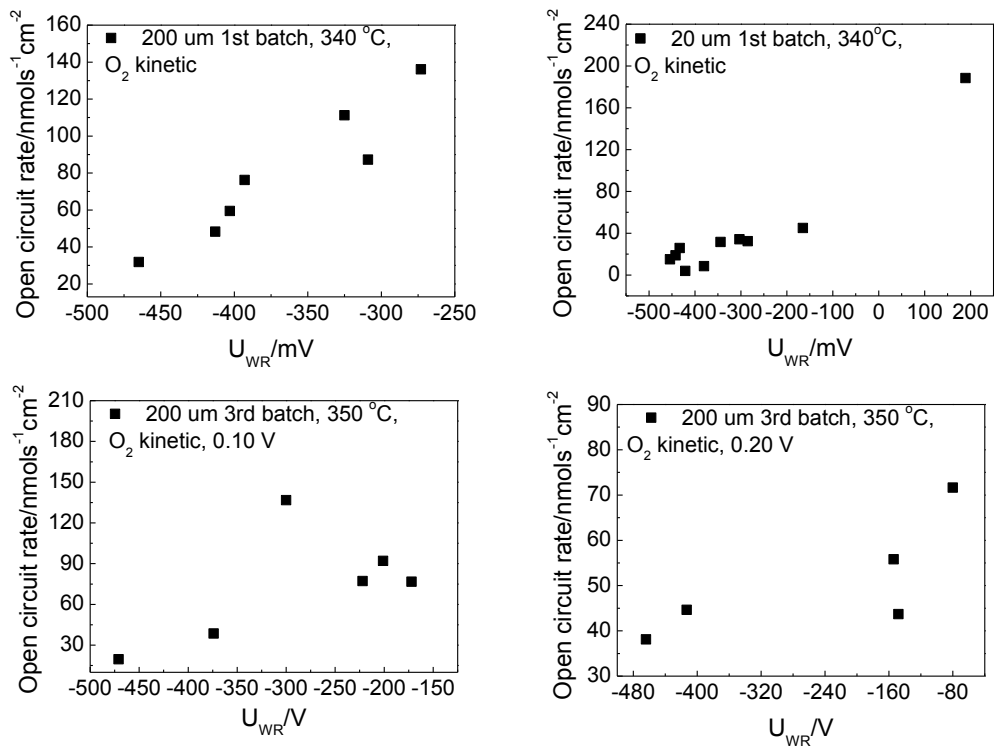


Figure 6.14: Open circuit rate and open circuit potential measured before the polarisation (a) 200 μm 1st batch, (b) 20 μm from the 1st batch, (c) 200 μm from the 3rd batch after electrochemical characterisation under nonreactive condition at 0.10 V, (d) 200 μm from the 3rd batch after electrochemical characterisation under nonreactive condition at 0.20 V

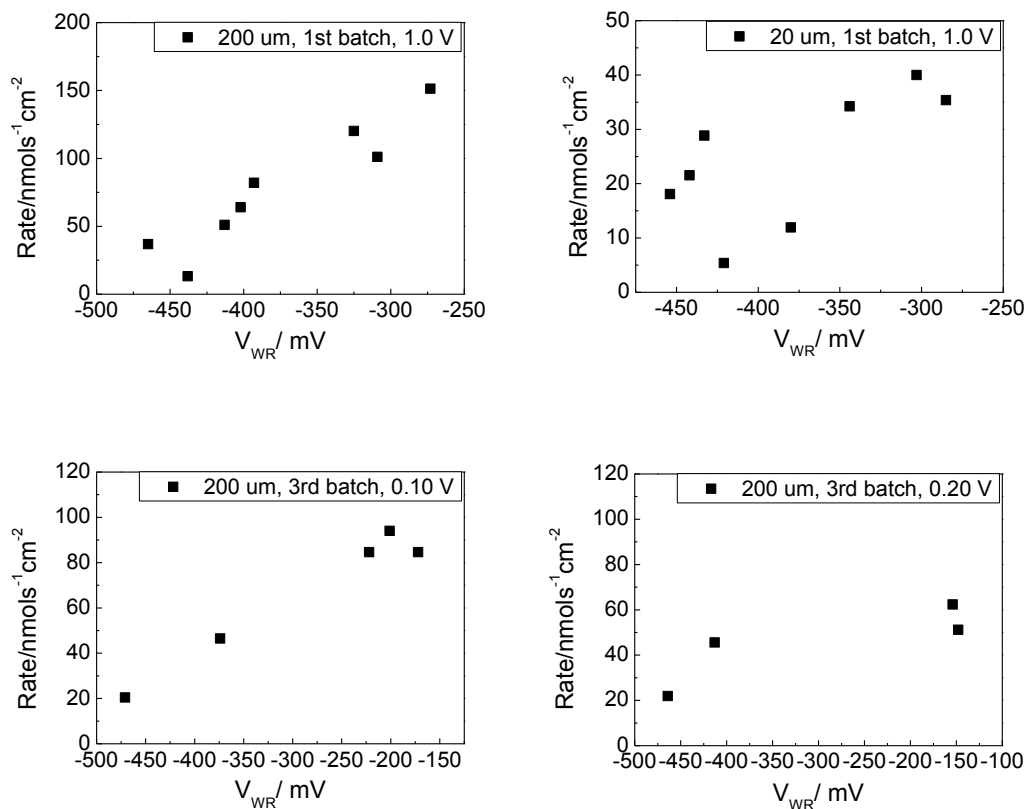


Figure 6.15: Electrochemical promoted rate and open circuit potential (a) 200 μm 1st batch, (b) 20 μm 1st batch, (c) 200 μm 3rd batch after electrochemical characterisation under nonreactive condition at 0.10 V, (d) 200 μm 3rd batch after electrochemical characterisation under nonreactive condition at 0.20 V

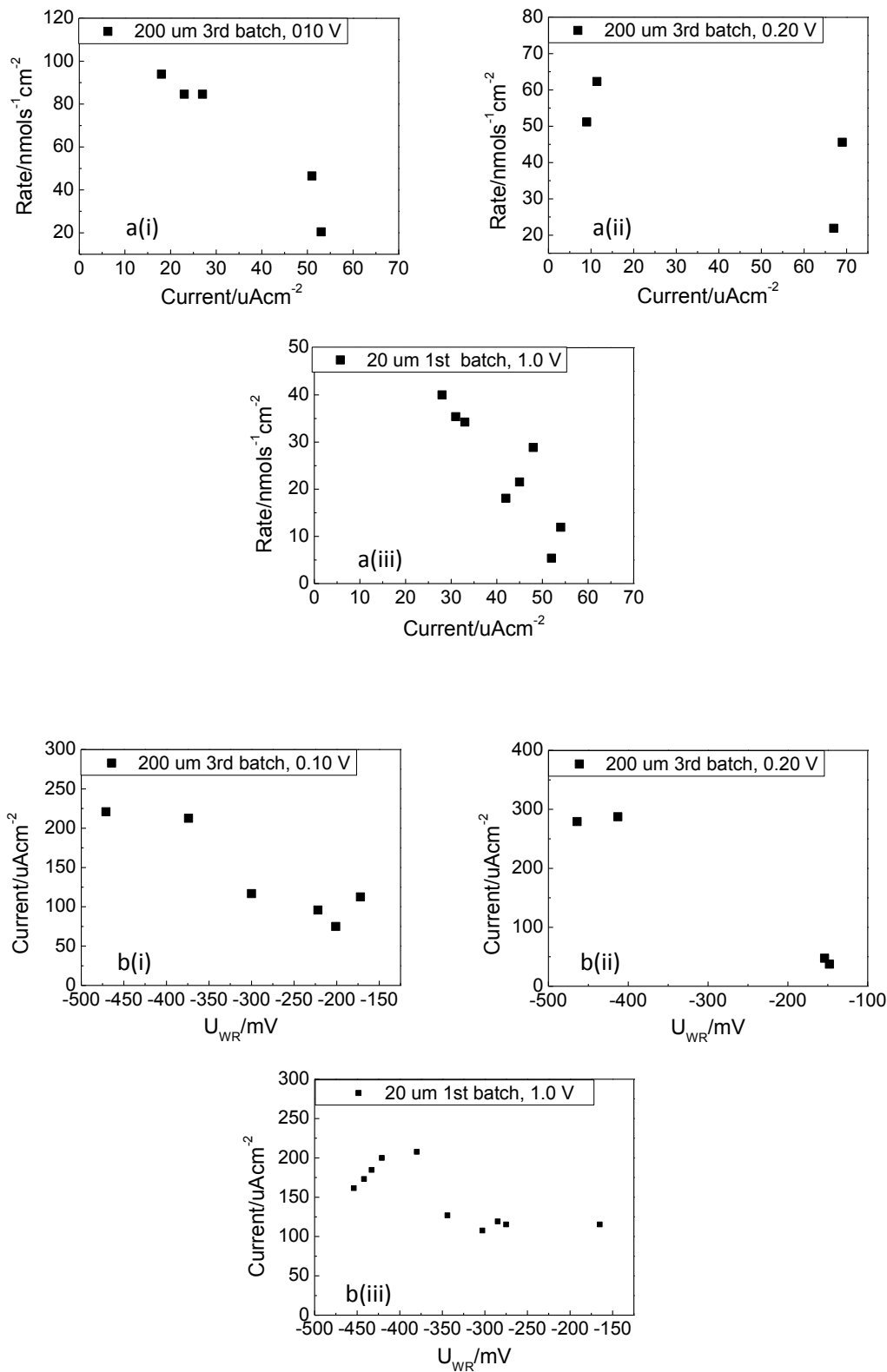


Figure 6.16: (a) Current and electrochemical promoted rate, (b) current and open circuit potential of the 20 μm and 200 μm from the 1st batch and the 200 μm from the 3rd batch

To further demonstrate the tpb dependence of both the open and close circuit catalytic rates, changes in the transient responses during the repeated experiments of the 20 μm from the 1st batch and the 200 μm from the 3rd batch are studied. For this analysis, it is assumed that the exposure to temperature and polarisation during the EPOC experiments causes changes in the electrode surface morphology or microstructure such as the formation of bubbles and or cracked bubbles, as indicated by SEM images in Table 5.1 and 6.1 which is known (in literatures) can change or increase the tpb length. Figure 6.17 demonstrates the transient results of the 20 μm from the 1st batch. As indicated in the figure a similarity is observed in the changes of the open and close circuit rates where both rates increased to a higher value during the repeated or 2nd EPOC experiment which was carried out at the same experimental conditions of the 1st experiment. The 2nd experiment was carried out on a different day and after EPOC experiments at different $p\text{O}_2$ and $p\text{CO}$ were completed at 340 $^\circ\text{C}$. The significant increase in the open and close circuit rates of approximately 86% and 85%, respectively, can be associated with the effect of exposing the sample to a large (1.0 V) anodic polarisation during EPOC experiments where the tpb length may have increased due to the formation of bubbles and or cracked bubbles.

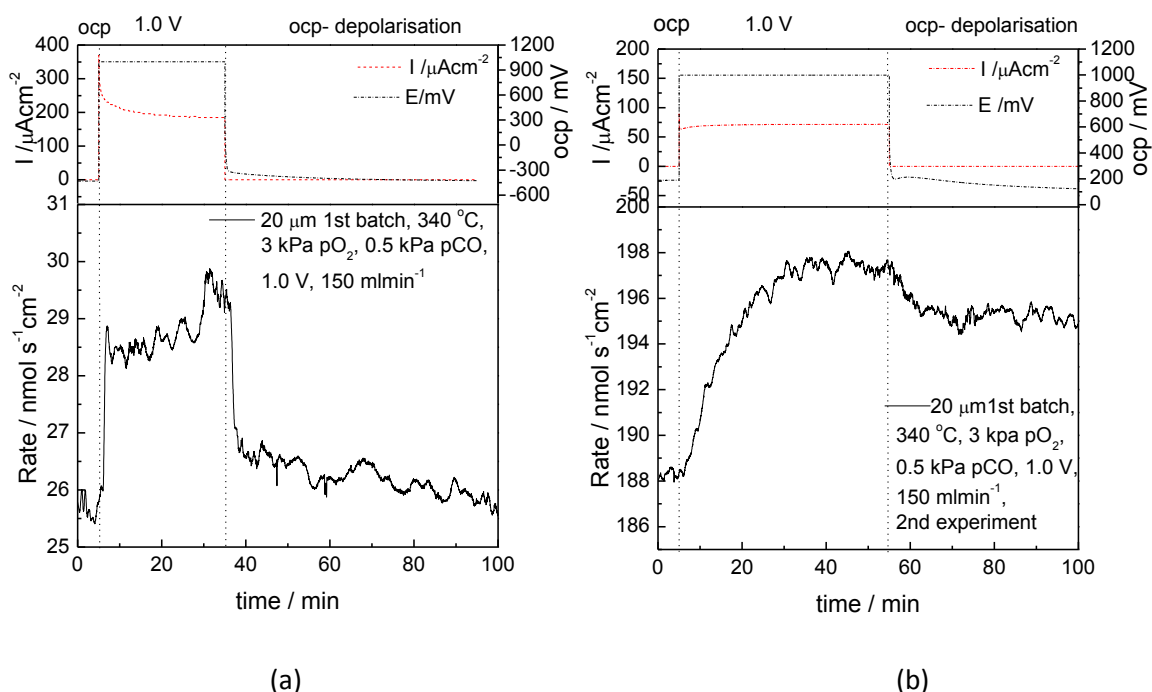


Figure 6.17: Transient responses of the 20 μm sample during EPOC studies at 340 $^\circ\text{C}$, 3kPa $p\text{O}_2$, 0.5kPa $p\text{CO}$, 1V, 150mlmin⁻¹ of the (a) first and (b) second experiments

Similar to the results of the 20 μm , as indicated in Figure 6.11(c and d) there is also an increase in both the open and close circuit rates when the EPOC experiment of the 200 μm from the 3rd batch was repeated within a short period of time. The factor of time is important for the description of the catalytic behaviour of the 200 μm because this sample was only exposed to a small anodic potential and the experimental data of this sample has been associated with the effect of surface oxides formation at tpb (when the sample was left in the reactor during no experimental works) as discussed in the previous section and in Chapter 5. The blocking effect of surface oxides may interact with the effect caused by the formation of new tpb due to the changes in electrode surface morphology on the catalytic rate and therefore this increase in the rate is not observed if the experiment is repeated after a longer period of time.

The blocking effect of surface oxides at tpb is suggested by the open and close circuit rates of the 200 μm from the 3rd batch, as indicated in Figure 6.5(b), which has been exposed up to 0.20 V and -1.0 V potentials. The transient experiments at 0.20 V were carried out after electrochemical experiments under nonreactive and reactive condition at 0.10 V and after electrochemical experiments under nonreactive condition at 0.20 V were completed at 350 °C, 400 °C and 450 °C. The rates during the experiments at 0.20 V were much lower than that of the experiments at 0.10 V. Exposures to the -1.0 V potential (under nonreactive and reactive conditions) may not be able to decompose the strongly adsorbed oxides at tpb and this is also indicated by the smaller currents measured during the transient experiments at 0.20 V than that measured during the transient experiments at 0.10 V. These results further verify the similarity of the open and close circuit catalytic rates where both are dependent on the tpb length.

Next, a correlation between (i) the current and the OCP and (ii) the current and the electrochemical promoted rate are studied where the data is presented in Figure 6.16. As demonstrated in Figure 6.16, an inversely proportional relationship is observed except between the current and OCP in the case of the 20 μm from the 1st batch as described in Figure 6.16 b(iii). The inversely proportional relationship correlations demonstrate that a lower oxygen activity at tpb (during a small amount of oxygen concentration available in the feed) led to an increase in the number of backspillover species which can migrate through tpb on the Pt surface. However, since the oxygen concentration in the feed was

small, there should be less reaction involving the normally chemisorbed atomic oxygen (which is more reactive than the spillover species) at this small concentration and thus resulted to the smaller electrochemical promoted rate. The developed correlations are described by equations (46 to 50).

$$r \propto pO_2 \quad (46)$$

$$r \propto \frac{1}{I} \quad (47)$$

$$pO_2 \propto \frac{1}{I} \quad (48)$$

$$I \propto \frac{1}{V_{WR}^o} \quad (49)$$

$$\Lambda \propto \frac{1}{I} \quad (50)$$

6.4 Summary

In summary, surface oxides formation at tpb has been discussed as a cause of (i) the difficulties in observing a correlation between the tpb length and the open circuit catalytic rate, (ii) the decrease in the open circuit catalytic rate over time of the 200 μm from the third batch (iii) the fluctuations of the open circuit rate and (iv) the permanent poisoning effect. Besides that, Pt/YSZ system utilising the patterned electrodes was found to exhibit EPOC, permanent EPOC and permanent poisoning EPOC effect. Most important, the occurrence of electrochemical backspillover species and its role during positive polarisation were able to be demonstrated. At least five types of oxygen species are suggested can present on the Pt/catalyst surface at most experimental conditions as demonstrated in Table 6.6. Type I species is the reactive chemisorbed oxygen from gas phase, type II species is the strongly adsorbed O as PtO_x from gas phase which blocks active sites, type III species is the thermally induced backspillover $\text{O}^{\delta-}$, type IV species is the electrochemically induced backspillover $\text{O}^{\delta-}$ and type V species is the stored oxygen upon anodic polarisation from non-gas exposed interface. The EPOC effect or the migration of the backspillover species during polarisation is strongly dependent on the coverage of those species on the Pt surface.

Table 6.6: Type of oxygen species on Pt surface.

Experimental Condition (O ₂ Kinetic)	Oxygen Species				
	I	II	III	IV	V
Less Oxidising	Present at low coverage	May present at a very low coverage	May present at a very low coverage	Mostly desorbed as O ₂	Present at low coverage
Moderate	Present	Present	Present	Present	Present
Oxidising	Present	Present	Present	Present	Present
Very Oxidising	Present	Present	Present	Present	Present

I: reactive chemisorbed oxygen from gas phase

II: strongly adsorbed O as PtO_x from gas phase which blocks active sites

III: thermally induced backspillover species

IV: electrochemically induced backspillover species

V: stored oxygen upon anodic polarisation from non-gas exposed interface

Chapter 7. Conclusions and Recommendations

7.0 Summary

This chapter summarises and concludes the findings of the current work in which the objective was to describe the backspillover phenomena and to determine factors controlling this process in a Pt/YSZ system utilising a model catalyst or patterned electrodes. This is because patterned electrodes of different width length scale, which were prepared by magnetron sputtering supported by YSZ, are well defined geometrically and should have a controlled amount of impurities (if any) on the catalyst surface. Most important, variables associated with the geometry characteristics are minimised and this allows the investigation of oxygen charge transfer at the three phase boundary (tpb). The electrodes are assumed geometrically simple because they have been fabricated by using a technology which causes less variation in the amount of Pt sputtered on the YSZ which should not be the case when the commercially available Pt pastes are painted manually on the YSZ pellets.

Prior to the study using the model catalyst, it is important first to demonstrate the presence of impurities in the commercially available catalysts (in this case from three providers) and hence on the sintered catalyst films. This has been obtained by carrying out impurity analyses by inductively coupled plasma in conjunction with atomic emission spectroscopy (ICP-OES). To show differences in the surface microstructure of the catalyst films of different providers, the sintered films were analysed by scanning electron microscopy (SEM). The results indicate that commercially available catalysts of different providers have different impurities where the type and amount of impurities of the sintered films (including the resulted surface morphology) are also vary which can also be associated with the differences in the sintering program suggested by the providers. These findings explain the variability in the electrochemical data often discussed in the literatures which is also proven in the current work by the CV results of the electrodes prepared by using the catalysts from the three providers under the nonreactive condition, at low temperature and under atmospheric condition. The effect of impurities is found to

interact with the effect of electrode microstructure or morphology and therefore a complex model is necessary to describe the electrochemical behaviour of such system.

Next, investigations of electrochemical behaviour of the Pt/YSZ system utilising the patterned electrodes were carried out also under the nonreactive condition at low temperature and under atmospheric condition in which various techniques were used which included scanning electron microscopy (SEM), cyclic voltammetry (CV), linear sweep, reverse potential, electrochemical impedance spectroscopy (EIS), current overpotential and hydrogen reduction experiments. First, the electrochemical data of patterned electrodes of different width length scale were compared. From this analysis, the tpb dependence of the oxygen charge transfer was not observed. This has been explained due to the changes of the patterned electrodes surface characteristics throughout the experimental works which include the formation of surface oxide at the tpb and the creation of new tpb due to bubble and cracked bubble formation.

Then, the results of repeatability study of the patterned electrode of one length scale (one sample) were analysed and it appears that this study can serve as another approach of observing the tpb dependence of the oxygen charge transfer (*This is similarly observed from the results of kinetic studies under the reactive condition*). From the repeatability study, oxygen activity (oxidation and reduction processes) at the binary (Pt/YSZ) interface is found to provide an insight into the activity at the tpb. Besides that, the presence of impurity oxides or Pt oxides of different oxidation state is suggested. Furthermore, the patterned electrodes are durable to the experimental conditions and can be reactivated by carrying out chemical treatments such as exposing the sample to hydrogen and by keeping the sample under a less oxidising condition during no experimental works.

After carrying out analyses on the results from the studies under the nonreactive condition, the focus was on the transient results from the experiments under the reactive conditions. The Pt/YSZ system using the patterned electrodes exhibits EPOC where permanent EPOC was also observed and permanent poisoning EPOC effect is first time reported in this work for CO oxidation. Through the utilisation of the patterned electrodes, EPOC was explained by the occurrence of backspillover species where the phenomenon was observed even with the application of very small anodic potentials of

0.10 V and 0.20 V at 350 °C. This finding therefore further verifies the existing theory or mechanism of the origin of the EPOC established by Vayenas and co-workers. However, the large differences in the electrode polarisability among the samples of different geometric characteristics suggests that EPOC effect and hence the backspillover phenomena in the present work is limited or controlled by electrode design and or processes taking place at the tpb.

In terms of the role of the backspillover species in the system during positive or anodic polarisation, the species was found not only to enhance the catalytic rate but also to stop rate oscillation by stabilising the effective double layer at the Pt/gas interface which formed by the thermally induced backspillover species. There are cases where after the positive current interruption, the catalytic rate remained stable at the highest limit of the rate oscillations. This is explained by the similarity in the role of the stored oxygen at the binary Pt/YSZ interface and Pt bulk with the backspillover species which controls the surface oxygen activity. In other words, an increase in the $O^{\delta-}$ coverage on the Pt surface, during the polarisation and after the positive current interruption, stabilises the effective double layer and therefore a stable catalytic rate at the higher limit of the rate oscillation can be observed. Another interesting finding is that there are five types of oxygen species can present on the Pt surface where the coverage of those species on the Pt surface controls the amount of the backspillover species which can migrate onto the Pt surface under the influence of the positive polarisation.

7.1 Conclusions

The present work concluded that

- (i) impurities influence the charge transfer reactions.
- (ii) the presence of either impurity oxides or Pt oxides of different oxidation state at the binary interface.
- (iii) the occurrence and the presence of backspillover species or the promoter (which in this case is $O^{\delta-}$) on the Pt surface caused the EPOC effect. Influences of impurities on EPOC cannot be excluded although not discussed in this work.
- (iv) EPOC is possible at small anodic potentials of 0.10 V and 0.20 V during CO oxidation at low temperature from the utilisation of the patterned electrodes. The catalytic reaction was electrophobic except at 1.3 kPa pO_2 and 0.5 kPa pCO .

- (v) the electrode design and the coverage of oxygen ionic species at the tpb and on the Pt surface control the backspillover processes.
- (vi) Pt/YSZ system using the patterned electrodes exhibited permanent EPOC and permanent poisoning EPOC effect.
- (vii) there is a similarity in the role of the stored oxygen at the binary Pt/YSZ interface and Pt bulk with the electrochemical backspillover species in controlling the surface oxygen activity, stabilising the effective double layer and enhancing the catalytic rate.
- (viii) the patterned electrodes are durable and can be applied in the field where the possible applications are in (i) sensor technology (CO oxidation catalytic rate sensor) and in (ii) EPOC.

7.2 Recommendations

Due to the limitations described in Chapter 1, the findings of the current work can be further explained by carrying out

- a. EPOC experiments by using the commercial catalysts under similar experimental conditions of the EPOC experiments carried out on the patterned electrodes. This is to further verify the influence of impurities on EPOC.
- b. EPOC experiments at a higher anodic potential (for the case of the patterned electrodes).
- c. kinetic study under open circuit conditions. This is to further verify the applications of the patterned electrodes in sensor technology.
- d. in situ analyses or measurement for better description or verifications of the mechanisms of the charge transfer and EPOC.
- e. sample pretreatment (in order to obtain approximately similar electrode morphology or microstructure) prior to the catalytic and electrochemical experiments.
- f. data analyses through the application of software such as those used in demonstrating the data obtained from EIS.

References

- [1] M. N. Tsampas and P. Vernoux, "Chapter 11 – Electrochemical Promotion of Catalysis for Automotive Post-Treatment and Air Cleaning," *New Futur. Dev. Catal. Catal. Remediat. Environ. Concerns*, pp. 281–302, 2013.
- [2] C. G. Vayenas, S. Brosda, and C. Pliangos, "Rules and Mathematical Modeling of Electrochemical and Chemical Promotion 1. Reaction Classification and Promotional Rules," *J. Catal.*, vol. 203, pp. 329–350, Oct. 2001.
- [3] S. Souentie, L. Lizarraga, E. I. Papaioannou, C. G. Vayenas, and P. Vernoux, "Permanent electrochemical promotion of C₃H₈ oxidation over thin sputtered Pt films," *Electrochem. commun.*, vol. 12, pp. 1133–1135, Aug. 2010.
- [4] E. Mutoro, C. Koutsodontis, B. Luerssen, S. Brosda, C. G. Vayenas, and J. Janek, "Electrochemical promotion of Pt(111)/YSZ(111) and Pt–FeOx/YSZ(111) thin catalyst films: Electrocatalytic, catalytic and morphological studies," *Appl. Catal. B Environ.*, vol. 100, pp. 328–337, Oct. 2010.
- [5] A. Nakos, S. Souentie, and A. Katsaounis, "Electrochemical promotion of methane oxidation on Rh/YSZ," *Appl. Catal. B Environ.*, vol. 101, pp. 31–37, Nov. 2010.
- [6] F. Matei, D. Ciuparu, C. Jiménez-Borja, F. Dorado, J. L. Valverde, and S. Brosda, "Electrochemical promotion of methane oxidation on impregnated and sputtered Pd catalyst-electrodes deposited on YSZ," *Appl. Catal. B Environ.*, vol. 127, pp. 18–27, Oct. 2012.
- [7] A. Jaccoud, C. Falgairrette, G. Fóti, and C. Comninellis, "Charge storage in the O₂(g),Pt/YSZ system," *Electrochim. Acta*, vol. 52, pp. 7927–7935, Nov. 2007.
- [8] E. Mutoro, B. Luerßen, S. Günther, and J. Janek, "The electrode model system Pt (O₂)/YSZ : Influence of impurities and electrode morphology on cyclic voltammograms," *Solid State Ionics*, vol. 180, pp. 1019–1033, 2009.
- [9] R. Imbihl, "Electrochemical promotion of catalytic reactions," *Prog. Surf. Sci.*, vol. 85, pp. 241–278, May 2010.
- [10] N. Ibrahim, D. Poulidi, and I. S. Metcalfe, "The role of sodium surface species on electrochemical promotion of catalysis in a Pt/YSZ system: The case of ethylene oxidation," *J. Catal.*, vol. 303, pp. 100–109, Jul. 2013.
- [11] N. Ibrahim, M. R. Jalil, D. Poulidi, and I. S. Metcalfe, "The role of low coverage sodium surface species on electrochemical promotion in a Pt/YSZ system," *Solid State Ionics*, vol. 225, pp. 386–389, Oct. 2012.

- [12] S. Radhakrishnan, R., Virkar, A.V. and Singhal, “Estimation of charge-transfer resistivity of Pt cathode on YSZ electrolyte using patterned electrodes,” *J. Electrochem. Soc.*, vol. 152, no. 5, pp. A927–A936, 2005.
- [13] A. K. Opitz, A. Lutz, M. Kubicek, F. Kubel, H. Hutter, and J. Fleig, “Investigation of the oxygen exchange mechanism on Pt|yttria stabilized zirconia at intermediate temperatures: Surface path versus bulk path,” *Electrochim. Acta*, vol. 56, pp. 9727–9740, Nov. 2011.
- [14] A. K. Opitz and J. Fleig, “Investigation of O₂ reduction on Pt/YSZ by means of thin film microelectrodes: The geometry dependence of the electrode impedance,” *Solid State Ionics*, vol. 181, pp. 684–693, Jun. 2010.
- [15] H. Pöpke, E. Mutoro, B. Luerßen, and J. Janek, “Oxygen reduction and oxidation at epitaxial model-type Pt(O₂)/YSZ electrodes – On the role of PtO_x formation on activation, passivation, and charge transfer,” *Catal. Today*, vol. 202, pp. 12–19, Mar. 2013.
- [16] H. Pöpke, E. Mutoro, C. Reiß, B. Luerßen, M. Amati, M. K. Abyaneh, L. Gregoratti, and J. Janek, “The role of platinum oxide in the electrode system Pt (O₂)/yttria-stabilized zirconia,” *Electrochim. Acta*, vol. 56, pp. 10668–10675, 2011.
- [17] J. Bandlow, P. Kaghazchi, T. Jacob, C. Papp, B. Tränkenschuh, R. Streber, M. P. A. Lorenz, T. Fuhrmann, R. Denecke, and H. Steinr, “Oxidation of stepped Pt (111) studied by x-ray photoelectron spectroscopy,” *Phys. Rev. B*, vol. 83, pp. 174107–1, 2011.
- [18] S. A. Krasnikov, S. Murphy, N. Berdunov, A. P. Mccoy, K. Radican, and I. V Shvets, “Self-limited growth of triangular PtO₂ nanoclusters on the Pt (111) surface and I V Shvets,” *Nanotechnology*, vol. 21, pp. 1–7, 2010.
- [19] S. Brosda, C. G. Vayenas, and J. Wei, “Rules of chemical promotion,” *Appl. Catal. B Environ.*, vol. 68, pp. 109–124, Nov. 2006.
- [20] I. Constantinou, D. Archonta, S. Brosda, M. Lepage, Y. Sakamoto, and C. G. Vayenas, “Electrochemical promotion of NO reduction by C₃H₆ on Rh catalyst-electrode films supported on YSZ and on dispersed Rh/YSZ catalysts,” *J. Catal.*, vol. 251, pp. 400–409, Oct. 2007.
- [21] C. . Vayenas and S. I. Bebelis, “Electrochemical promotion,” *Solid State Ionics*, vol. 94, pp. 267–277, 1997.

- [22] D. Poulidi, C. Anderson, and I. S. Metcalfe, "Remote control of the activity of a Pt catalyst supported on a mixed ionic electronic conducting membrane," *Solid State Ionics*, vol. 179, pp. 1347–1350, Sep. 2008.
- [23] D. Tsiplakides, S. Neophytides, and C. G. Vayenas, "Investigation of electrochemical promotion using temperature- programmed desorption and work function measurements," *Solid State Ionics*, vol. 136–137, pp. 839–847, 2000.
- [24] A. Katsaounis, Z. Nikopoulou, X. E. Verykios, and C. G. Vayenas, "Comparative isotope-aided investigation of electrochemical promotion and metal–support interactions 1. 18O₂ TPD of electropromoted Pt films deposited on YSZ and of dispersed Pt/YSZ catalysts," *J. Catal.*, vol. 222, pp. 192–206, Feb. 2004.
- [25] R. Imbihl and J. Janek, "Spatially resolved measurements of electrochemically induced spillover on porous and microstructured Pt/YSZ catalysts," *Solid State Ionics*, vol. 136–137, pp. 699–705, 2000.
- [26] E. Mutoro, S. Gunther, B. Luersen, I. Valov, and J. Janek, "Electrode activation and degradation: Morphology changes of platinum electrodes on YSZ during electrochemical polarisation," *Solid State Ionics*, vol. 179, pp. 1835–1848, Oct. 2008.
- [27] A. De Lucas-consuegra, F. Dorado, C. Jiménez-Borja,, A. Caravaca, P. Vernoux, and J. L. Valverde, "Use of potassium conductors in the electrochemical promotion of environmental catalysis," *Catal. Today*, vol. 146, pp. 293–298, 2009.
- [28] S. P. Yoon, S. W. Nam, J. Han, T.-H. Lim, S.-A. Hong, and S.-H. Hyun, "Effect of electrode microstructure on gas-phase diffusion in solid oxide fuel cells," *Solid State Ionics*, vol. 166, pp. 1–11, Jan. 2004.
- [29] V. Perrichon, L. Retailleau, P. Bazin, M. Daturi, and J. C. Lavalley, "Metal dispersion of CeO₂–ZrO₂ supported platinum catalysts measured by H₂ or CO chemisorption," *Appl. Catal. A Gen.*, vol. 260, pp. 1–8, Mar. 2004.
- [30] J. Dawody, L. Eurenus, H. Abdulhamid, M. Skoglundh, E. Olsson, and E. Fridell, "Platinum dispersion measurements for Pt/BaO/Al₂O₃, NO_x storage catalysts," *Appl. Catal. A Gen.*, vol. 296, pp. 157–168, Dec. 2005.
- [31] C. Guizard and A. Princivalle, "Preparation and characterization of catalyst thin films," *Catal. Today*, vol. 146, pp. 367–377, Aug. 2009.
- [32] C. G. Vayenas, I. Ioannides, and S. Bebelis, "Solid Electrolyte Cyclic Voltammetry for in Situ Investigation of Catalyst Surfaces," *J. Catal.*, vol. 129, pp. 67–87, 1991.

- [33] C. G. Vayenas, S. Bebelis, C. Pliangos, S. Brosda, and D. Tsiplakides, "*Electrochemical Activation Of Catalysis Promotion, Electrochemical Promotion and Metal Support Interactions*," Kluwer Academic/Plenum Publishers New York, 2001.
- [34] C. G. Vayenas and C. G. Koutsodontis, "Non-Faradaic electrochemical activation of catalysis.," *J. Chem. Phys.*, vol. 128, p. 182506, May 2008.
- [35] A. Hammad, S. Souentie, E. I. Papaioannou, S. Balomenou, D. Tsiplakides, J. C. Figueroa, C. Cavalca, and C. J. Pereira, "Electrochemical promotion of the SO₂ oxidation over thin Pt films interfaced with YSZ in a monolithic electropromoted reactor," *Appl. Catal. B Environ.*, vol. 103, pp. 336–342, Apr. 2011.
- [36] C. G. Vayenas and D. Tsiplakides, "On the work function of the gas-exposed electrode surfaces in solid state electrolyte cells," *Surf. Sci.*, vol. 467, pp. 23–34, Nov. 2000.
- [37] S. Ladas, S. Bebelis, and C. G. Vayenas, "Work function measurements on catalyst films subject to in situ electrochemical promotion," *Surf. Sci.*, vol. 251–252, pp. 1062–1068, 1991.
- [38] C. G. V. Ilan Riess, "Fermi level and potential distribution in solid electrolyte cells with and without ion spillover," *Solid State Ionics*, vol. 159, pp. 313–329, Apr. 2003.
- [39] A. Jaccoud, "*Electrochemical Promotion of Pt Catalysts for Gas Phase Reactions*," École Polytechnique Fédérale De Lausanne, 2007.
- [40] C. G. Vayenas and S. Bebelis, "Electrochemical promotion of heterogeneous catalysis," *Catal. Today*, vol. 51, pp. 581–594, Jul. 1999.
- [41] J. Nicole, D. Tsiplakides, C. Pliangos, X. E. Verykios, C. Comninellis, and C. G. Vayenas, "Electrochemical Promotion and Metal–Support Interactions," *J. Catal.*, vol. 204, pp. 23–34, Nov. 2001.
- [42] I. V Yentekakis and G. Moggridge, "In Situ Controlled Promotion of Catalyst Surfaces via NEMCA: The Effect of Na on the Pt-Catalyzed CO Oxidation," *J. Catal.*, vol. 146, pp. 292–305, 1994.
- [43] F. H. M. Dekker, J. G. Nazloomian, A. Bliet, F. Kapteijn, J. A. Moulijn, D. R. Coulson, P. L. Mills, and J. J. Lerou, "Carbon monoxide oxidation over platinum powder: A comparison of TAP and step-response experiments," *Appl. Catal. A Gen.*, vol. 151, pp. 247–266, Mar. 1997.

- [44] A. D. Frantzis, S. Bebelis, and C. G. Vayenas, "Electrochemical promotion (NEMCA) of CH₄ and C₂H₄ oxidation on Pd/YSZ and investigation of the origin of NEMCA via AC impedance spectroscopy," *Solid State Ionics*, vol. 136–137, pp. 863–872, 2000.
- [45] P. Vernoux, F. Gaillard, L. Bultel, E. Siebert, and M. Primet, "Electrochemical Promotion of Propane and Propene Oxidation on Pt/YSZ," *J. Catal.*, vol. 208, pp. 412–421, Jun. 2002.
- [46] P. Vernoux, F. Gaillard, C. Lopez, and E. Siebert, "In-situ electrochemical control of the catalytic activity of platinum for the propene oxidation," *Solid State Ionics*, vol. 175, pp. 609–613, Nov. 2004.
- [47] A. Thursfield, S. Brosda, C. Pliangos, T. Schober, and C. G. Vayenas, "Electrochemical promotion of an oxidation reaction using a proton conductor," *Electrochim. Acta*, vol. 48, pp. 3779–3788, Nov. 2003.
- [48] N. Kotsionopoulos and S. Bebelis, "Electrochemical promotion of the oxidation of propane on Pt/YSZ and Rh/YSZ catalyst-electrodes," *J. Appl. Electrochem.*, vol. 35, pp. 1253–1264, Sep. 2005.
- [49] C. Jiménez-Borja, F. Dorado, A. de Lucas-Consuegra, J. M. García-Vargas, and J. L. Valverde, "Complete oxidation of methane on Pd/YSZ and Pd/CeO₂/YSZ by electrochemical promotion," *Catal. Today*, vol. 146, pp. 326–329, Aug. 2009.
- [50] M. N. Tsampas, F. M. Sapountzi, and C. G. Vayenas, "Electrochemical promotion of CO oxidation on Pt/YSZ: The effect of catalyst potential on the induction of highly active stationary and oscillatory states," *Catal. Today*, vol. 146, pp. 351–358, Aug. 2009.
- [51] L. Lizarraga, S. Souentie, L. Mazri, A. Billard, and P. Vernoux, "Investigation of the CO oxidation rate oscillations using electrochemical promotion of catalysis over sputtered-Pt films interfaced with YSZ," *Electrochem. commun.*, vol. 12, pp. 1310–1313, Oct. 2010.
- [52] A. de Lucas-Consuegra, A. Princivale, A. Caravaca, F. Dorado, C. Guizard, J. L. Valverde, and P. Vernoux, "Preferential CO oxidation in hydrogen-rich stream over an electrochemically promoted Pt catalyst," *Appl. Catal. B Environ.*, vol. 94, pp. 281–287, Feb. 2010.
- [53] P. Vernoux, F. Gaillard, R. Karoum, and A. Billard, "Reduction of nitrogen oxides over Ir/YSZ electrochemical catalysts," *Appl. Catal. B Environ.*, vol. 73, pp. 73–83, Apr. 2007.

- [54] A. Lintanf, E. Djurado, and P. Vernoux, "Pt/YSZ electrochemical catalysts prepared by electrostatic spray deposition for selective catalytic reduction of NO by C₃H₆," *Solid State Ionics*, vol. 178, pp. 1998–2008, Mar. 2008.
- [55] A. de Lucas-Consuegra, F. Dorado, C. Jiménez-Borja, and J. L. Valverde, "Influence of the reaction conditions on the electrochemical promotion by potassium for the selective catalytic reduction of N₂O by C₃H₆ on platinum," *Appl. Catal. B Environ.*, vol. 78, pp. 222–231, Feb. 2008.
- [56] G. Pekridis, N. Kaklidis, M. Konsolakis, C. Athanasiou, I. V. Yentekakis, and G. E. Marnellos, "A comparison between electrochemical and conventional catalyst promotion: The case of N₂O reduction by alkanes or alkenes over K-modified Pd catalysts," *Solid State Ionics*, vol. 192, pp. 653–658, Jun. 2011.
- [57] C. Pliangos, C. Raptis, T. Badas, D. Tsiplakides, and C. . Vayenas, "Electrochemical promotion of a classically promoted Rh catalyst for the reduction of NO," *Electrochim. Acta*, vol. 46, pp. 331–339, Nov. 2000.
- [58] E. I. Papaioannou, S. Souentie, A. Hammad, and C. G. Vayenas, "Electrochemical promotion of the CO₂ hydrogenation reaction using thin Rh, Pt and Cu films in a monolithic reactor at atmospheric pressure," *Catal. Today*, vol. 146, no. 3–4, pp. 336–344, 2009.
- [59] S. Bebelis, H. Karasali, and C. G. Vayenas, "Electrochemical promotion of CO₂ hydrogenation on Rh/YSZ electrodes," *J. Appl. Electrochem.*, vol. 38, pp. 1127–1133, May 2008.
- [60] S. Bebelis, H. Karasali, and C. G. Vayenas, "Electrochemical promotion of the CO₂ hydrogenation on Pd/YSZ and Pd/β"-Al₂O₃ catalyst-electrodes," *Solid State Ionics*, vol. 179, pp. 1391–1395, Sep. 2008.
- [61] R. H. Venderbosch, W. Prins, and W. P. M. Van Swaaij, "Platinum catalyzed oxidation of carbon monoxide as a model reaction in mass transfer measurements," *Chem. Eng. Sci.*, vol. 53, no. 19, pp. 3355–3366, Oct. 1998.
- [62] C. Xia, M. Hugentobler, Y. Li, G. Foti, C. Comninellis, and W. Harbich, "Electrochemical promotion of CO combustion over non-percolated Pt particles supported on YSZ using a novel bipolar configuration," *Electrochem. commun.*, vol. 13, pp. 99–101, Jan. 2011.
- [63] P. Vernoux, M. G. And, and X. Li, "Ionically Conducting Ceramics as Alternative Catalyst Supports," *Electrochemical Solid-State Lett.*, vol. 12, no. 7, pp. E9–E11, 2009.

- [64] L. Lizarraga, M. Guth, A. Billard, and P. Vernoux, "Electrochemical catalysis for propane combustion using nanometric sputtered-deposited Pt films," *Catal. Today*, vol. 157, pp. 61–65, Nov. 2010.
- [65] R. Karoum, A. de Lucas-Consuegra, F. Dorado, J. L. Valverde, A. Billard, and P. Vernoux, "Towards a new definition of EPOC parameters for anionic electrochemical catalysts: case of propene combustion," *J. Appl. Electrochem.*, vol. 38, pp. 1083–1088, Mar. 2008.
- [66] C. Yentekakis, I.V. and Vayenas, "The Effect of Electrochemical Oxygen Pumping on the Steady-State and Oscillatory Behavior of CO Oxidation on Polycrystalline Pt," *J. Catal.*, vol. 111, pp. 170–188, 1988.
- [67] C. Jiménez-Borja, a. de Lucas-Consuegra, F. Sapountzi, F. Dorado, a. Katsaounis, and J. L. Valverde, "Oscillatory behavior of Rh/YSZ under electropromoted conditions," *Chem. Phys. Lett.*, vol. 519–520, pp. 89–92, Jan. 2012.
- [68] S. Souentie, C. Xia, C. Falgairrette, Y. D. Li, and C. Comninellis, "Investigation of the 'permanent' electrochemical promotion of catalysis (P-EPOC) by electrochemical mass spectrometry (EMS) measurements," *Electrochem. commun.*, vol. 12, pp. 323–326, Feb. 2010.
- [69] C. Falgairrette and G. Fóti, "Oxygen storage in O₂/Pt/YSZ cell," *Catal. Today*, vol. 146, pp. 274–278, Aug. 2009.
- [70] C. Falgairrette, A. Jaccoud, G. Fóti, and C. Comninellis, "The phenomenon of 'permanent' electrochemical promotion of catalysis (P-EPOC)," *J Appl Electrochem*, vol. 38, pp. 1075–1082, 2008.
- [71] C. Xia, C. Falgairrette, Y. Li, G. Foti, C. Comninellis, and W. Harbich, "Electrochemical promotion of CO combustion over Pt/YSZ under high vacuum conditions," *Appl. Catal. B Environ.*, vol. 113–114, pp. 250–254, Feb. 2012.
- [72] D. Poulidi, M. E. Rivas, B. Zydorczak, Z. Wu, K. Li, and I. S. Metcalfe, "Electrochemical promotion of a Pt catalyst supported on La_{0.6}Sr_{0.4}Co_{0.2}Fe_{0.8}O_{3-δ} hollow fibre membranes," *Solid State Ionics*, vol. 225, pp. 382–385, Oct. 2012.
- [73] C. López-Gándara, J. M. Fernández-Sanjuán, F. M. Ramos, and A. Cirera, "Estimation of the electrodes' three phase boundary sites in electrochemical exhaust gas sensors before and after electric polarization," *Sensors Actuators B Chem.*, vol. 175, pp. 225–233, Dec. 2012.

- [74] R. Lewis and R. Gomer, "Adsorption of oxygen on platinum," *Surf. Sci.*, vol. 12, no. 2, pp. 157–176, 1968.
- [75] J. Will, A. Mitterdorfer, C. Kleinlogel, D. Perednis, and L. J. Gauckler, "Fabrication of thin electrolytes for second-generation solid oxide fuel cells," *Solid State Ionics*, vol. 131, pp. 79–96, 2000.
- [76] J. Sunarso, S. Baumann, J. M. Serra, W. A. Meulenber, S. Liu, Y. S. Lin, and J. C. Diniz da Costa, "Mixed ionic–electronic conducting (MIEC) ceramic-based membranes for oxygen separation," *J. Memb. Sci.*, vol. 320, pp. 13–41, Jul. 2008.
- [77] L. and R. B. Velho, "Diffusivity and solubility of oxygen in platinum and Pt-Ni alloys," *Metall. Mater. Trans. B*, vol. 3, no. 1, pp. 65–72, 1972.
- [78] D. Archonta, A. Frantzis, D. Tsiplakides, and C. G. Vayenas, "STM observation of the origin of electrochemical promotion on metal catalyst-electrodes interfaced with YSZ and β "-Al₂O₃," *Solid State Ionics*, vol. 177, pp. 2221–2225, Oct. 2006.
- [79] G. Pekridis, K. Kalimeri, N. Kaklidis, E. Vakouftsi, E. F. Iliopoulou, C. Athanasiou, and G. E. Marnellos, "Study of the reverse water gas shift (RWGS) reaction over Pt in a solid oxide fuel cell (SOFC) operating under open and closed-circuit conditions," *Catal. Today*, vol. 127, pp. 337–346, Sep. 2007.
- [80] A. Piram, X. Li, F. Gaillard, C. Lopez, A. Billard, and P. Vernoux, "Electrochemical promotion of environmental catalysis," *Ionics (Kiel)*, vol. 11, pp. 327–332, Sep. 2005.
- [81] T. Neubrand, S. Günther, A. Fenske, and R. Imbihl, "Work function changes and electrochemical pumping of platinum electrodes on yttrium stabilized zirconia," *Phys. Chem. Chem. Phys.*, no. 13, pp. 3569–3575, 2004.
- [82] S. Balomenou, D. Tsiplakides, A. Katsaounis, S. Thiemann-Handler, B. Cramer, G. Foti, C. Comninellis, and C. G. Vayenas, "Novel monolithic electrochemically promoted catalytic reactor for environmentally important reactions," *Appl. Catal. B Environ.*, vol. 52, pp. 181–196, Sep. 2004.
- [83] A. de Lucas-consuegra, F. Dorado, J. L. Valverde, R. Karoum, and P. Vernoux, "Low-temperature propene combustion over Pt/K- β Al₂O₃ electrochemical catalyst: Characterization, catalytic activity measurements, and investigation of the NEMCA effect," *J. Catal.*, vol. 251, pp. 474–484, Oct. 2007.
- [84] S. P. S. Badwal and F. T. Ciacchi, "Microstructure of Pt electrodes and its influence on the oxygen transfer kinetics," *Solid State Ionics*, vol. 18–19, pp. 1054–1059, 1986.

- [85] J. Janek, B. Luerßen, E. Mutoro, H. Fischer, and S. Günther, “In situ imaging of electrode processes on solid electrolytes by photoelectron microscopy and microspectroscopy – the role of the three-phase boundary,” *Top. Catal.*, vol. 44, no. 3, pp. 399–407, Jun. 2007.
- [86] S. P. Yoon, S. W. Nam, S.-G. Kim, S.-A. Hong, and S.-H. Hyun, “Characteristics of cathodic polarization at Pt/YSZ interface without the effect of electrode microstructure,” *J. Power Sources*, vol. 115, pp. 27–34, Mar. 2003.
- [87] J.H. Phark, S. Duarte Jr., H. Kahn, M. B. Blatz, and A. Sadan, “Influence of contamination and cleaning on bond strength to modified zirconia,” *Dent. Mater.*, vol. 25, pp. 1541–1550, Dec. 2009.
- [88] J. J. H. Pöpke, E. Mutoro, and B. Luerssen, “Oxidation of Platinum in the Epitaxial Model System Pt(111)/YSZ(111): Quantitative Analysis of an Electrochemically Driven PtOx Formation,” *J. Phys. Chem.C*, vol. 116, no. 2, pp. 1912–1920, 2012.
- [89] V.F.Lvovich, *Impedance Spectroscopy: Applications to Electrochemical and Dielectric Phenomena*, Wiley, New Jersey, 2012.
- [90] S. N. Reddy, A. S. Chary, and T. Chiranjivi, “ac impedance analysis of single crystals of $\text{Sr}(\text{NO}_3)_2$ and $\text{Sr}(\text{NO}_3)_2\text{:Na}$,” *Solid State Ionics*, vol. 42, no. 1–2, pp. 101–107, 1990.
- [91] J. L. Hertz, A. Rothschild, and H. L. Tuller, “Highly enhanced electrochemical performance of silicon-free platinum–yttria stabilized zirconia interfaces,” *J. Electroceram*, vol. 22, pp. 428–435, Apr. 2008.
- [92] H. Pöpke, E. Mutoro, B. Luerßen, and J. Janek, “The potential of in situ-scanning electron microscopy — Morphology changes of electrically polarized thin film Pt(O₂)/YSZ model electrodes,” *Solid State Ionics*, vol. 189, pp. 56–62, May 2011.
- [93] C. Ellinger, A. Stierle, I. K. Robinson, A. Nefedov, and H. Dosch, “Atmospheric pressure oxidation of Pt(111),” *J. Phys. Condens. Matter*, vol. 20, p. 184013, May 2008.
- [94] L. K. Ono, B. Yuan, H. Heinrich, and B. R. Cuenya, “Formation and Thermal Stability of Platinum Oxides on Size-Selected Platinum Nanoparticles: Support Effects,” *J. Phys. Chem.C*, vol. 114, pp. 22119–22133, 2010.
- [95] M. Peuckert and H. P. Bonzel, “Characterization of oxidized platinum surfaces by x-ray photoelectron spectroscopy,” *Surf. Sci.*, vol. 145, pp. 239–259, 1984.

- [96] X. Zhang, H. Li, and Y. Yang, "Determination of impurities in highly pure platinum by inductively coupled plasma-atomic emission spectrometry," *Talanta*, vol. 42, pp. 1959–1963, 1995.
- [97] L. Bultel, P. Vernoux, F. Gaillard, C. Roux, and E. Siebert, "Electrochemical and catalytic properties of porous Pt–YSZ composites," *Solid State Ionics*, vol. 176, pp. 793–801, Feb. 2005.
- [98] K. Hennebrüder, R. Wennrich, J. Mattusch, H.-J. Stärk, and W. Engewald, "Determination of gadolinium in river water by SPE preconcentration and ICP-MS," *Talanta*, vol. 63, pp. 309–16, May 2004.
- [99] C. Cui, M. He, and B. Hu, "Membrane solid phase microextraction with alumina hollow fiber on line coupled with ICP-OES for the determination of trace copper, manganese and nickel in environmental water samples," *J. Hazard. Mater.*, vol. 187, pp. 379–85, Mar. 2011.
- [100] E. J. Llorent-Martínez, P. Ortega-Barrales, M. L. Fernández-de Córdova, A. Domínguez-Vidal, and A. Ruiz-Medina, "Investigation by ICP-MS of trace element levels in vegetable edible oils produced in Spain," *Food Chem.*, vol. 127, pp. 1257–1262, Aug. 2011.
- [101] Y. Qing-hua, Y. Li, W. Qing, and M. Xiao-qin, "Determination of major and trace elements in six herbal drugs for relieving heat and toxic by ICP-AES with microwave digestion," *J. Saudi Chem. Soc.*, vol. 16, pp. 287–290, Jul. 2012.
- [102] A. K. Opitz, M. P. Hörlein, T. Huber, and J. Fleig, "Current-Voltage Characteristics of Platinum Model Electrodes on Yttria-Stabilized Zirconia," *J. Electrochem. Soc.*, vol. 159, no. 5, pp. B502–B513, 2012.
- [103] L. Winkel, J. Wochele, C. Ludwig, I. Alxneit, and M. Sturzenegger, "Decomposition of copper concentrates at high-temperatures: An efficient method to remove volatile impurities," *Miner. Eng.*, vol. 21, pp. 731–742, Sep. 2008.
- [104] H. Maleszewska and R. Dybczyński, "Determination of trace impurities in platinum by neutron activation analysis," *J. Radioanal. Chem.*, vol. 31, no. 1, pp. 177–193, 1976.
- [105] K. Arul Raj, I. Vasu, "Electrochemical and oxygen reduction behaviour of solid silver-bismuth/antimony electrodes in KOH solutions," *J. Appl. Electrochem.*, vol. 23, no. 7, pp. 728–734, 1993.

- [106] S. N. Kapura, B. Shana, J. Hyuna, and L. Wanga, "First-principles study of CO oxidation on bismuth-promoted Pt(111) surfaces," *Mol. Simul.*, vol. 37, no. 8, pp. 648–658, 2011.
- [107] A. Jaccoud, G. Fóti, and C. Comninellis, "Electrochemical investigation of platinum electrode in solid electrolyte cell," *Electrochim. Acta*, vol. 51, pp. 1264–1273, Jan. 2006.
- [108] C. G. Vayenas, "Thermodynamic analysis of the electrochemical promotion of catalysis," *Solid State Ionics*, vol. 168, pp. 321–326, Mar. 2004.
- [109] A. Katsaounis, Z. Nikopoulou, X. E. Verykios, and C. G. Vayenas, "Comparative isotope-aided investigation of electrochemical promotion and metal support interactions2. CO oxidation by $^{18}\text{O}_2$ on electropromoted Pt films deposited on YSZ and on nanodispersed Pt/YSZ catalysts," *J. Catal.*, vol. 226, pp. 197–209, Aug. 2004.

Appendix A

Table 1: Patterned electrodes geometric characteristics of the (a) 1st, (b) 2nd and 3rd batch

Length scales (μm)	No of fingers	Pt block surface (mm^2)	Pt block length (mm)	Fingers surface (mm^2)	Finger length	Total surface (mm^2)	Total tpb length (mm)	Tpb (mm^{-1})
2	363	12	19	2.5	2542	14.5	2561	177
20	200	12	19	14	1404	26	1423	55
200	36	12	19	25.2	259	37.2	278	7

(a)

Length scales (μm)	No of fingers	Pt block surface (mm^2)	Pt block length (mm)	Fingers surface (mm^2)	Finger length	total surface (mm^2)	total tpb length (mm)	Tpb (mm^{-1})
4	1000	12	19	12	3004	24	3023	126
40	100	12	19	12	304	24	323	13
200	20	12	19	12	64	24	83	3
400	10	12	19	12	34	24	53	2

(b)

Appendix B

1. Reactive condition

Reaction rate calculation

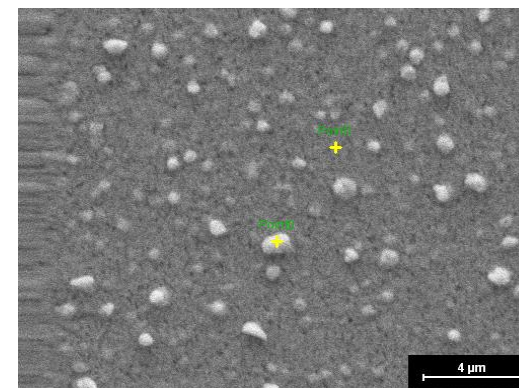
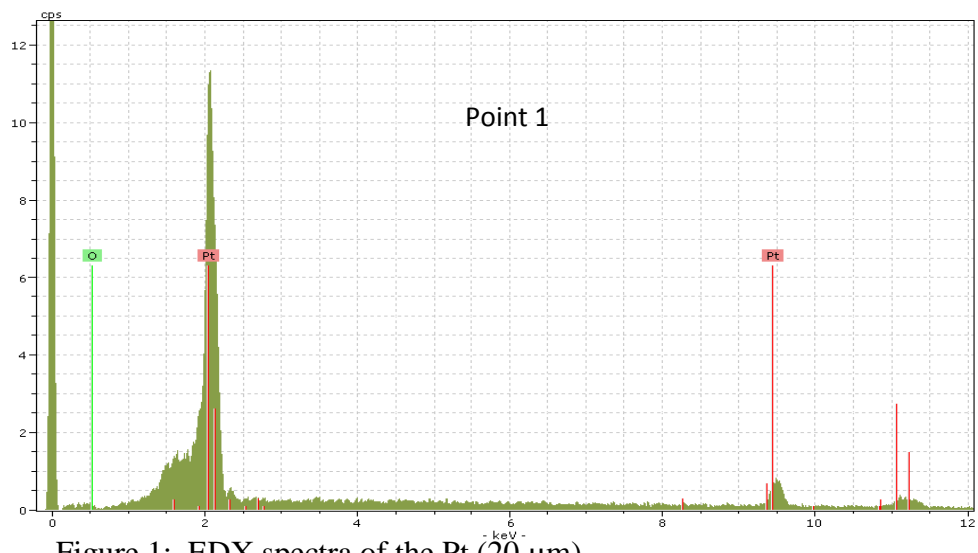
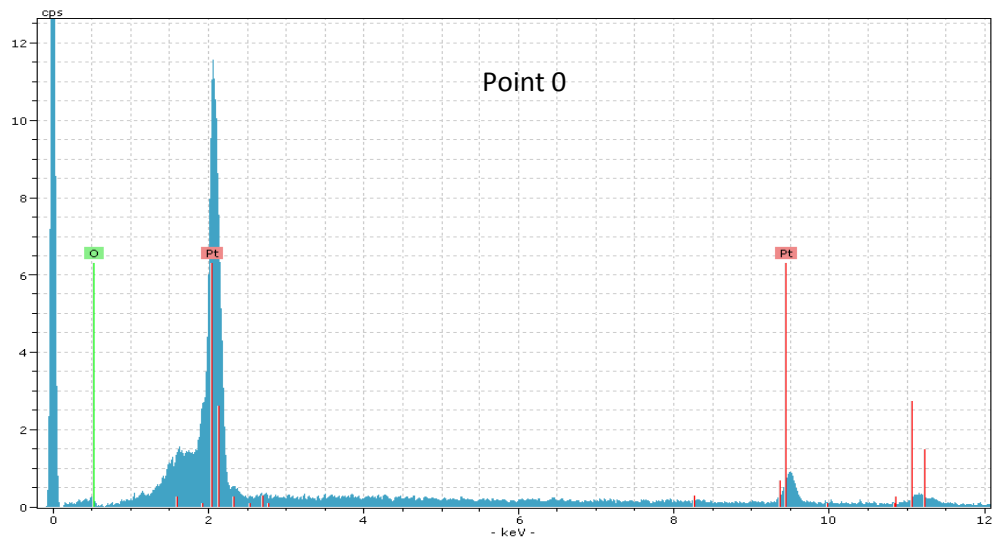
$$\text{Rate } CO_2 = \frac{\text{Volumetric flow rate (mlmin}^{-1}\text{)}}{\text{Pt area (cm}^2\text{)} \times 60 \text{ (smin}^{-1}\text{)}} \times [CO_2] \times \frac{10^9 \text{ (nmol)}}{22400 \text{ (ml)}}$$

2. Nonreactive condition

The charge transfer resistance (diameter of a semicircle) calculation

$$\text{radius} = \frac{Z_1^2 + Z_2^2}{2 Z_1}$$

Appendix C



Pt (20 μm)

Figure 1: EDX spectra of the Pt (20 μm)

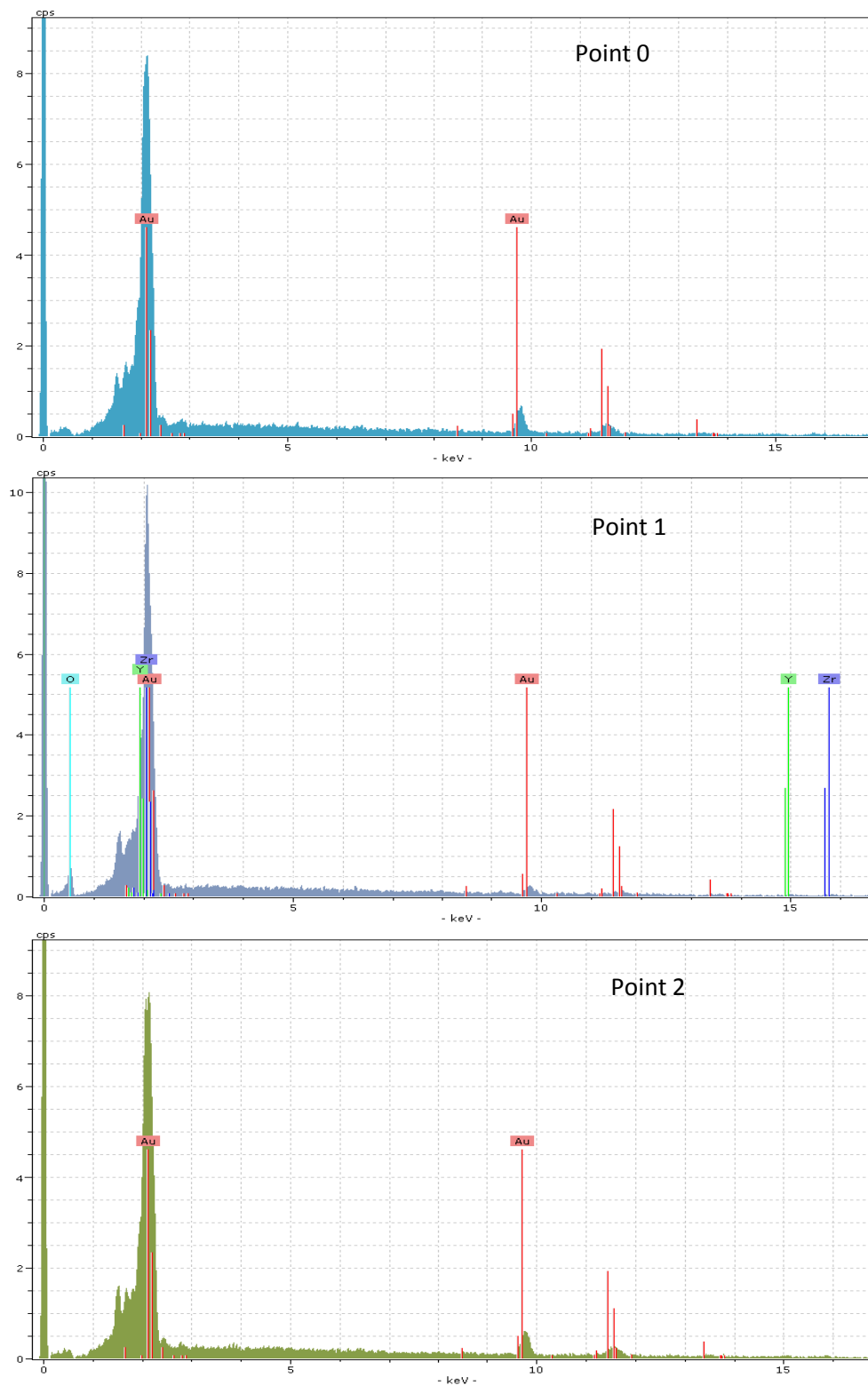


Figure 2: EDX spectra of the Au (200 μm)

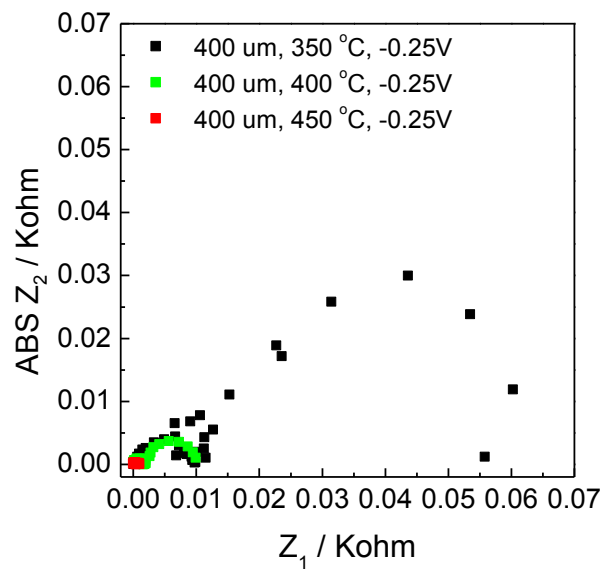
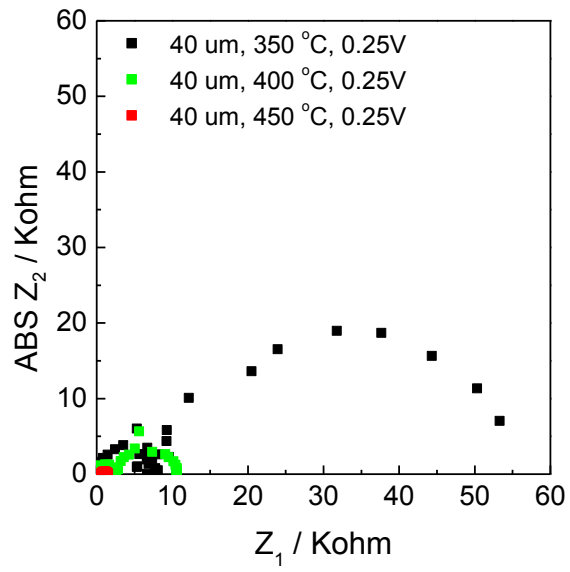


Figure 3: Impedance spectra of the patterned electrode samples at different temperature (frequency from 1E6 to 1E-1 Hz)

Table 2: Conductance values from the impedance spectra of 4 μm , 40 μm and 400 μm at each applied potential, at 350 $^{\circ}\text{C}$, 400 $^{\circ}\text{C}$ and 450 $^{\circ}\text{C}$ by using the equation of a circle. The experiments were carried out under the flow of 20% O_2/He .

Applied Potential (V)	1/Temperature (K^{-1})	Conductance (ohm^{-1})		
		4 μm	40 μm	400 μm
-0.04V to-0.10V	1.61E-3	5.88E-5	1.27E-5	3.40E-5
	1.49E-3	2.27E-4	3.88E-5	3.57E-5
	1.38E-3	3.03E-4	4.08E-4	1.34E-4
-0.28 V	1.61E-3	2.94E-5	1.35E-4	5.81E-5
	1.49E-3	6.25E-5	2.94E-4	1.11E-4
	1.38E-3	3.33E-3	1.25E-3	1.75E-3
-0.40 V	1.61E-3	3.13E-5	1.00E-4	5.38E-5
	1.49E-3	NA	3.33E-4	7.14E-5
	1.38E-3	NA	1.67E-3	1.25E-3
0.35 V	1.61E-3	8.37E-6	1.09E-5	5.15E-5
	1.49E-3	3.33E-5	2.94E-5	5.00E-5
	1.38E-3	3.85E-4	1.72E-4	7.14E-4

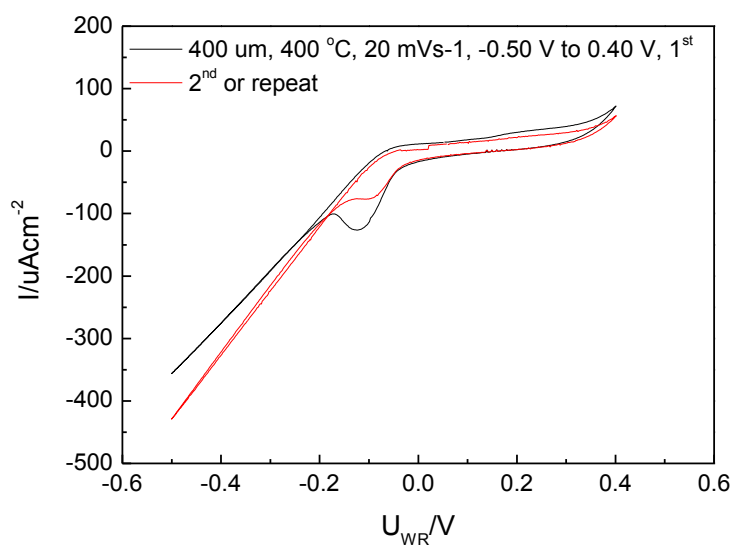


Figure 4: Voltammograms of the 400 μm at 400 $^{\circ}\text{C}$ under a nonreactive condition from reverse potential experiments after the exposure to a 0.50 V anodic potential

Table 3: Bubble diameter which is observed in the SEM images of the electrode surface of the patterned electrode samples

Bubble Diameter	4 μm (electrochemical)	40 μm (electrochemical)	200 μm (kinetic)	200 μm 550 $^{\circ}\text{C}$ (kinetic)	2 μm (kinetic)
Minimum	1.17E-1	8.60E-2	9.61E-2	1.92E-2	1.54E-1
Maximum	4.22E-1	7.01E-1	1.12	1.27	4.04E-1
Average	2.41E-1	3.28E-1	4.08E-1	4.35E-1	2.61E-1
Average /length scale	6.03E-2	8.21E-3	2.04E-3	2.18E-3	1.31E-1
Average/surface area (μm^{-1})	1.00E-10	1.37E-10	1.7E-10	1.81E-10	1.80E-10

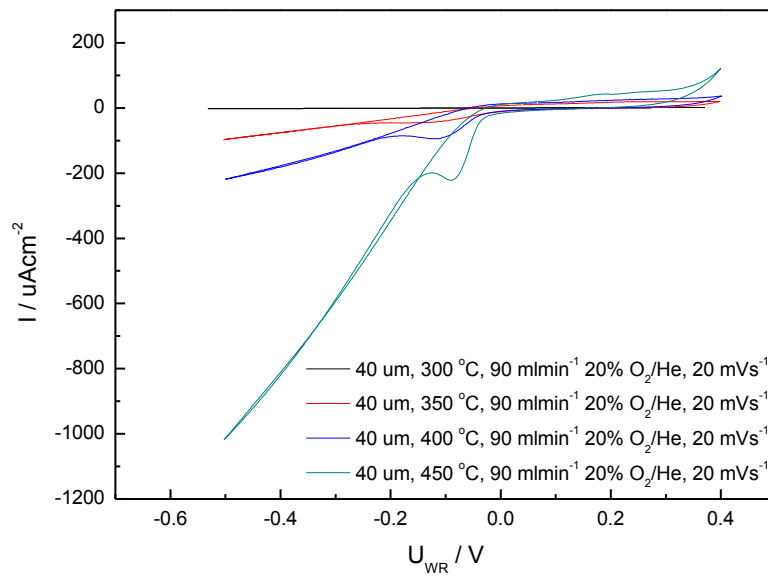


Figure 5: Voltammograms of 40 μm at 300 °C to 450 °C, scan rate of 20 mVs^{-1} , 90 to 100 mlmin^{-1} 20% O_2/He

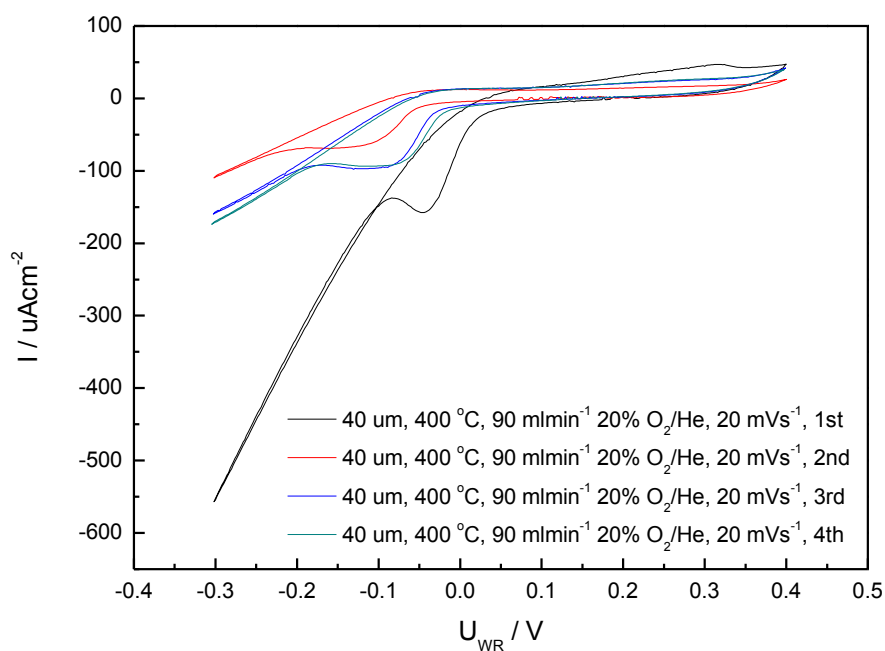
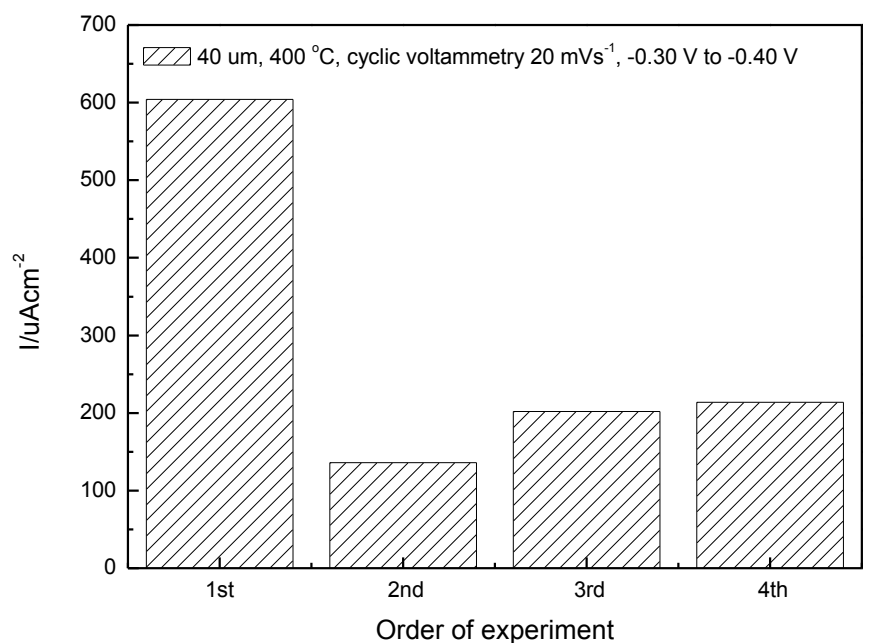


Figure 6: (a) Current range and (b) voltammograms of 40 μm sample at scan rates of 20 mVs^{-1} , 400 $^{\circ}\text{C}$, 90 mlmin^{-1} 20 % O_2/He , (2nd experiment was carried out after a complete study of CV, EIS and current overpotential for the 40 μm , 3rd and 4th experiments were carried out in sequence)

Table 4: Data from current overpotential study at 350 °C

U_{WR} , V	4 μm	40 μm	400 μm
-3.49E-1	-9.29E1		
-2.76E-1	-6.56E1		
-2.01E-1	-4.17E1		
-1.32E-1	-1.75E1		
-9.37E-2	-6.89		
-4.80E-2	-2.11		
7.00E-4	-3.55E-1		
2.93E-1	4.91E-1		
3.52E-1	1.52E		
3.97E-1	5.87E		
4.55E-1	2.03E1		
5.33E-1	6.60E1		
5.51E-1	1.42E2		
-2.87E-1		-4.39E1	
-2.80E-1		-4.19E1	
-1.81E-1		-2.62E1	
-1.32E-1		-1.73E1	
-1.05E-1		-1.10E1	
-5.48E-2		-4.79	
-1.51E-2		-2.02E	
3.50E-1		6.54E-1	
3.90E-1		1.50	
4.50E-1		6.61	
4.82E-1		2.04E1	
5.29E-1		4.24E1	
5.69E-1		7.60E1	
5.91E-1		1.02E2	
-4.15E-1			-4.71E1
-2.58E-1			-2.50E1
-2.23E-1			-1.90E1
-1.49E-1			-1.05E1
-1.26E-1			-6.89
-7.01E-2			-2.64
-3.83E-2			9.10E3
5.10E-3			-4.70E1
4.28E-2			-2.14E2
1.19E-1			5.20E3
2.88E-1			1.58
3.44E-1			2.85
4.37E-1			1.87E1
4.53E-1			6.14E1
4.36E-1			1.14E2
4.37E-1			1.57E2

Table 5: Data from current overpotential study at 400 °C

UWR, V	4 μm	40 μm	400 μm
-2.79E-1	-1.63E2		
-2.61E-1	-1.63E2		
-1.10E-1	-1.02E2		
-7.88E-2	-3.46E1		
-3.61E-2	-9.23E		
1.70E-2	-1.23E		
2.47E-1	1.14E		
3.07E-1	4.94E		
3.65E-1	2.29E1		
4.17E-1	1.08E2		
5.25E-1	1.63E2		
5.80E-1	1.63E2		
-3.71E-1		-1.63E2	
-2.82E-1		-1.63E2	
-1.80E-1		-1.02E2	
-1.22E-1		-3.46E1	
-5.39E-2		-9.23	
-5.88E-2		-1.23	
-1.51E-2		1.14	
2.53E-1		4.94	
3.64E-1		2.29E1	
4.24E-1		1.08E2	
4.51E-1		1.63E2	
4.65E-1		1.63E2	
4.89E-1			
-3.84E-1			-2.18E2
-3.28E-1			-1.83E2
-2.61E-1			-1.34E2
-1.84E-1			-6.52E1
-1.21E-1			-1.40E1
-9.96E-2			-5.74
-5.75E-2			-2.17
-2.00E-2			5.71E-1
5.78E-2			2.32E-1
9.20E-2			2.24
1.62E-1			1.82
2.62E-1			3.78
3.52E-1			1.95E1
4.23E-1			2.22E2
4.36E-1			4.43E2
4.38E-1			7.27E2

Table 6: Data from current overpotential study at 450 °C

UWR, V	4 μm	40 μm	400 μm
-4.31E-1	-1.63E2		
-3.29E-1	-1.63E2		
-2.29E-1	-1.63E2		
-1.29E-1	-1.63E2		
-8.01E-2	-1.63E2		
-3.52E-2	-7.52E1		
1.08E-2	-1.60E1		
1.66E-1	1.53		
2.24E-1	3.61		
3.22E-1	2.99		
3.71E-1	1.11E2		
4.38E-1	1.63E2		
5.72E-1	1.63E2		
6.05E-1	1.63E2		
-3.31E-1		-9.32E2	
-2.64E-1		-6.85E2	
-2.03E-1		-4.21E2	
-1.38E-1		-2.08E2	
-9.18E-2		-8.60E1	
-6.52E-2		-2.11E1	
-2.47E-2		-3.89	
2.33E-1		3.30	
2.86E-1		1.58E1	
3.33E-1		5.35E1	
3.63E-1		1.84E2	
3.97E-1		5.83E2	
4.29E-1		1.09E3	
4.49E-1		1.62E3	
-2.12E-1			-1.80E3
-1.68E-1			-1.21E3
-1.28E-1			-7.47E2
-1.44E-1			-3.31E2
-1.24E-1			-1.51E2
-8.50E-2			-4.24E1
-3.81E-2			-1.21E1
-1.47E-2			-4.86
3.33E-2			3.27
5.96E-2			5.51
1.09E-1			7.46
2.06E-1			1.34E1
2.68E-1			4.12E2
2.85E-1			1.30E3
3.01E-1			2.18E3

Appendix D

Publication

Title: Influence of Impurities and Catalyst Surface Characteristics on the Oxygen Charge Transfer Reaction in the Pt/YSZ System

Authors: Mas Rahayu Jalil, Naimah Ibrahim, Danai Poulidi, Ian S. Metcalfe

Journal: Solid State Ionics, 2012

doi:10.1016/j.ssi.2012.06.011

